CENTER FOR SPACE RESEARCH

MASSACHUSETTS INSTITUTE OF TECHNOLOGY

Design Studies of a Large Electronically Steerable Phased Array

MIT CSR TR-69-4 February 1969

ABSTRACT

Design studies relating to a VHF, electronically controlled, 50 db antenna are presented. This antenna will be a low noise dipole phased array covering the range 70 to 80 MHz. The purpose and evolution of the array are outlined. The objective has been the design of a large versatile tracking array maximizing the performance per unit cost.

Also included, are site survey reports, a proposal for the addition of a transmitting function, a description of the Sunblazer spacecraft, and an evaluation of a 128 dipole narrow band pilot system.

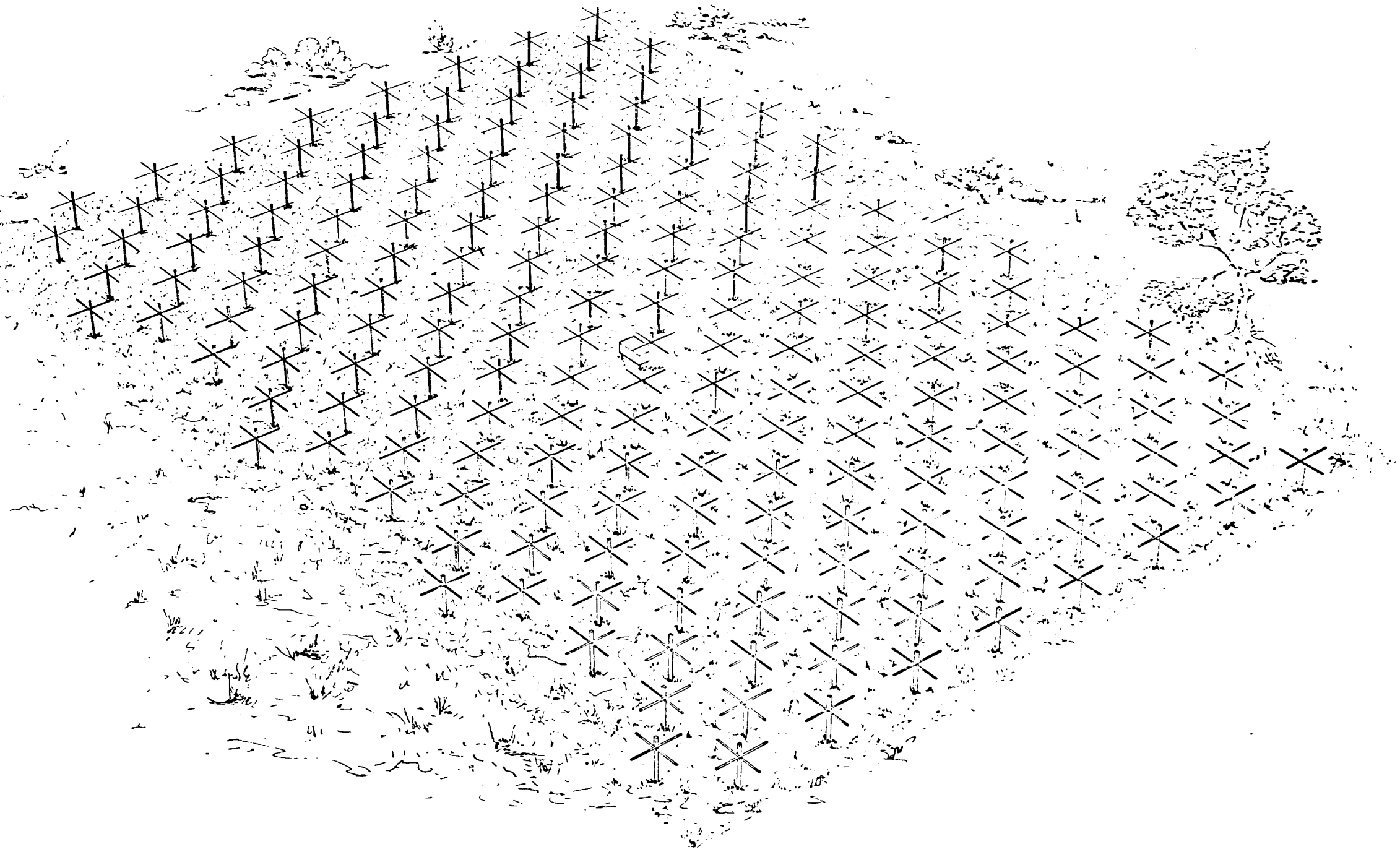

192 DIPOLE PILOT ARRAY

MASSACHUSETTS INSTITUTE OF TECHNOLOGY

CENTER FOR SPACE RESEARCH

LABORATORY FOR SPACE EXPERIMENTS

MIT CSR TR-69-4

Design Studies of a Large Electronically Steerable Phased Array

February 1969

Research and Development Work Under

National Aeronautics and Space Administration

Contract Number NASr-249

CONTRIBUTING EDITORS

R. H. Baker

J. V. Harrington

W. T. Higgins

J. C. James

CONTRIBUTORS

W. W. Cooper

and

L. H. Bannister

D. H. Galvin

R. H. Thompson

E. K. Weinschenk

TABLE OF CONTENTS

LIST OF FIGURES

INTRODUCTION

The Sunblazer mission is designed to provide the first accurate measurement of the solar coronal electron density in regions beyond the visible corona and yet where direct in situ satellite measurements are not possible. Stated in broader terms, the prime mission goal is to obtain the coronal electron density profile from regions near the earth's orbit to regions as close to the sun as possible. A second mission objective, which is of importance almost equal to the first, is to obtain quantitative data related to both turbulent and anisotropic phenomena within the expanding corona.

These data will be obtained by placing in solar orbit a small, relatively inexpensive spacecraft equipped with a pulsed radio frequency transmitter. The permutations suffered by coherent pulses on several frequencies will be observed from a terrestial site with a large aperture receiving system. The current results of design studies on the realization of such a receiving system comprise the bulk of this report. The remainder covers related topics about the mission, spacecraft, etc.

For reasons of time and space, only a small fraction of the results obtained during the many man-years of study that have gone into advancing the Sunblazer program to its present state can be reported here. All work not directly related to the receiving system is omitted (see Section 1) and much work which does relate to the receiving system but which is not essential in the understanding or description of the current

design is relegated to previous progress reports, technical reports, memos, etc.

Without attempting to justify specific conclusions, a general summary of the results may prove useful at this point. To be specific, it is shown elsewhere (see MIT/CSR-TR-69-1, Conceptual Design of a Small Solar Probe, Sunblazer, by Baker et al, 1969) that the accomplishment of the scientific objectives of the Sunblazer mission requires the transmission of short high power phase coherent R.F. pulses on two frequencies and that the required receiving aperture must have an effective area on the order of 1.2×10^5 (meters)^2. In order to enhance the scientific content of the experiment, a base frequency of about 75 MHz was chosen. At lower frequencies certain disruptive effects of the medium (the solar corona) dominate and destroy the communications path while at higher frequencies certain disruptive effects that contain essential scientific data about turbulent phenomena within the corona are eliminated completely.

Finally, for reasons of spacecraft and ground receiving system simplicity and to reduce overall cost, a "closely-packed" two frequency (70 MHz and 80 MHz) propagation experiment was chosen. This allows a single broadband ground antenna to be used for the mission. The required aperture together with the chosen frequency range thus dictates an antenna gain of 50 db. It is felt that an antenna of this magnitude can best be obtained in the form of a dipole phased array composed of roughly 27,000 dipoles for each of two polarizations. The receiving system

will incorporate polarization diversity reception.

One might consider the possiblity of using either a single large paraboloid or a collection of many smaller paraboloids to realize the required aperture. Assuming an aperture efficiency of 50%, the required gain can be obtained with a single reflector of 1870 feet diameter, 56 reflectors of 250 feet diameter, or 350 reflectors of 100 feet diameter. Stated another way, the 1000 foot spherical reflector at Arecibo, which has an aperture efficiency less than 50%, can realize somewhat less than 40 db gain at 75 MHz. Based on these and other considerations, principally financial, a structurally simple and electronically effective dipole phased array is proposed.

Consistent with cost effectiveness, the dipoles are organized in a modular form consisting of multi-level hierarchy in which the basic grouping, the "element", is composed of six individual dipoles sharing a common low-noise R.F. amplifier. These elements are then grouped to form the next level of organization which is called the "pilot" and which is in turn grouped to form a level called the "40 db array". Ten such 40 db arrays are joined to produce a full 50 db array. A combination of manual and electronically controlled phase shifters, providing appropriately fine increments of phase delay, can be used to electronically steer the main lobe of this array. It should be noted that the broadband requirement dictates a need for frequency insensitivity of the beam pointing system. Stated another way, the required steering is accomplished through the introduction

of increments of fixed time delay rather than increments of phase shift. For descriptive simplicity these delay elements will be usually referred to throughout this report as "phase shifters" and the increments will be labeled "λ/2", etc. However, one should remember the essential distinction.

Throughout the study effort performed to date, several underlying "boundary conditions" have served to guide our thinking. First and foremost is of course the accomplishment of the scientific objectives of the mission. However a second condition has had an impact which permeates this report. That is a strongly felt desire to maintain a high degree of scientific return per dollar spent. This consideration has resulted in many features which, although of proven effectiveness, lack cosmetic beauty. A final selection of the characteristics and hardware for this array will naturally depend upon the balance between these sometimes conflicting aspects.

Two final notes may be appropriate before the reader embarks on the long and somewhat arduous journey through this tome. First, the report is the product of several authors and the reader will experience a diveristy of grammatical style. Second, the material ranges from the pragmatic to the esoteric; from the thread pitch of a wood screw to the mathematical theory of arrays. The reader will do well to either skim or skip at first reading those sections which require detailed study. In particular, an inclusion of Section 2.1, 2.2, 2.3 will prove instructive for first reading while much of the remainder of

Chapter 2 should be left for later more leisurely study. Similarly, the appendices (Chapter 7) may be omitted. Bon Voyage!

CHAPTER 1

1.0 HISTORICAL REVIEW OF THE PHASED ARRAY PROGRAM

1.1 Initial Proposal

When the Sunblazer experiment was first proposed, it was hoped that the relatively high signal energy transmitted from the spacecraft[1,2] would allow one of the existing metric wavelength radio astronomical telescopes to be employed as the ground receiving antenna. After several unsuccessful attempts to get a commitment of more than a few hours a week of observing time on a number of suitable facilities such as the Arecibo Radio Telescope and a local 120-foot paraboloid, we concluded that the only way in which observing time consistent with the investment in spacecraft and launch costs could be guaranteed was for Sunblazer to have its own receiving antenna. We believed that the least expensive means of obtaining a suitable aperture was through an array of dipoles patterned after the 38 MHz solar radar telescope at El Campo, Texas, which we had operated for some time. Some differences in design were required by the higher 75 and 225 MHz frequencies which were initially proposed for the Sunblazer experiment. Furhter, we proposed to take advantage of new developments in solid state circuitry to make the array automatically phaseable, as opposed to the time

consuming cable-plugging method then in use at El Campo.

To investigate the feasibility of this approach, we developed and tested a laboratory model of the electronic amplifier and phasing package which were to be associated with each dipole element. When the design of these units was sufficiently firm, bids were solicited from several electronic manufacturers so that realistic cost data on the electronic components of the array were obtained. These outside estimates indicated two things: (1) that more than 90 percent of the cost of the two-frequency array was in the electronics, and (2) that the cost of a dual polarization, two-frequency, 4000-dipole array with amplifiers at every dipole was likely to be considerably in excess of the $3 million estimate which we had earlier postulated. These somewhat discouraging but realistic conclusions were reported to a group from NASA Headquarters and Langley at a meeting held in Cambridge in May, 1967.

1.2 High Gain Elements

As a result of this meeting a fundamental redirection of the array program was made. Since the major cost items of the array were in the electronic system, any attempt at significant cost reduction required a less complex electronic system. For a given overall system gain this implies replacement of the individual 6 db dipole elements with higher gain types. It was further indicated that an array of 14 db to 20 db elements would yield a reduction of an order of magnitude in electronic system

complexity over the previous individual dipole system. Several typical high gain elements were considered but no decision was taken as to the final element design.

The approach was discussed at a Sunblazer coordinating committee meeting in Washington on 13 July 1967 and again in Cambridge on 23 August 1967. At the August meeting it was agreed; (1) that the installation of the 128 element 75 MHz pilot array at El Campo would continue and that dipoles would be used as the elements, and (2) that the 225 MHz array would be redesigned to achieve 25 db gain using an array of high gain elements. Subsequently work on the 75 MHz array was carried out as planned and work was begun on the 225 MHz array. A backfire configuration was selected and designed for the 225 MHz element; typical antenna patterns were taken and a complete set of electronic and mechanical hardware was prepared. However, this system was not installed or developed further because at this time new scientific results became available and dictated a change in the pulse frequencies and format as described below in Section 1.3.

1.3 Change to Closely Packed "Single" Frequency Experiment

About two years ago information became available from the Mariner 4 solar occultation experiment[3]. This experiment measured for the first time the frequency broadening which a coherent signal undergoes when transmitted on ray paths within four to six solar radii of the solar corona. When the 2200 MHz

Mariner 4 results were scaled to 75 MHz by theoretical methods justified by some recent work in our laboratory[4,5], they strongly suggested that the 25 millisecond pulse which we had earlier proposed for Sunblazer should be reduced to a pulse no longer than three milliseconds if coherent integration and coding within the pulse was to be employed.

If the Mariner 4 results are taken at face value they lead to the conclusion that two receiving antennas (one at 75 MHz and one at 225 MHz) of 50 db gain are required to completely carry out the Sunblazer experiment. Obviously it was impossible to proceed along these lines because of the much larger costs involved in constructing the required ground antenna.

Several possibilities were considered and discarded. Among these there are two—increasing the peak power and using a directional antenna on the spacecraft—which are impractical at present but may provide increased capability in the future.

Our solution, which solves the cost problem and does not compromise the science, was to simplify the experiment by using a separation between the probing and reference frequencies of some 10 percent such that both frequencies can be received within the bandwidth achievable in a single antenna array. In principle the accuracy of the delay experiment is slightly reduced but in practice this effect is not serious and does not compromise the experimental results. On the other hand, the elimination of the 225 MHz array represents a substantial saving in cost.

Based on the 3 ms pulse duration and constrained by the

maximum power output available from the transmitter, it can be shown[7] that the required receiving antenna gain is 50 db. This array provides a 16 db signal-to-noise ratio on the 3 msec pulse and results, we believe, in a better and simpler experiment.

There remained the question of the choice of the element for the 75 MHz array. Although the backfire configuration was satisfactory for the 225 MHz system, it possessed mechanical disadvantages at 75 MHz due to the relatively large (4 meter) wavelength. Based upon cost figures obtained from the construction of an in-house model and estimates obtained from outside vendors, it was determined that the cost per unit of gain of this antenna type was inordinately high ($400 for a 14 db element excluding mechanical steering costs). Our approach to this problem was to keep the element gain constant at 14 db while investigating other elements of equivalent gain.

As a result of this investigation, an element in which six dipoles are paralleled was proposed to replace the backfire. Basically it has been determined that a 14 db antenna element is less expensive and has better performance when constructed by connecting six fixed or mechanically steerable dipole elements together as opposed to employing single or multiple backfire or other slow wave type elements. The particular physical layout chosen for the six dipole element has lead to a natural choice of name for this element; we call it the "Twin Tee" or "Double Tee". (See Figure 2.2-1). A detailed description of the Double Tee element is given in Section 6.2. Most of the

remainder of this report consists of a system analysis and description of the proposed 50 db array using this six dipole interconnection.

1.4 Additional Advantages of the 50 db Broadband Array

A further benefit of the use of a 50 db ground terminal is the rather high bit rate (approximately 1 bit per second) which can be made available for the telemetry of data from on-board experiments over distances as great as 2 A.U. This is a matter of some considerable importance for on-board experimenters and to the future use of Sunblazer as an interplanetary observatory.

As a radio telescope the array also has important uses such as the observation of the newly discovered pulsars at a frequency somewhat below that on which they have thus far been observed. The high gain and directivity of this array at 75 MHz may well provide important new information and improved resolution of the signals from the sources observed thus far, and its greater sensitivity may lead to the discovery of other sources.

The modular nature of the array also makes it practicable to provide small solid state power amplifiers in the 250 to 1000 watt range on each element to convert the array into a radar telescope and to provide an up-link to future Sunblazer spacecraft. The power amplifiers required are essentially identical to those developed for the spacecraft and, while some design work is involved in adapting and packaging them for the ground array, their addition to the array is largely a matter of cost. That

is, the overall transmitter power could be somewhere between one and four megawatts, depending on the funds available and the interest in adding the transmitter facility. This was an item in the original proposal, but was eliminated at an early stage because of cost considerations. It is, however, a growth item which should be considered in future planning.

Solar radar echoes have never been observed at 75 MHz, and we believe the reason for this is that sufficient radar telescope sensitivity has never been available to counteract the additional absorption losses in the corona which occur along a ray path prior to the reflection point. The great advantage in making solar radar observations with this instrument would be an improved sensitivity and a greatly improved angular resolution, which would make it possible to resolve quadrants of the solar disk and improve the capability for observing average Doppler and Doppler broadening of the signals which contain important and otherwise unobtainable information on the motion of the solar corona at distances close to the photosphere.

As a planetary radar it would appear to be the first instrument that could detect reflections from the planet Jupiter and could make important observations on Venus and Mars at a much lower frequency than has heretofore been used. The rather surprising oscillation in radio cross section of the planet Venus which has been observed at 38 MHz[6] could be better studied with the additional sensitivity and the greater range of this new instrument.

1.5 References

1. Harrington, J. V.; Summary Report of Sunblazer Part I, Study of a Small Solar Probe—Radio Propagation Experiment, CSR-PR-5255-5, June 21, 1965.

2. Baker, R. H., et al.; Summary Report of Sunblazer Part II, Spacecraft and Payload Design, CSR-PR-5255-5, June 21, 1965.

3. Goldstein, R. M.; Jet Propulsion Laboratory Technical Report No. 32-1092 (1967).

4. Hollweg, J. V.; "A Statistical Ray Analysis of the Scattering of Radio Waves by an Anisotropically Turbulent, Non-Homogeneous Solar Corona", CSR-T-67-6, 1967.

5. Hollweg, J. V., and J. V. Harrington; "The Properties of Solar Wind Turbulence Deduced by Radio Astronomical Measurements", Journal of Geophysical Research, Vol. 73 pp 7221-7230, December 1, 1968.

6. James, J. V., R. P. Ingalls, and L. P. Rainville; "Radar Echoes from Venus at 38 Mc/sec." Astronomical Journal 72, #8 pp 1047-1050, 1967.

7. Baker, R. H., et al, "The Conceptual Design of a Small Solar Probe, Sunblazer", MIT/CSR-TR-69-1, 1969.

CHAPTER 2

2.0 DESCRIPTION OF THE DOUBLE TEE GROUND ARRAY SYSTEM

2.1 Function of the Ground Array

The array provides coupling between an incident radiation field, originating from the spacecraft, and earth station data processing equipment. Thus the array must interface with the on-board electronics system and the correlation receiver, both of which are briefly described in other sections of this document (Section 7.5). The antenna itself is characterized by its effective area or gain, frequency response, polarization, noise characteristics and tracking capability. The interrelationship of these quantities with the on-board electronics and the correlation receiver is given below. Section 2.2 of this paper presents a system analysis of the array while Section 2.3 is a detailed description of the Sunblazer array electronic organization and hardware.

2.1.1 Relationship to the Sunblazer Spacecraft

In order to be compatible with the Sunblazer communications system the antenna characteristics such as gain and noise figure must be maintained at the frequencies radiated by the on-board transmitter plus an allowance for modulation bandwidths

and dispersion due to Doppler, attenuation and plasma effects. Three specific frequency bands listed in Table 2.1.1-1 are of primary interest.

TABLE 2.1.1-1

Signal Frequency Bands

69.72 MHz ± 500 KHz
74.70 MHz ± 500 KHz
79.68 MHz ± 500 KHz

Since it is impractical to provide separate band tuning networks for each of the frequency bands, the array system is being designed to operate over the range 69.2 MHz to 80.2 MHz.

In addition to bandwidth considerations, the polarization of the transmitted signal from the spacecraft is of some importance. The on-board antenna is linearly polarized; but the radiating elements rotate at a mean angular velocity of about 1 rpm with respect to a fixed direction in the plane of the receiving array. Thus the polarization of the received energy varies with time. In addition, expected Faraday rotation effects will cause displacement of the received electric field vector. Therefore, to insure a maximum received signal and to estimate the effects of Faraday rotation the ground array must be capable of receiving orthogonally polarized waves.

For the remainder of this paper a dual cross polarized array is assumed unless explicitly stated otherwise.

2.1.2 Relationship to Receiver and Singal Processing Equipment

The array output is amplified, translated in frequency and then fed to signal processors and recorders. One processor, the correlation receiver, cross correlates the received signal with replicas of transmitted pulses. In order to attain the required accuracy in the propagation experiment, the signal-to-noise ratio of the video signal at the input to the correlation receiver must be maintained as high as possible. This implies the following array constraints.

1) The array gain must be maintained as high as practicable (50 db).
2) The system noise figure must be as low as feasible (less than 5 db).
3) Intermodulation and cross modulation products must be held to a minimum while system dynamic range must be high.
4) Losses prior to the first amplifier, i.e. mutual coupling, mismatch or attenuation must be held to a minimum.
5) Pattern grating lobes and side lobes must be held to a minimum.
6) The array gain must be known at all times.

More quantitative values are given in Section 2.2 and 2.3 for these system parameters. For the present it should be noted that every design compromise which reduces the array gain or increases its system noise contribution, reduces the quality of the experiment.

2.1.3 Cost vs Antenna Performance

The general requirement for the array design is to provide a tracking and receiving facility for the Sunblazer spacecraft. The nominal specifications are a 50 db system gain with a 5 db noise figure and a minimum viewing time of two hours per day. The above requirements are within the state of the art at VHF frequencies. The large effective aperture of the proposed array will make it unique compared to existing telescope antennas as discussed in Section 1.4.

In the proposed antenna design, the performance is limited by budgetary rather than technical restraints. Our objective has been the design of a large versatile tracking array maximizing the performance per unit cost. To this end we have made, in our judgment, realistic technical compromises between state-of-the-art performance and cost. This is especially true in the design of the dipole elements and time-delay networks.

2.2 The Gain Requirements

The power received, P_R, with an antenna having an effective

aperture, A_R, is:

$$P_R = P_T \frac{G_T}{4\pi R^2} A_R \eta\rho \qquad \text{(MKS units)} \qquad (2.2\text{-}1)$$

where P_T is the transmitted power from the spacecraft, G_T is the transmitting antenna gain in the direction of the earth, R is the distance from the spacecraft to earth, η is the transmission coefficient of the medium, which is probably near unity except when the signal path is near the sun, and ρ is the polarization misalignment factor.

On the basis of this equation and a desired S/N of 16 db, an array gain of 50 db is required. (See Appendix 7.5.3 and Reference 8 for details of calculation).

The beam width, which varies inversely as the aperture dimensions, is less than 0.6°. The exact array dimensions and beam characteristics are dependent on the latitude of the site selected for the final array. The system outlined in this paper will be suitable for a latitude of ±30°.

In considering the problem of synthesizing a phased array to satisfy the conflicting requirements of high gain, wide bandwidth and low noise, two concepts are of fundamental importance: (1) the superposition principle and (2) the pattern multiplication rule. The superposition principle requires that in the far field of an array of elements, the resulting field at a point is the vector sum of the fields

due to the individual elements. The pattern multiplication rule as applied to an array of identical elements states the resulting antenna pattern of an array is the product of the element pattern and a polynomial characteristic of the array. The ploynomial is commonly referred to as the array factor. In general terms the beam pattern function $E(\theta,\phi)$ may be expressed as a product of the form:

$$E(\theta,\phi) = E_e(\theta,\phi)A(\theta,\phi) \qquad (2.2\text{-}2)$$

where E_ϵ is element factor, and A is the array factor. When the array geometry is symmetric, Equation 2.2-2 may be used in this simplified form and permits a straightforward representation of the salient features of the array.

The pattern multiplication rule however, must be applied with caution since its use includes the implicit assumption that mutual coupling between elements may be neglected. The element pattern will, in general, change when it is brought to close proximity to other elements and the fact that all elements are physically identical does not insure that all elements of the array have the same pattern[1]. When the array elements are spaced "far enough" apart and are highly directive the superposition principle requires that the resultant array power gain is merely the product of the number of elements in the array and the gain per element. However, the array gain is a function of the element factor, the number of

elements, and the element spacing.[2,3]

To a first order approximation then, the gain of the proposed array is:

$$NG_E = 10^5 \qquad (2.2\text{-}3)$$

where N is the number of elements in the array and G_E is the power gain per element. If N is restricted to values of the form 2^q where q is an integer, the element gain is also specified. Table 2.2-1 gives the values of the total number of elements N as function of the gain per element.

TABLE 2.2-1

G_E (db)	N
23	512
20	1024
17	2048
14	4096
11	8192

The value N = 4096 and G_E = 14 db have been selected as a compromise between a very large number of elements and high gain per element. (In the final array N is made somewhat larger than 4096).

The characteristics of the 14 db element are of primary importance to the array design since they determine the general

level of complexity of the electronics system. A description of array electronics is given in Section 5.0.

A fundamental question is the physical realization of the 14 db element: "Of the many types of elements available in this frequency range, which element exhibits the desirable properties of low cost, wide bandwidth and high gain?" During the course of this program many antenna types were evaluated and each was found to have limitations. A detailed description of the evolution of the element design and selection is given in Section 1.2 of this report and in the document entitled "History and Design Summary, Sunblazer Phased Array", (Baker, Harrington, Higgins, James; September, 1968).[4]

In summary, a system parametric study was made for each of the element types including a cost evaluation of mechanical and electrical array components. These cost performance studies led to the following conclusion concerning the element:

> "The best method, in terms of satisfying the Sunblazer tracking requirements (both engineering and science) at minimum overall cost (initial installation, operation and maintenance) is to construct a cross polarized wideband dipole array at El Campo, Texas."[4]

Basically, it has been determined that a 14 db antenna element arrayed through electronic means is less expensive and has better performance when constructed by connection six dipole elements together as opposed to employing single or

multiple backfire, yagis or helices. A detailed description of the 14 db dipole element is given below. Figure 2.2-1 shows the physical layout of the 6 dipole (Double Tee) 14 db element. Details of the various costs are given in Appendix 7.4.

2.3 Functional Description of the Array

2.3.1 Realization of the Required Element Gain

A single half wavelength dipole in free space has a gain of 2.14 db above an isotropic radiator. When this same dipole is positioned a quarter of a wavelength above a perfect ground plane, its gain is increased by 5.34 db. Subject to the qualifications outlined in Section 2.2 (principally mutual coupling effects), the gain of an array of six dipoles above a ground plane is 7.78 db greater than the gain of a single dipole a quarter wavelength over a ground plane. The gain of the six dipole array has a maximum value of about 15.26 db over an isotropic radiator. If a one db allowance is made for losses and inefficiencies and for a non-perfect ground, the gain of a six dipole array will vary, as a function of scan angle, from 11 to 14 db.

The problem of realizing a 14 db element is centered not upon gain considerations, because a six dipole array appears to have adequate gain, but rather upon beam patterns considerations. Since a fundamental objective of the array is

NOTE:
CROSS DIPOLES 1 THROUGH 6 ARE
POSITIONED NS AND EW

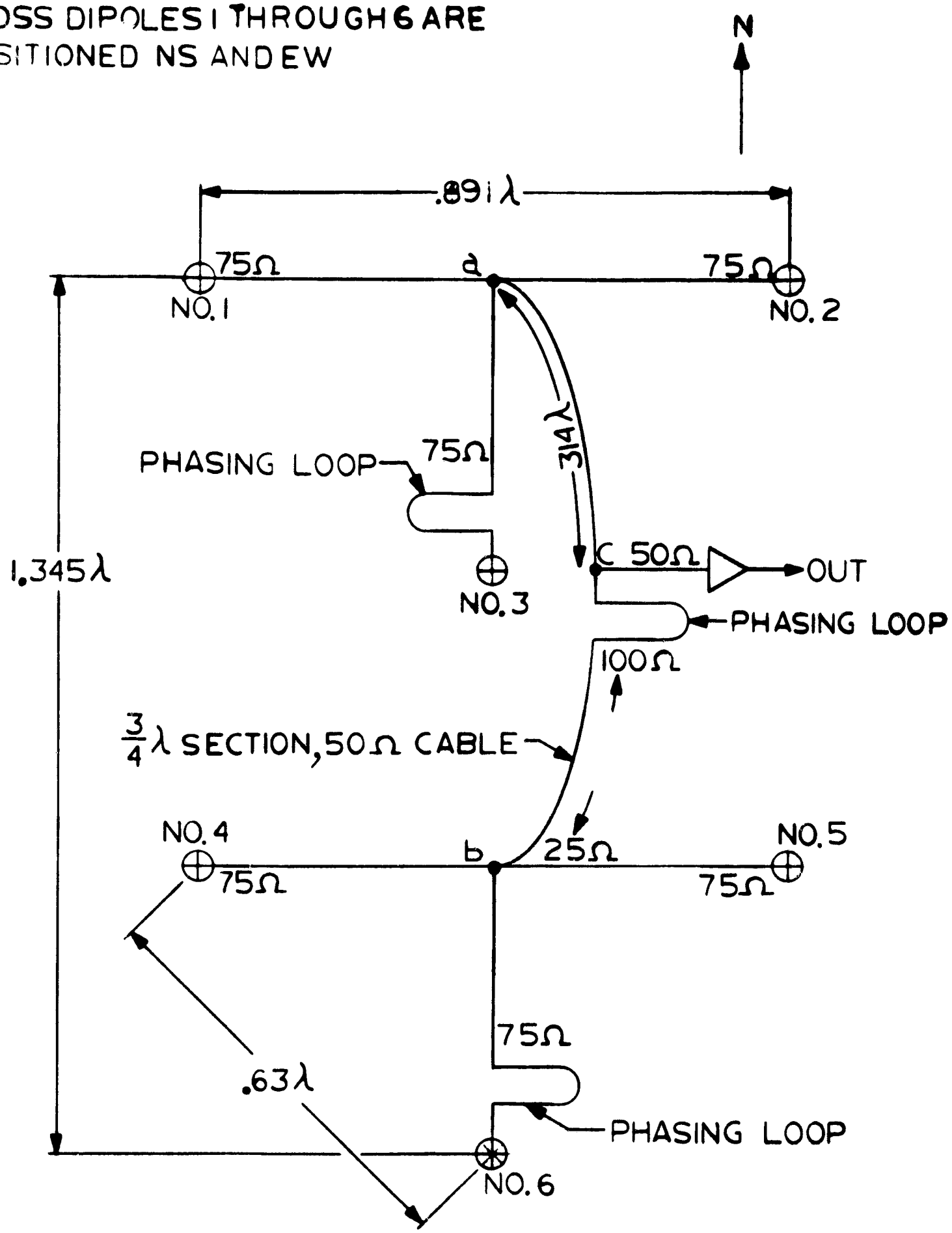

DOUBLE TEE LAYOUT
FIG. 2.2-1

two hours per day of view time, the element pattern, in the EW plane must have a total 3 db beamwidth in excess of 30°. On the other hand, the spacecraft does not have major day-to-day positional displacements that require a large element beamwidth in the NS plane. Therefore, the NS dimension of the element may be somewhat larger than the EW dimensions. The limiting factor for the NS extent of the element is related to the position of the grating lobes which have the net effect of reducing overall system gain and degrading system noise performance.

Figure 2.2-1 shows the physical layout of the Double Tee six dipole 14 db element. Impedance matching and interconnection with the electronic system is accomplished as follows: Each dipole has an output impedance of approximately 75 ohms. Separate cables of 75 ohm characteristic impedance are used to return the signals from the dipoles to point "a". At point "a" the 75 ohm cables are directly paralleled. Since the system is matched, the impedance at point "a" is 25 ohms. The signals from dipoles 4, 5, and 6 are combined in a similar way and returned to point "b". Phasing loops are included to provide element beam positioning. At both point "a" and point "b", 3/4 wavelength transformers of 50 ohm characteristic impedance are used to realize a 100 ohm input impedance at the respective transformer inputs. These two transformers are then paralleled at point "c" to yield an input impedance of 50 ohms. An advantage of this sub-array is that all interconnecting cables are standard RG types and

no cables of unusual characteristic impedance are required.

A major consideration is frequency response of the element which depends upon both the variation of the dipole impedance and the behvaior of the 3/4 wavelength transformer with frequency. Under idealized impedance conditions the 3/4 wavelength transformer adds about 0.04 db insertion loss to the system which corresponds to an input VSWR of 1.22:1. Field measurements of the complete element were taken and variation in input admittance was approximately ±10%. In this test, where phasing and mutual coupling effects are present, measurements showed that the mismatch corresponded to an insertion loss of .12 db and a VSWR of 1.4:1. These measurements also included the mismatch associated with dipole unbalance. From experience with the 38 MHz solar radar dipole array as well as the Sunblazer 75 MHz narrow band array, it has been determined that the feed cable may be connected directly to the dipole without the use of a balun. The individual dipole and cable connection is shown in detail in Figure 6.2.2-1.

Alternate element types have been evaluated. Details of these measurements are given in Section 7.7.

2.3.2 Manual Phasing

The combination of six dipoles in the Double-Tee configuration yields an essentially zenith looking element. It is comparable to a 14 db yagi and backfire which is mechanically fixed in the zenith looking position. A mechanically

fixed 14 db element would be unsatisfactory if it were not for the fact that the daily change in declination is small, thereby permitting the use of a manual phasing system at the element level. A more rapid element phasing system would be necessary for tracking earth orbiting satellites.

Manual phasing is accomplished by delaying the signal from dipole number three with respect to dipoles one and two and from dipole number six with respect to dipoles four and five. Since the distance between point "a" and dipole 3 is .445λ (.63λ × sin 45°) and the maximum declination of the sun at El Campo is 52°, then the maximum excess delay required in this cable is: .445λ sin 52° = .35λ. Assuming delay increments of λ/8; a two section time delay circuit composed of an λ/8 and λ/4 sections lengths (Figure 2.3.2-1) will provide the required range of delay variation. In a similar way the signals from points "a" and "b" are delayed. Here the maximum required delay is .7λ and therefore a three section circuit consisting of λ/8, λ/4, and λ/2 sections are used to provide the required delay variation.

The cable switching can be accomplished with mercury switches which exhibit excellent R.F. performance (insertion loss .04 db isolation 30 db) and are judged to be more reliable than connectors which must be plugged and unplugged. Based upon several years of site experience with the manually phased 1000 dipole 38 MHz El Campo solar radar, it has been estimated that the required phasing time is about .005 hours/switch which for a 40 db array amounts to about 8 man hours. Another

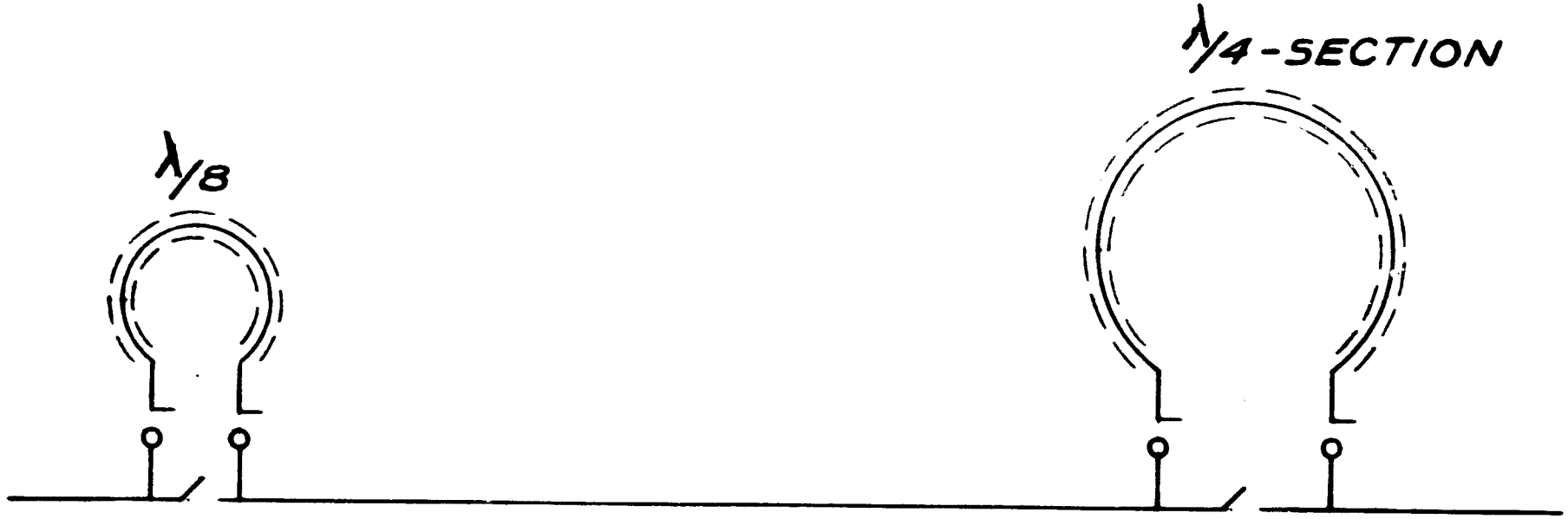

λ/8 AND λ/4 TIME DELAY

FIG. 2.3.2.-1

important advantage of this design is that this switching system may in the future be made fully automatic by replacing the manual switches with mercury relays.

2.3.3 Physical Layout of the Array

The physical layout of the final 50 db antenna is essentially specified by the spacing within the 14 db element. Although a uniform array of approximately 4000 -14 db elements is not required to satisfy the gain requirement and density tapers may be applied to the aperture; it is desirable to fill the aperture in a uniform way because the system is greatly simplified. However, the use of a uniform array does not preclude the addition of gain, phase or density tapers to the aperture at some later date.

The 50 db array is partitioned into sub-arrays (pilot arrays) of 192 elements each shown in Figure 2.3.3-1. The pilot array which is the basic building block of the 50 db system, consists of 8 columns of four 14 db elements. The phase centers of the elements in each column are colinear, but there is a displacement of .445λ between the phase centers of adjacent columns. Within a pilot array the individual dipoles are spaced at a distance of .63λ between the phase centers and the parallel distance between dipoles is .445λ (i.e. an echelon array of dipoles). Figure 2.3.3-2 shows the configuration of the proposed 50 db antenna which is composed of a 14 × 10 matrix of pilot arrays, a total of

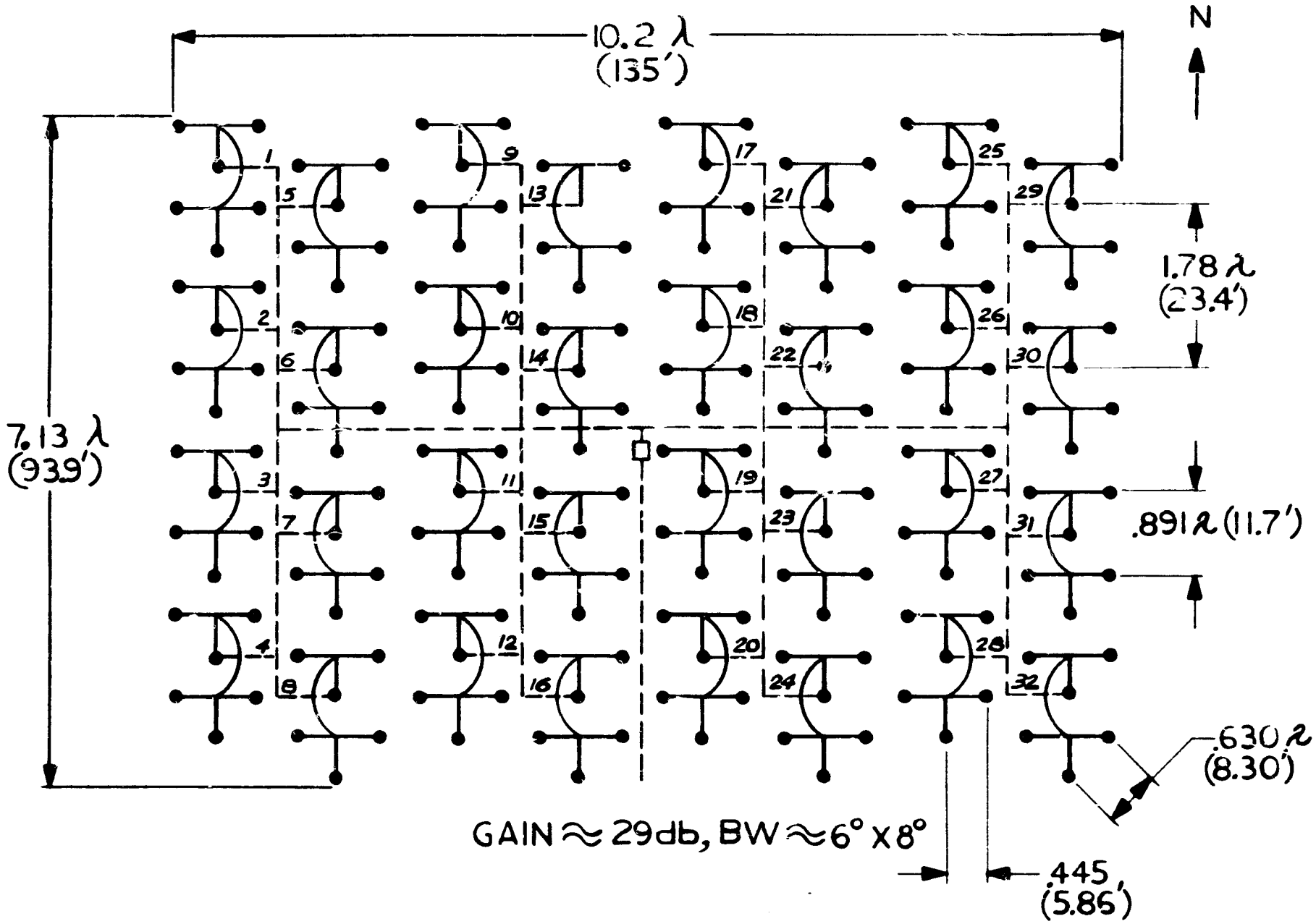

PILOT ARRAY PHYSICAL LAYOUT
FIGURE 2.3.3-1

NOTES:

EACH NUMERAL (1-32) CORRESPONDS TO THE OUTPUT POINT OF 1 DOUBLE TEE.

DIPOLES ARE POSITIONED NS AND EW.

ARRAY APERTURE 10.7λ BY 7.13λ (140' BY 93.9')

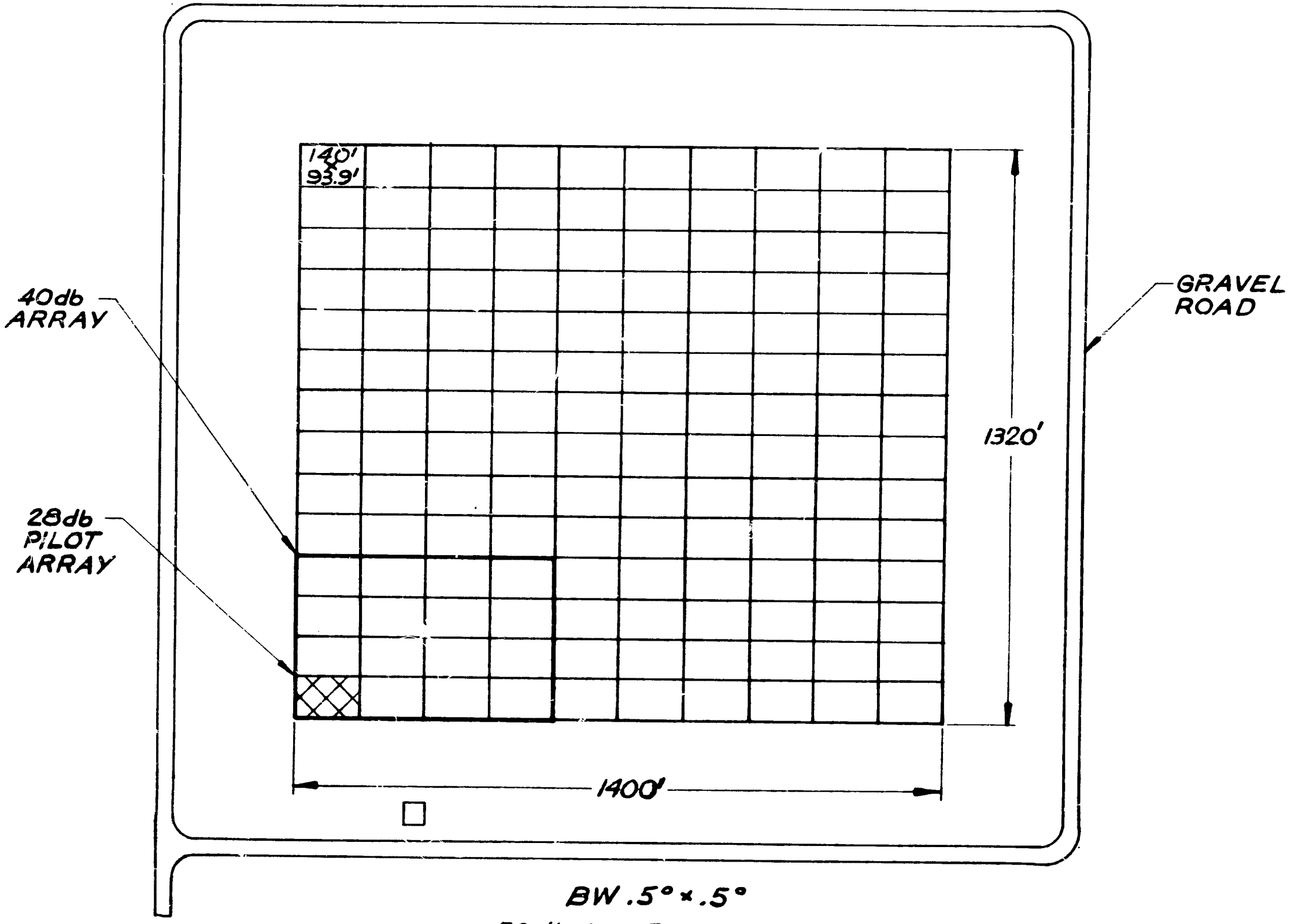

BW .5° x .5°
50db ANTENNA ARRAY
FIG. 2.3.3-2

26,880 crossed dipoled uniformly distributed across the 1400' EW by 1320' NS aperture. Alternate layouts are given in Figures 2.3.3-3 and 2.3.3-4.

It is proposed to build the 50 db array in three steps. The first step is to build one 192 dipole pilot array which will provide the experimental evidence to substantiate the design both in terms of performance and cost. Following the evaluation of the pilot system a larger expanded array, having a 40 db gain, which can be used for the Sunblazer engineering shot should be constructed.

The 50 db array can be realized by expansion of the 40 db system. The electronics, cable trench system and construction techniques are all identical in each of the 140 pilot arrays and therefore technical difficulties in expanding the 40 db system to 50 db should be minimized. In essence, the modular nature of the array, coupled with the orderly growth concept proposed, minimizes the risk in the development of the 50 db array. Table 2.3.3-1 gives a design summary of all three proposed arrays.

2.3.4 Electronic System

In general the philosophy of the array development consists of (1) designing the pilot array as a model of the final 50 db system and (2) making system compromises regarding electronics, R.F. cabling and mechanical hardware, etc. at the pilot level. Several different system organizations

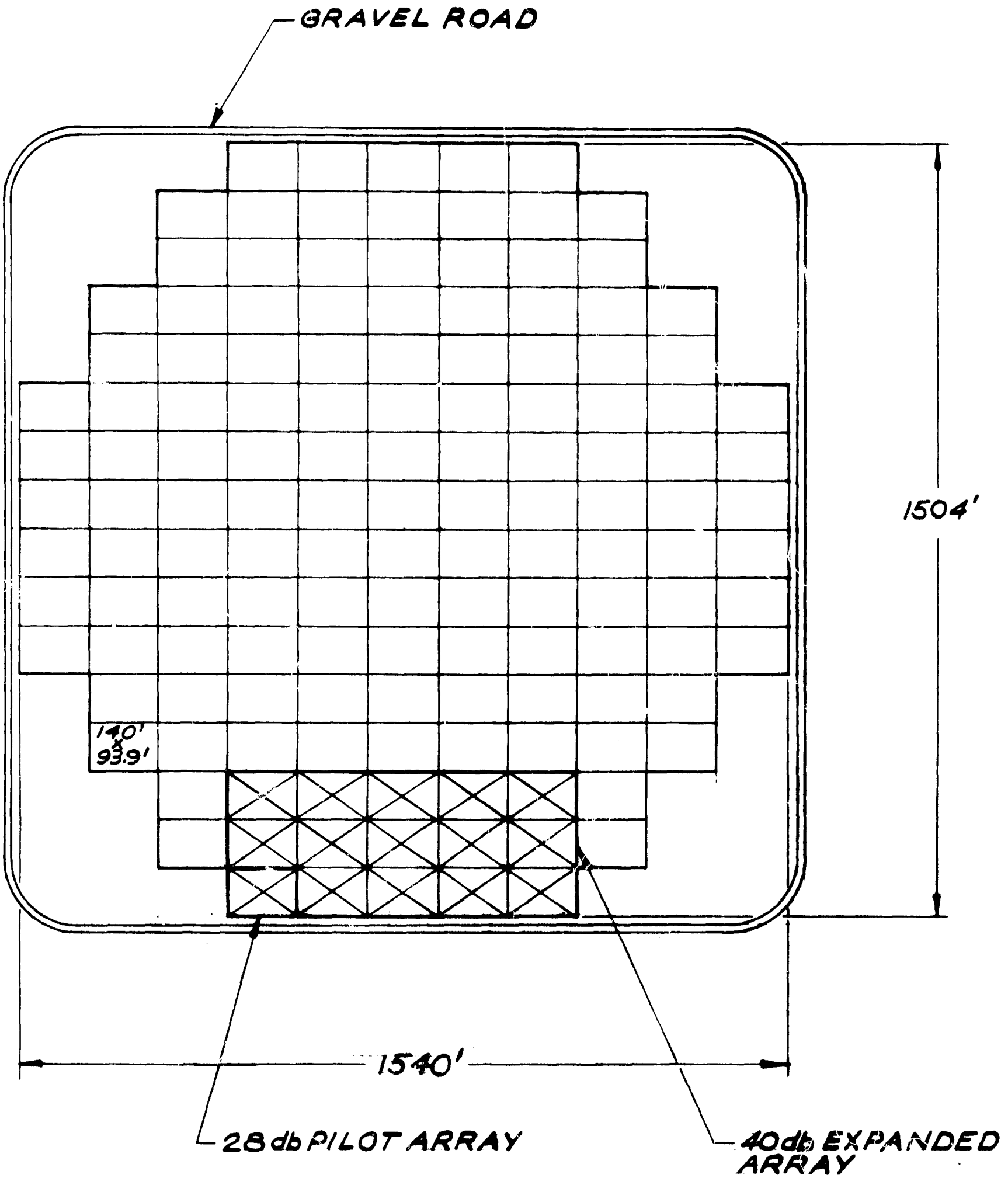

ALTERNATE 50db ARRAY LAYOUT
(15 PILOT EXPANDED ARRAY)
FIG. 2.3.3-3

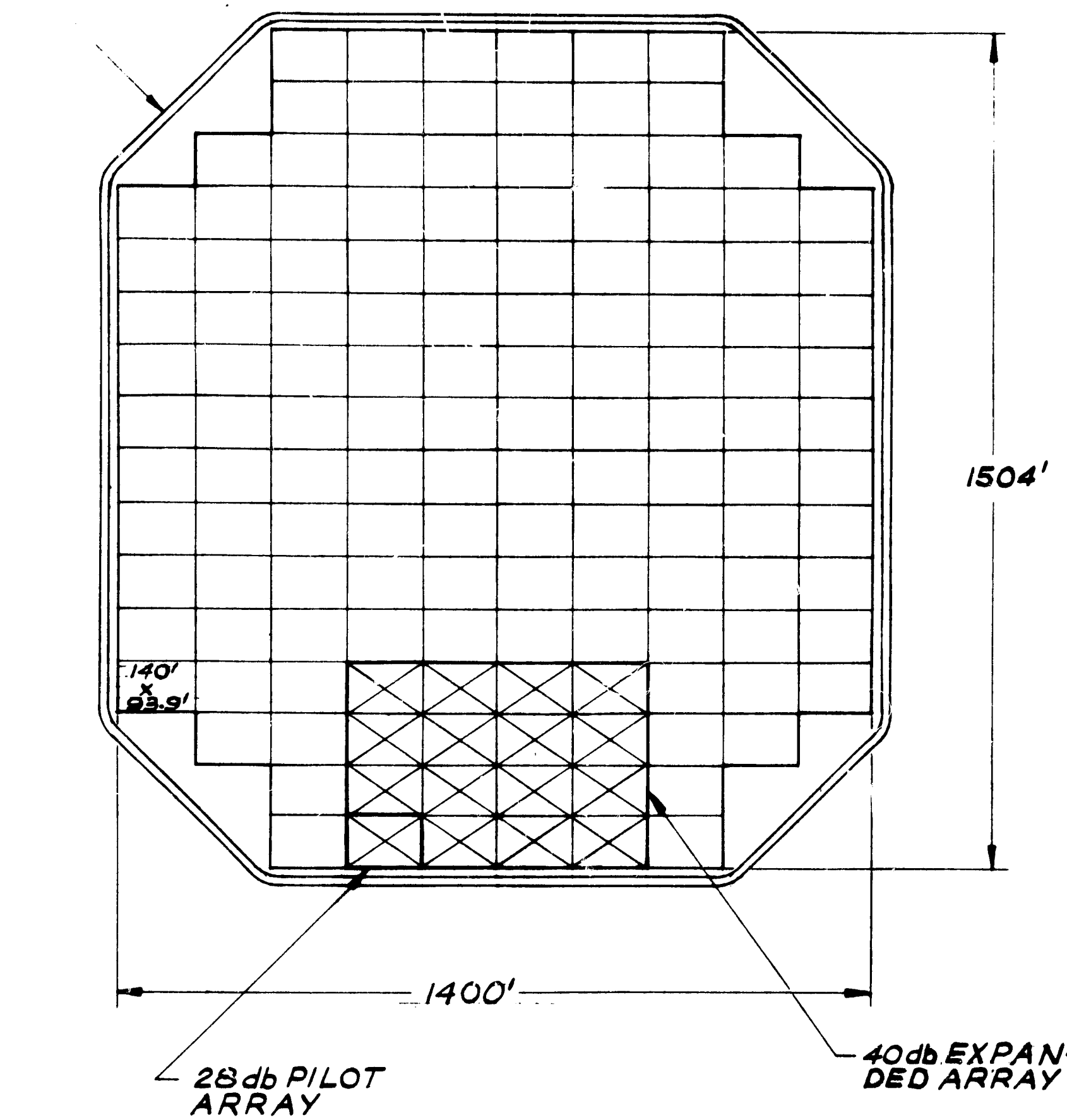

ALTERNATE 50db ARRAY LAYOUT
(16 PILOT EXPANDED ARRAY)

FIG. 2.3.3 -4

TABLE 2.3.3-1

Design Summaries

28 db Pilot Array

Operating Frequencies	69.72 MHz, 74.7 MHz, 79.68 MHz
Total Array Gain	28.8 db
Element Type	λ/2 dipole λ/4 above a ground plane
Realized Gain Per Dipole	6 db
Number of Dipoles	192
Dipole Grouping	6 per group in Double-Tee interconnection
Dipole Spacing	.63λ echelon
Array Aperture	10.7λ by 7.13λ (140' by 93.9')
Grating Lobes	None in Zenith pointing array.
Polarization	Two independent polarizations NS and EW
Beamwidth	6° × 8°
Phasing	Hybrid System: rapid electronic scan short-term tracking manual phasing using mercury switches for long-term (declination) scans.

40 db Array

Operating Frequencies	69.72 MHz, 74.7 MHz, 79.68 MHz
Total Array Gain	40.9 db
Gain per Dipole	6 db
Total Number Dipoles	3072
Dipole Grouping	Double-Tee
Dipole Spacing	.63λ
Array Area	42.8λ by 28.5λ (560' by 376')
Beamwidth	1.3° × 1.9°

50 db Array

Operating Frequencies	69.72 MHz, 74.7 MHz, 79.68 MHz
Total Array Gain	50.2 db
Gain Per Dipole	6 db
Total Number of Dipoles	26880
Dipole Grouping	Double Tee
Dipole Spacing	.63λ
Array Area	107λ by 99.9λ (1400' by 1320')
Beamwidth	.5° × .5° (Zenith)

have been considered; for example, the outputs of individual dipole elements could be returned to a central point in which all time delay and control equipment is located. On the other hand, it is possible to distribute the electronics evenly over the array aperture where the various combining and control functions are performed at many points in the field. The compromise solution proposed utilizes the more desirable features of the above extremes reducing both cable and enclosure costs while maintaining performance.

To present a detailed picture of the pilot array organization, it is helpful to start at the individual dipoles and follow the signal path to the pilot level output. The design concept is to provide for manual phasing in declination by means of mercury switches within the individual 14 db elements (see Section 5.1), and return the output of the 14 db element to a central enclosure where the phasing and control is accomplished electronically.

The pilot array layout is shown in Figure 2.3.3-1 and Figure 2.3.4-1 shows the block diagram of the electronic combining system. The amplifier signals from each of the 14 db elements are returned to the geometric center of the group of 192 dipoles where they are appropriately delayed, and combined. For example, the signal arriving from the 14 db element designated as point 1 in Figure 2.3.3-1 is first amplified in a low noise broadband amplifier and then supplied to network W. The signal from point 2, which is adjacent to point 1 in the first column is also amplified and

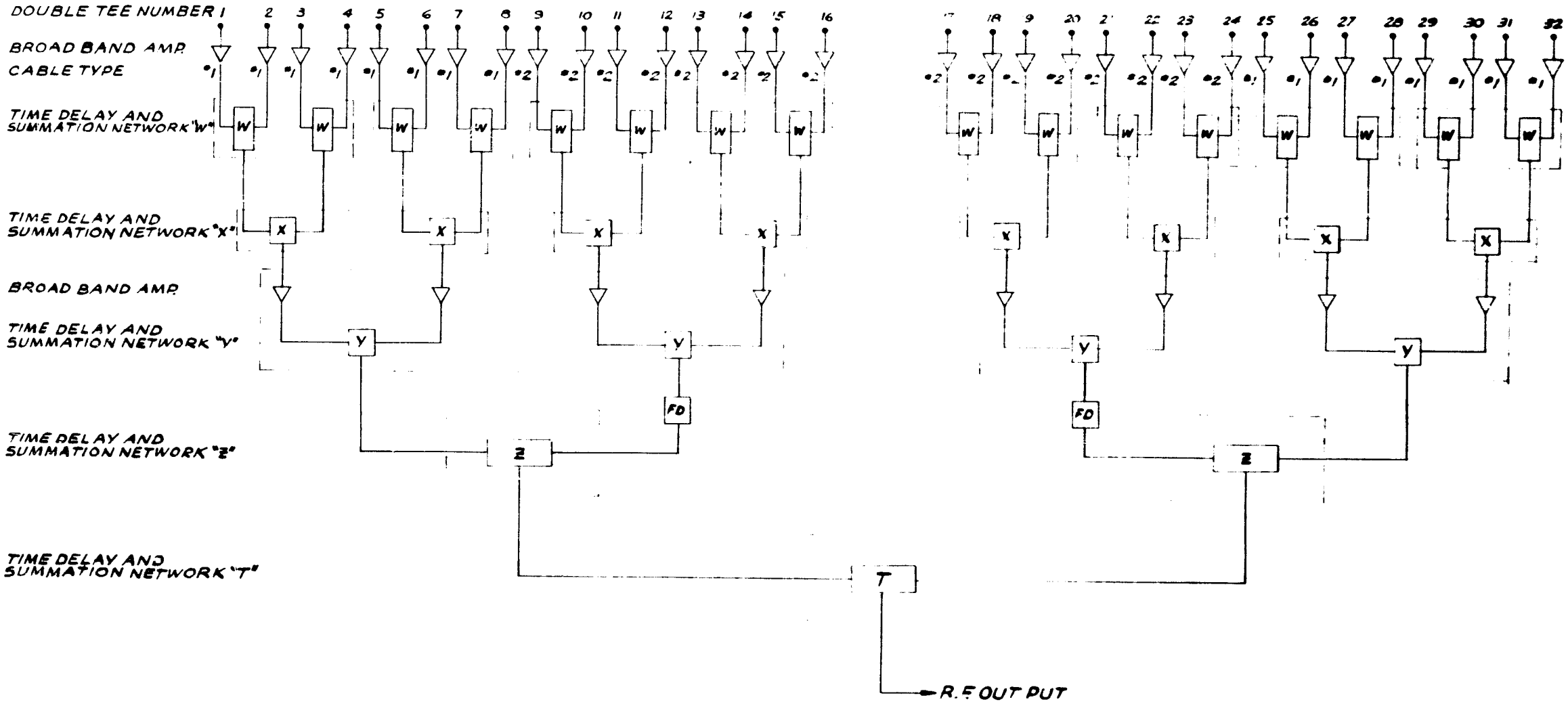

BLOCK DIAGRAM OF THE ELECTRONIC COMBINING SYSTEM FOR 192 DIPOLE PILOT ARRAY PER POLARIZATION

FIG 2.3.4 - 1

supplied to network W. In this circuit these signals are delayed an amount, dependent upon the desired array look angle, and then summed coherently. A second level of combining is performed by network X which delays and sums the output from two adjacent " " networks. The output of network X is a complete column output of the pilot array. There are eight such column outputs in the array. These outputs are delayed and combined in a way similar to the above by the operation networks Y, Z, and T. The R.F. output of network T represents the sum of all 192 dipoles. All of the combining networks are of the same general design and there are only two basic types of R.F. circuits used in the combining system; (1) a broadband amplifier and (2) a time delay-summation network.

There is one amplifier at each 14 db element and it is basically the "receiver front end". However, it is also used at other levels in the system as a linear amplifier to make up for the insertion loss of the various time delay and signal combining networks.

In the amplifier design the principal problem is reproducibility, since variations between units in gain, phase, impedance match and linearity will have a deteriorating affect on the resultant system R.F. output. To solve the problem of system alignment the amplifier circuit is designed to permit amplitude and phase adjustment.

Noise figure is another important design consideration. An overall system noise figure of 5 db implies a front end noise figure of 3 db which in turn requires that the transistor

used in the front end has a noise figure of somewhat less than 3 db. Fortunately the gain required in the front is relatively low, permitting a design for minimum noise rather than for maximum gain. This low gain requirement yields a more stable circuit and is a factor that simplifies the amplifier design.

The amplifier frequency response and linearity are also important considerations. Because it is impractical in a low cost, high volume production design, to provide independent R.F. passbands for each of the design frequencies, the amplifier must be designed to have a 3 db bandwidth from 60 MHz to 90 MHz. This frequency band is a region of high RFI interference due to local TV and other commercial services. Therefore, amplifier linearity, i.e. dynamic range, cross modulation and inter-modulation, is of prime importance because the affects of non-linearities cannot be eliminated by filtering at later stages in the system. Details of the amplifier design are given in Section 5.2.

2.4 Planar Array Pattern Description

2.4.1 General

The ground array is analyzed as a doubly-periodic rectangular structure which gives the array pattern a simple description in terms of a doubly-periodic function of x and y, or direction cosines in the horizontal plane. The basic

unit in the array is taken to be the Double-Twin-Tee, which is necessarily the smallest unit because of the North-South staggering of columns in the array. The array pattern naturally has a sequence of peaks, grating lobes, at doubly-periodic locations in the x-y plane, with spacing given by the reciprocals of the dimensions between units in the N-S and E-W directions. Based on the spacings between Double-Twin-Tees, there are about 15 grating lobes in the visible space at any time, although for scans within about ± one-half hour from local noon and about ± 15° in declination from manual set point, the grating lobes are better than 10 db below the main lobe. Scan points out to about ± one hour are possible before some grating lobes are bigger than the main lobe.

This analysis is done primarily for the large or nominal 50 db rectangular array. Some patterns are shown as functions of x and y (cosines): (1) for scan points on the meridian at different declinations and (2) for scan points at constant declination, varying time. In addition, directivity of the large array is calculated using a grating-lobe summation to approximate the scattering loss. This directivity is plotted for scans varying in time and also for scan points varying in x and y giving contours of constant directivity. The gain of the array will be less than the directivity shown, because (1) this analysis neglects ohmic loss in the array and (2) also neglects reflection loss due to variation of active impedance caused by mutual coupling in the array.

In order to make this analysis, mutual coupling between elements is neglected. This enables one to consider the elements as independent and to neglect edge effects in the array.

One feature of the array which is being investigated is its noise performance. This is a very complicated problem because noise reception depends on the location of the sun and of galactic noise sources relative to the spacecraft, all of which vary with time of year and time of day. However, there is promise that this problem can be solved in practice because of three proposed features of the array: (1) the overall periodicity and rectangular structure of the array, (2) the use of parallel or independent phasing of rows and columns of the array and (3) the use of a digital computer to select patterns minimizing noise reception.

For the purpose of a logical derivation of the array pattern and performance, the remaining material is arranged as follows:

2.4.1.1 Pattern Properties

2.4.1.2 Assumptions about Array

2.4.2 Grating Lobe Structure

2.4.3 Side Lobe Structure

2.5 Planar Array Performance Characteristics

2.5.1 Gain and Beamwidth

2.5.2 Gain vs. Time and Declination

2.5.3 Noise and Side Lobes (& Grating Lobes)

2.4.1.1 Pattern Properties

The important pattern properties are as follows:

1) Beamwidth of the array. The beamwidth of the main beam is inversely related to the gain of the array. The main beam is really the main grating lobe. The detailed pattern near the main beam is revealed by a calculation of the side lobe structure (Section 2.4.3). The size of the main beam is roughly inversely proportional to the overall area of the array but a detailed description of the shape of the main beam will have to wait until the patterns have been derived and analyzed (Sections 2.4.3, 2.5.1).

2) Grating lobe structure of large (50 db) ground array. The grating lobes contribute to scattering loss (reducing gain) and to noise reception (from radio sources). When the location and intensity of the grating lobes are known it is possible to calculate the approximate directive gain of the array and the approximate galactic and solar noise contribution for any given scan angles and for a known celestial noise density. These calcuations can be made either in terms of pure coordinates (scan directions) giving 2-dimensional or contour plots, or as a function of time (on a rotating earth) with declination of celestial source as a

parameter (this is tracking information). The grating lobe structure, which is mainly determined by the nature of the smallest unit in the array (the Twin-Tee) and of how it is repeated in space, is analyzed in Section 2.4.2 below.

3) Side lobe structure, superimposed on the grating lobe structure. Here the side lobes are the details which fill the pattern between the grating lobes. The side lobes can contribute to noise (from a strong radio source) but are typically too small to detract appreciably from the gain. This problem is related to the overall organization and quantization errors of the array and is treated in Section 2.4.3 below.

2.4.1.2 Array Assumptions

In order to make a pattern analysis, certain assumptions are made:

1) No mutual coupling between elements. This enables one to consider the elements as independent and to neglect edge effects in the array. In addition, this analysis neglects mismatch loss due to variation of active impedance with scan angle. (See Section 2.8 for an analysis of mutual coupling effects)
2) The 50 db ground array is considered as a large, uniform (periodic) array. This assumption enables one to represent the pattern by its grating lobes

(and the strongest side lobes are on lines connecting the grating lobes) and to use a grating lobe series to determine the scattering loss (which reduces the gain). Most of the discussion in this Section 2.4 and the following (Section 2.5) is primarily relevant to the large (50 db) array, which justifies the approximations mentioned.

2.4.2 Grating Lobe Structure

2.4.2.1 Coordinate Systems

Here the general separation of pattern into grating lobe pattern and side lobe pattern will be made, so that the grating lobe pattern can be analyzed here, and the side lobe pattern in Section 2.4.3. First an illustration of the geometrical layout of a section of the array and an illustration of the fundamental coordinates, direction cosines, are shown in Figures 2.4.2.1-1 and 2.4.2.1-2 below. The direction cosines, x, y, and z, are related to the azimuth and zenith angles, ϕ and θ:

$$x = \sin\theta \sin\phi \qquad (2.4.2.1\text{-}1)$$

$$y = \sin\theta \cos\phi \qquad (2.4.2.1\text{-}2)$$

$$z = \cos\theta \qquad (2.4.2.1\text{-}3)$$

The x-, y-, and z-cosines are not to be confused with spacial

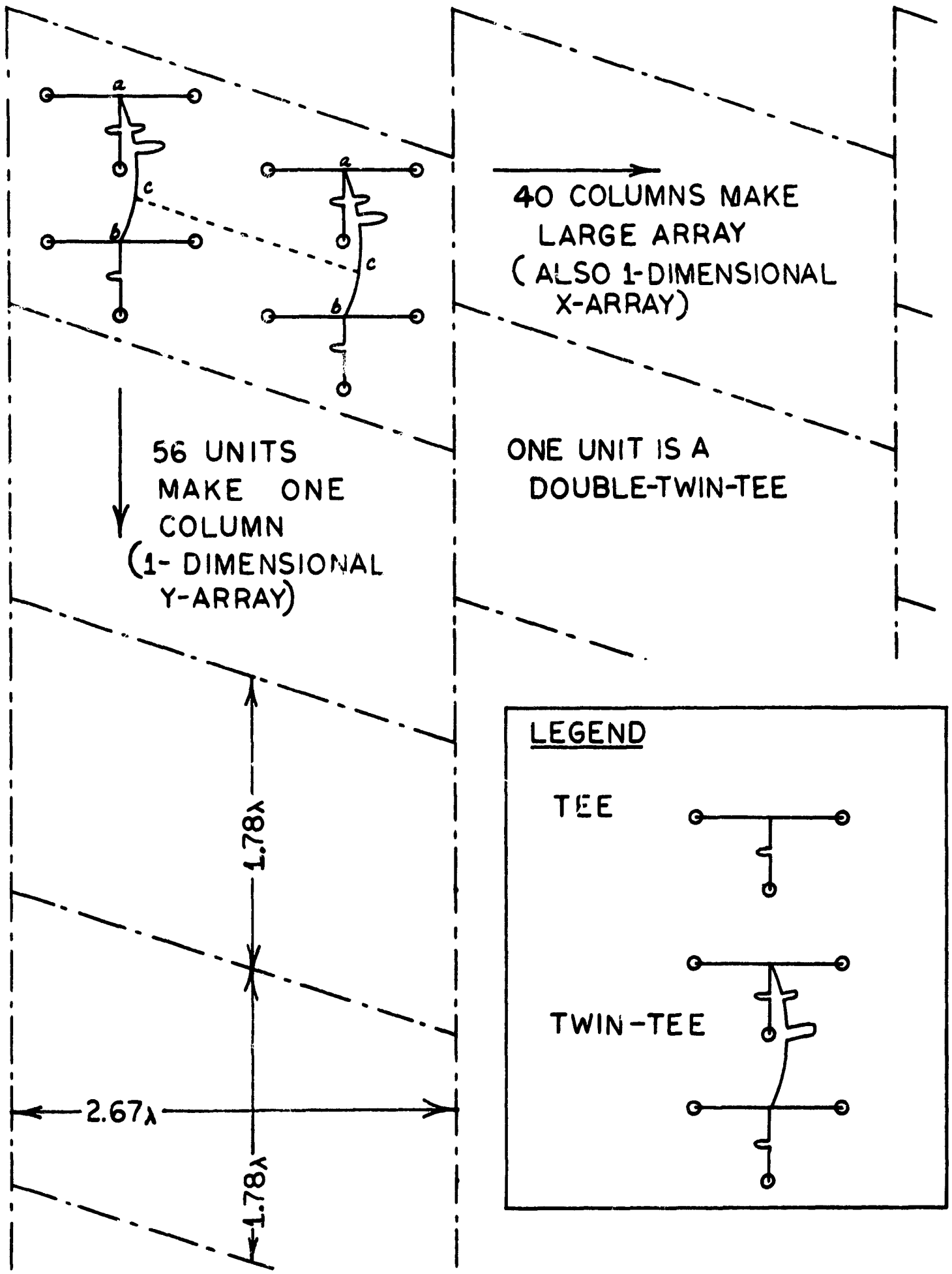

Figure 2.4.2.1-1 (a) Array Geometry

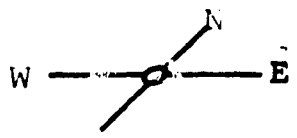

$$[\text{dipole pattern}] = \begin{cases} 1-x^2, & \text{EW dipole} \\ 1-y^2, & \text{NS dipole} \\ 1, & \text{istropic element} \end{cases}$$

Hertzian dipoles

ideal elements aligned North-South or East-West

Figure 2.4.2.1-1(b) Element Pattern

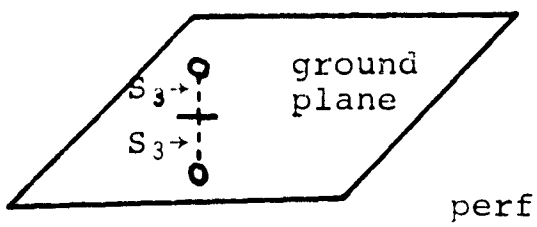

$$[\text{z-array factor}] = \sin(\pi 2 S_3 Z)$$

perfect ground plane, reflected image of element

Figure 2.4.2.21-1(c) Element above Ground Plane

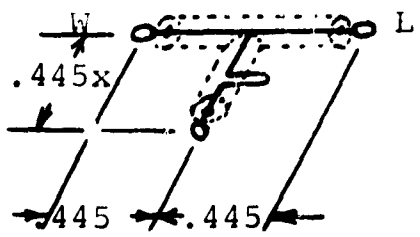

$$[\text{single-tee pattern}] = \sum_{m=1}^{3} e^{i(\vec{K}\cdot\vec{r}_m - \phi_m)}/3$$

$$[\text{single-tee pattern}] = [1+2e^{i2\pi.445(y-y_1)}\cos(2\pi.445x]/3.$$

no phasing East-West within Tee
one manual phasing loop North-South giving $\phi_1 = 2\pi.445y,/3.$

Figure 2.4.2.1-1 (d) Single-Tee Pattern -- manually phased

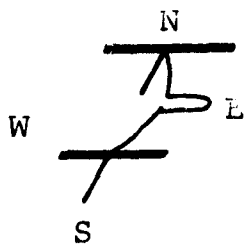

$$[\text{TT-array factor}] = \cos 2\pi.445(y-y_\star)$$

phase shift between two Tees is $\phi = 2\pi.445y_\star$ (radians)
$y_\star$ adjusted manually to approximate a desired y-value

Figure 2.4.2.1-1 (e) Twin-Tee Array - manually phased

$$\vec{r}=.445(3,-1,0)$$

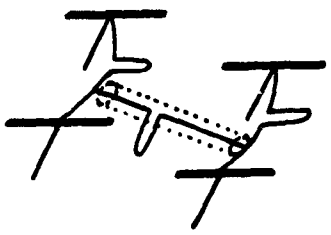

$$[\text{double-TT-array factor}] = \cos(\pi.445(\vec{K}\cdot\vec{r}-\vec{K}_0\cdot\vec{r}))$$

phase shift between staggered TT's = $\pi.445(\vec{K}_0\cdot\vec{r})$
$\vec{K}_0\cdot\vec{r}$ $\vec{K}\cdot\vec{r}$ within $\lambda/16$ (nearest quantization of delay line)

Figure 2.4.2.1-1 Double Twin-Tee Array - electrically phased

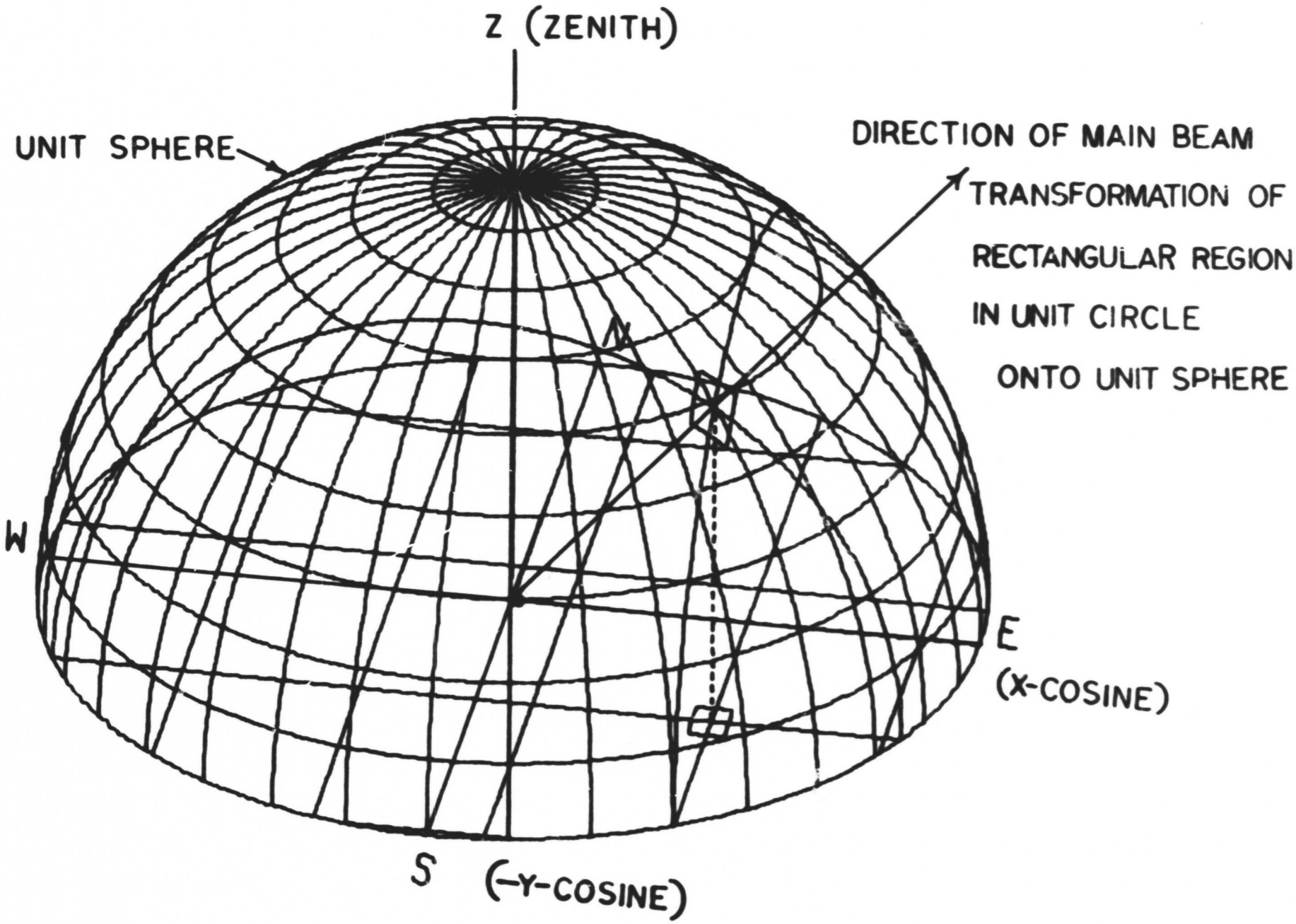

Figure 2.4.2.1-2 Direction Cosines

coordinates, as the cosines represent a direction in space; consequently, the length of the vector (x,y,z) is normalized to unity. The two cosines, x and y, are projections of the direction vector in the easterly and northerly directions, respectively, and are sufficient to represent any direction above the horizon, as:

$$z = \sqrt{1 - x^2 - y^2} \qquad (2.4.2.1\text{-}4)$$

In the following analysis, directions will be represented by their projections, x and y, within the unit circle, although a more familiar representation would be by points on the unit sphere, as in Figure 2.4.2.1-2.

2.4.2.2 Case of Exact Phasing

In Figure 2.4.2.1-1, the Double-Twin-Tee (staggered pair) is the smallest geometrical unit which can be repeated periodically to fill the entire array. If the phasing and currents within each Double-Twin-Tee are the same and if the phasing from each Double-Twin-Tee to each other is exact*, then the array of Double-Twin-Tees will be doubly-periodic electrically

---

*This exactness will result from quantizing the allowed scan directions as mentioned in Section 2.4.3.3, resulting in exactness at some of the points needed to cover the visible space, and approximate exactness at all other points.

and geometrically, with 40 units EW and 56 units NS in the 50 db ground array. In this case, the overall pattern can be represented as the product of the pattern for the Double-Twin-Tee multiplied by a (periodic) array factor, giving:

$$E(x,y) = [\text{x-array factor}] \cdot [\text{y-array factor}] \cdot [\text{Double-Twin-Tee pattern}] \qquad (2.4.2.2\text{-}1)$$

where

$$[\text{x-array factor}] = \frac{1}{40} \frac{\sin 40\pi\ 2.67(x - x_o)}{\sin \pi\ 2.67(x - x_o)} \qquad (2.4.2.2\text{-}2)$$

$$[\text{y-array factor}] = \frac{1}{56} \frac{\sin 56\pi\ 1.78(y - y_o)}{\sin \pi\ 1.78(y - y_o)} \qquad (2.4.2.2\text{-}3)$$

$$(x_o, y_o) = \text{scan point} \qquad (2.4.2.2\text{-}4)$$

$$2.67\lambda = \text{period in x-direction} \qquad (2.4.2.2\text{-}5)$$

$$1.78\lambda = \text{period in y-direction} \qquad (2.4.2.2\text{-}6)$$

The [x-array factor] and the [y-array factor] produce a series of peaks, grating lobes, at doubly periodic locations in the x-y plane, displaced from the main lobe by multiples of the respective x and y periods:

$$\Delta x = 1/2.67 \approx .3745 \qquad (2.4.2.2\text{-}7)$$

$$\Delta y = 1/1.78 \approx .5618 \qquad (2.4.2.2\text{-}8)$$

In the case of exact phasing, a grating lobe* can be defined as a part of the array pattern in a rectangular domain between two consecutive nulls in the [x-array factor], between two consecutive nulls in the [y-array factor], and containing a point where the denominators in the [x-array factor] both go to zero, producing what will ordinarily be a single relative maximum within the domain. Ordinarily the magnitude of the grating lobe will be larger than the magnitude of neighboring side lobes, arising from other peaks in the [x-array factor] and [y-array factor]. Although the detailed pattern will be of interest in Sections 2.4.2.4, 2.4.3, and 2.5.3 concerning noise and side lobes and in Section 2.5.1 concerning the main beam, this derivation will first consider the overall pattern in the entire unit circle, as the overall pattern is strongly

---

*The grating lobes are simply caused by periodicities in the array, such that a wave is at the same phase (mod 2π) at all the units in the array. The overall array can be considered as a conjunction of two one-dimensional arrays: a one-dimensional array of 56 units in the y-direction, making one column, and a one-dimensional array of 40 columns in the x-direction, for which the [x-array factor] is equal to magnitude to:

$$\left| \frac{1}{40} \sum_{k=1}^{40} e^{i2\pi s(x-x_o)} \right| = \left| \frac{\sin 40\pi s(x - x_o)}{40 \sin \pi s(x - x_o)} \right| \qquad (2.4.2.2\text{-}9)$$

where s = spacing = 2.67 wavelengths. The [y-array factor] is similarly represented by Equation (2.4.2.2-3).

related to the periodic grid of lines, parallel to x,y axis intersecting in the grating lobes.

Based on the periods $\Delta x, \Delta y$ given by Equations 2.4.2.2-7 and 2.4.2.2-8, there are about 15 grating lobes in the unit circle at any time, although it should be noted that for scan points close to the manually-adjusted peak of the Twin-Tee pattern, as shown in Figure 2.4.2.5-1 and derived in Sections 2.4.2.5 and 2.4.2.6, all of the grating lobes except the main lobe will be reduced by the [Double-Twin-Tee pattern]. In addition, for a small set of "exact phasing points" [which are a subset of the points mentioned in Section 2.4.3.3(1)] when the electrical and the manual phasings are exact, then all of the grating lobes except the main lobe and possibly a diagonal lobe are identically cancelled.

In order to facilitate a visualization of the overall pattern, the high frequency variation of the [x-array factor] and the [y-array factor], as evidenced in their numerators, will be eliminated, as the factors will be replaced by approximate envelopes or upper limits in the following Section 2.4.2.3.

2.4.2.3 Envelope of Array Factors for Exact Phasing

The region between the grating lobes is filled by a number of side lobes, as shown for example in the numerators of the [x-array factor] and the [y-array factor] for exact phasing. To remove the high-frequency oscillation in the

[x-array factor] and the [y-array factor], each of their numerators will be replaced by unity, except near a grating lobe where the envelope will be chopped to unity, which is the maximum value of the array factors. These relatively simple modifications to Equation 2.4.2.2-2 and 2.4.2.2-3 result in:

$$[\text{x-envelope}] = \begin{cases} 1 \quad , & |x-x_o| \leq \varepsilon_1 \pmod{1.} \\ 1 \quad , & |x-x_o| \geq 1 - \varepsilon_1 \pmod{1.} \\ \dfrac{1}{40 \sin \pi 2.67|x-x_o|} \quad , & \text{otherwise} \end{cases} \qquad (2.4.2.3\text{-}1)$$

$$\varepsilon_1 = \frac{1}{\pi 2.67} \sin^{-1}\left(\frac{1}{40}\right) \qquad (2.4.2.3\text{-}2)$$

$$[\text{y-envelope}] = \begin{cases} 1 \quad , & |y-y_o| \leq \varepsilon_2 \pmod{1.} \\ 1 \quad , & |y-y_o| \geq 1 - \varepsilon_2 \pmod{1.} \\ \dfrac{1}{56 \sin \pi 1.78|y-y_o|} \quad , & \text{otherwise} \end{cases} \qquad (2.4.2.3\text{-}3)$$

$$\varepsilon_2 = \frac{1}{\pi 1.78} \sin^{-1}\left(\frac{1}{56}\right) \qquad (2.4.2.3\text{-}4)$$

The [Double-Twin-Tee pattern], the [x-envelope] and the [y-envelope], are slowly varying functions of x and y; the product of all these gives an overall nominal envelope pattern which will be used to show the overall structure of the pattern in the unit circle:

[nominal envelope pattern] =

[Double-Twin-Tee pattern] · [x-envelope] · [y-envelope]

(2.4.2.3-5)

This simplification of Equation 2.4.2.2-1 is used to show the overall features of the pattern, to be discussed in Sections 2.4.2.5 and 2.4.2.6.

2.4.2.4 Side Lobe Pattern Separation

The high-frequency oscillating parts of the [x-array factor] produce what will be called the side lobe pattern. In the more general case when the phasing between Double-Twin-Tees is not exact, the [x-array factor] and the [y-array factor] are replaced by sums of the form:

$$[\text{x-array summation}] = \sum_{m=1}^{40} e^{i2\pi 2.67(mx-\phi_m)} \qquad (2.4.2.4\text{-}1)$$

$$[\text{y-array sumation}] = \sum_{n=1}^{56} e^{i2\pi 1.78(ny-\phi_n)} \qquad (2.4.2.4\text{-}2)$$

where the $\{\phi_m\}$ and $\{\phi_n\}$ are quantized phases, adjusted to produce a desired side lobe pattern, as treated in Section 2.4.3 below. Investigation of these sums shows that their side lobe patterns are quite similar to the corresponding array factors, because they all have (1) periodic grating lobes of approximately the same shape and period as in the nominal case and (2) side lobes which die off more or less (depending on how the array is organized) like the nominal envelope. Therefore, for all scan directions, the overall behavior of the pattern will be represented by the nominal envelope pattern, and the separate problem of the details of the side lobe pattern will be treated in Section 2.4.3, 2.5.1 and 2.5.3.

2.4.2.5 Double-Twin-Tee Pattern

The [x-envelope] and the [y-envelope] are respectively periodic in x and y (as is the side lobe pattern, treated in Section 2.4.3). The peaks in the [x-envelope] and the [y-envelope] are of unit magnitude and are periodic with the respective periods $\Delta x \approx .3745$, $\Delta y \approx .5618$. Since there are about 15 peaks (grating lobes) in the visible space (unit circle) at any time, it is essential that all of the peaks

except the main peak (main lobe) should be reduced to a low magnitude by the [Double-Twin-Tee pattern]. Fortunately, there is a large region in the unit circle where the desired scan point does produce the greatest peak, as shown in Figure 2.4.2.5-1 below. The allowed scan region, as shown, is only restricted by east-west lack of phasing and by an uncompensated diagonal lobe. There should also be a daily restriction of y-phasing; so the net daily scan region would be roughly a rectangle, or a rectangle less a part of two circular areas.

Reference to geometrical layout of the Double-Twin-Tee reveals that the [Double-Twin-Tee pattern] is composed of several factors, which are defined below:

[Double-Twin-Tee pattern] =

[dipole pattern]·[z-array factor]·[single tee pattern]·

[TT-array factor]·[Double-TT-array factor]

(2.4.2.5-1)

In the coordinates chosen (x and y direction cosines), the pattern of the Hertzian dipole (proportional to cosine squared (θ), θ = angle between the dipole axis and the direction vector), is normalized to:

$$[\text{dipole pattern}] = \begin{cases} 1 & x^2, \text{ east-west dipole} \\ 1 - y^2, & \text{north-south dipole} \end{cases} \qquad (2.4.2.5\text{-}2)$$

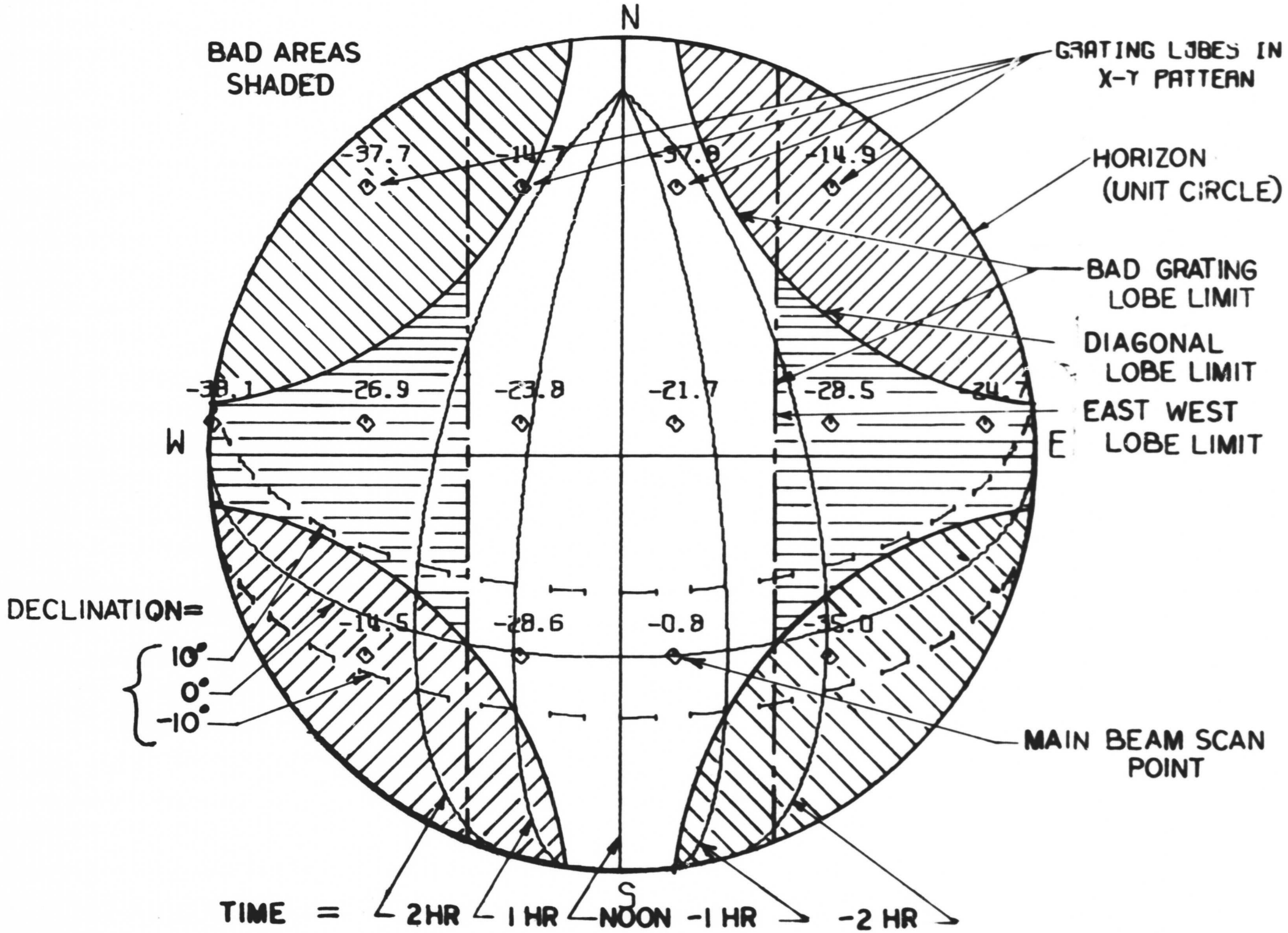

Figure 2.4.2.5-1 Unit Circle Plot of Scan Regions

The [z-array factor] arises from the reflected image of a dipole below a ground-plane:

$$[\text{z-array factor}] = \sin(\pi 2 S_3 z) \qquad (2.4.2.5\text{-}3)$$

$$S_3 = \text{dipole-ground spacing (wavelength)} = .25 \qquad (2.4.2.5\text{-}4)$$

The [single tee pattern] is formed as an exponential sum of terms from 3 point sources in the tee:

$$[\text{single tee pattern}] = [1 + 2e^{i2\pi.445(y-y_1)} \cos(2\pi.445x)]/3 \qquad (2.4.2.4\text{-}5)$$

where y_1 is fixed by a mechanical phase-shifter (quantized to $\lambda/8$). The [TT array factor] comes from the juxtaposition of two tees on the north-south line to form a Twin-Tee:

$$[\text{TT-array factor}] = \cos[2\pi.445(y-y_*)] \qquad (2.4.2.5\text{-}6)$$

where y_* is also fixed by a mechanical phase-shifter (quantized to $\lambda/8$).

Finally, the [Double-TT-array factor] comes from the staggering of two tees to form the basic geometrical unit which can be repeated geometrically to produce the entire array:

[Double-TT-array factor] =

$$\cos\left[\pi .445(\vec{K}\cdot\vec{R} - \vec{K}_o\cdot\vec{r})\right] \qquad (2.4.2.5\text{-}7)$$

$\vec{K}$ = scan direction = (x, y, z) (2.4.2.5-8)

$\vec{K}_o$ = electronically quantized (λ/ℓ) scan direction (2.4.2.5-9)

The product of all these factors, which are normalized to unity, produce the [Double-Twin-Tee pattern]. The [dipole pattern] and the [z-array factor] are slowly-varying and do not have too much effect on the overall results. The other factors are vital in their effect on grating lobes, as outlined below and illustrated in Figures 2.4.2.5-2, 2.4.2.5-3, and 2.4.2.5-4: Table 2.4.2.5-1 on page 48 gives the legend and notes for all figures.

set	factor	zero	approximate cancellation
A	Double-TT	Diagonal lines, slope 3, offset $\pm\Delta x$, $\pm 3\Delta x$,...	∿2-5 zeros, can be scanned electronically.
B	TT-array	Lines for $y=y_* \pm \Delta y$, $y_* \pm 3\Delta y$,...	∿5-10 zeros, fixed in y
C	Single Tee	Isolated zeros at $(y_1, \pm 2\Delta x)$, $(y_1 \pm 2\Delta y, \pm \Delta x)$,...	2-4 zeros, fixed x and y.

(A) and (B) produce the major cancellation of grating lobes in the unit circle, particularly the cancellation which is

PROJECTION PLOTS
X-Y PATTERN
0. TO -50. DB.
NOMINAL COORDINATES
XO = 0.00000
YO = -0.10054
ZENITH = 5.76998
AZIMUTH = 180.000
DIPOLE IS ISOTROPIC
GAIN = 51.0108.
MONTH = 0.00
HOUR = 0.00
DECLINATION = 23.4500
LATITUDE = 29.22

(A) ZEROS OF DOUBLE-TT ARRAY

(B) ZEROS OF TT-ARRAY

(C) ISOLATED ZEROS OF TEE

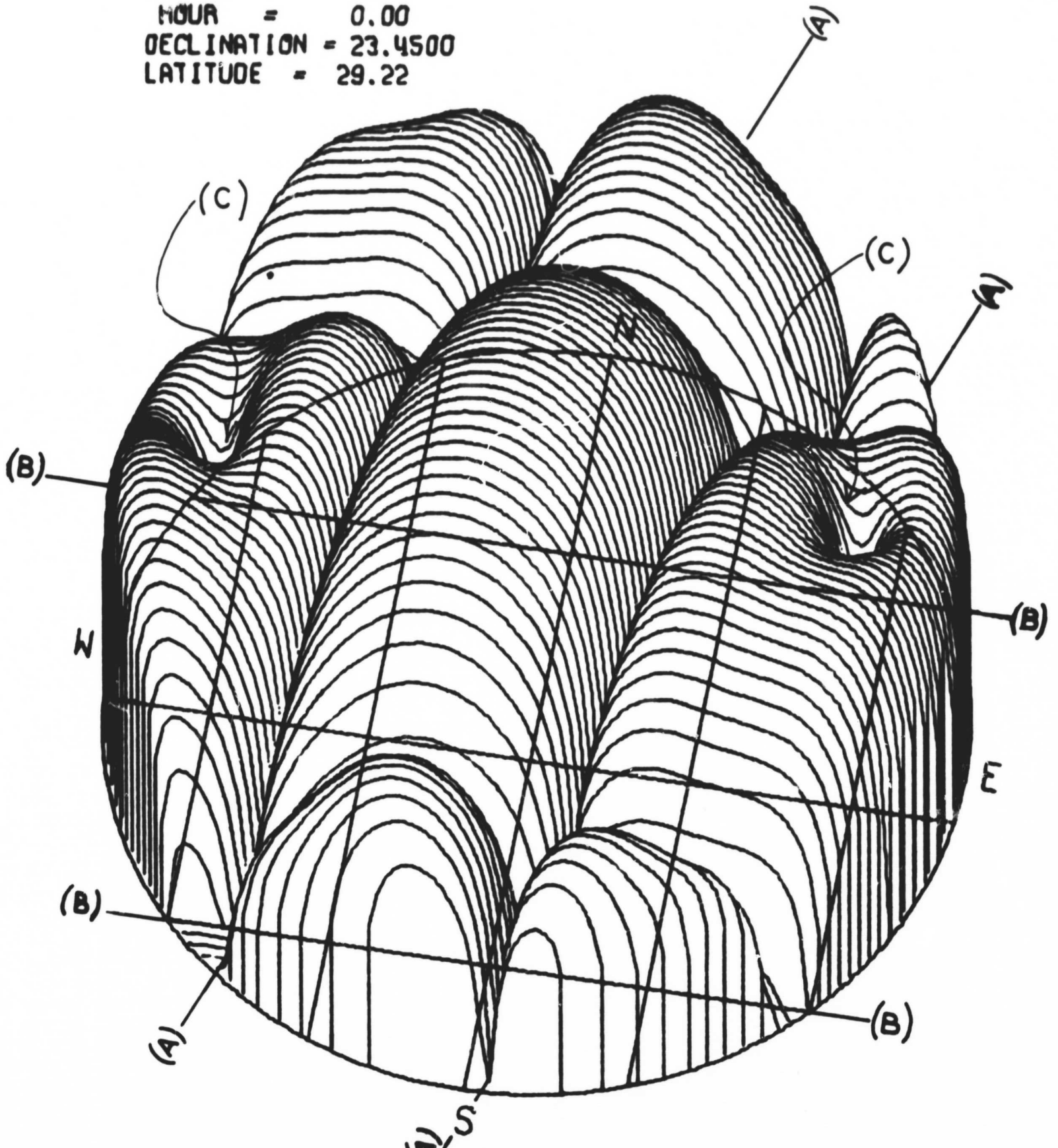

Figure 2.4.2.5-2 Double-Twin-Tee Pattern

PROJECTION PLOTS
X-Y PATTERN
0. TO -50. DB.
NOMINAL COORDINATES
XO = 0.00000
YO = -0.10054
ZENITH = 5.76996
AZIMUTH = 180.000
DIPOLE IS ISOTROPIC
GAIN = 51.0108.
MONTH = 0.00
HOUR = 0.00
DECLINATION = 23.4500
LATITUDE = 29.22

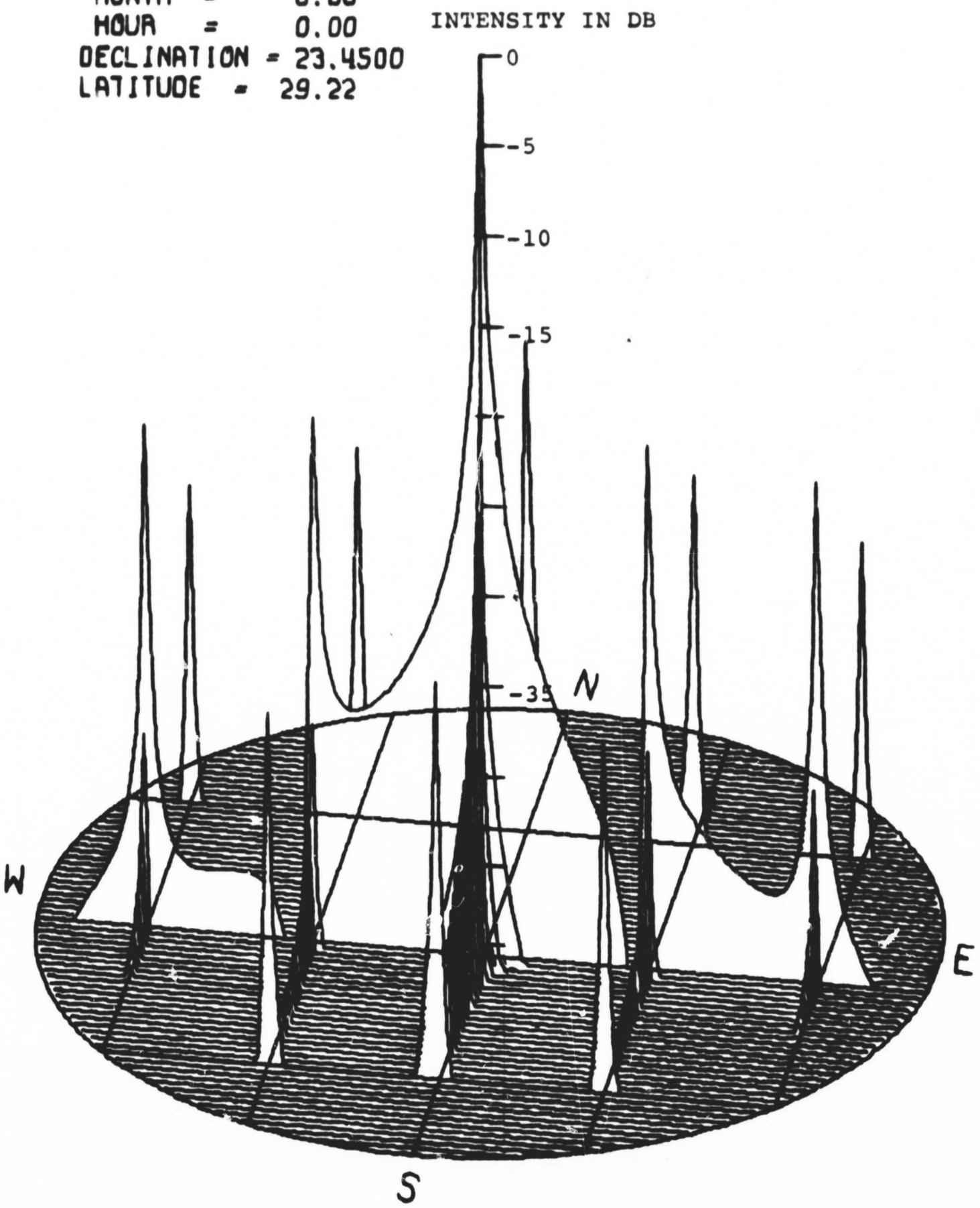

Figure 2.4.2.5-3 Overall Envelope Projection, Mo.=0,Hr.=0.

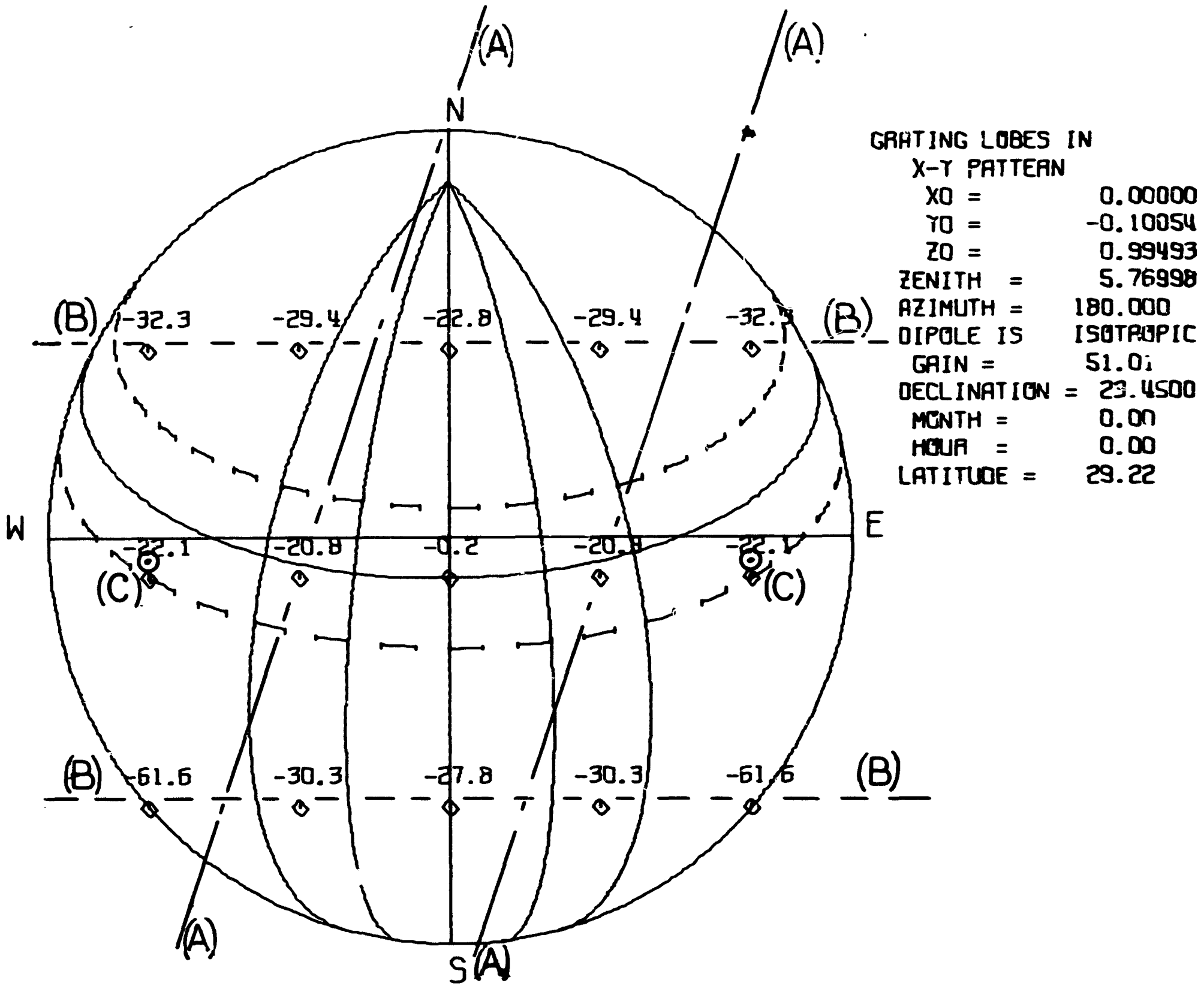

Figure 2.4.2.5-4 Unit Circle Plot, Mo.=0.,Hr.=0.

effective as the main beam is scanned in x (or in time, for ± an hour or two from local noontime). (B) restricts the scan in y. (C) does not remain effective as the main beam is scanned either in x or y.

2.4.2.6 Overall Envelope Pattern

The product of the [Double-Twin-Tee pattern], as shown in Figure 2.4.2.5-2 above, multiplied by the [x-envelope] and the [y-envelope], which are respectively periodic in x and y, as shown in Equations 2.4.2.3-1 and 2.4.2.3-3 above, produces a nominal envelope pattern with a sequence of peaks at doubly-periodic locations in the x-y coordinate plane, with the magnitude at the peaks being the magnitude of the [Double-Twin-Tee pattern]. As mentioned in Section 2.4.2.5, the [Double-Twin-Tee pattern] should approximately cancel most of the peaks except the main peak, for which all of the factors composing the [Double-Twin-Tee pattern] should be approximately maximum (unity).

This desired state of affairs holds only near the meridian (local noon) and near the y-direction for which the manual components in the array are phased. As shown in the figures below, the nominal envelope pattern will change with local time and with y-phasing. Figure 2.4.2.5-3 shows the nominal envelope for the same time (local noon) and the same declination (5.77°, corresponding to declination of sun at 0. months from the summer solstice) as chosen for

TABLE 2.4.2.5-1

Legend and Notes for Curves

All curves for nominal 50 db rectangular array

Assuming no mutual coupling between elements.

No East- est phasing within Twin-Tee

Manual North-South phasing with Twin-Tee (quantized).

Target coordinates month and hour referred to Sun:

Month: 0.00 at Summer Solstice to 6.00 at Winter Solstice

Hour: 0.00 at local noon

Other targets in ecliptic plane specified by declination and local hour (relative to meridian).

x and y are direction cosines, related to spherical coordinates of zenith and azimuth angles.

Basic elements of array can be: NS dipole, Hertzian
EW dipole, Hertzian
Isotropic element

Latitude of array approximately: 17.67 St. Croix
29.22 El Campo
35.40 Goldstone

the plot of the [Double-Twin-Tee pattern] in Figure 2.4.2.5-2 above. The latter plot is merely the former mulitplied by the doubly-periodic envelope of the array factor. Figure 2.4.2.5-4 below shows the same conditions in a normal view, also printing the nominal intensities at the grating lobes, and superimposing ellipses of: (1) constant declination, for target $\pm 10°$ and (2) constant time for ± 1, ± 2 hours from noon.

Figures 2.4.2.6-1 through 2.4.2.6-6 below show similar plots of the nominal envelope pattern and the grating lobes for a declination of 0° (corresponding to declination of sun at an equinox) and for varying time in increments from local noon.

Figures 2.4.2.6-7 and 2.4.2.6-8 below show a similar set of plots for maximum declination of target in ecliptic (sun at winter solstice, declination = -23.45°), at local noon.

As shown in Figures 2.4.2.6-1 and 2.4.2.6-2 above, the main beam, when it is on the meridian, is the largest lobe in the visible space (unit circle) when the main beam is phased approximately to the y-coordinate for which the manual phasings in the array are set. When the time from local noon is changed, with declination remaining constant, as shown in Figures 2.4.2.6-3 through 2.4.2.6-6 above, it is seen that within two hours, the main lobe has been supplanted as the largest lobe by one $2\Delta x$ ($\Delta x = .3745$) over on the same

PROJECTION PLOTS
X-Y PATTERN
0. TO -50. DB.
NOMINAL COORDINATES
XO = 0.00000
YO = -0.46816
ZENITH = 29.21994
AZIMUTH = 180.000
DIPOLE IS ISOTROPIC
GAIN = 50.4408.
MONTH = 3.00
HOUR = 0.00
DECLINATION = 0.0000
LATITUDE = 29.22

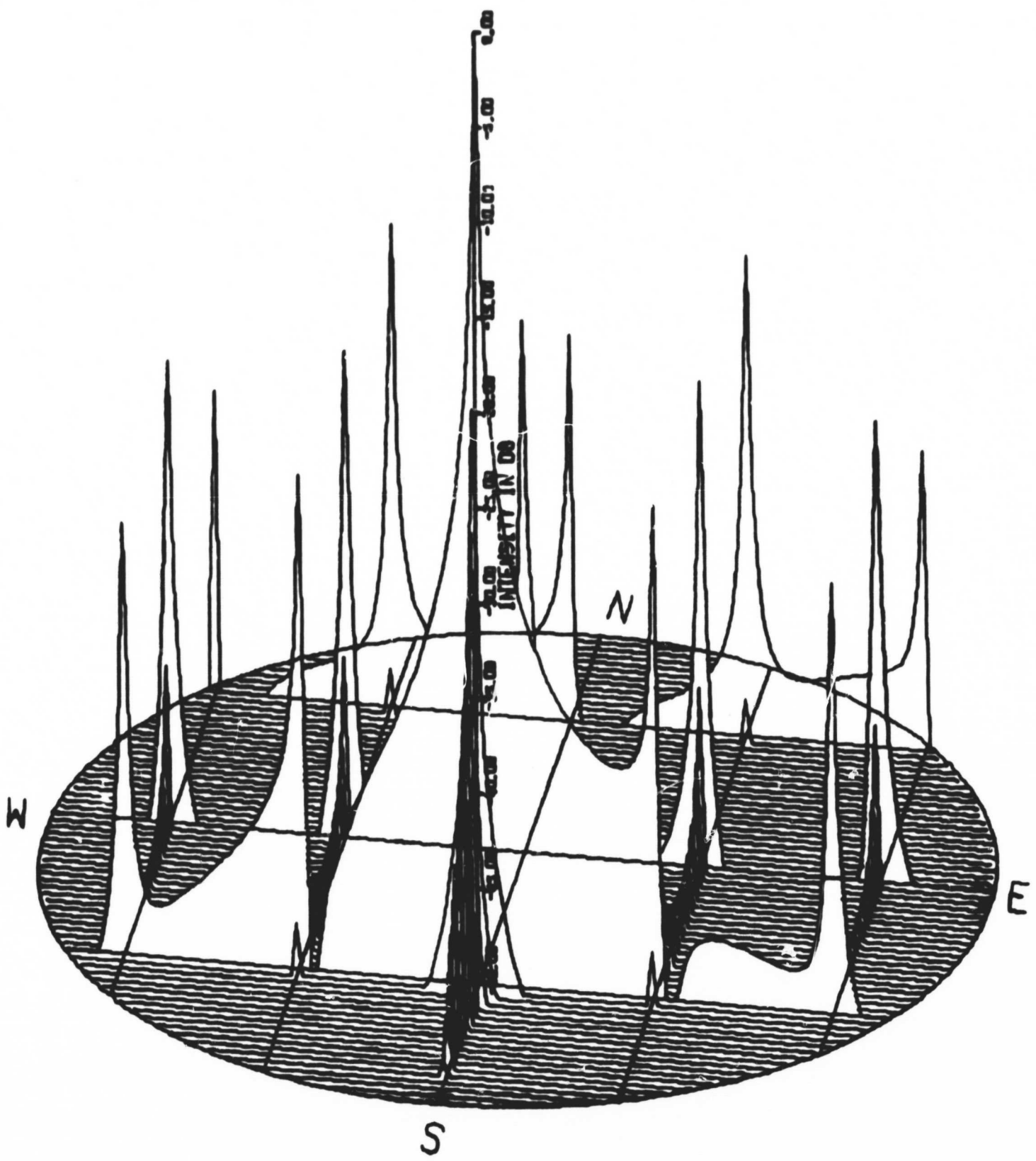

Figure 2.4.2.6-1 Overall Envelope Projection, M0.=3.,Hr.=0.

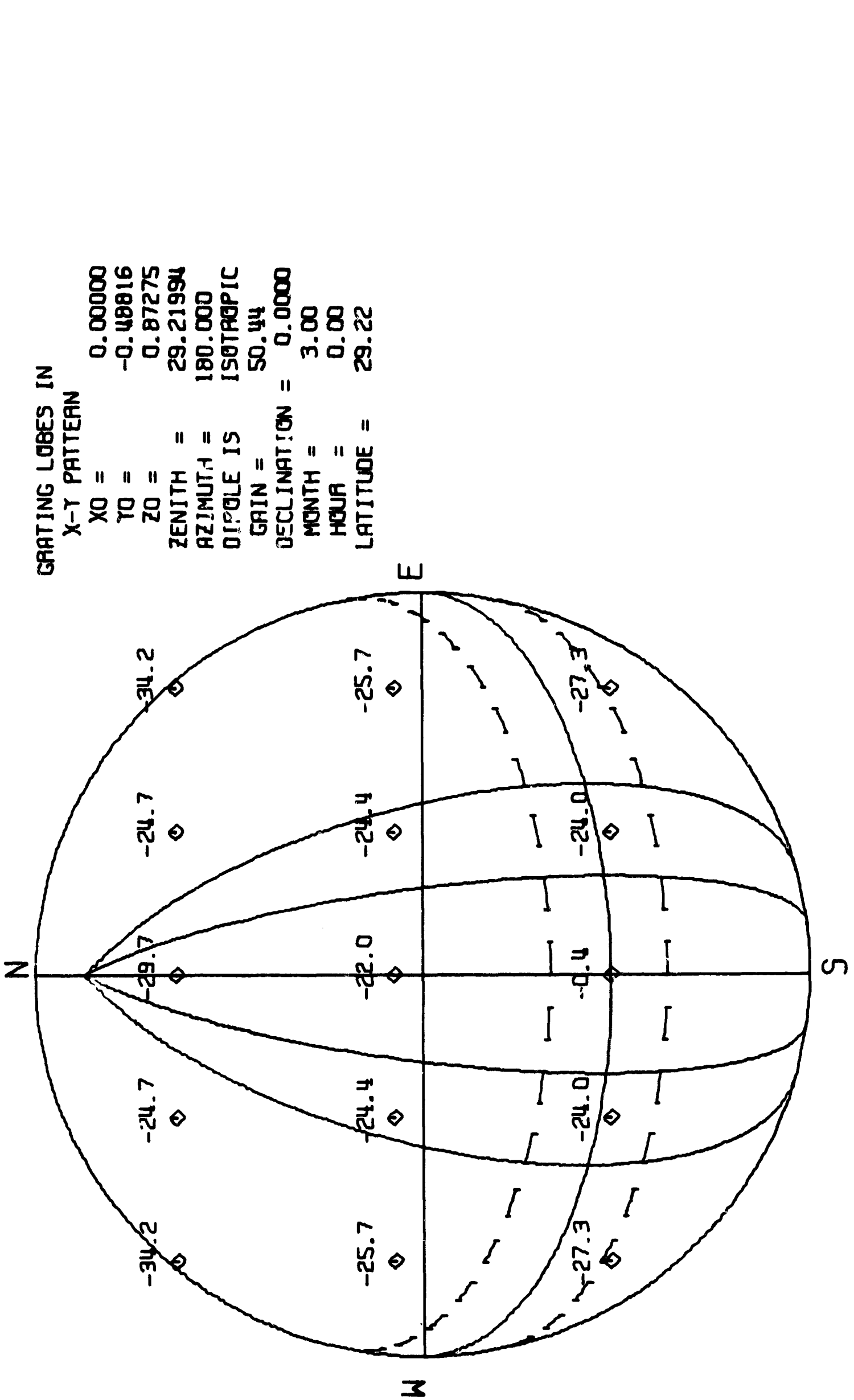

Figure 2.4.2.6-2 Unit Circle Plot, Mo.=3.,Hr.=0.

PROJECTION PLOTS
X-Y PATTERN
0. TO -50. DB.
NOMINAL COORDINATES
XO = 0.25882
YO = -0.47153
ZENITH = 32.54025
AZIMUTH = 151.238
DIPOLE IS ISOTROPIC
GAIN = 48.0008.
MONTH = 3.00
HOUR = 1.00
DECLINATION = 0.0000
LATITUDE = 29.22

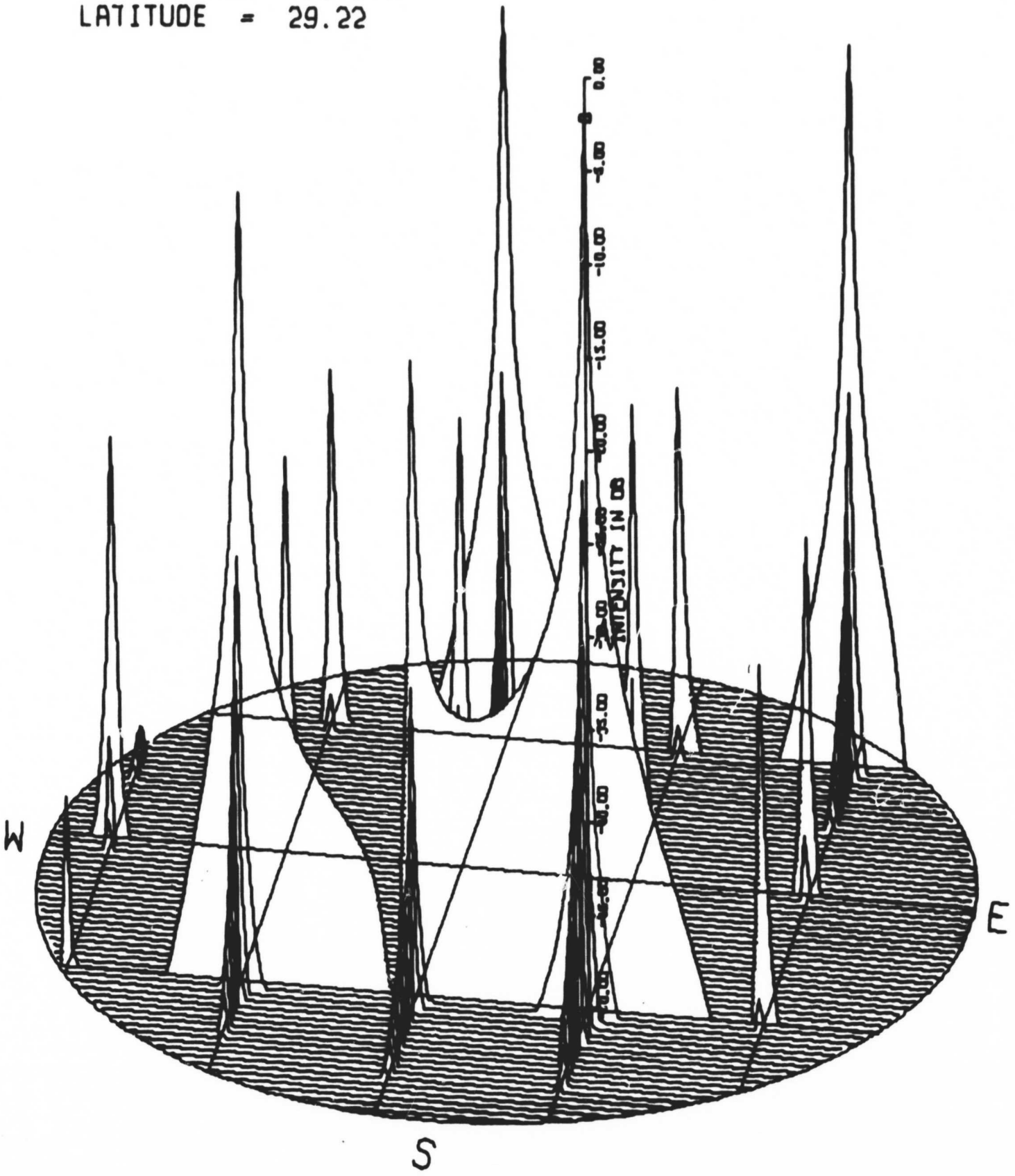

Figure 2.4.2.6-3 Overall Envelope Projection, Mo.=3.,Hr.=1.

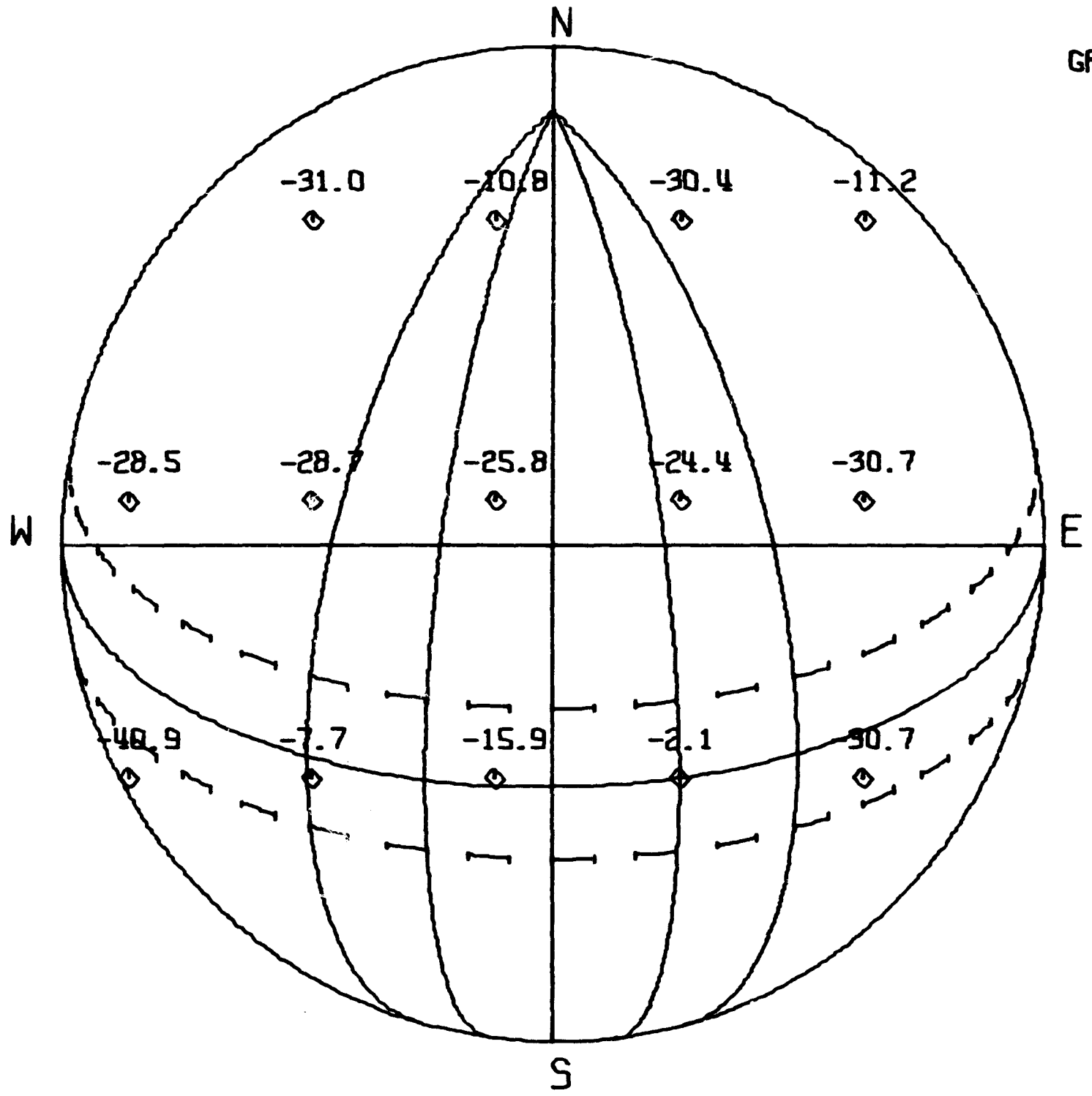

GRATING LOBES IN
X-Y PATTERN

XO =	0.25882
YO =	-0.47153
ZO =	0.84301
ZENITH =	32.54025
AZIMUTH =	151.238
DIPOLE IS	ISOTROPIC
GAIN =	48.00
DECLINATION =	0.0000
MONTH =	3.00
HOUR =	1.00
LATITUDE =	29.22

Figure 2.4.2.6-4 Unit Circle Plot, Mo.=3.,Hr.=1.

PROJECTION PLOTS
X-Y PATTERN
0. TO -50. DB.
NOMINAL COORDINATES
XO = 0.50000
YO = -0.42276
ZENITH = 40.90243
AZIMUTH = 130.215
DIPOLE IS ISOTROPIC
GAIN = 42.4808.
MONTH = 3.00
HOUR = 2.00
DECLINATION = 0.0000
LATITUDE = 29.22

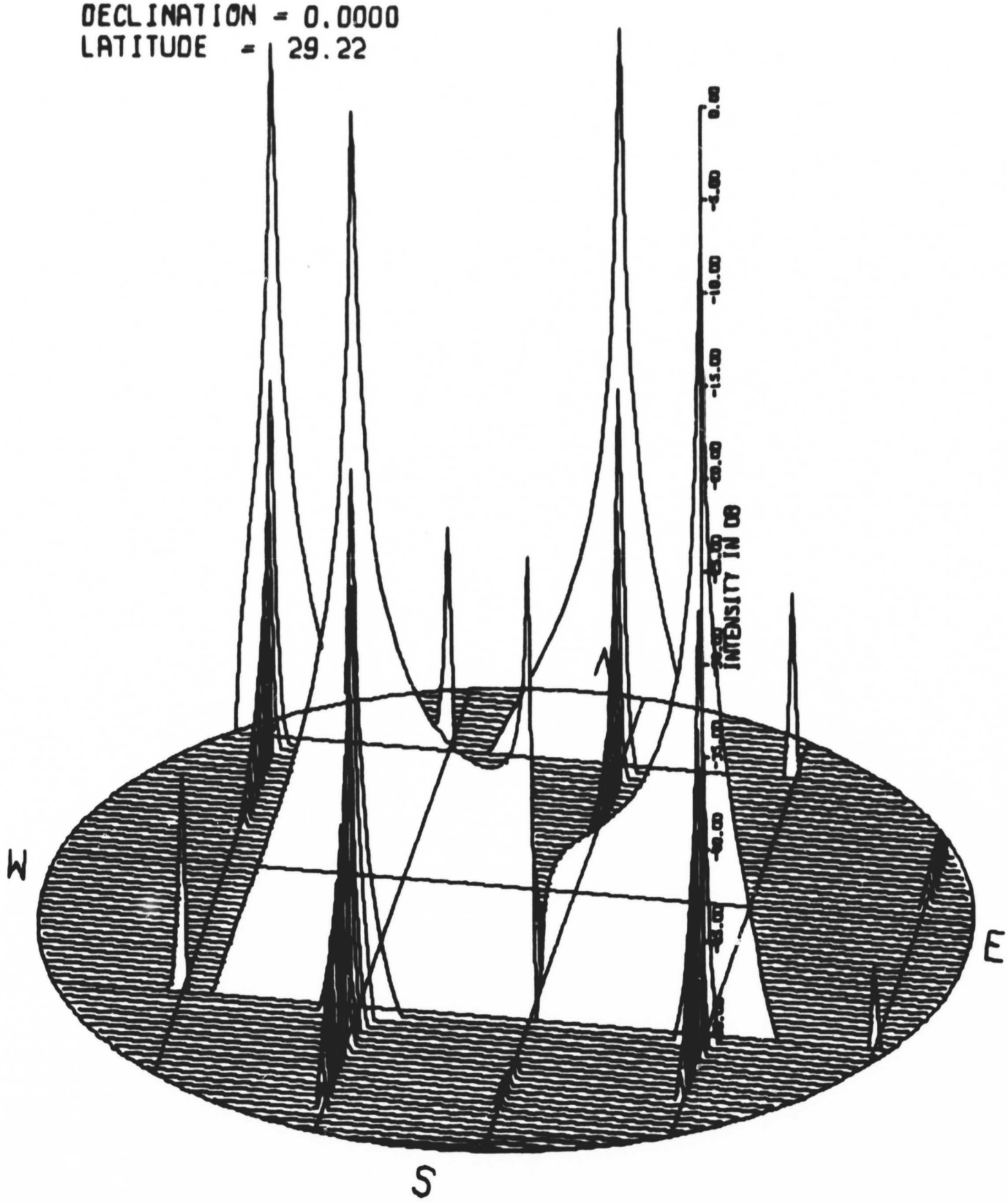

Figure 2.4.2.6-5 Overall Envelope Projection, Mo.=3.,Hr.=2.

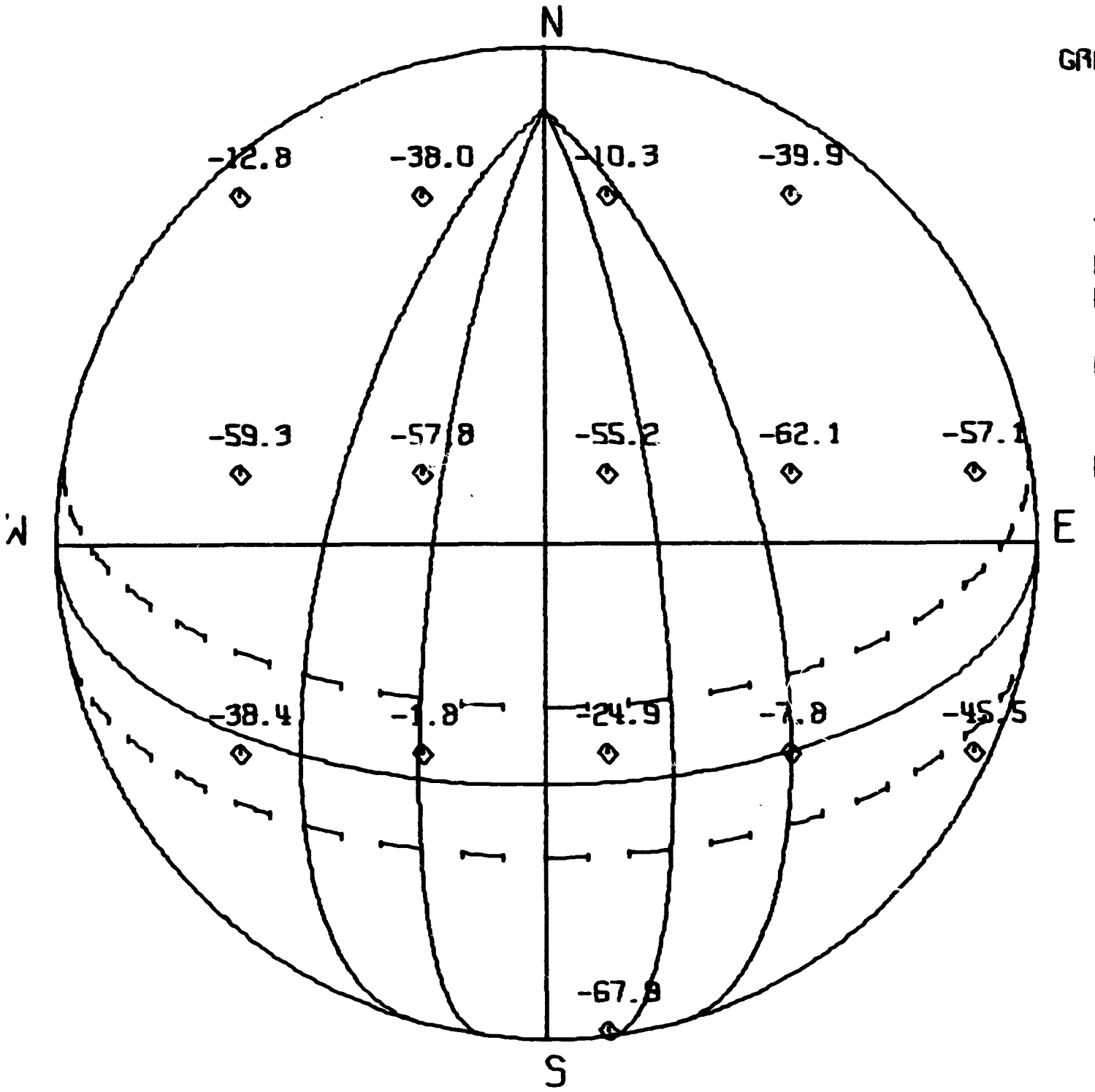

GRATING LOBES IN
X-Y PATTERN

XO =	0.50000
YO =	-0.42276
ZO =	0.75583
ZENITH =	40.90243
AZIMUTH =	130.215
DIPOLE IS	ISOTROPIC
GAIN =	42.48
DECLINATION =	0.0000
MONTH =	3.00
HOUR =	2.00
LATITUDE =	29.22

Figure 2.4.2.6 - 6 Unit Circle Plot, Mo.=3.,Hr.=2.

PROJECTION PLOTS
X-Y PATTERN
0. TO -50. DB.
NOMINAL COORDINATES
XO = 0.00000
YO = -0.78516
ZENITH = 52.66995
AZIMUTH = 180.000
DIPOLE IS ISOTROPIC
GAIN = 48.9608.
MONTH = 6.00
HOUR = 0.00
DECLINATION =-23.4500
LATITUDE = 29.22

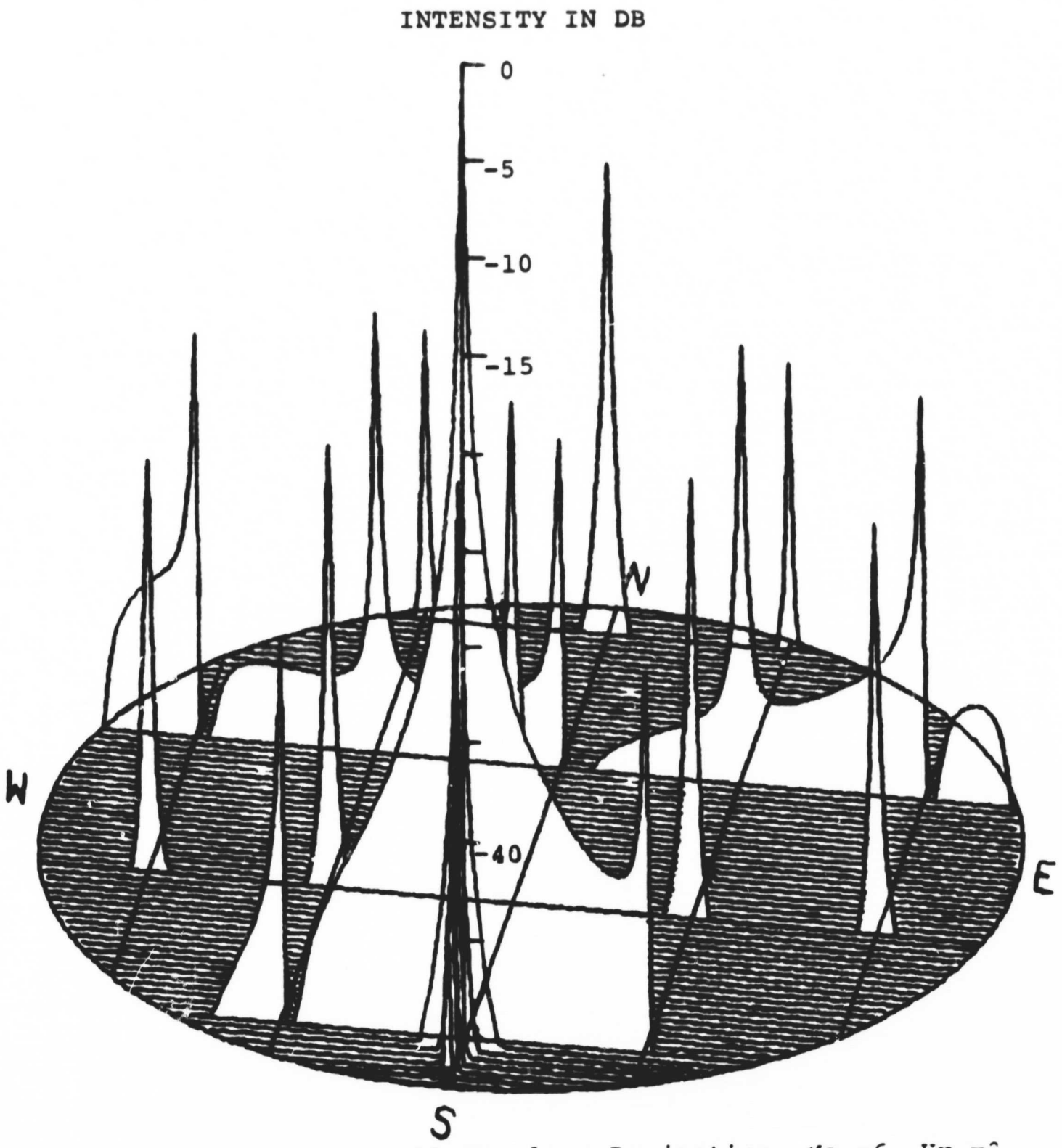

Figure 2.4.2.6. - 7 Overall Envelope Projection, Mo.=6.,Hr.=0.

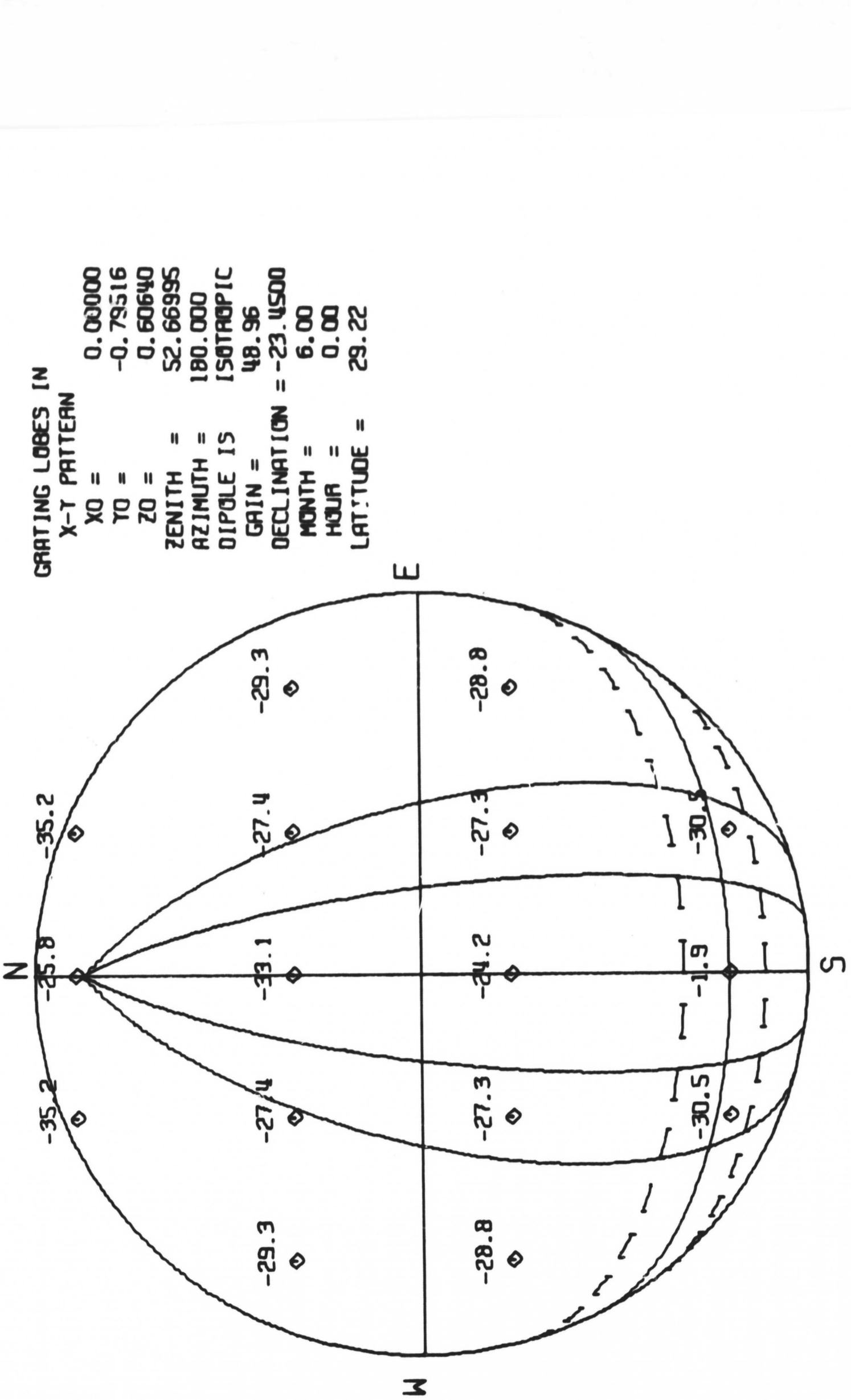

Figure 2.4.2.6 - 8 Unit Circle Plot, Month=6.,Hour=0.

EW line. This occurs, because, as explained in Section 2.4.2.5, this lobe is initially cancelled by a fixed, isolated zero in the [single tee pattern]; the fixed zero, resulting from fixed EW-phasings in the tee, cannot be phased EW; therefore, as the pattern of grating lobes is phased eastward, the extraneous lobe moves away from the fixed zero, and the desired main lobe moves toward the other symmetrically-located fixed zero on the other side of the meridian.

Similarly, as the main beam is phased NS away from the y-value for which the array is manually phased, the main beam would be supplanted as the largest lobe by another grating lobe, as other rows of grating lobes move away from the lines of zeros fixed by manual y-phasing (NS) in the array.

The net effect of this reduction in the magnitude of the main lobe and increase of the other grating lobes with phasing is manifested by a loss in gain, or scattering loss, reducing the receiving area of the array proportionally to the fraction of power which would be scattered in the directions of the other grating lobes (divided by the total power). Quantitatively, this reduction in gain is covered in Section 2.5.1 and 2.5.2 where results are given in the form of gain contours, gain vs. time, and some analytic results. In addition, the rise of a bad grating lobe can result in an increase in received noise power if the lobe moves into a galactic noise source (which is likely to be found in the galactic equator), as mentioned in Section 2.5.3 below.

Noise due to side lobes is treated in Section 2.4.3, 2.5.3.

2.4.3 Side Lobe Patterns

2.4.3.1 Overall Behavior of Side Lobes

As mentioned above (Sections 2.4.1.1(3), 2.4.2.5) the main effect of side lobes is a potential increase in received galactic noise power, proportional to the magnitude of the side lobes. For gross purposes, the side lobes are represented by a nominal envelope (Section 2.4.2.6), an approximate upper limit of the side lobes for exact phasing between Double-Twin-Tees. A secondary effect of the side lobe pattern is the effect on the main beam; however, the only significant effect on the main beam is a slight ripple in gain caused by a slight misalignment of the main beam as it is moved in quantized steps throughout the x-y coordinate plane. The width of the main beam in x-y coordinates is not expected to change very much with phasing; therefore, the discussion of the main beam in Section 2.5.1 will be based on the nominal array factors.

In the overall envelope pattern (Sections 2.4.2.3 and 2.4.2.6) it can be seen that the side lobes tend to lie along lines connecting grating lobes in the x-y coordinate plane. Thus, the side lobes tend to form ridges in the x-y plane along which ridges the pattern will typically be of greater magnitude than in the larger areas between the ridges. Since the overall array is rectangular NS and EW, the ridges of side lobes are also aligned along lines parallel to the x- and

--axes in the space of direction cosines. This overall structure of the pattern makes it possible to see when a ridge of side lobes is potentially close enought to a noise source to produce appreciable received noise power. The exact noise power would depend on the detailed pattern of the side lobes, which can deviate appreciably from the nominal pattern, as covered immediately below in Section 2.4.3.2.

2.4.3.2 Side Lobes for Tree vs Parallel Phasing

The detailed side lobe pattern can have side lobes 10 and 20 db above the nominal envelope pattern, depending upon the method of phasing the array. It has been seen that the tree, or digital number, method of phasing the array can produce some side lobes on the order of -10 to -20 db, because of the assimulated growth of phasing errors as the signals from the Twin-Tees are combined through successive phase shifters, each with a maximum error of $\lambda/16$, producing an accumulated maximum error of $3\lambda/8$. In certain cases, this tree method of phasing was shown to produce side lobes on the order of 10 db below the main lobe, where the nominal envelope was about 30 db below the main lobe. In an effort to improve this situation, a study was made of various methods of parallel phasing of the array. Approximate least-mean-squared-error phasing was shown to produce a predictable side lobe on the order of 17 db below the main lobe (this was simply a result of dividing the array into

groups of roughly equal numbers of elements, each of which groups simply approximates a sub-array of elements at the same phase, plus an exact tilt). This results in a significant reduction in the level of the worst side lobe, and corresponding results apply to the levels of other bad side lobes in the same patterns. In addition, parallel phasing of the array leaves open a degree of freedom which can be used to tailor the side lobes relative to a given galactic noise distribution.

Formulas for the side lobe patterns can be derived from the basic expressions 2.4.2.4-1 and 2.4.2.4-2. This was essentially done in deriving Equations 2.4.2.2-2, 2.4.2.2-3 and 2.4.2.2-9. For tree or parallel phasing, the expressions are more complicated than for a uniform array, and have been evaluated by a digital computer (Figures 2.4.3.2-1 and 2.4.3.2-2). For tree phasing (single digital number method) the array is broken into successive sub-arrays, each containing two units, each half as large as the next-higher-level sub-array. This is basically a method of successively dividing the array in halves. The tree phasing produces an [x-array summation] of the form:

$$[\text{x-array summation}] = \cos(\pi dx_1)\cos(2\pi dx_2)\cos(4\pi dx_3)\cdot \frac{1}{5}\{4\cos(8\pi dx_4)\cos(16\pi dx_5) + \epsilon^{i2\pi(32dx_6-8dx_5-4dx_4)}\} \qquad (2.4.3.2\text{-}1)$$

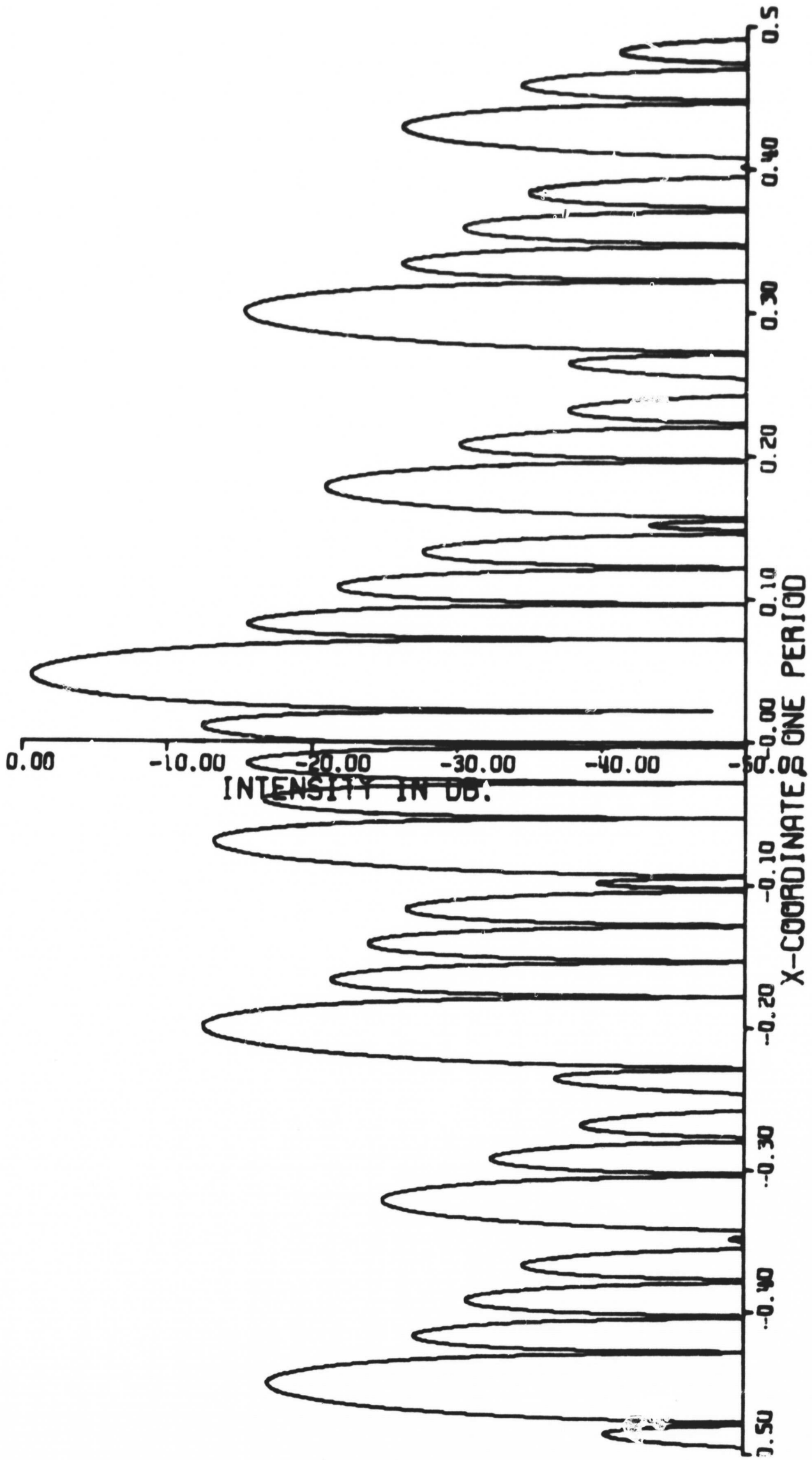

Figure 2.4.3.2 - 1 Detailed Sidelobe Pattern, Tree Phasing

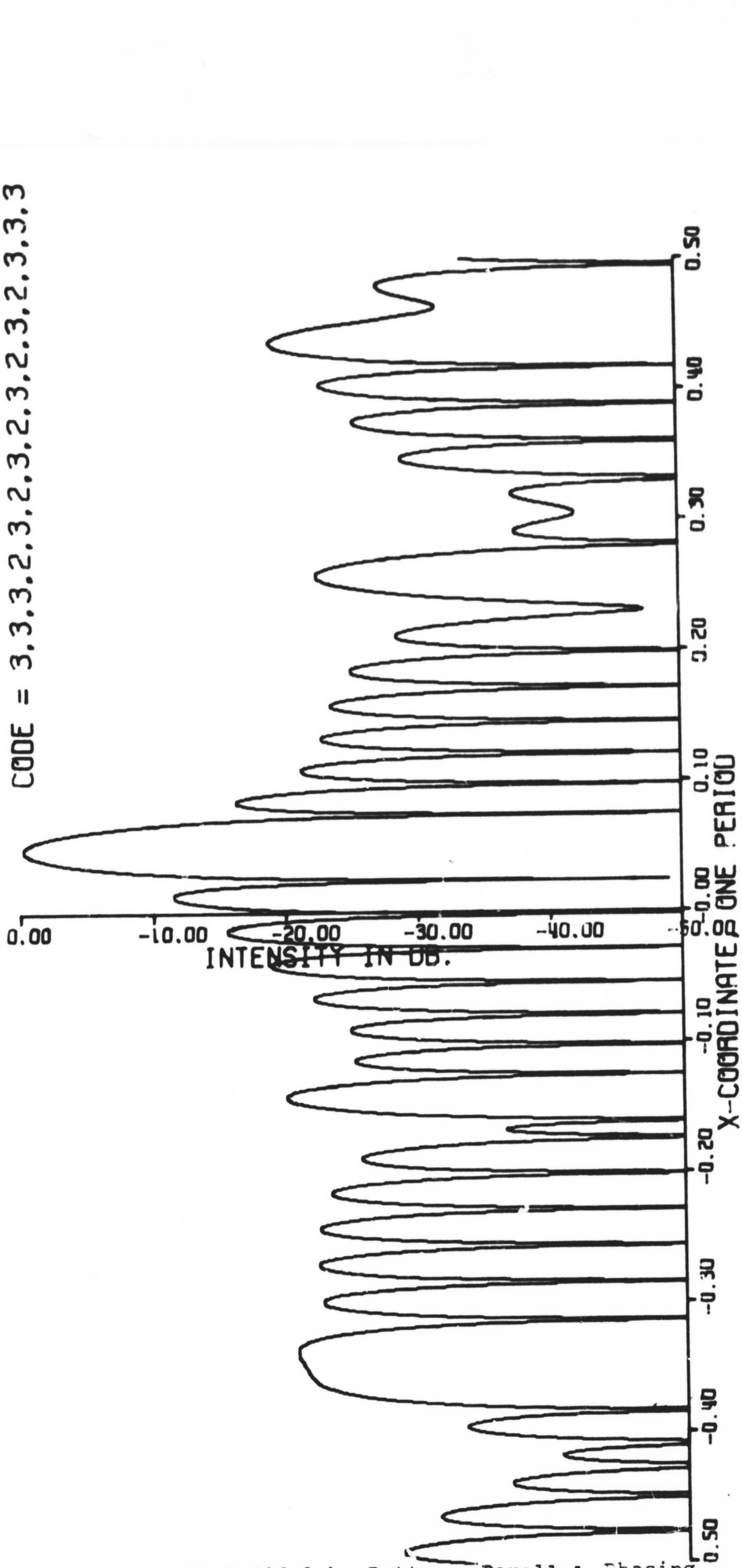

Figure 2.4.3.2 - 2 Detailed Sidelobe Pattern. Parallel Phasing

where $dx_1 = 2.67(x - \Delta_1), \ldots, dx_6 = 2.67(x - \Delta_6)$ with the $\{\Delta_m\}$ selected to phase the given sub-arrays as closely to x as possible using phase shifters quantized to $\lambda/8$. The $\{\Delta_m\}$ are simply obtained from the single digital number by eliminating an insignificant digit from the end of the number for each successive level of the tree from top to bottom. Parallel phasing divides the array into groups with the phase at each unit in a group given by a constant plus an exact tilt. By grouping the terms of Equation 2.4.2.4-1, this produces an [x-array summation] of the form:

$$[\text{x-array summation}] = \sum_{k=1}^{\max} S_{N_K}(x - x_o) e^{i2\pi 2.67[(x-x_o)\sum_{j=1}^{K-1} N_K - \Delta(K-1)]} \quad (2.4.3.2\text{-}2)$$

$$S_{N_K}(x - x_o) = \sum_{m=1}^{N_K} e^{i2\pi 2.67m(x-x_o)} \quad (2.4.3.2\text{-}3)$$

where x_o is an exact phase point giving the exact phase tilt (see Section 2.4.3.3(1),(2) bleow, and Δ is the phase step from one group to the next (Δ usually will be the minimum quantized step = $\Delta x/8 \approx .0468$, from Equation 2.4.2.2-7). The code of numbers on Figure 2.4.3.2-2 shows the division of the

array into groups at the same phase plus an exact tilt (thus there are 3 units at "zero" phase, then 3 units at $\lambda/8$, then 3 units at $2\lambda/8$, then 2 units at $3\lambda/8$, etc.; all plus an exact tilt).

2.4.3.3 Quantization of Look Directions

In either case, tree or parallel phasing, it is acceptable to quantize the allowed look directions in the x-y coordinate plane (as mentioned in Section 2.4.2.2). This quantization can be thought as occurring at two levels:

1) First, there is a quantization of points in the x-y plane at which the phasing can be set exactly between every Double-Twin-Tee and every other. This quantization produces a rectangular grid in the x-y plane with grid spacings exactly 1/8 of the spacing between grating lobes; because the grating lobes are points where the phase difference between Double-Twin-Tees is a multiple of one wavelength, and the exact phasing points are points where the phase difference is a multiple of one-eighth wavelength (the quantization of the phase shifters).
2) Second, between the exact phasing points, the space can be quantized into a sufficinet number of points which will allow any point in the space to be covered by the main beam with less than, say, .5 db ripple in intensity. Therefore, since the pattern is a

product including an [x-array factor] and a [y-array factor], the quantization should be such that for any point (x,y) in the space, there should be grid points (x_k,y_k) such that if the main beam is at (x_k,y_k), then the [x-array factor] and the [y-array factor] at (x,y) are both within, say, .25 db of the peak.

Investigation of the tree method of phasing based on a single digital number to specify an x-coordinate or a y-coordinate makes it evident that the digital numbers automatically quantize the allowed look points as discussed in (1) and (2) above. The fineness of the quantization corresponds to the length of the digital number but the quantization is not significant beyond the number which is necessary to specify the phasing of the array. For the parallel method of phasing, the level of quantization is almost arbitrary but is limited practically by the number of different side lobe patterns one wishes to allow in the system's memory. Practically, the same level of quantization for the allowed patterns in both methods of phasing give about the same coverage by the main beam (but different side lobe levels relative to the main beam).

2.4.3.4 Results

For an illustration of the type of side lobe patterns which have been considered, a typical sample is included in Figures 2.4.3.2-1 and 2.4.3.2-2.

The final trade-off on the phasing of the array will involve several factors:

1) Main lobe coverage. This problem seems to be solved by the quantization methods discussed above.
2) Side lobe levels and noise. Since the sun will be roughly EW of the target near conjunction, a mongrel system with better control of EW phasing than NS may be economical.

3) Flexibility. To optimize patterns and reduce noise, some independent or parallel phasing of groups will be necessary.

2.5 Planar Array Performance Characteristics

Certain properties of the planar array pattern, which were derived in Section 2.4 above, will be related to important performance characteristics of the array, including: antenna gain, antenna noise reception, and the variation of antenna gain and noise power with right ascension and declination of target. Again, the assumptions which were stated in Section 2.4.1.2 will apply. In particular, the discussion will apply mainly to the large (50 db) ground array, for which the separation of pattern into side lobe and overall envelope parts is particularly valid. The coordinate system of direction cosines (Figure 2.4.2.1-2) will again be used, as these are fundamental coordinates in which a rectangular array

"thinks", and which give the pattern the periodicities discussed throughout Section 2.4.

2.5.1 Gain and Beamwidth

2.5.1.1 Gain vs Inverse Beamwidth

The gain of the array is perhaps the single most important factor in the performance of the array, as the gain can be shown to be proportional to the effective receiving area of the array for a plane wave. Neglecting ohmic losses in the array, neglecting mismatching reflection losses due to variation of active impedance at the terminals leading from the Twin-Tees*, and assuming that the pattern can be represented as exactly one unit in the grating lobe pattern (this assumption is good if the [Double-Twin-Tee pattern] is slowly varying in the neighborhood of the main lobe, and if all other grating lobes are small), then the array gain is inversely proportional to the product of the x- and y-beamwidths, normalized by the cosine of the zenith angle.

2.5.1.2 Expressions for Beamwidth

It is expected that the x and y half-power beamwidths are

---

*The problem of variation of active impedance does not appear at present to be satisfactorily solved, even for a uniform array of dipoles, in which an unrealistic assumption of a sinusoidal dipole current is often made. See Section 2.7 for a description of active impedance variation.

roughly independent of the method of phasing the array, so long as the phasing errors do not get out of hand (this still is a question for investigation, in connection with the organization of the array, and the side lobe patterns, Section 2.4.3). So long as the x and y half-power beamwidths are independent of the phasing, the beamwidths will be given for the case of exact phasing, for which the pattern in the vicinity of the main beam is approximately proportional to the product of the [x-array factor] and the [y-array factor] which are of the form $\sin N\pi s_1(x - x_o)/N \sin \pi s_1(x - x_o)$ and $\sin M\pi s_2(y - y_o)/M \sin \pi s_2(y - y_o)$ from Equations 2.4.2.2-2 and 2.4.2.2 -3 above. The power in the vicinity of the main beam is approximately the square of the product of these factors, hich looks somewhat like a cosine-squared function in both x and y. The half-power width of a cosine-squared function is exactly half the distance between the first (symmetric) nulls in the function, so the half power beamwidths will approximately equal the distance in x and y, respectively, from the center of the main lobe to the first nulls.

2.5.1.3 Numerical Results

It can be seen from Equations 2.4.2.2-2 and 2.4.2.2-3 that the distances from the peak to the first nulls in the [x-array factor] and the [y-array factor], respectively, are given by

$$XBW = \frac{1}{40 \times 2.67} = \frac{.3745}{40} = .00936 \qquad (2.5.1.3\text{-}1)$$

$$YBW = \frac{1}{56 \times 1.78} = \frac{.5618}{56} = .01032 \qquad (2.5.1.3\text{-}2)$$

These half-widths are inversely proportional to the overall dimensions of the array, so that the directive gain of the array is directly proportional to the overall area of the array, under the assumptions stated at the beginning of Section 2.5.1.

The beamwidths, in addition to being related to the gain, give an indication of the angular resolution of the system and an indication of the noise rejection capabilities of the system for noise sources within a few beamwidths of the main beam (beamwidths given above transform to $\sim .5°$).

2.5.2 Gain vs Time and Declination

2.5.2.1 Gain - Scattering Loss Relationship

The relationship between gain and beamwidth or between gain and overall area of the array is reasonably good if the main lobe is much larger than all the other grating lobes. As discussed in Section 2.4.2.6, the main lobe is not always larger than the other grating lobes. As the array is scanned away from the meridian (x = 0) and the y-value (corresponding

to declination) for which the manual components of the array are set, the main lobe will decrease in amplitude and the other grating lobes will increase as the manually-phased factors of the array pattern become more favorable for them than for the main lobe. The gain of the array will decrease, depending strongly on the scattering loss, which is the ratio of the main beam power to the total power in the pattern, which will be approximated below by a summation over all the grating lobes within the unit circle.

2.5.2.2 Expressions for Gain

Considering the array for the moment as a transmitting array, the effect of the other grating lobes is to radiate power which should be radiated from the main lobe for maximum efficiency. Considered as a receiving array, the reciprocal effect on performance is due to scattered or reradiated power which can never be absorbed by the receiving terminals of the array. In order to account for these effects, it is necessary to have an accurate expression for the gain of the array. The gain of the array will be given by:

$$[\text{gain}] = [\text{directive gain}] + [\text{mismatch loss}] + [\text{ohmic loss}] \qquad (2.5.2.2\text{-}1)$$

in decibels, where, for the following, the [mismatch loss] and the [ohmic loss] will be neglected. The [directive gain] is

given by the following:

$$[\text{directive gain}] = 10 \log_{10} \left| \frac{4\pi P(x_o, y_o)}{\iint P(x,y)\, dxdy/z} \right| \qquad (2.5.2.2\text{-}2)$$

(for reference, see Antenna Analysis, E.A. Wolff, Wiley, New York, 1967, PP 12). Following the separation of pattern into side lobe and envelope (or grating lobe) parts, the expression for [directive gain] will be separated into parts for the main beam and parts for the grating lobes, as follows:

$$[\text{directive gain}] = G_o + 10 \log_{10} Z_o +$$

$$10 \log_{10} \left| \frac{P(x_o, y_o)/Z_o}{\sum_{\substack{\text{all lobes in} \\ \text{unit circle}}} P(x_o + i\Delta x, y_o + j\Delta y)/Z_{ij}} \right| \qquad (2.5.2.2\text{-}3)$$

where G_o is the ideal gain for main beam alone (as in Section 2.5.1), or $4\pi/\lambda^2$ times the overall array area:

$$G_o = 10 \log_{10} (4\pi 40 * 2.67 * 56 * 1.78) \qquad (2.5.2.2\text{-}4)$$

The term $10 \log_{10}(Z_o)$ accounts for the spreading of the main beam in the transformation from x-y to angular coordinates, and the third term is the scattering loss or the ratio of

power in the main beam to the total power (in this summation Z_{ij} is the third, vertical, direction cosine for the point x_i, y_j so that $Z_{ij} = \sqrt{1 - x_i^2 - y_j^2}$). The use of a grating lobe summation as an approximation to the integral in Equation 2.5.2.2-2 is justified for the large (50 db) array by the fact that the pattern is only significant in a small neighborhood of each grating lobe (in fact, approximately 70% of the contribution to the integral comes from the single main beam within each rectangular period of the grating lobe pattern).

2.5.2.3 Digital Computation of Gain Curves

This computation has been implemented on a digital computer and the antenna gain has been calculated for many points (x_o, y_o) in the unit circle according to one of three different modes of operation*:

1) Isolated point. For certain isolated points in the x-y plane, the gain has been calculated as an adjunct

---

*Legend for Curves

Months are given in decimals from Summer solstice (0.00) to Winter solstice (6.00). When the month is given the corresponding y-value at local noon, which is the sine of the zenith angle, is also given. In some cases, the zenith angle at local noon is also given. The month is given for a target at the Sun; other targets in the ecliptic plane, like a spacecraft, can be specified by their declinations which would enable the appropriate gain curves to be located.

When month and y-value are given for Twin-Tee sub-array phasing, these values are for the closest quantized values which can be set by manual adjustment.

Dipole specifies the element, which can be "East-West" Hertzian, "North-South" Hertzian, or "Isotropic".

Latitude is given for the East-based receiving array.

to the intensity patterns, such as shown in Figures 2.4.2.5-3, 2.4.2.5-4 and 2.4.2.6-1 through 2.4.2.6-8 above.

2) Gain vs time. For this mode of operation, the manual phasings of the array are calculated as closely as possible to the exact phasing which would be used for a target at the given declination on the meridian. Then, with the manual phasings set, the electrical phasings of the array are varied so as to move the main beam in an ellipse within the unit circle, corresponding to a target at the given declination but at different times of day relative to the meridian (or local noon). For a plot of such an ellipse and a detailed picture of how the pattern changes with time, see Figures 2.4.2.6-1 through 2.4.2.6-6. The curves of gain vs time are arranged in families of 7, corresponding to the sun at monthly increments from summer solstice to winter solstice. The families shown are arranged to illustrate the change in the gain curves vs the type of element (or dipole) and vs the latitude of the array on the earth:

a) Fig. 2.5.2.3-1 Lat. = 29.22, Dipole is NS

b) Fig. 2.5.2.3-2 Lat. = 29.22, Dipole is EW

c) Fig. 2.5.2.3-3 Lat. = 29.22, Radiator is Isotropic

d) Fig. 2.5.2.3-4 Lat. = 17.67, Radiator is Isotropic

e) Fig. 2.5.2.3-5 Lat. = 35.4, Radiator is Isotropic

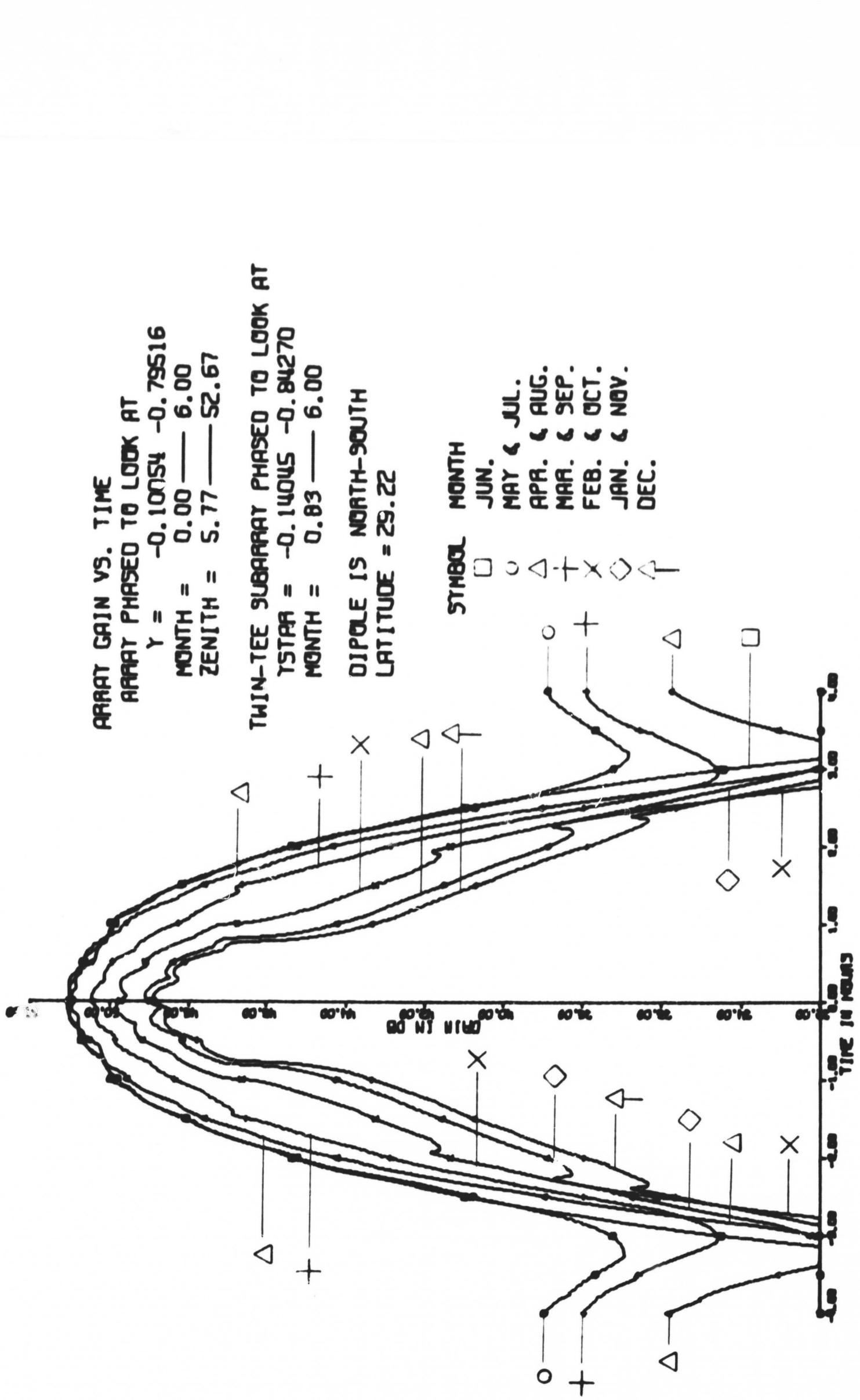

Figure 2.5.2.3 - 1 Gain vs. Time, Latitude = 29.22,Dipole is NS

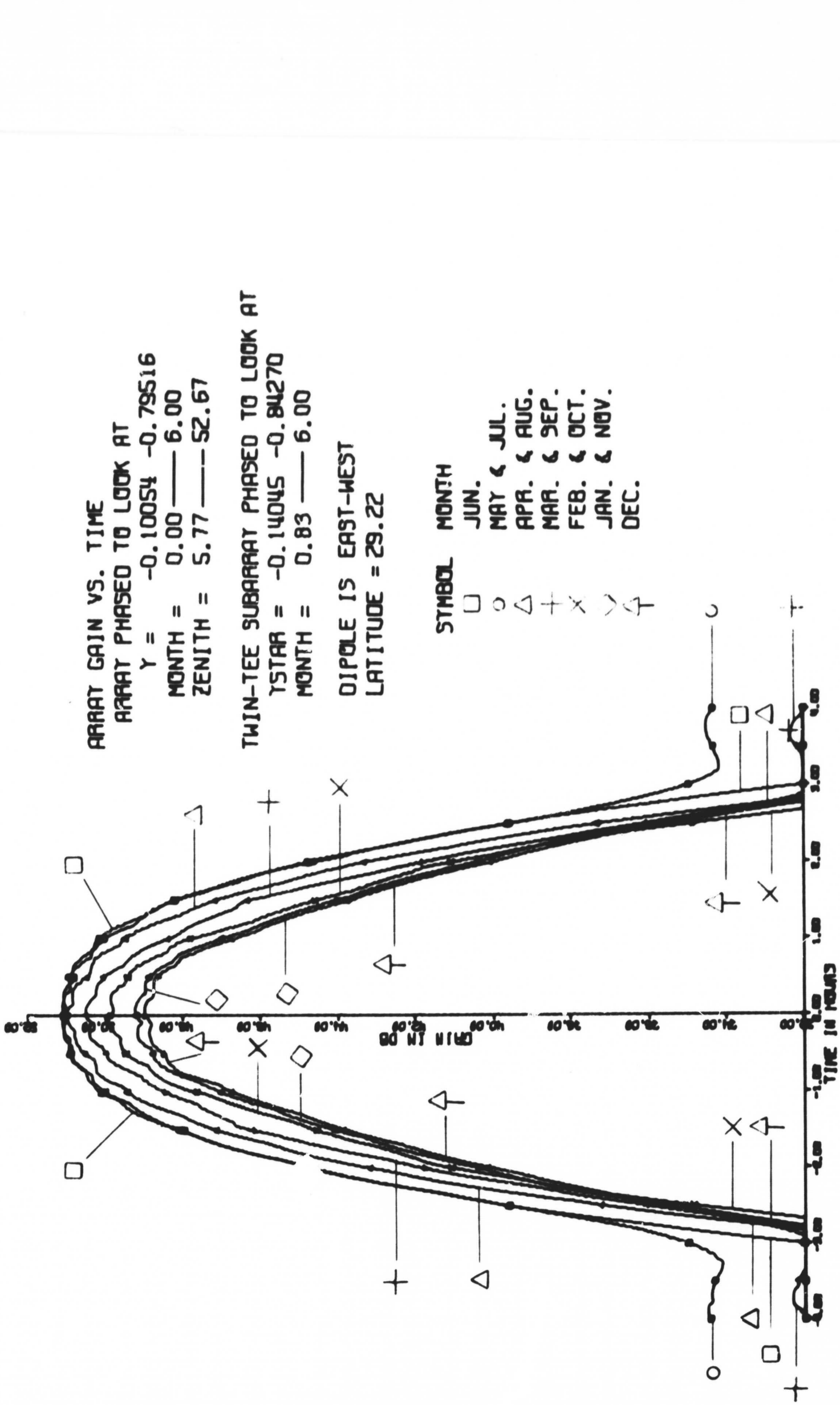

Figure 2.5.2.3 - 2 Gain vs. Time, Latitude = 29.22, Dipole is EW

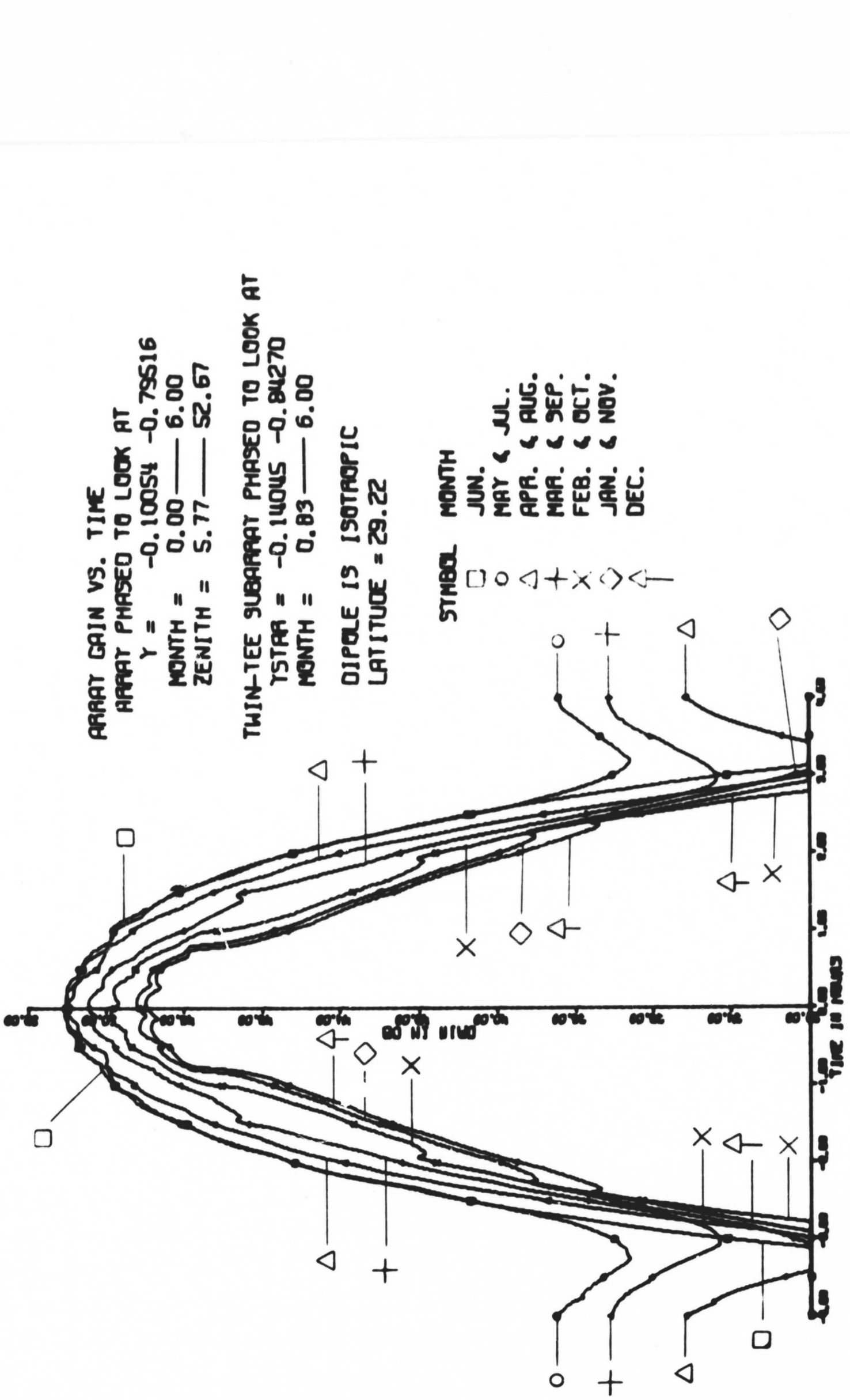

Figure 2.5.2.3 - 3 Gain vs. Time, Latitude = 29.22, Radiator is Isotropic

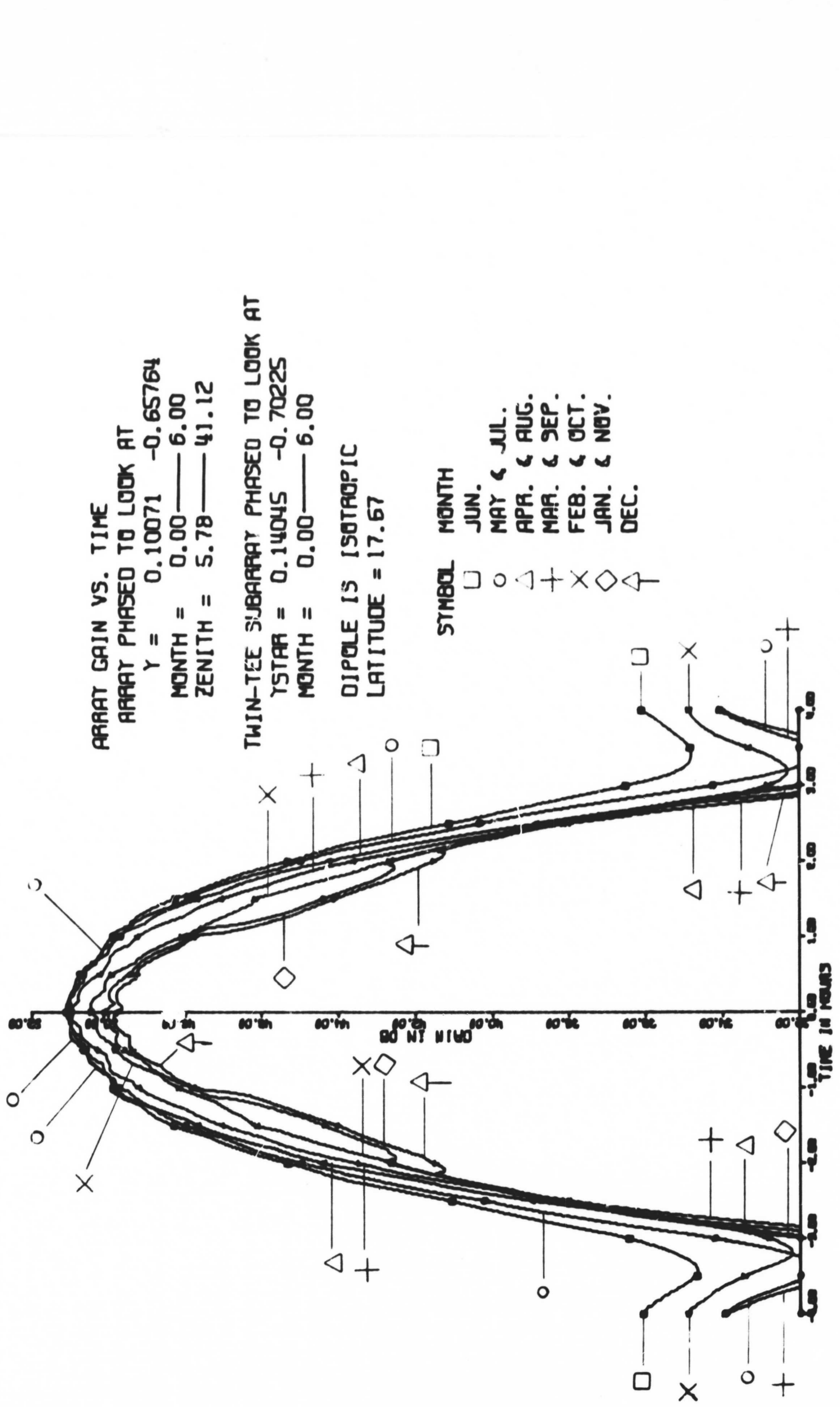

Figure 2.5.2.3 - 4 Gain vs. Time, Latitude = 17.67, Radiator is Isotropic

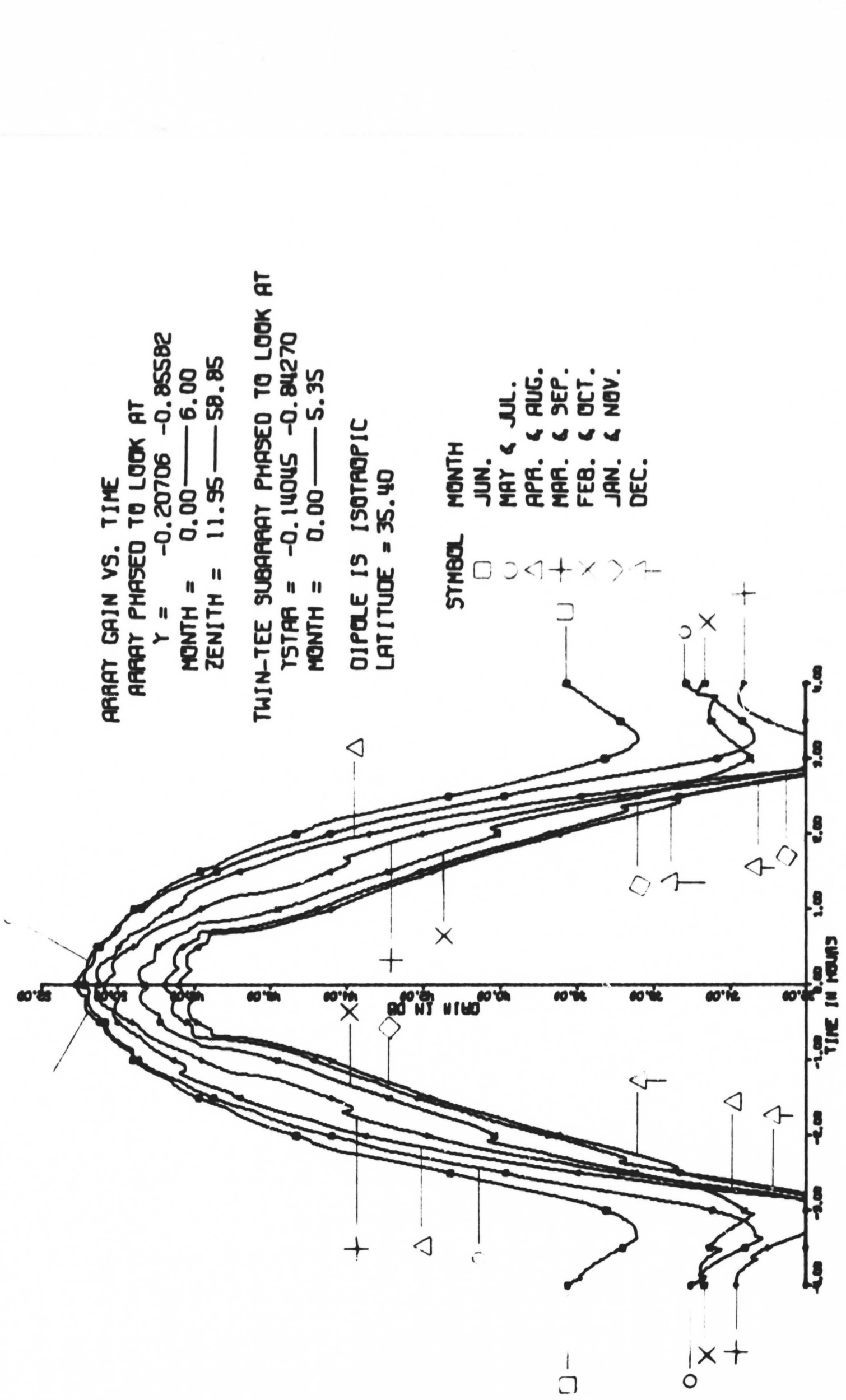

Figure 2.5.2.3 - 5 Gain vs. Time,Latitude = 35.4, Radiator is Isotropic

Figures (c) - (e) show the degradation in performance at higher latitudes.

3) Gain contours. Gain contours show a) the fixed point for which the manual phasings are set (before quantizing), b) ellipses showing variation in time (±1, ±2 hr.) and variation in declination (±10°), c) contours of constant gain in steps of 2 db from 40 db up to a maximum. These contours are intended to show variation of gain vs x and y, and vs time and declination (rather than just vs time for fixed declination, as in (2)). Representative plots here show variation of gain vs month (or declination) of target and vs latitude of array on earth:

a) Fig. 2.5.2.3-6 Lat. = 29.22, Month = 0 (summer)

b) Fig. 2.5.2.3-7 Lat. = 29.22, Month = 3 (spring, fall)

c) Fig. 2.5.2.3-8 Lat. = 29.22, Month = 6 (winter)

d) Fig. 2.5.2.3-9 Lat. = 35.4, Month = 6 (winter)

e) Fig. 2.5.2.3-10 Lat. = 17.67, Month = 6 (winter)

Again the highest latitude is worst, particularly at low declinations, in winter. The irregularity of these contours, and the previous gain curves, is due to the discontinuous manner in which grating lobes appear and disappear on the horizon. The curves show the shrinkage in gain at low declination, near the horizon (particularly at high latitudes).

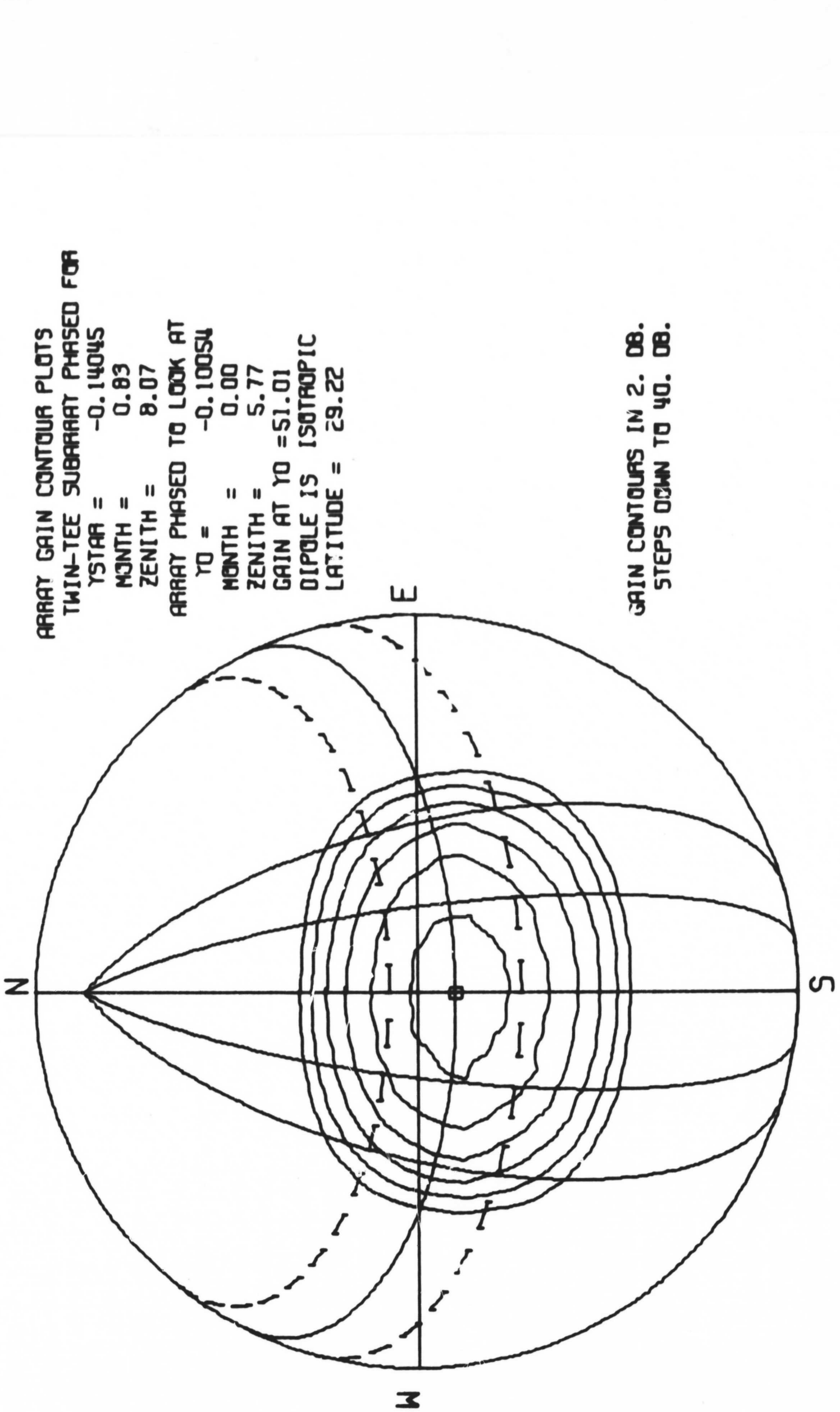

Figure 2.5.2.3 - 6 Gain Contours, Latitude = 29.22, Month = 0.

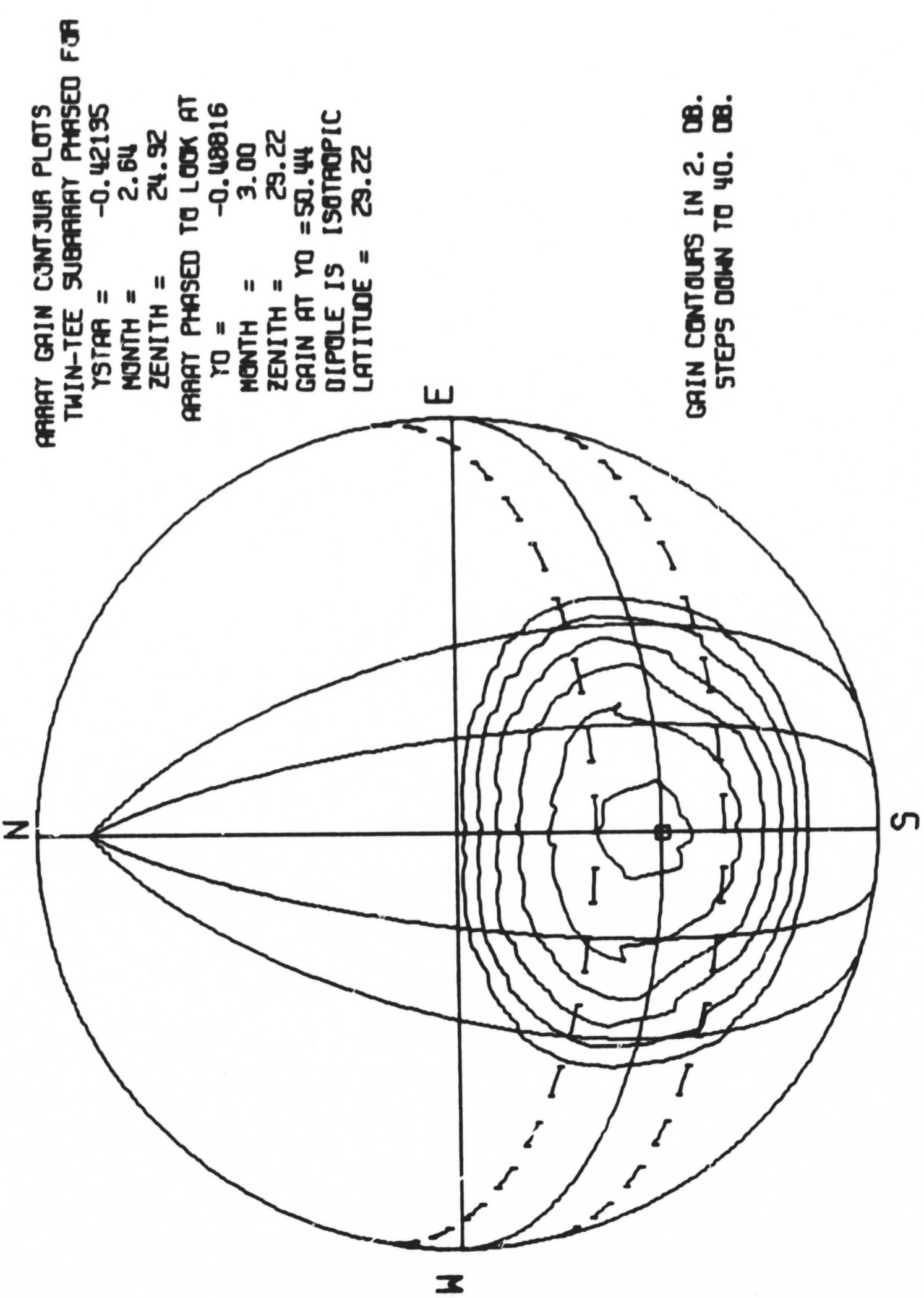

Figure 2.5.2.3 - 7 Gain Contours, Latitude = 29.22, Month = 3.

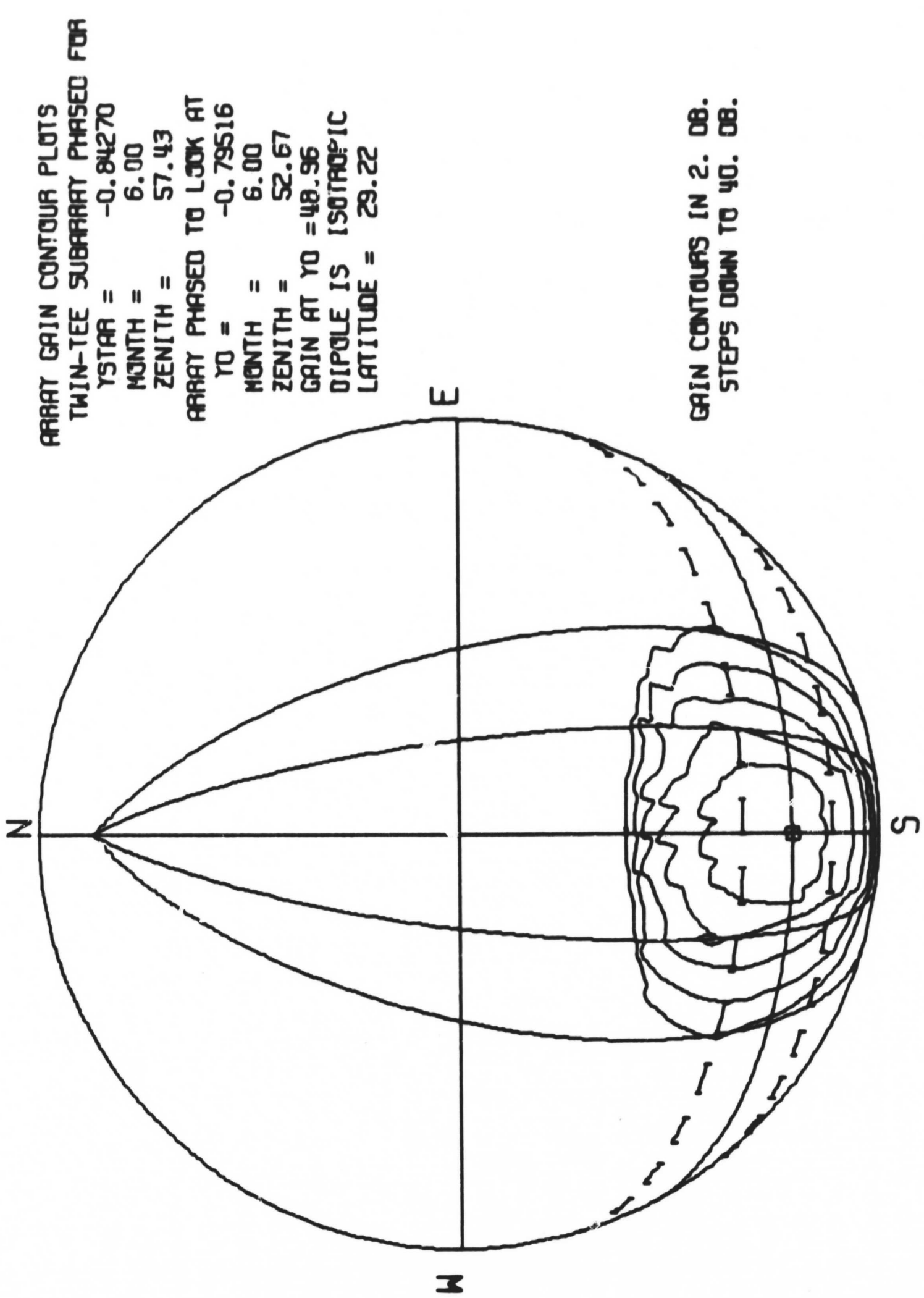

Figure 2.5.2.3 - 8 Gain Contours, Latitude = 29.22, Month = 6.

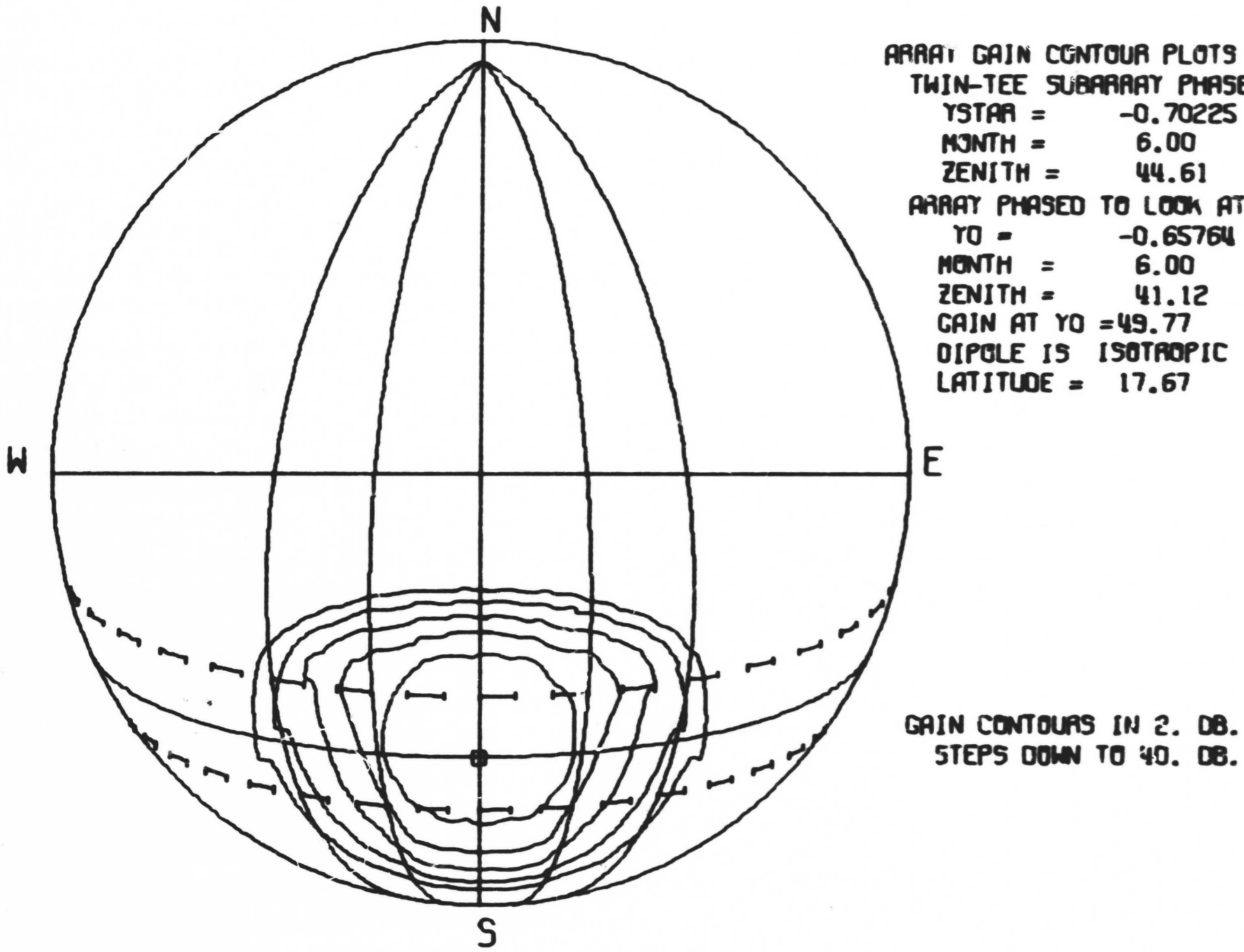

Figure 2.5.2.3 - 9 Gain Contours, Latitude = 17.67, Month = 6.

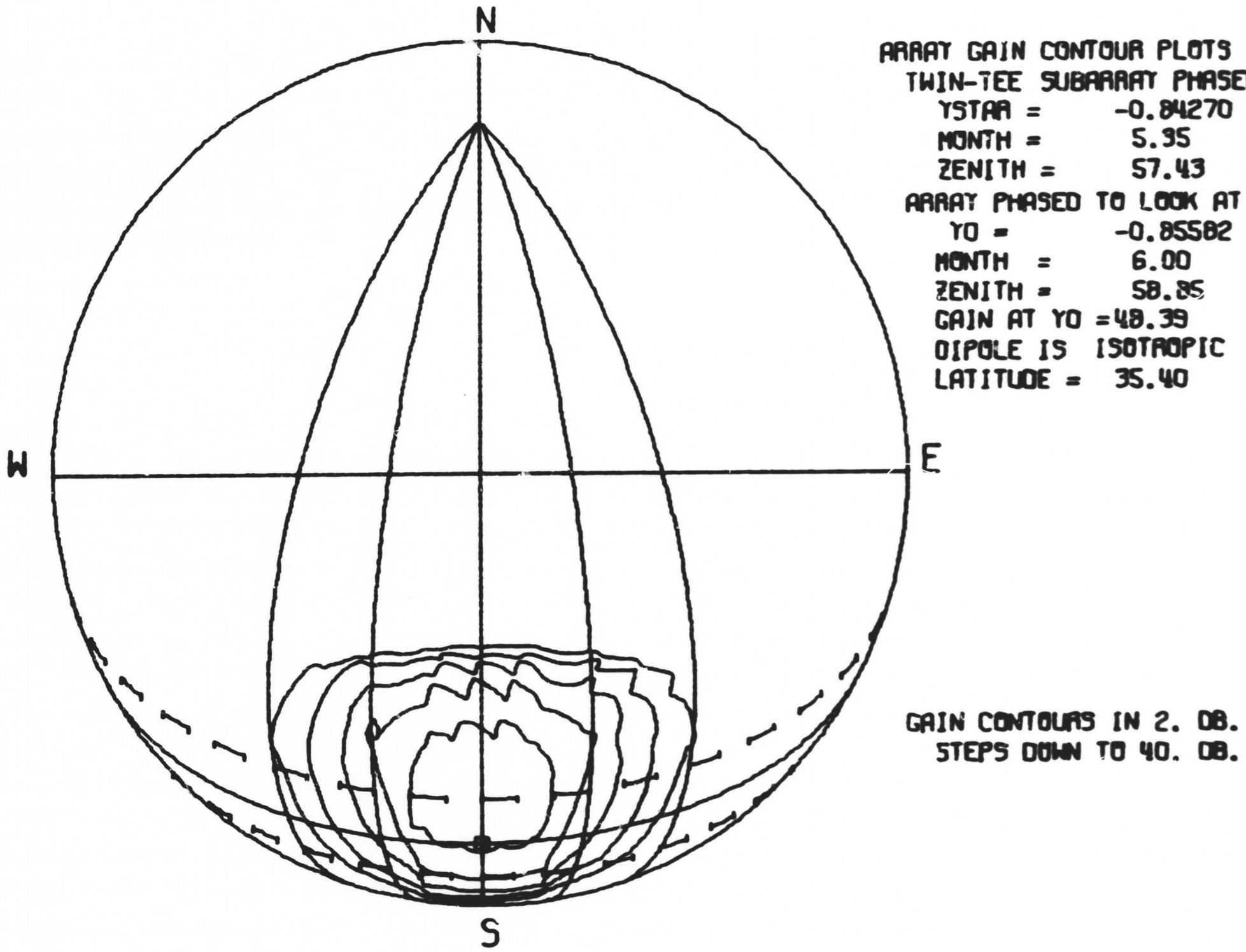

Figure 2.5.2.3 - 10 Gain Contours, Latitude = 35.4, Month = 6.

2.5.3 Noise and Sidelobes

The main reason for deriving a detailed side lobe pattern in Section 2.4.2 (the basic formulas are given at 2.4.2.4-1 and 2.4.2.4-2) is to determine their effect on received noise power in the system. As discussed in Section 2.4.3, the normal location of the largest side lobes is along ridges parallel to the x-y axes in the unit circle, and intersecting at the grating lobes; the detailed nature of the side lobes depends greatly upon the method of phasing the array and the associated phasing errors.

It is apparent that side lobes along the ridges can have a significant effect on the system noise figure, even when the side lobes are in the range of the nominal array factor, or about -30 db relative to the main peak. This level of significance is roughly the amount of solar noise rejection which is necessary to produce about an 1800°K front-end noise temperature, for the typical noise emission of the sun in a neighborhood of 75 MHz. The typical solar noise density, referred to the Earth's surface at 75 MHz is in the range of 2×10^{-22} to 10^{-21} watts/m^2-cps. (See Introduction to Radar Systems, M.I. Skolnik, McGraw-Hill, New York, 1962, PP 370)*. For an array with an area of 1.272×10^5 m^2, corresponding to a gain

---

*Theoretical calculations cited by J.C. James in Radar Astronomy, J.V. Evans and T. Hagfors, McGraw-Hill, New York, 1968, PP 328 indicates that a quiet Sun noise flux of about 1.5×10^{-22} watts/m^2-cps might be expected.

of 50 db, the total incident noise power on the array is in the range k (Boltzmann's constant) times an effective noise temperature of 1.846 to 9.22 million °K. In order to reduce this noise temperature to about 1800°K, a side lobe rejection on the order of 30 to 37 db is required. In fairness, it should be stated that these are averaged side lobe levels, which are expected to be 3 to 6 db below the peak side lobe levels which have been discussed up to this point.

Because side lobe levels of -30 to -37 db are not easy to obtain, it is felt that there may be an unavoidable loss in performance when the Sun (or some other noise source) is at a region in the sky where there is a large side lobe unless means are provided for tailoring the side lobe levels relative to a given noise source. Between the ridges of side lobes, the noise should be relatively low, although there may be some points where solar or galactic noise can hurt if the phasing is particularly ineffective in reducing side lobes.

In theory, it is possible to run curves of receiver noise vs time (similar to the curves of gain vs time, Figures 2.4.2.3-1 through 2.5.2.3-5). However, the problem is very complicated because the noise depends on (1) the detailed side lobe patterns, which depend on the method of phasing which is finally selected, (2) time of year at launch of spacecraft, and (3) time of year at observation. Items (2) and (3) determine the declination of target and the differential right ascension between target and Sun as a function of time.

Practically, a reasonable program might be expected to give launch dates and observation times for which the Sun will pass through a ridge or a region of high side lobes.

2.6 Frequency Sensitivity

When a phased array has a principal beam orientation that is a function of frequency, it is said to have frequency sensitivity. For example, for a given phasing condition the beam axis at 30 MHz may differ from the beam axis at 70 MHz by an angle, $\Delta\theta$. Such an array would have frequency sensitivity, if $\Delta\theta \neq 0$, and would have limitations that may or may not be serious depending upon the application. This limitation would be serious even for a very small $\Delta\theta$, if the average received noise at 70 MHz were subtracted from that at 80 MHz in a signal integration process, and the background noise level were a function of position such as on the Sun.

The amount of frequency sensitivity in a given antenna will depend upon the way in which the phasing is done, and upon the lengths of cables connecting the various elements together. By way of illustration consider the phased array sketched in Figure 2.6-1. This is a line of n dipoles extending over a distance of $100\lambda_1$ (the λ's and f's refer to wave lengths and frequencies at each end of the 70 to 80 MHz band). All dipoles are connected to the receiver by cables of equal length except for small phasing increments, $\phi_k (k = 1, n+1)$. Suppose these phasing increments are adjusted so that the beam axis is at an

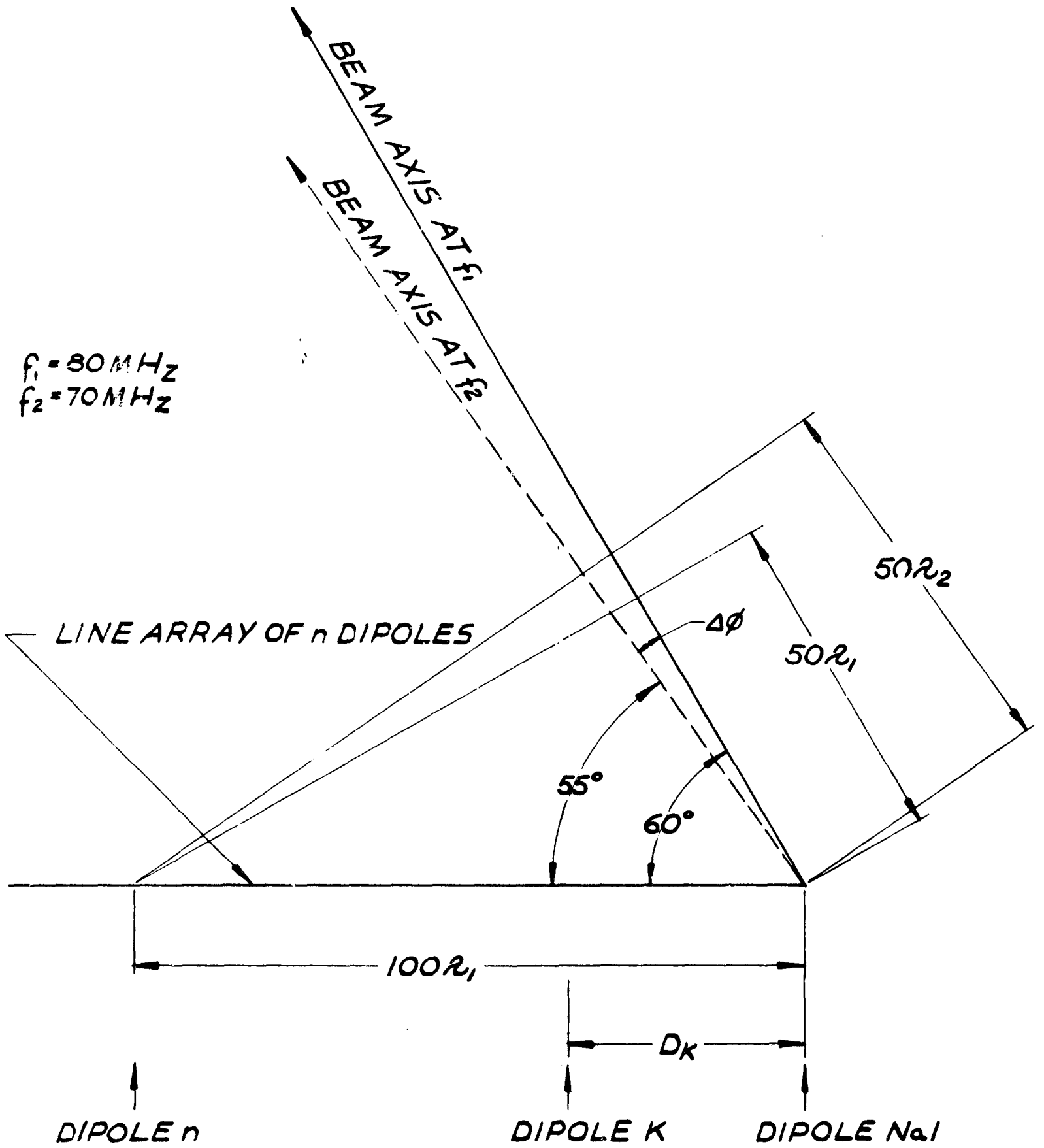

FREQUENCY SENSITIVITY
IN A PHASED ARRAY

FIG. 2.6-1

elevation angle of 60° at f_1. Then for $\phi_1 = 0$ it can be shown that $\phi_{n+1} = 0$, $\phi_{\frac{n+1}{2}} = 0$, $\phi_{\frac{n+1}{4}} = \pi$, and in general

$$\phi_k = N\lambda_1 - \frac{D_k}{\lambda_1} \cos 60° \qquad (2.6\text{-}1)$$

where N is an integer and D_k is the distance from dipole 1 to dipole k. At frequency f_2 this array would have the main beam oriented at elevation angle θ such that for every dipole the following relation would be approximately correct.

$$\frac{D_k}{\lambda_1} \cos \theta + \phi_k = N\lambda_2 \qquad (2.6\text{-}2)$$

A few examples should convince one that θ is about 55° so that $\Delta\theta \approx 5°$. This is large compared with the beamwidth of this array which is about 0.6°, and could not be tolerated for the Sunblazer application.

The straightforward method of eliminating frequency sensitivity is to arrange the feed cable lengths so that the travel times of all signal components from any wave front in space to the receiver is the same. Phasing cables longer than one-half wavelength may be used to phase such an array, and the array might more properly be called a time-delay array.[5] Some compormise between a time delay and a phased array system

are allowable provided that a small amount of frequency sensitivity can be tolerated.

2.7 Mutual Coupling

An analysis of mutual coupling effects, is usually simplified by assuming an infinite array of elements. Of the proposed three arrays, pilot, expanded, and 50 db; the 50 db system qualifies as an infinite array since it is approximately 100λ by 100λ. For example, in the 50 db system the perimeter to area ratio is $.04\lambda^{-1}$ while in the expanded array this ratio is $.11\lambda^{-1}$ and in the pilot array $.44\lambda^{-1}$. The array may be considered to be composed of two zones; the central zone in which all the elements may be considered to be in an infinite array environment, and an edge effect zone.

The significance of edge effects is not pattern degradation due to mismatch, because it can be argued that the periphiral elements are less effected by mutual coupling and therefore more closely matched to their connecting transmission lines. Edge effects contribute to impedance variations across the aperture and interact with the electronic signal combining systems. In this sense they add phase and gain variations to elements near the perimeter of the array. In general each element along the periphery of the antenna has an output impedance which is different from its neighbors, while all the elements in the central portion of the array have the same output impedance. Analytically edge effects are difficult to

estimate since the specific array geometry must be considered and coupling coefficients computed between every element in the array. This usually involves the summation of slowly convergent series and yields little insight into the problem of mutual coupling.

A more convenient and physically intuitive method of considering the mutual coupling problem is to view the large array as an infinitely large periodic structure. Since there are no edge effects to consider, each dipole has the same active impedance, $Z_a(\theta,\phi)$ and Z_a is only a function of the angular position (θ,ϕ) of the main beam. The periodic structure concept is particularly useful since it permits a scale model simulation of the infinite array. A simulation, which utilizes waveguide imaging properties, is described in the literature.[3,7] It has been used at the Center to study the expected mutual coupling effects of the large dipole array. The results of this study are given below.

The infinite array waveguide simulation method permits a rapid measurement of active resistance and reactance as a function of scan angle. This impedance variation interacts with the input impedance of the electronic system and results in a mismatch loss. In the large array, phase and amplitude errors due to edge effects will be small because the impedance of most of the elements change in the same way. Under the assumption that only impedance mismatch degrades system performance the realized gain $G_r(\theta,\phi)$, in any direction, relative

to the idealized or peak directive gain in that direction may be expressed as:

$$\frac{G_r(\theta,\phi)}{G_d(\theta,\phi)} = 1 - |R(\theta,\phi)|^2 \qquad (2.7\text{-}1)$$

where $|R(\theta,\phi)|^2$ is the ratio of returned power to incident power due to mismatch loss and is a function of beam position. For the cases of practical interest $R(\theta,\phi)$ may be related to the active impedance Z_a and the antenna connecting transmission line characteristic impedance Z_o by the relationship:

$$R(\theta,\phi) = \frac{Z_a(\theta,\phi) - Z_o}{Z_a(\theta,\phi) + Z_o} \qquad (2.7\text{-}2)$$

For a large uniformity excited planar array in which no grating lobes are present the directive gain is a function of beam pointing angle and is given by

$$G_d(\theta,\phi) = \frac{4\pi NA}{\lambda^2} \cos\theta \qquad (2.7\text{-}3)$$

where A is the physical area associated with each element, N is the total number of elements and θ is the beam pointing angle measured from the zenith. The cos θ factor accounts for the reduced array aperture as the beam is steered from the zenith. For a 50 db array; N = 26,880, A = $(.63\lambda)^2$ and for the

zenith looking array (cos θ = 1) the gain, G, is 51.2 db. The net realized gain per element is denoted as g where:

$$\frac{G}{N} = g = 6.95 \text{ db} \qquad (2.7\text{-}4)$$

Now at each element the net realized gain will be reduced due to mismatch. This effect may be expressed as a function of beam position by combining the above expressions as:

$$g_r(\theta,\phi) = \frac{4\pi A}{\lambda^2} \cos\theta \left[1 - |R(\theta,\phi)|^2\right] \qquad (2.7\text{-}5)$$

Now if a one db mutual coupling gain loss is allowed (g = 5.95 db) and assuming θ = 15°, then the maximum permissible value of |R| is .44. This implies the connecting transmission lines may be mismatched to the dipoles with a VSWR of about 2.6:1 before there is a significant mutual coupling gain loss.

In the above example it appears that mutual coupling does have a determental effect on the gain of the proposed large antenna. On the other hand these effects are of manageable proportions and do not impose a fundamental limit on array operation. Array performance depends not so much on one parameter, but the compromises between many conflicting design considerations. This point may be illustrated by considering the selection of the dipole spacing which represents a compromise between low mutual coupling and grating lobe free operation. This final selection of .63λ echelon

dipole spacing was made on the basis of experience with the 38 MHz solar radar which has been confirmed by additional laboratory and field experiments.

For a large uniformly excited array, in which all elements are individually phased, the maximum angle θ_{max} to which the beam may be scanned without grating lobe interference is related to the element spacing D/λ by:

$$D/\lambda = \frac{1}{1 + \sin \theta_{max}} \qquad (2.7\text{-}6)$$

For a spacing of 0.63λ, θ_{max} is limited to 36°. It should be noted that Equation (2.7-6) is only approximately valid for the Double-Tee configuration since all the elements of the Double-Tee are not individually phased. In addition, grating lobes may be enhanced or reduced according to the electronic system organization and for precise results these effects should be taken into account. However, Equation (2.7-6) does give a first order estimate of the region of grating lobe free operation. In general, reduced grating lobes require a high element density per unit area whereas low mutual coupling for non-directive elements, requires a low element density. The $.63\lambda$ spacing was selected as a compromise value based upon equivalent electrical area. From this point of view the gain of single dipole above a ground plane is 7.48 db. This corresponds to an equivalent effective area of $(.67\lambda)^2$. When the spacing is reduced to $.63\lambda$, the net gain per dipole is

reduced to 6.95 db. This gain penalty is in addition to the mismatch loss outlined above and represents another system loss due to mutual coupling considerations. Conversely the grating lobe problem has been reduced somewhat. The region of grating lobe free operation has been increased from 30° for .67λ spacing to 36° for the .63λ spacing.

Several experiments were conducted, using the .63λ spacing, to determine the extent of the mismatch loss. A series of measurements were made at the El Campo, Texas field site using a small aperture (16 element array). Input VSWR was measured on all elements as a function of scan angle from 0° to 60°. The tests were repeated for various dipole lengths and it was determined that a 68 inch dipole (.43λ) yielded the lowest r.m.s. value of the voltage standing wave ratio. The highest VSWR was 3.94 and the lowest was 1.05 with the r.m.s. value of all elements for all scan angles being 1.76. As expected the center elements displayed a higher VSWR than the periphiral elements[6].

An independent estimate of the expected VSWR was made by the waveguide simulation method[7]. In these measurements the active input impedance of an infinite array of half wavelength crossed dipoles spaced a quarter of a wavelength above a ground plane was measured using an L band waveguide simulator. The results of these measurements are shown in Figure 2.7-1. Here a maximum VSWR of 2.3 was observed when beam scanning was limited to the grating lobe free region. As the beam scan angle was increased to include grating lobe affects the observed

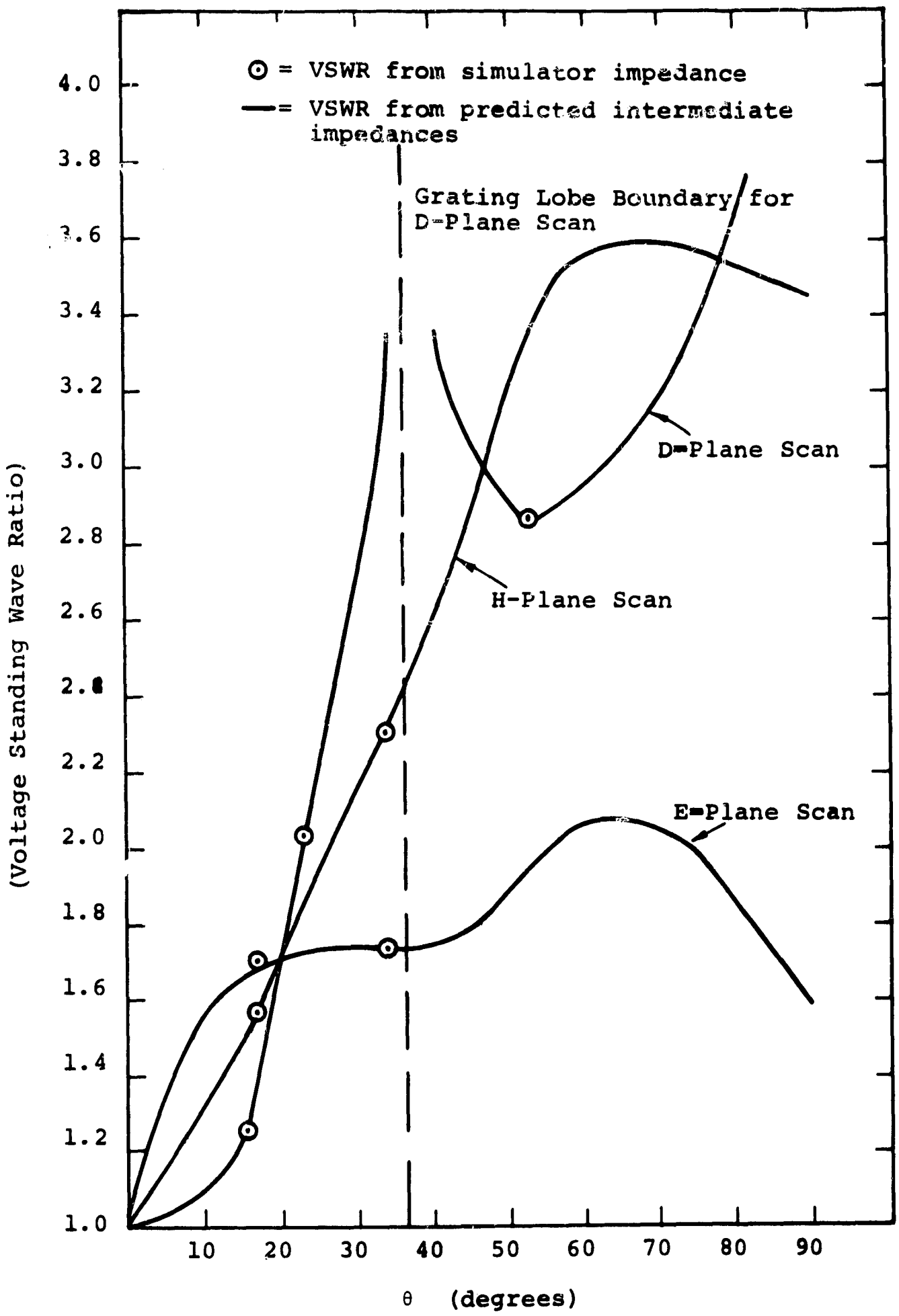

Figure 2.7-1 Dipole Feed Line Voltage Standing Wave Ratio vs Array Scan Angle

For an infinite .63λ echelon array of $\lambda/2$ dipoles, $\lambda/4$ above ground plane

VSWR increased to 2.8:1. However, in this mode of operation, the simulator studies are only approximate. In the grating lobe free region good correlation was obtained between the finite array and the simulator studies. It is expected that the design experience gained from evaluating mutual coupling in the pilot array will be directly applicable to both the expanded (40 db) array and the 50 db array.

2.8 Noise Considerations

2.8.1 Noise Model

This section will define some of the factors which contribute to the total system noise. In the final array, each 14 db element will have its own amplifier. However, for noise analysis purposes it is sufficient to consider the entire array as one antenna followed by a single amplifier as shown in the array system noise model of Figure 2.8.1-1. Noise may enter the system or be generated by each of the components, the antenna, connecting cables, and receiver. The major contributions to the system noise are as follows:

1) Background sky noise characterized by the brightness temperature T_B. The intensity of this quantity is primarily a function of the system operating frequency, and the direction of beam pointing. For the Sunblazer ground array an average value of 1800°K is characteristic.
2) Noise due to antenna side lobes and grating lobes

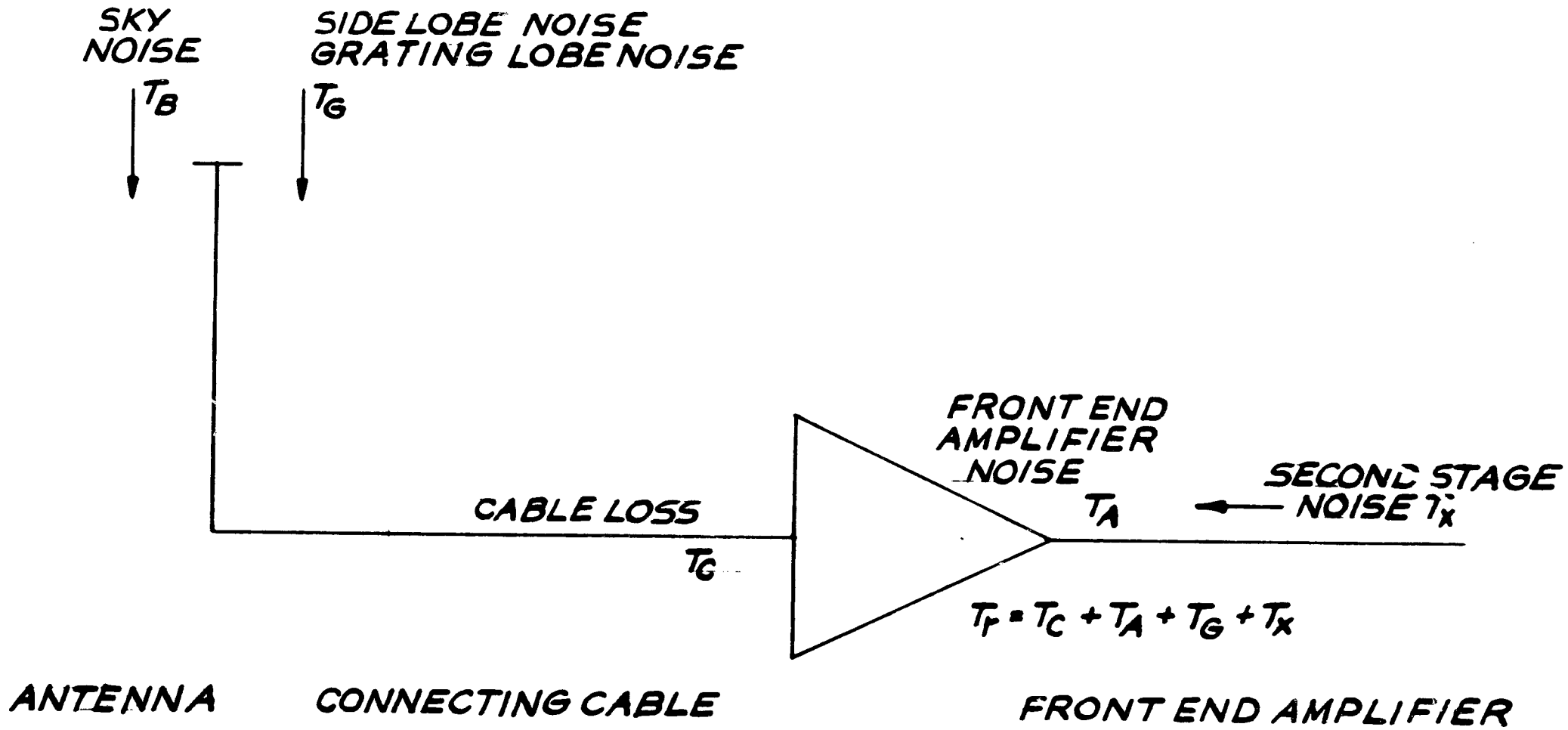

NOISE MODEL

FIG. 2.8.1-1

pointing at galactic hot spots. (T_G) The average value of this quantity has been estimated as 250°K. Over short periods of time, when system grating lobes and galactic hot spots are favorably aligned the peak value of T_G will be much higher than 250°K. Under certain rare conditions a total system black-out may occur. Estimates of the effect of side lobes are given in Section 2.5. The peak value of T_G is very much dependent upon the pattern and system organization and will vary over a wide range.

3) Noise due to antenna element losses, cable losses, impedance mismatches, mutual coupling, etc. The major component in this class of losses is mutual coupling. An allowance of 1 db or 75°K has been made for these effects, as outlined in Section 2.7.

4) Front-end amplifier noise. For the design under consideration a value of 3 db or 290°K is typical. Section 5.2 discusses the noise properties of the front-end amplifier.

5) Second stage noise contribution. Due to the insertion loss of the time delay networks the noise generated by the second and later stages of the receiver will contribute to overall system temperature. In Section 2.8.2, a detailed analysis of the second stage noise contribution is given. The second stage adds approximately 100° to the receiver temperature.

6) Spurious man-made noise entering the antenna at or near the desired signal frequencies. Additional noise may be added by intermodulation and cross modulation products due to high level signals entering the amplifier. The exact specification of intermodulation and cross modulation depends upon local conditions but as an example; for competing TV signals of the order of 50μ volts intermodulation and cross modulation products should be down by 80 db for good system performance. These specifications and high system dynamic ranges are related and both are required for a highly linear system. Section 5.2 discusses intermodulation in more detail.

Neglecting the intermodulation noise, the total receiver temperature is 665°. Therefore, the total equivalent system noise temperature is $T_n + T_R = 2500° = T_s$.

2.8.1.1 Antenna Calibration Using Extraterrestrial Radio Sources

Although discrete sky sources (hot spots) may contribute to total system noise, they are useful in a practical way for antenna calibration purposes. In the 50 db array, the near field of the antenna $(\frac{2D^2}{\lambda})$ extends to an altitude of approximately 100 kilometers above the surface of the earth. This distance is so large that only a system utilizing a satellite could be expected to perform conventional far field pattern measurements. However, a radio star such as Cassiopeia A,

provides a solution for this measurement problem. The measurement is performed by directing the beam of the array toward a source of known intensity and spectral distribution. As the beam is allowed to pass through the source, the output of the array is a measure of the gain of the antenna elements, the electronics and the beamwidth of the antenna. This test is also an indication of the accuracy with which the beam may be steered. A similar method was used to test the narrow band 75 MHz 128 dipole experimental receiving array which was constructed at El Campo in connection with this study (Appendix 7.2).

2.8.2 Second Stage Noise Contribution

In the R.F. signal combining system the received energy is coherently combined by a series of time delay networks. The design details of these circuits are given in Section 5.3. The sertion loss of these networks contributes to overall system noise temperature by an amount which depends not only upon the overall system gain, but upon the placement of the various stages of amplification and the amount of insertion loss between these stages.

There are four cases to be considered. These are shown in simplified form in Figure 2.8.2-1, and correspond to variations in the placement of the second level of amplification. In Case I, this second amplifier is placed between the "y" and "z" time delay circuits. In Case II, the amplifier

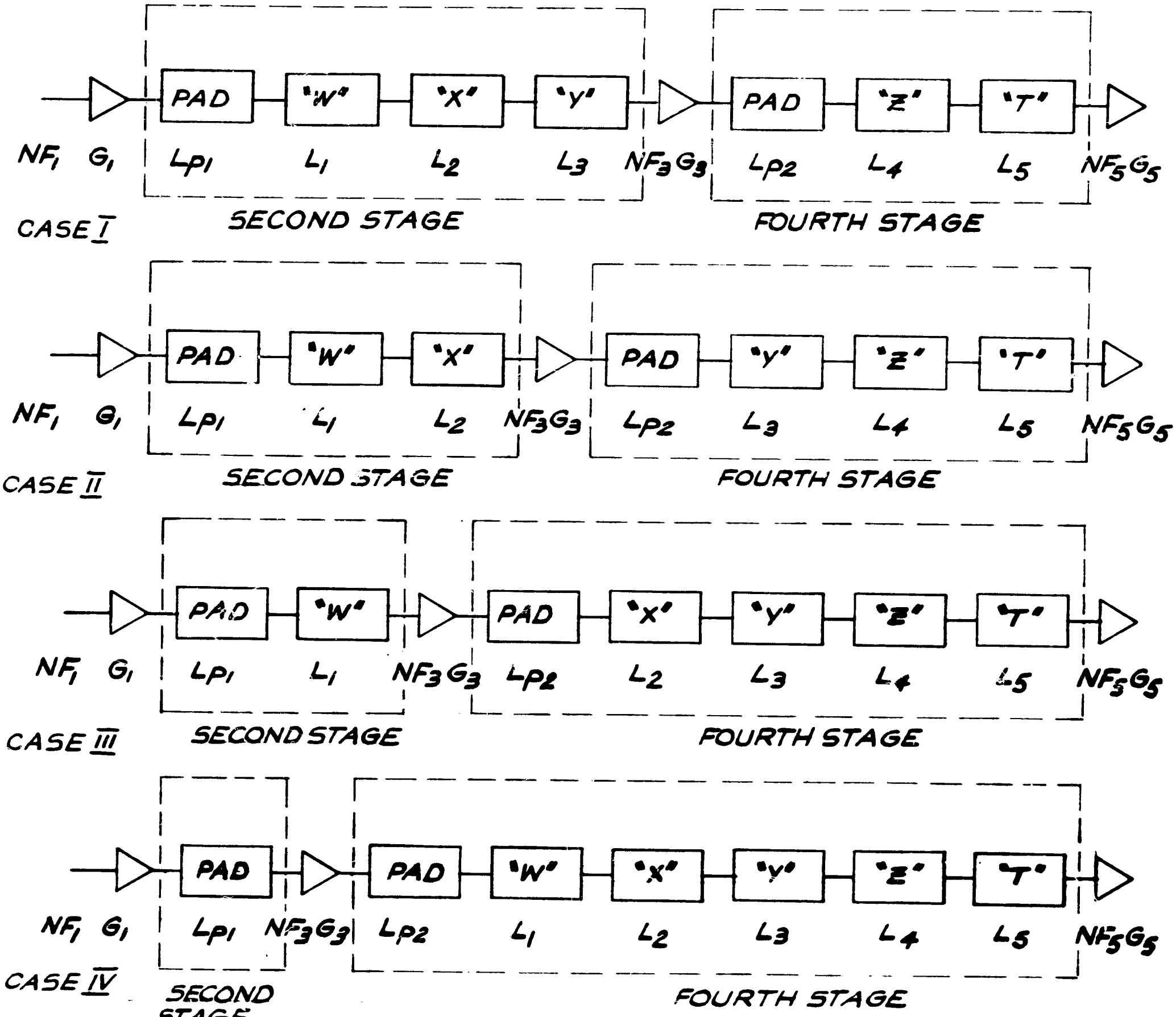

AMPLIFIER PLACEMENT FIG. 2.8.2 -1

is between the "x" and "y" time delay circuits. In Case III, the amplifier is between the "w" and "x" networks and finally Case IV is for a two-stage input amplifier. Note that in each case the receiver is composed of five stages and it is merely the boundary of the stages that changes from case to case.

The active devices are characterized by power gains G_1, G_3, and G_5 and noise factors NF_1, NF_2, NF_5. The combination of device and pad losses is equivalent to the net circuit gain. The pads and time delay networks are characterized by power loss factors L_{P1}, L_{P2}, L_1, L_2, L_3. L_4, L_5. The noise factor of a passive lossy network is 1/L where L is power loss factor of the network. Table 2.8.2-1 gives the gains and noise factors of each stage for Cases I through IV. By applying the cascade formula for a five-stage receiver the system noise factor, NF_s, is obtained in terms of the component stage power gains G_1, G_2, G_3, G_4, and noise factors NF_1, NF_2, NF_3, NF_4, NF_5 as:

$$NF_s = NF_1 + \frac{NF_2 - 1}{G_1} + \frac{NF_3 - 1}{G_2G_1} + \frac{NF_4 - 1}{G_1G_2G_3} + \frac{NF_5 - 1}{G_1G_2G_3G_4}$$

Direct substitution of the values from Table 2.8.2-1 yields the following expressions for system noise factor in each case:

Case I

$$NF_{s1} = NF_1 + \frac{1}{G_1}\left[\frac{1}{L_{P1}L_1L_2L_3} - 1\right] + \frac{1}{G_1L_{P1}L_1L_2L_3}[NF_3 - 1] +$$

$$+ \frac{1}{G_1 G_3 L_{P1} L_1 L_2 L_3}\left[\frac{1}{L_{P2} L_4 L_5} - 1\right] +$$

$$+ \frac{1}{G_1 G_3 L_{P1} L_{P2} L_1 L_2 L_3 L_4 L_5}[NF_5 \quad 1]$$

Case II

$$NF_{s2} = NF_1 + \frac{1}{G_1}\left[\frac{1}{L_{P1} L_1 L_2} - 1\right] + \frac{1}{G_1 L_{P1} L_1 L_2}[NF_3 - 1] +$$

$$+ \frac{1}{G_1 G_3 L_{P1} L_1 L_2}\left[\frac{1}{L_{P2} L_3 L_4 L_5} - 1\right] +$$

$$+ \frac{1}{G_1 G_3 L_{P1} L_{P2} L_1 L_2 L_3 L_4 L_5}[NF_5 - 1]$$

Case III

$$NF_{s3} = NF_1 + \frac{1}{G_1}\left[\frac{1}{L_{P1} L_1} - 1\right] + \frac{1}{G_1 L_{P1} L_1}[NF_3 - 1] +$$

$$+ \frac{1}{G_1 G_3 L_{P1} L_1}\left[\frac{1}{L_{P2} L_2 L_3 L_4 L_5} - 1\right] +$$

$$+ \frac{1}{G_1 G_3 L_{P1} L_{P2} L_1 L_2 L_3 L_4 L_5}[NF_5 - 1]$$

Case IV

$$NF_{s4} = NF_1 + \frac{1}{G_1}\left[\frac{1}{L_{P1}} - 1\right] + \frac{1}{G_1 L_{P1}}[NF_3 - 1] +$$

$$+ \frac{1}{G_1 G_3 L_{P1}}\left[\frac{1}{L_{P2} L_1 L_2 L_3 L_4 L_5} - 1\right] +$$

$$+ \frac{1}{G_1 G_3 L_{P1} L_{P2} L_1 L_2 L_3 L_4 L_5}[NF_5 - 1]$$

In Figure 2.8.2-2 these four equations have been plotted as functions of the amplifier noise figure using the assumed values:

$$G_1 = G_3 = 23 \text{ db}$$

$$L_{P1} = L_{P2} = L_1 = L_2 = L_3 = L_4 = L_5 = 5 \text{ db}$$

In Figure 2.8.2-3 system excess noise temperature has been plotted as a function of amplifier noise figure using Case IV as a standard. In other words, Figure 2.8.2-3 represents the difference in °K between Cases IV and III, IV and II, and finally IV and I.

Examination of these sets of curves show that either Case II, III or IV is satisfactory from the system noise point of view. However, Case II is utilized because it is considerably less complex.

	STAGE I		STAGE II		STAGE III		STAGE IV		STAGE V	
	Power Gain G_1	Noise Factor NF_1	Power Gain G_2	Noise Factor NF_2	Power Gain G_3	Noise Factor NF_3	Power Gain G_4	Noise Factor NF_4	Power Gain G_5	Noise Factor NF_5
CASE I	G_1	NF_1	$L_{P1}L_1L_2L_3$	$\frac{1}{L_{P1}L_1L_2L_3}$	G_3	NF_3	$L_{P2}L_4L_5$	$\frac{1}{L_{P2}L_4L_5}$	G_5	NF_5
CASE II	G_1	NF_1	$L_{P1}L_1L_2$	$\frac{1}{L_{P1}L_1L_2}$	G_3	NF_3	$L_{P2}L_3L_4L_5$	$\frac{1}{L_{P2}L_3L_4L_5}$	G_5	NF_5
CASE III	G_1	NF_1	$L_{P1}L_1$	$\frac{1}{L_{P1}L_1}$	G_3	NF_3	$L_{P2}L_2L_3L_4L_5$	$\frac{1}{L_{P2}L_2L_3L_4L_5}$	G_5	NF_5
CASE IV	G_1	NF_1	L_{P1}	$\frac{1}{L_{P1}}$	G_3	NF_3	$L_{P2}L_1L_2L_3L_4L_5$	$\frac{1}{L_{P2}L_1L_2L_3L_4L_5}$	G_5	NF_5

TABLE 2.8.2-1

GAIN AND NOISE FACTORS

FIG. 2.8.2-2

SYSTEM NOISE FIGURE
VS
DEVICE NOISE FIGURE

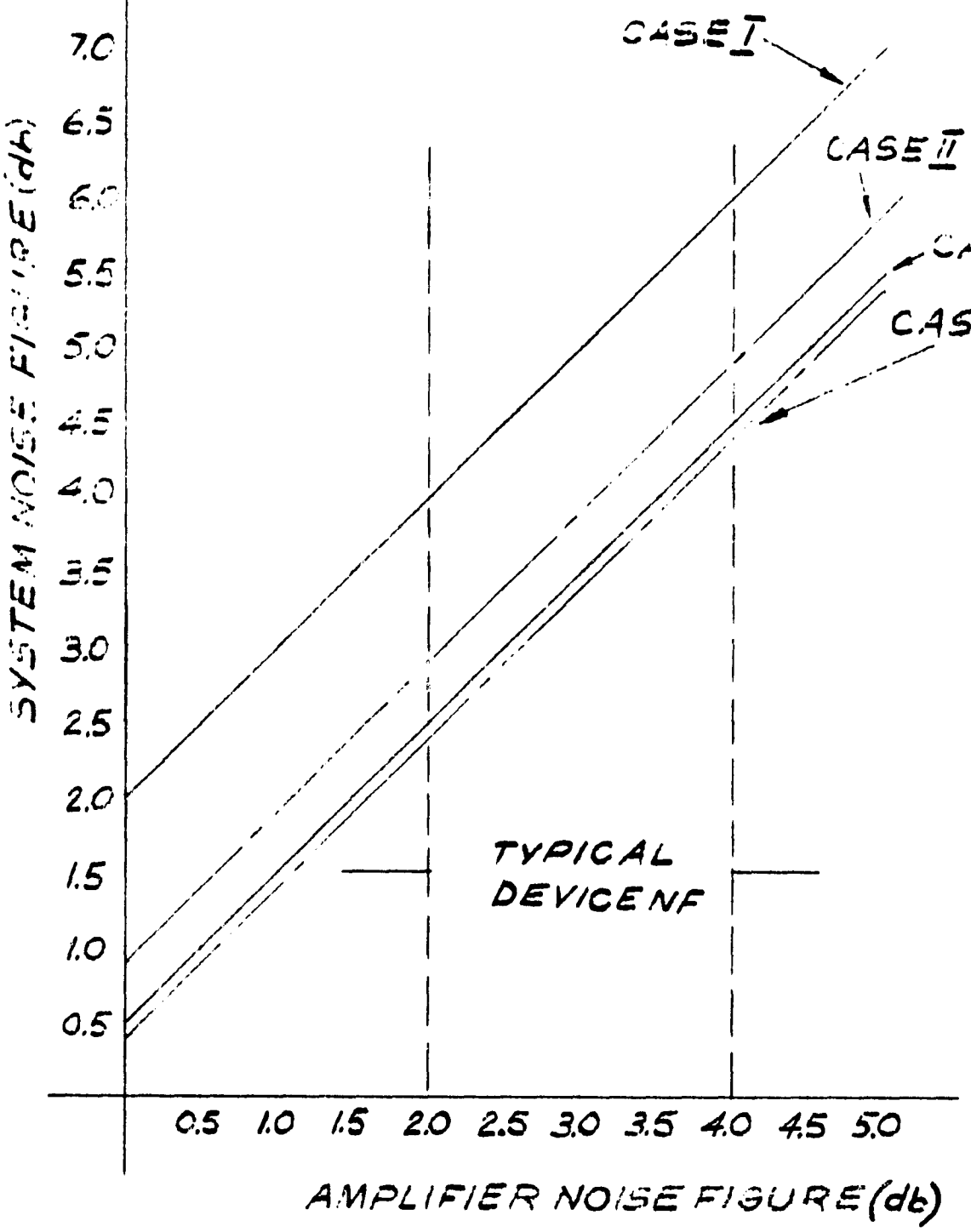

FIG. 2.8.2-3

EXCESS NOISE TEMPERATURE
VS
AMPLIFIER NOISE FIGURE

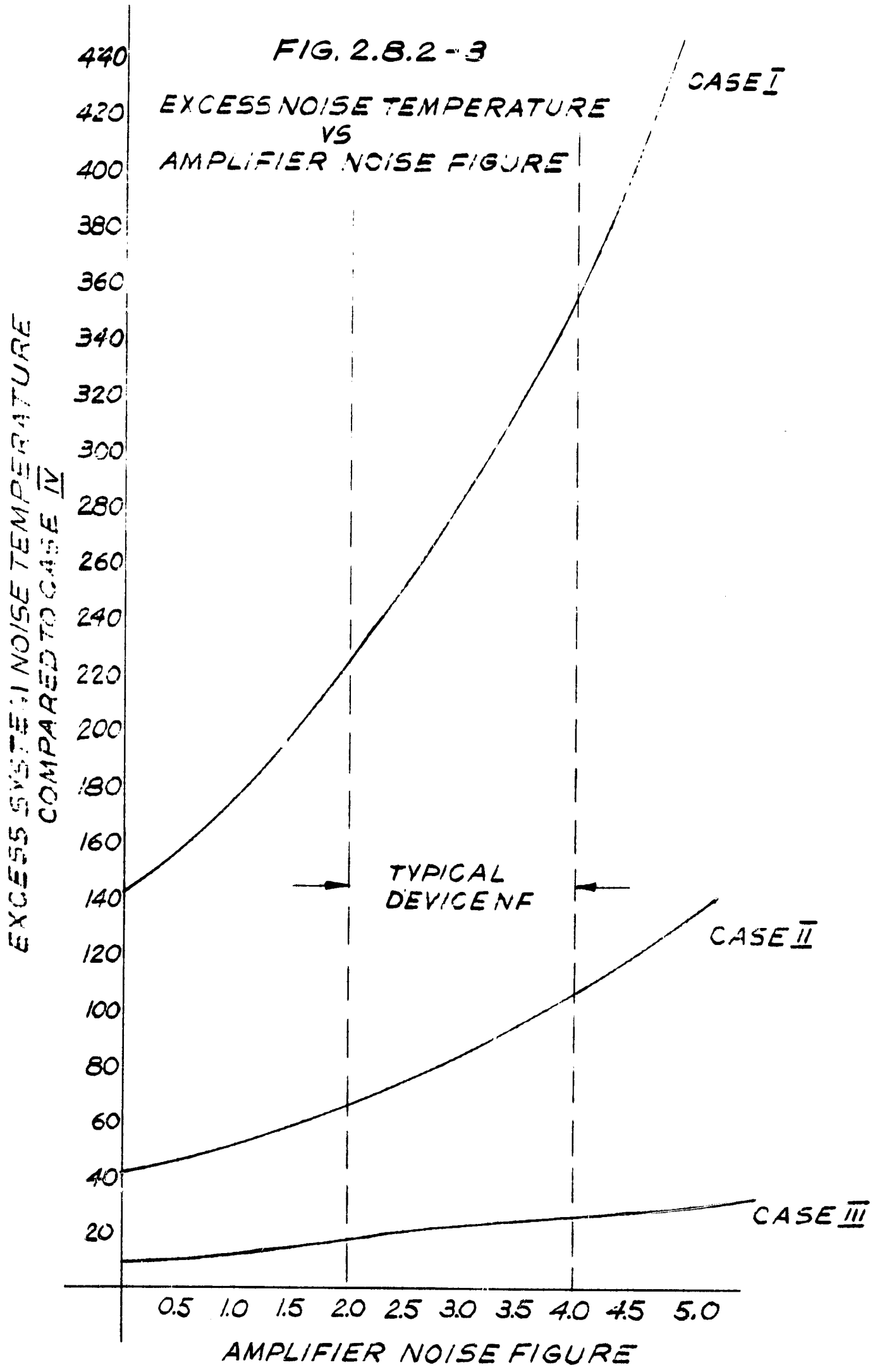

2.8.3 Site Noise Considerations

Because the background noise temperature T_B is relatively large compared to the receiver noise temperature T_r, improvements in receiver noise performance will have only a second order effect on the overall system noise temperature. However even when $T_B > T_R$, T_R has a large effect on the effective noise of band comparison experiments. System noise performance can be improved by careful site selection and seriously degraded by a high interference environment. Local RFI conditions are of primary importance and the final site selected for the 50 db array should be shielded from unwanted frequency interference or be located in a remote area free of man-made noise. Section 7.1 gives the details of recent surveys of potential sites.

El Campo, Texas is over 125 miles from the nearest co-channel TV station. At this distance and because dipole elements are close to the ground, little interference difficulty is to be expected. Indeed, experience with the existing dipole antenna (128 dipole 75 MHz narrow band system) confirms this conclusion because to date no interferring signals near 75 MHz have been observed with this system. However, with a directive yagi antenna which has been used to conduct an RFI survey several weak signals near 75 MHz have been observed. In general, average man-made noise is low due to the remoteness of the site.

The existing 38 MHz array has experienced RFI interference caused by ionospheric bounce on certain occasions when solar

activity was very high. At 75 MHz this effect will not occur because the ionosphere is not highly reflective in this frequency range. The 38 MHz array, when transmitting, is also a source of potential interference. In a recent test of the 75 MHz narrow band dipole array, the only observable effect due to the 38 MHz transmissions was an increase of about 1/2 db in overall system noise. This is surprisingly small considering the close proximity of the 500 KW transmitter operating near the first sub-harmonic of the 75 MHz array. During the critical periods of the Sunblazer tracking operations the solar radar will not transmit and therefore no interference from the existing 38 MHz system is expected.

2.9 References

1. E. A. Wolff, "Antenna Analysis", John Wiley and Son, January 1968, Page 243.

2. J. L. Allen, "The Theory and Array Antennas (with emphasis on radar applications)", Lincoln Laboratory Technical Report 323, July 1963, Page 10.

3. R. C. Hansen, "Microwave Scanning Antennas", Academic Press, 1964, Pages 29-35.

4. R. H. Baker, et al., "History and Design Summary, Sunblazer Phased Array, CSR, September 1968.

5. J. L. Allen, "Array Antennas: New Applications for an Old Technique", IEEE Spectrum, November 1964, Pages 115-130.

6. J. C. James, "75 Mc Test Array", CSR, July 1967.

7. M. A. Bucciarelli, "Dipole Array Simulation by Means of a Waveguide Obstacle Array Model," CSR-T-64-4, January 1969.

8. R. H. Baker, et al., "The Conceptual Design of a Small Solar Probe", MIT-CSR-TR-69-1, 1969.

CHAPTER 3

3.0 REALIZATION OF THE 50 db ARRAY

The governing design philosophy for the 50 db array is to: (1) design and construct a pilot array, (2) thoroughly test this pilot array, and (3) based on these tests finalize the design and construct a large array by joining these self-contained pilot units together to obtain the desired system gain. The array electronic system concept has been presented in Section 2.3.4. In this Chapter, we will detail the signal combining system in regard to types of cables and components, the number of circuits for each of the three arrays, pilot, expanded and 50 db system. The detail circuit description, i.e. component and transistor types, used in laboratory experiments is given in Section 5.

3.1 Pilot Array

3.1.1 Pilot Array General Consideration

The radio energy incident upon the dipoles of the double tee element is combined by means of a cable and mercury switch phasing system. As shown in Figure 2.2-1,

the cables which connect the dipoles to summing points a and b and the 75 ohm phasing cables are of the R.G. 11 A/U type. The three-quarter wavelength matching transformers and the output cables are of the RG 8 A/U cable type. The 100 ohm phasing cable is currently constructed of RG 62 A/U (Z_o = 93 ohm), but a larger cable, similar to RG 133 should be used in the final array. The output of the double tee element is supplied to a low noise broadband amplifier.

The outputs from the field amplifiers are returned to a central electronics enclosure via a direct burial aluminum sheathed cable. This cable, Foamflex, is manufactured by Phelps Dodge Corp. and the recommended type is FXA-38-50H. The phase-temperature stability is 25 ppm/°C and the attenuation is 0.7 db per 100 feet at 75 MHz. The cost of Foamflex is $257/1000 feet and connectors are available at approximately $7 each. The final system uses only a limited number of connectors because most field interconnections are hard wired. Therefore, the relatively high cost connectors for Foamflex are not expected to add significantly to overall system cost. Trenching is required to insure relatively constant operating temperature and resulting phase stability for all buried cables.

The Foamflex cable returns the R.F. signals to a central electronics enclosure which houses all the R.F. and

control circuits required to coherently sum the received signals. In Table 3.1.1-1 these circuits are listed according to type and number required for the pilot array. A brief statement of the major circuit specifications is also given in the table. Table 3.1.1-2 summarizes the number of circuits required for each array. Table 3.1.1-3 gives a summary of the various system components.

TABLE 3.1.1-1
Pilot Array Electronics (Cross Polarized)

Circuit Type	Number Required	Description and/or Major Specifications
Broadband * Amplifier	80	Noise Figure = 3 db 3 db Bandwidth = 30 mc Gain = 17.5 db average
Time Delay and Summation Network "W"	32	Maximum Delay = 1 7/8λ_o in λ_o/8 steps Insertion Loss = 6 db max. Amplitude Variation = 1 db Coherently combines two signals from 14 db element
Time Delay and Summation Network "X"	16	Maximum Delay = 3 7/8λ_o in λ_o/8 steps Insertion Loss = 6 db max. Amplitude Variation = 1 db Coherently combines two signals from network "W"
Time Delay and Summation Network "Y"	8	Maximum Delay = 1 7/8λ_o in λ_o/8 steps Insertion Loss = 6 db max. Amplitude Variation = 1 db Coherently combines two signals from network "X"
Time Delay and Summation Network "Z"	4	Maximum Delay = 3 7/8λ_o in λ_o/8 steps Insertion Loss = 6 db max. Amplitude Variation = 1 db Coherently combines two signals from network "Y"
Time Delay and Summation Network "T"	2	Maximum Delay = 7 7/8λ_o in λ_o/8 steps Insertion Loss = 7 db max. Amplitude Variation = 1 db Coherently combines tow signals from network "Z"
Fixed Delay	4	2.67λ_o phase equalizing cable
Power Supply	1	120 v ac @ 1.1 amp 130.0 watts input 3 v dc @ 1.2 amp 3.6 watts 8 v dc @ 10.0 amp 80.0 watts 15 v dc @ .4 amp 6.0 watts
Logic	4	5 and 6 bit counters with SCR drivers for beam pointing control

Quantities for El Campo System

	PILOT	EXPANDED PILOT	50 db
Field RF Amplifier	64	1024	8960
Time Delay 1W	16	256	2240
Time Delay 2X	8	128	1120
Time Delay 3Y (plus amp.)	4	64	560
Time Delay 4Z	4	64	560
Time Delay 5T	2	32	280
Power Supply	1	16	140
Logic Digital Control Circuit	1	16	140

TABLE 3.1.1-2

TABLE 3.1.1-3

System Type	Number of Dual Double Tee Elements	Number of Mercury Switches	Number of Field Amplifier	Number of Central Enclosures
Pilot	32	448	64	1
Expanded 40 db	512	7168	1024	16
50 db	4480	61720	8960	140

3.1.2 Testing Considerations

The primary reason for the construction of a pilot array is to obtain engineering data on design and performance problems such as amplifier and phase shifter uniformity, mutual coupling effects precise antenna gain, losses, etc. that cannot be precisely calculated. An exact determination of such effects will be made as the array is constructed and tested. The theoretical performance including gain and effect of grating lobes and mutual coupling will be experimentally verified. The reliability of the field electronics will be determined under actual weather and working conditions.

After the array is constructed an overall evaluation will be made by using known celestial sources. Cassiopeia, Cygnus, and the Sun may be used for the pilot array, and Virgo, Taurus, and several others including pulsating sources may be used to test the 40 db array.

3.2 Expanded Array

3.2.1 General Comments

Since the pilot array is completely self-contained, i.e. it is designed as a "module", an increase in array effective aperture may be obtained by adding pilot array modules to realize the desired gain. Two pilot modules

will yield a gain improvement of 3 db, four modules will result in 6 db improvement, etc. For the Sunblazer engineering payload, the required minimum receiving system gain which will provide satisfactory telemetry and tracking data is about 40 db which can be realized by expanding or adding 15 pilot arrays as indicated in Figure 3.2.1-1. A summary of the antenna system characteristics for the expanded array is given in Table 2.3.3-1. A breakdown of system components is given in Table 3.1-3.

3.2.2 Expanded 40 db Array Electronics

Each of the pilot array outputs are returned to a central building. The electronic circuits for each of the 16 pilot arrays are identical to the system described above, but additional electronics to shift the phase of the R.F. signal from each pilot and sum the results must be constructed.

Figure 3.2.2-1 shows a block diagram of the electronic system to shift the phase and sum the signals. As for the pilot, the signal energy from adjacent segments is summed in pairs, then the two pairs are summed and finally the columns are treed together to form one output per polarization.

The time delay networks W', X;, Y', and Z' are identical in design to those of the pilot array (W, X, Y, and Z) except that extra stages of cable loops are added to

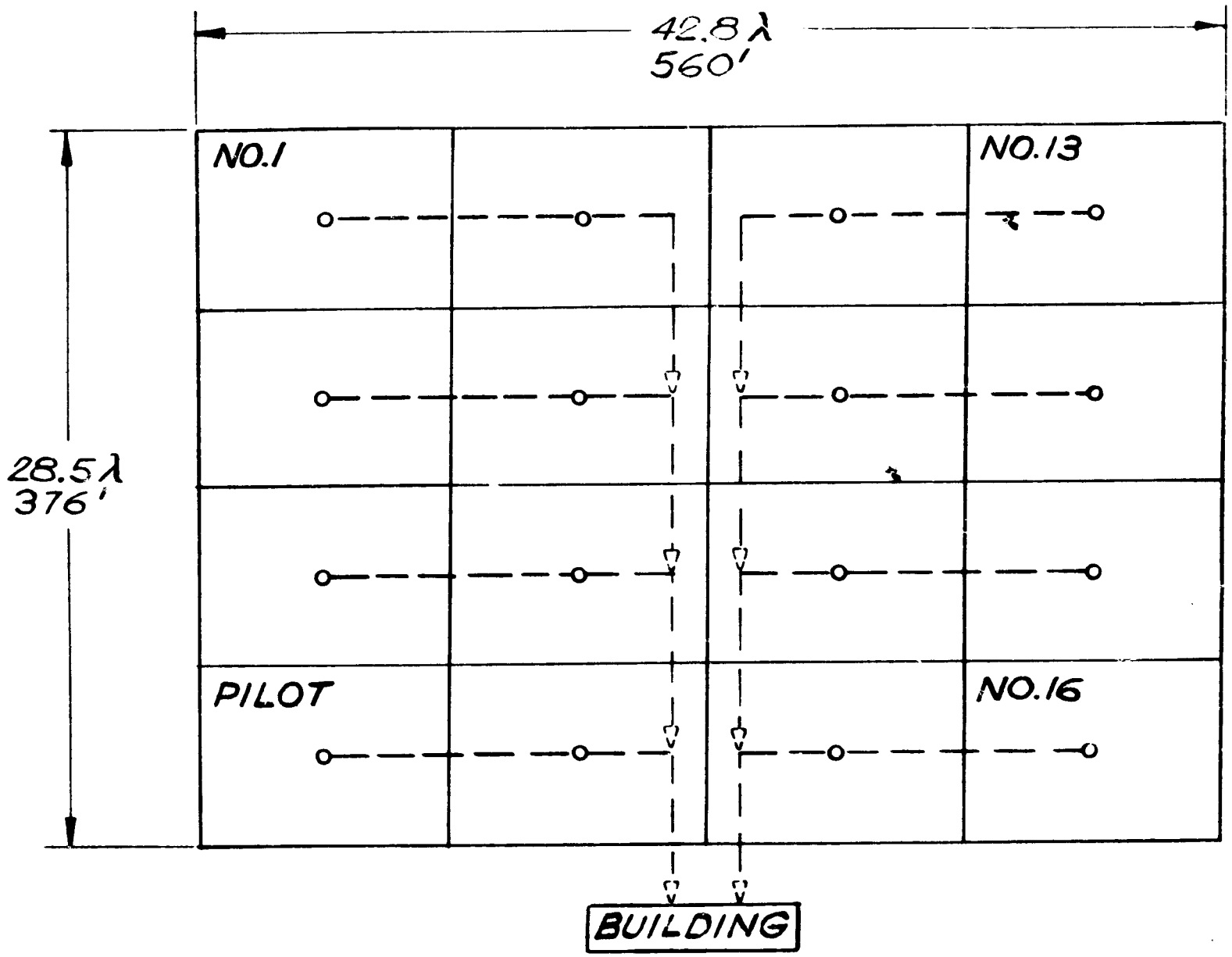

EXPANDED 40db ARRAY

FIG. 3.2.1-1

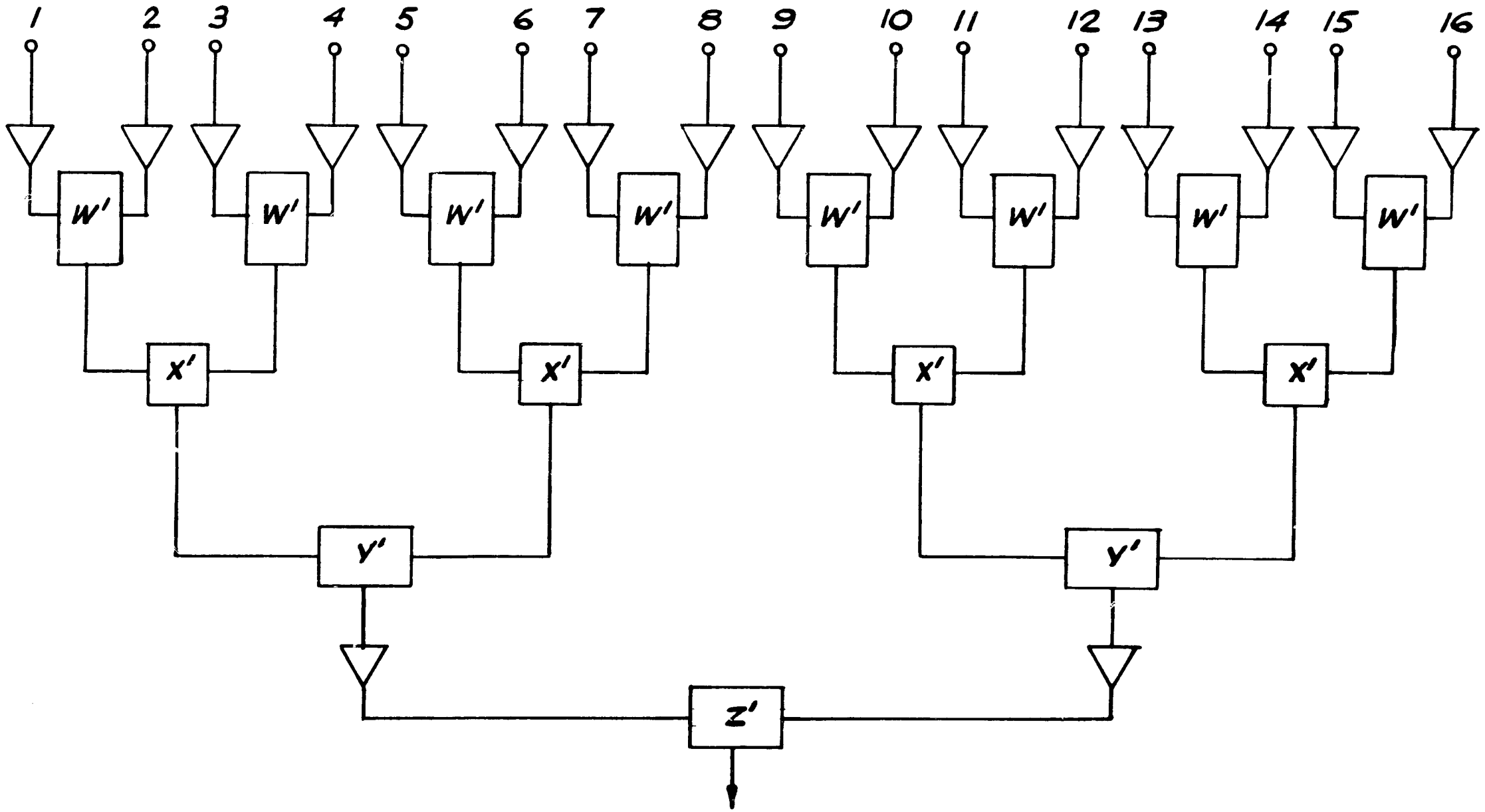

FIG. 3.2.2-1
ELECTRONIC SYSTEM
PHASE SHIFT AND SIGNAL
SUMMATION

accommodate increased delay resulting from the fact that the signals come from phase centers which are more widely separated in physical distance.

3.2.3 Testing

Each segment of the expanded array will be tested individually as an antenna in a similar manner as the original pilot section, and then the resulting sum will be characterized for gain, noise figure, beamwidth, bandwidth, etc. The central building (control center) for the array will contain the necessary equipment to operate; i.e. steer, receive, record signals, etc. from the Sunblazer engineering shot. System noise performance will be evaluated and necessary changes in the electronic system organization will be made at this time, if required (see Section 2.5.3 for a discussion of the system trade-offs).

3.3 50 db System

The experience gained in the electronic system design, element design, mutual coupling effects, construction and test of both the expanded array and pilot system would provide an excellent foundation for the realization of the 50 db array. Design difficulties encountered in expanding the 40 db system into a 50 db array should be minimal.

The orderly growth and expansion procedure will minimize the likelihood of any fundamental problem remaining unsolved prior to the construction of the final system and therefore the cost of realizing the final 50 db system would largely be in materials and services. These items will be purchased to specifications, which are currently in preliminary form, but which are to be finalized during the construction and test of the pilot and expanded array systems.

The 50 db array concept and layout is shown in Figure 2.3.3-2. It consists of 140 pilot systems arrayed in a physically square 14 x 10 matrix. The outputs of each of the pilot array is returned to central building which houses all the higher level phasing circuits, monopulsing, receiving and control subsystems, the 140 field enclosures and amplifiers located at each double tee will be similar to the circuits described in this report. The final designs will be modified by the experience gained in the 40 db system construction, especially in regard to site hardening, environmental considerations, and installation procedures.

The delay and summation circuits for the higher level signal combining system have not as yet been designed. Additional study is required here to optimize the signal combining system to reduce the effect of phasing errors, at the higher levels, on side lobe and grating lobe pattern structure.

3.4 Site Installation and Testing

3.4.1 Installation Requirements

After the site has been selected and preliminary surveying done, the first task in constructing the array is to level the land. When the ground is used as a reflecting screen, its flatness and roughness affect the antenna characteristics. The rms deviation of ground level should be no more than six inches over the entire plot, except for a few well placed drainage ditches. The use of an artificial ground screen may change this requirement.

Ground excavation is expensive and care should be taken in selecting the site so that a minimum amount of excavation is required. A 16-acre plot was excavated at El Campo with a bulldozer and maintainer so that the plot is now flat with an rms deviation of about 0.2 foot about a plane with a slope of zero in the east-west direction and a slope of 1/1000 toward the south. Initially, the plot was flat except for a 9 inch ridge along the center. This excavation work cost us a little less than $2,000 which is a reminder that ground flattening is expensive even for rockless, relatively flat, ground.

Other items of ground preparation may include a road and perhaps a fence around the plot. Also some thought must be given to the type of ground cover that is to be used. A ground cover is needed to prevent mud, dust, and erosion. Gravel, shell, or crushed rock would be satisfactory but is expensive. Most grasses would require some type of mowing either by a mechanical mower or by animals such as sheep. The antenna will not be usable when a gasoline driven mower is mowing in the field. A mower with an electric induction motor might be satisfactory provided its silhouette is low enough so that it can mow under the dipoles. Another problem with the grass is the fire hazard during the wintertime. However, the danger of fire can be reduced if proper precautions are taken. A type of grass called Ophiopogon Japonica is evergreen and requires no mowing. It has been used in some areas at the El Campo site. However this grass is probably too expensive at 5¢/ft^2. The ground-cover solution will probably be a native grass which is controlled with mowing and with herbicides. Herbicides exist and have been used in El Campo that do such things as kill the weeds without killing the grass, slow the growth of all plants, and prevent seeds from germinating.

The next task in the construction of the array is the installation of the posts that support the dipoles. These posts may either be aluminum or treated wood. Treated wood posts are easier to work with and are cheaper,

and have lifetimes of at least 20 years.

Over 1000 creosoted fir posts have been in use for 9 years at El Campo and none have failed. About 500 pentachlorophenal treated yellow pine posts have been in service for 6 years and none of them have failed. The pentacholorophenol preservative is more pleasant than the creosote to work with. The posts should be pressure treated by the supplier, but the buyer should have samples tested to be sure the proper amount of preservative was added. A U.S. Forest Service test on 96 pertachlorophenal yellow pine posts showed only one failure due to decay after 22 years of service. (See "Comparison of Wood Preservatives in Mississippi Post Study, 1961 Progress Report," January, 1961, No. 1757, U.S. Department of Agriculture, Forest Service.)

An accurate surveying job is required for the placement of the posts. No posts should be placed more than six inches from its ideal location. Trenches for the underground cables also should be accurately dug and records kept of their location. Posts can be easily and quickly installed by having a tractor with an auger dig a post hole about three feet deep. The post is then inserted and the hole backfilled with sand. These suggested procedures have been used at El Campo.

The first cables installed should be for the 110 volt power outlets which should be distributed well over

the entire plot. These cables should be followed by the installation of the control cables, the R.F. cables, and the aluminum power cables for the transmitting devices. Communication lines should also be installed in the same trenches. The phase length of each R.F. cable should be accurately measured, preferably with an admittance bridge. A time-domain reflectometer can be used provided a standard cable is used as a pattern and frequent checks are made with the standard cable. After all lines are installed the trenches should be covered, the ground surface smoothed, and grass planted.

The R.F. amplifier will likely be supplied with the flexible harness attached. If so, these should be installed after the other cables.

The next task to perform is the installation of electronics which includes the central amplifiers and the phase shifters. This task will require electronic technicians whereas much of the installation requires unskilled labor. The receiving amplifiers should be placed under the ground, but the power amplifiers should be placed above the ground for ventilation.

Finally, the dipoles are installed on the posts and lead cables attached to the dipoles. Any ground screen cables should be installed just before the dipoles.

Over a period of five years various experimental dipoles and mounts have been time and weather tested at

El Campo. A very strong yet lightweight dipole is a section of 1 1/2" x 0.050" wall tubing. This can be fully supported by a wooden dowel which has been impregnated with paraffin, and which attaches directly to the post. These wooden mounts have excellent weathering properties and have resistances no lower than one megohm even during a rain. Many have been in service at El Campo for several years. A tool has been designed and used for quickly inserting the dipoles onto the mount. Most plastic mounts deteriorate in the sun, and are more expensive.

A balun is not needed for a half-wave dipole. This is especially true when the dipole is one-fourth wavelength above ground. None of the several El Campo arrays have baluns. Two former arrays did, but the performance was no better due to the baluns. An extensive series of impedance measurements were made at 75 MHz on a dipole with and without a balun. For this series of tests, various length feed lines were used. The feed lines were better matched to the dipoles without baluns. The reason for this was the self inductance of the short length of wire used to connect the balun to the dipole. The reason no balun is needed for the half-wave dipole is illustrated in Figure 3.4.1-1. The impedance of a single long line is several hundred ohms, and the impedance of a line that is partially shorted

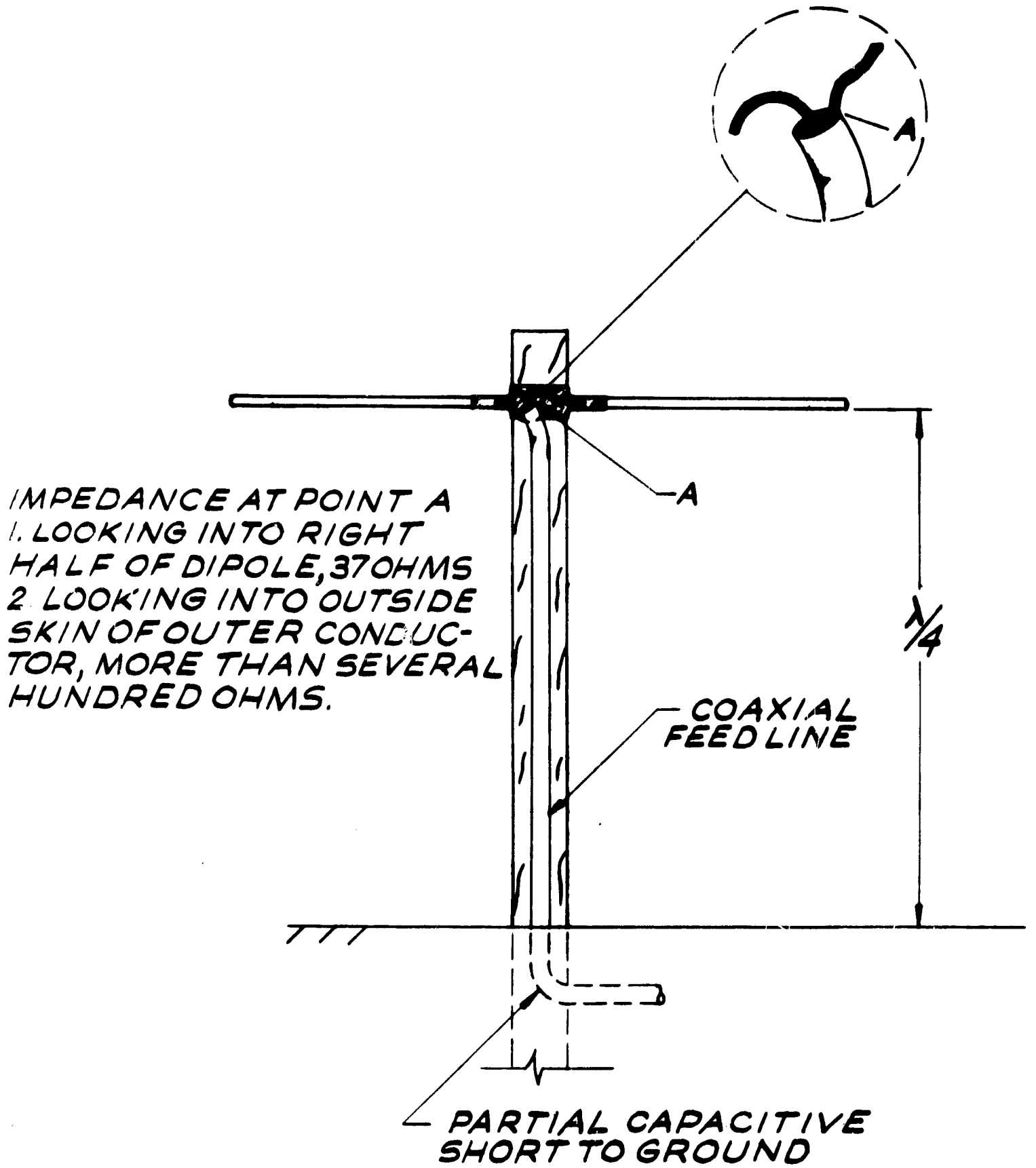

IMPEDANCE AT POINT A
1. LOOKING INTO RIGHT HALF OF DIPOLE, 37 OHMS
2. LOOKING INTO OUTSIDE SKIN OF OUTER CONDUCTOR, MORE THAN SEVERAL HUNDRED OHMS.

A SKETCH ILLUSTRATING WHY NO BALUN IS NEEDED ON A HALF-WAVE DIPOLE

FIG 3.4.1-1

at one-quarter wavelength is much larger, whereas the impedance of one-half the dipole is 37 ohms.

The two cross-polarized dipoles may be mounted on the same post, one or two inches above the other. With this arrangement the measured coupling between the two dipoles is about 25 db down, which is very good.

3.4.2 Site Testing

The testing of each amplifier should be done as the amplifier is installed and before the lead-in cables are attached to the dipoles. During this phase of testing, the gain and phase shift of each amplifier is checked. After the installation is completed, checking consists of determining only whether or not each amplifier is functioning at all. This is easily done by radiating a small signal from a generator in the vicinity of each dipole and observing the outputs at some central location.

In the pilot array at El Campo, weak amplifiers and faulty cables were easily and quickly found by exciting each dipole with a small hand-held transmitter. The response was heard on a receiver at the array output. With a little experience the technician soon became proficient with this procedure. There were several variations in this general method that worked equally well. A more precise method of checking the gain and

phase shift of each field unit in the pilot array involved the sending of a reference signal into the field over a standard cable. A sample of the input signal triggered an oscilloscope at the control center that also monitored the array output. The relative gain and phase shift were then direc tly on the oscilloscope. This procedure works well, but is time consuming and hopefully will not be needed in the final array.

The testing and calibration of the complete array will be done using standard celestial radio sources. The sources Cassiopeia A, Cygnua A, Virgo A, and Tamus A will be used for the 192 element pilot array. For the 50 db array, there exist more than 500 sources that may be used for checking the gain and beam position without integration. About 25 sources will be of sufficient intensity for the 40 db array. Cassiopeia and Cygnus were extensively used in testing the narrow-band pilot array. The 50 db array will be divided into 140 separate "bays" each of which may be controlled separately from the central building so that the gain and beam pointing characteristics of each bay can be periodically monitored using Cassiopeia and Cygnus. This monitoring may be done automatically by a computer upon command.

The gain and positional accuracy of the 1024 element, 38.2 MHz array at El Campo is periodically checked using celestial radio sources. This has proven to be much better than a signal source flown by a high-altitude

aircraft, which was used on several occasions. The cosmic noise from this array is continually recorded on a continuously moving paper chart to keep a check on gain, line losses, etc. The galactic maximum which appears daily around 1800 local sidereal time is especially useful for this purpose, and no doubt will be also for the 50 db array. (See Figures 7.2-6 and 7.2-7.)

When the 1024 dipole, 38.2 MHz array was constructed at El Campo, it had not been preceded by a pilot array. This was a mistake because many details of design and construction had to be worked out after the 1024 elements were in place. This was a much more difficult task than it would have been had only 128 or 256 elements been used initially as a pilot system. It is this experience that leads us to say, unequivocally, that it is wise to first construct a pilot system for any antenna array for which an identical model has not previously been constructed.

In addition to receiving, the 38.2 MHz array also transmits 500KW of power. When one of the 1024 elements arcs under power, it incapacitates the entire array for protection purposes. Within the first year after the array was constructed, such an arc was usually found within five minutes in spite of the fact that the array consists of eight bays. The trouble-shooting success with this array is due largely to three things: (1) knowing the probability of various failure modes,

(2) experience with various fault-finding procedures for the particular antenna, and (3) using the power-of-two elimination rule.

Experience with the narrowband antenna at El Campo has convinced us that the testing and trouble-shooting features will not be as great as were expected initially. The best insurance against trouble is the proper design and installation of the antenna in the beginning, and the solving of practical problems in the pilot array stage.

3.4.3 Expansion for Transmitter Capability

The addition of a transmitting facility can be added for less cost if plans are made for it in the beginning. The best procedure is to install both the receiving and transmitting features simultaneously. However, a satifactory procedure would be to install only part of the transmitting feature as the receiving system is installed. For example, the installation of the secondary voltage busses for the transmitter should be installed with the other cables because all the trenches should be dug during a given phase of construction. A complete description of the proposed transmitter facility is given in Section 7.6.

3.5 References

1. R.H. Baker, J.V. Harrington, W.T. Higgins, J.C. James, "History and Design Summary of Sunblazer Phased Array, CSR, September 1968. (Internal Memorandum).

CHAPTER 4

4.0 BEAM POINTING AND CONTROL CONSIDERATIONS

In this section the method by which main beam scanning is accomplished is presented. Ancillary data relating to tracking requirements and therefore the array control is also presented.

4.1 General System Requirements and Constraints

Beam positioning (tracking) is but one function of a much larger, but as yet not completely defined computer operated system. The major functions of this system are:

1) Generation and distribution of phase angle control signals to the sub-array modules (i.e., the 140 pilot systems in the 50 db array).
2) Station keeping such as array test, fault isolation, local time dignal generation, etc.
3) Correlation receiver control including frequency and time estimation.
4) Adaptive pattern analysis including side lobe reduction.
5) Spacecraft acquisition.

6) Other computations such as data reduction which are accomplished during "off peak hours".

This section is primarily concerned with items (1) and (5). The correlation receiver, item (3), is briefly described in the Sunblazer Documentation (January 1969) and items (2), (4) and (6) are currently being studied.

For discussion the general tracking requirement is a two hour per day viewing time at El Campo. This corresponds to an east-west scan of about ±15° daily, and a declination scan angle range of 6° to 52° annually. East-west scanning and the higher level declination scanning is obtained by the time delay system. At the element level, the declination scan is obtained with manual mercury switches located at each element.

An important item is the rate at which the tracking angles change. During the daily tracking of the spacecraft, the approximate rate of change of the east-west view angle is 15° per hour. Since the array beam width is .5°, the target moves through the beam in about 1/30 of an hour. Therefore, rephasing of the array should occur about once every 15 seconds. A minimum of six digital numbers are required to steer the array. This corresponds to a relatively slow computation for the computer and is well within the capability of the smallest commercially available computer.

The problem of repositioning (daily acquisition) has not been fully investigated, but the mid-day angular position

of the spacecraft changes very slowly from day to day. This point is illustrated in encounter profiles given in Figures 4.1-1 through 4.1-6 which snow the differential declination-right ascension angles for the Sunblazer spacecraft in a 3/4 year orbit as a function launch data. The circular points indicated on the profile path are 10 days apart. These curves show that during the period of superior conjunction the rate of change of both the differential right ascension and declination change about 0.1° per day.

If all other launch parameters are assumed constant, then the spacecraft-sun encounter profile is a function of the launch date. It is pointed out in Section 2.8 that peak solar noise entering the system via the antenna side lobes and grating lobes may cause system blackout. The amount of peak solar noise will be a function of launch date, since the array side lobe structure will, in general, be different for each encounter profile. However, the side lobe structure of the array pattern which determines the amount of peak noise, is a function of array organization and control. Additional study of the relationships between the encounter profile and noise characteristics of the array system is required.

4.2 Phased Angle Generation and Distribution

The amount of time delay required at each 14 db element depends upon the beam pointing position and the array geometry.

SUNBLAZER-SUN ENCOUNTER PROFILE

DIFFERENTIAL DECLINATION
VS
DIFFERENTIAL RIGHT ASCENSION

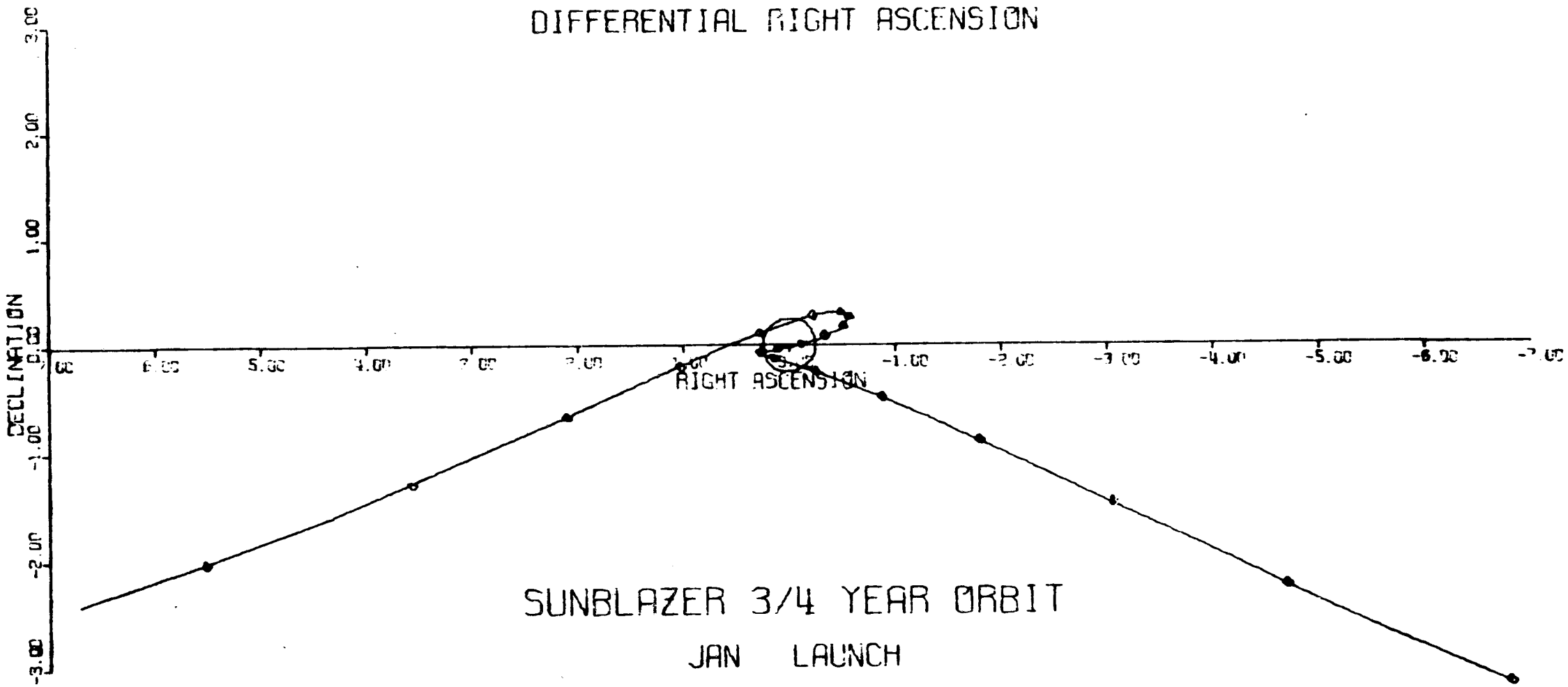

SUNBLAZER 3/4 YEAR ORBIT

JAN LAUNCH

FIG 4.1-1

SUNBLAZER-SUN ENCOUNTER PROFILE

DIFFERENTIAL DECLINATION
VS
DIFFERENTIAL RIGHT ASCENSION

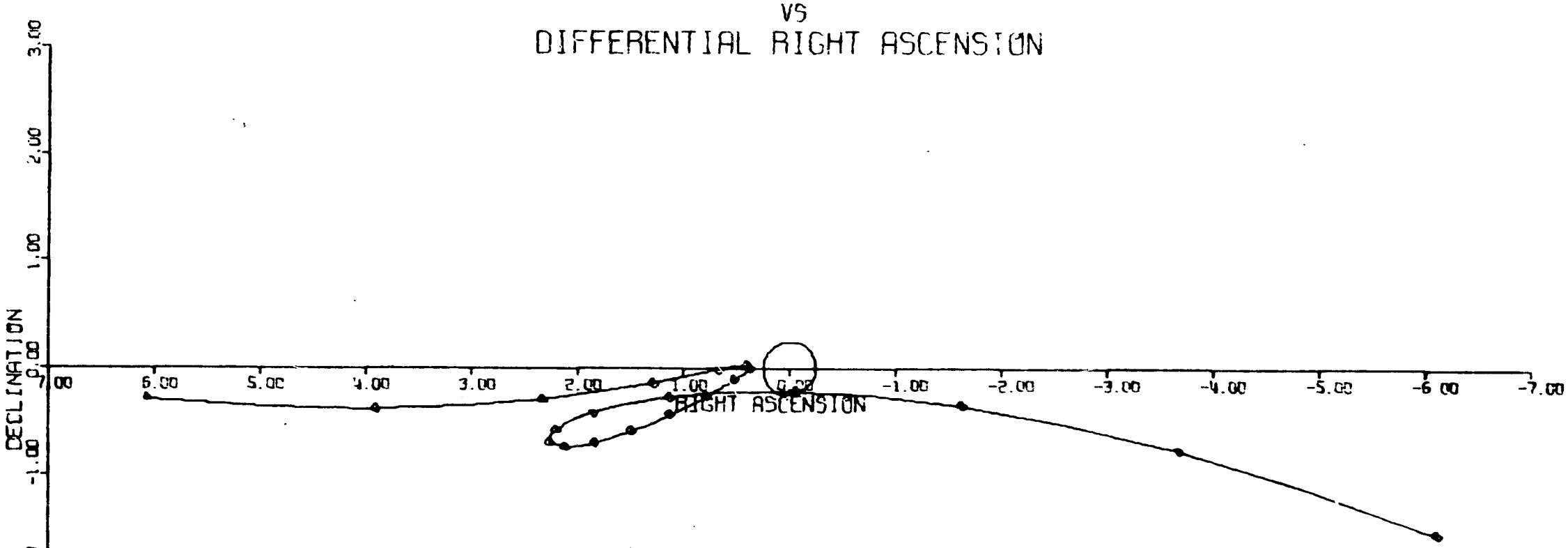

SUNBLAZER 3/4 YEAR ORBIT

MAR LAUNCH

FIG. 4.1-2

SUNBLAZER-SUN ENCOUNTER PROFILE

DIFFERENTIAL DECLINATION
VS
DIFFERENTIAL RIGHT ASCENSION

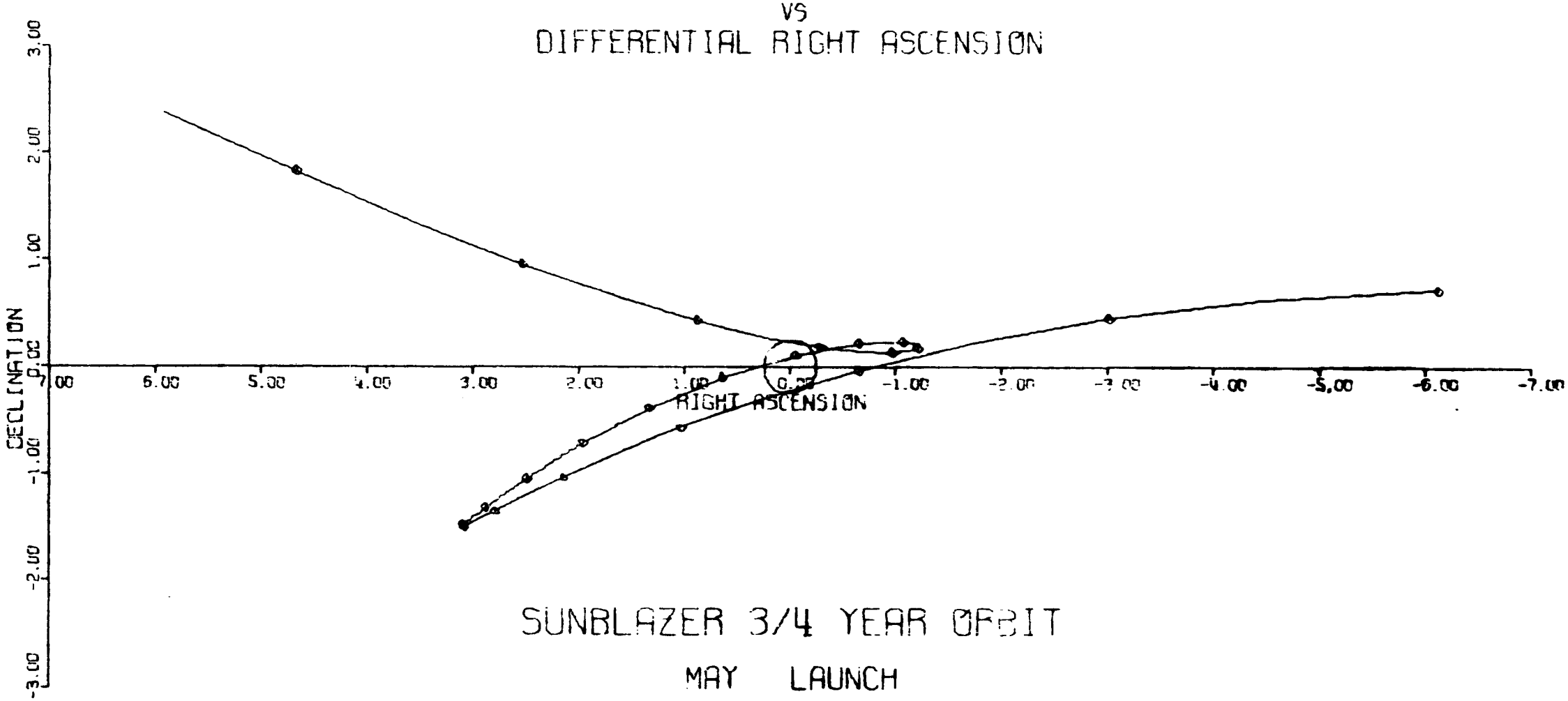

SUNBLAZER 3/4 YEAR ORBIT

MAY LAUNCH

FIG. 4.1-3

SUNBLAZER-SUN ENCOUNTER PROFILE

DIFFERENTIAL DECLINATION
VS
DIFFERENTIAL RIGHT ASCENSION

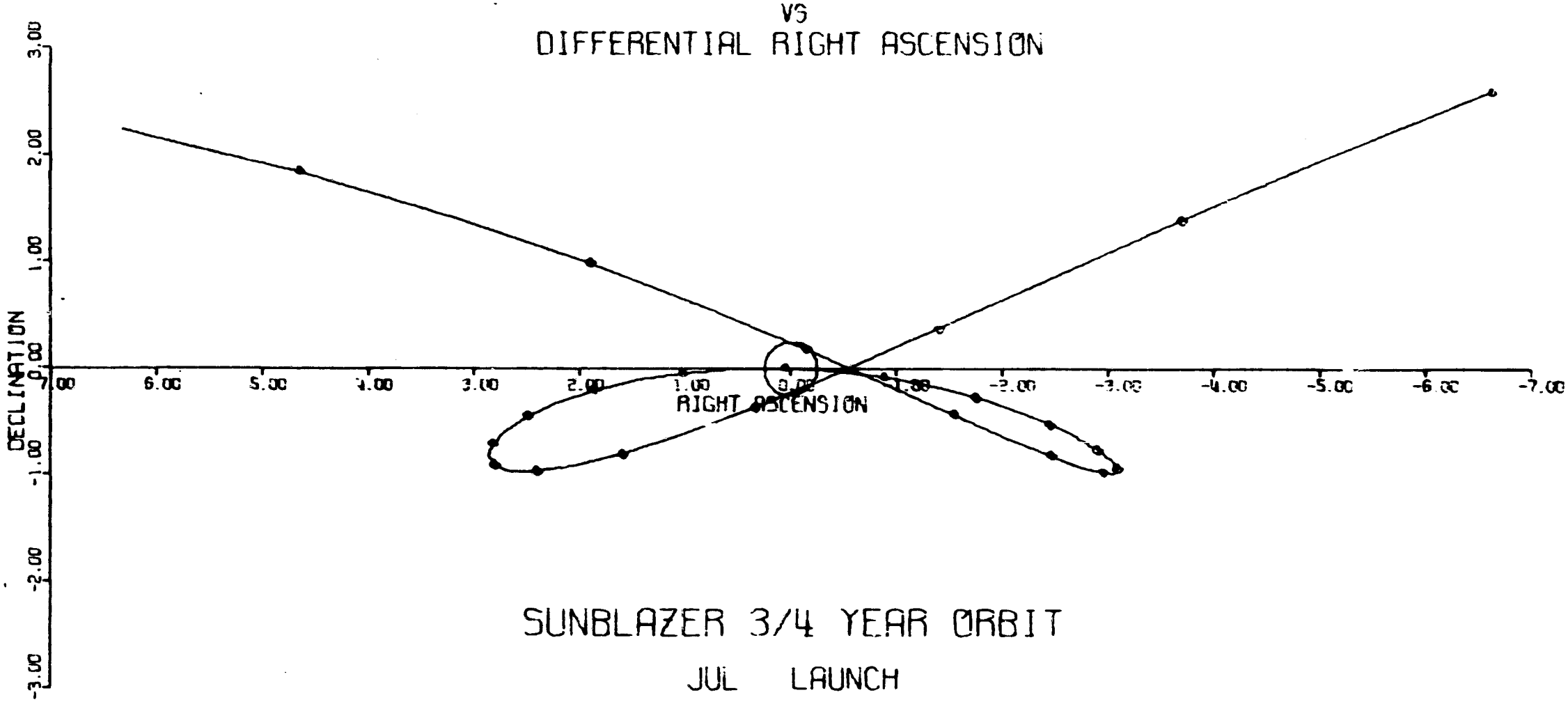

SUNBLAZER 3/4 YEAR ORBIT

JUL LAUNCH

FIG. 4.1-4

SUNBLAZER-SUN ENCOUNTER PROFILE

DIFFERENTIAL DECLINATION
VS
DIFFERENTIAL RIGHT ASCENSION

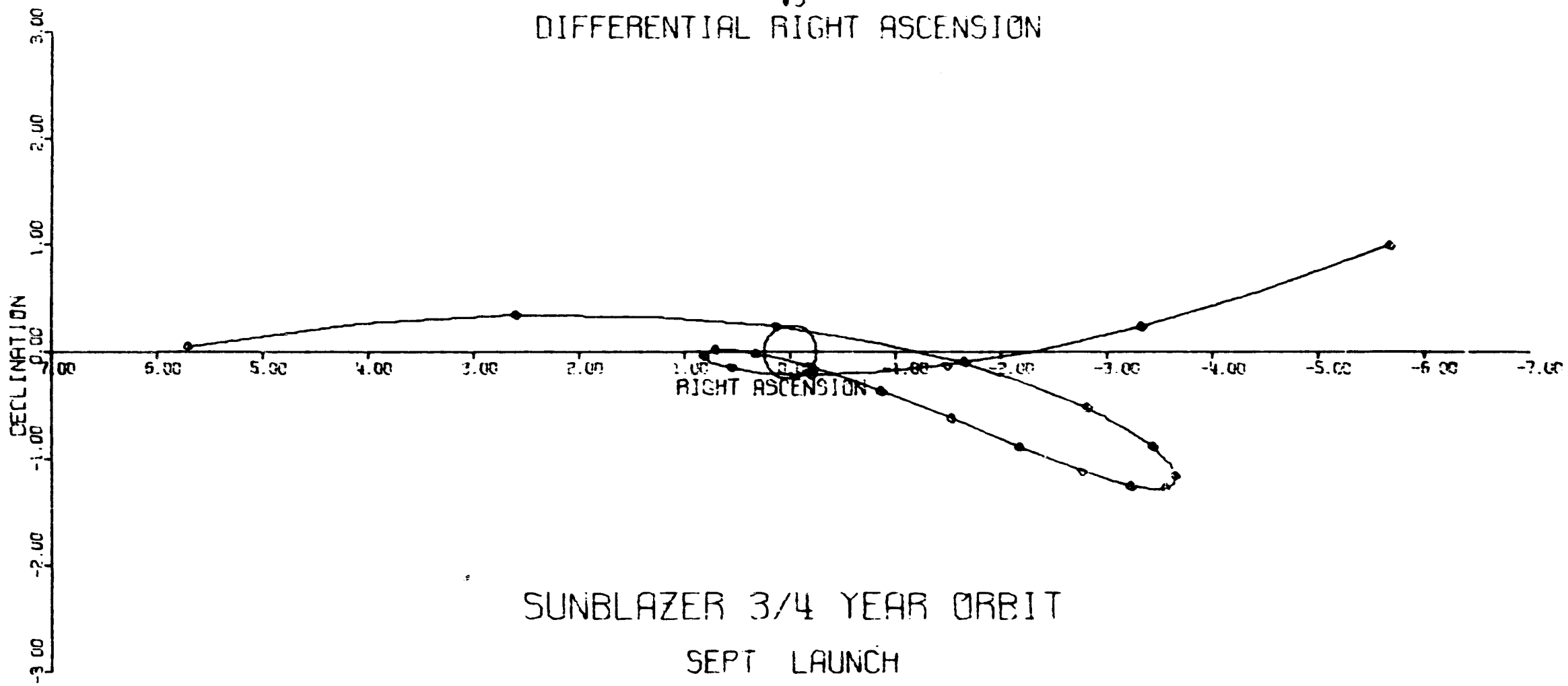

SUNBLAZER 3/4 YEAR ORBIT

SEPT LAUNCH

FIG. 4.1-5

SUNBLAZER-SUN ENCOUNTER PROFILE

DIFFERENTIAL DECLINATION
VS
DIFFERENTIAL RIGHT ASCENSION

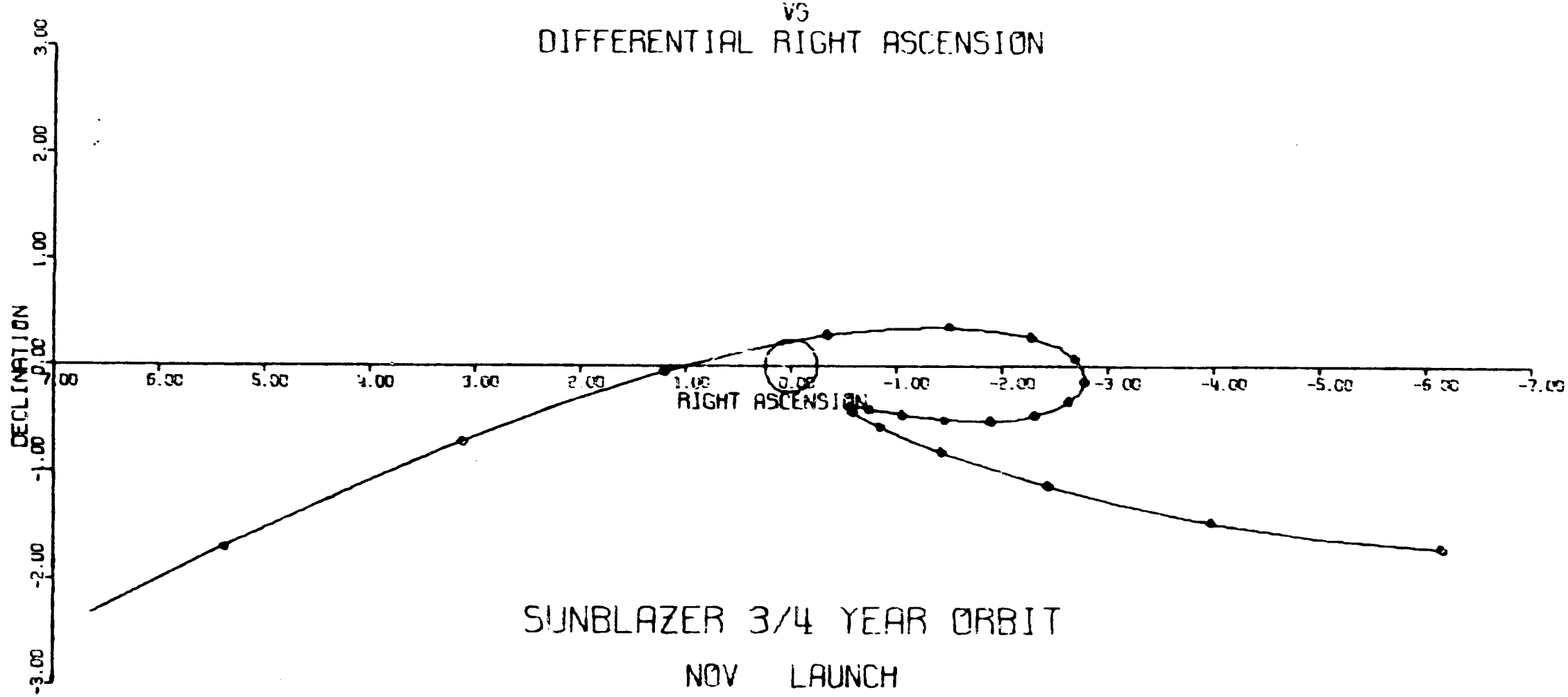

SUNBLAZER 3/4 YEAR ORBIT

NOV LAUNCH

FIG. 4.1-6

Depending on the system organization, "Christmas tree feed" or "parallel" feed as outlined in Section 3, combining is initially accomplished by delaying signals from adjacent 14 db elements and then summing coherently. In the regularly spaced, echelon, array considered here, the time delay is a function of the spacing between the adjacent 14 db elements, and the beam pointing angle. Therefore, the time delay at all the first level combining points (i.e. the "w" networks) are the same, and one four-bit number per polarization will control all of these 2240 first level time delay circuits.

The "x" networks combine the outputs from adjacent pairs of sources. For a given beam angle, the required time delay in the "x" networks is twice that of the"w" networks because the signal here comes from phase centers that are twice the separation of the individual 14 db elements. The "x" networks therefore require a five fit control signal or an extra bit over that of the "w" networks. However, the first four bits of the "x" network control is identical to that of the "w" network. By continuing the symmetry argument, it can be shown that subsequent (higher level) control numbers are related to the "w" and "x" network control numbers and consequently only three numbers are required to unambiguously control the array. Essentially one number controls declination, one number controls east-west scanning of the array, and the third number accounts for the .445λ displacement between adjacent columns. The Twin-Tee to Twin-Tee phasing is described in

Section 2.4.1. When the array is utilized in a sub-divided mode, i.e. into four separate independent quadrants for closed loop tracking (monopulsing), then each of these sub-arrays must be independently controlled. In this case, a dual polarized array requires 24 control numbers.

Some aspects of array control are being further studied because an analysis of the "tree" organization (see Section 2.5.3) indicates a more nearly optimum lobe structure for solar noise rejection may be attained with parallel phasing (see Section 2.4.2), for which the distribution of control signals would be somewhat modified.

CHAPTER 5

5.0 PILOT ARRAY ELECTRONICS SUBSYSTEM

In this section design details, including schematic diagrams of representative electronic circuits will be given. We will start with a description of the mercury switch, located at each Double Tee, and proceed through the amplifier, time delay, logic and power supply circuits. Operating data along with circuit specifications is presented. Section 7.3 gives a master list of all circuit drawings and hardware used in the electronic system.

5.1 Mercury Switch

5.1.1 Design Approach

The resultant pattern of the 14 db element is more directive than the individual component dipoles and therefore the individual dipole elements must be phased to accommodate changes in declination. For this reason, mercury switches are used to insert or remove phasing cables in the signal path within the Double Tee configuration. Physically, in the Double Tee element, one $3/8\lambda_o$ and one

$7/8\lambda_o$ delay circuit may be located near point a, (Figure 2.2-1) while one $3/8\lambda_o$ delay circuit may be located near point b.

A schematic diagram of the $7/8\lambda_o$ phasing network, which includes a double pole double throw switching network is shown in Figure 5.1.1-1. The double pole double throw switch permits element scanning in both the northerly and southerly directions. The mercury switches shown here, S_1 to S_{11} are hermetically sealed in glass tubes having sealed-in electrodes and containing a quantity of mercury which makes or breaks contact when the switch is tilted through a small angle. The tubes are filled with an inert gas which acts as an arc suppressor in high current applications.

The operation of the phasing system is as follows: When switches S_1 and S_2 are in position ADB input A is delayed with respect to input B, and when switches S_1 and S_2 are in position BDA input B is delayed with respect to input A. Time delay increments are obtained by the setting of switches S_3 and S_{11} and depending on the state (on or off) of these switches any time delay from 0 to $7/8\lambda$ may be obtained. Each group of three switches S_3, S_4, S_5; S_6, S_7, S_8; and S_9, S_{10}, S_{11} control the delay sections in a binary manner. For example, when S_4 is open switches S_3 and S_5 are closed, a time delay corresponding to $\lambda/8$ is obtained. In the proposed

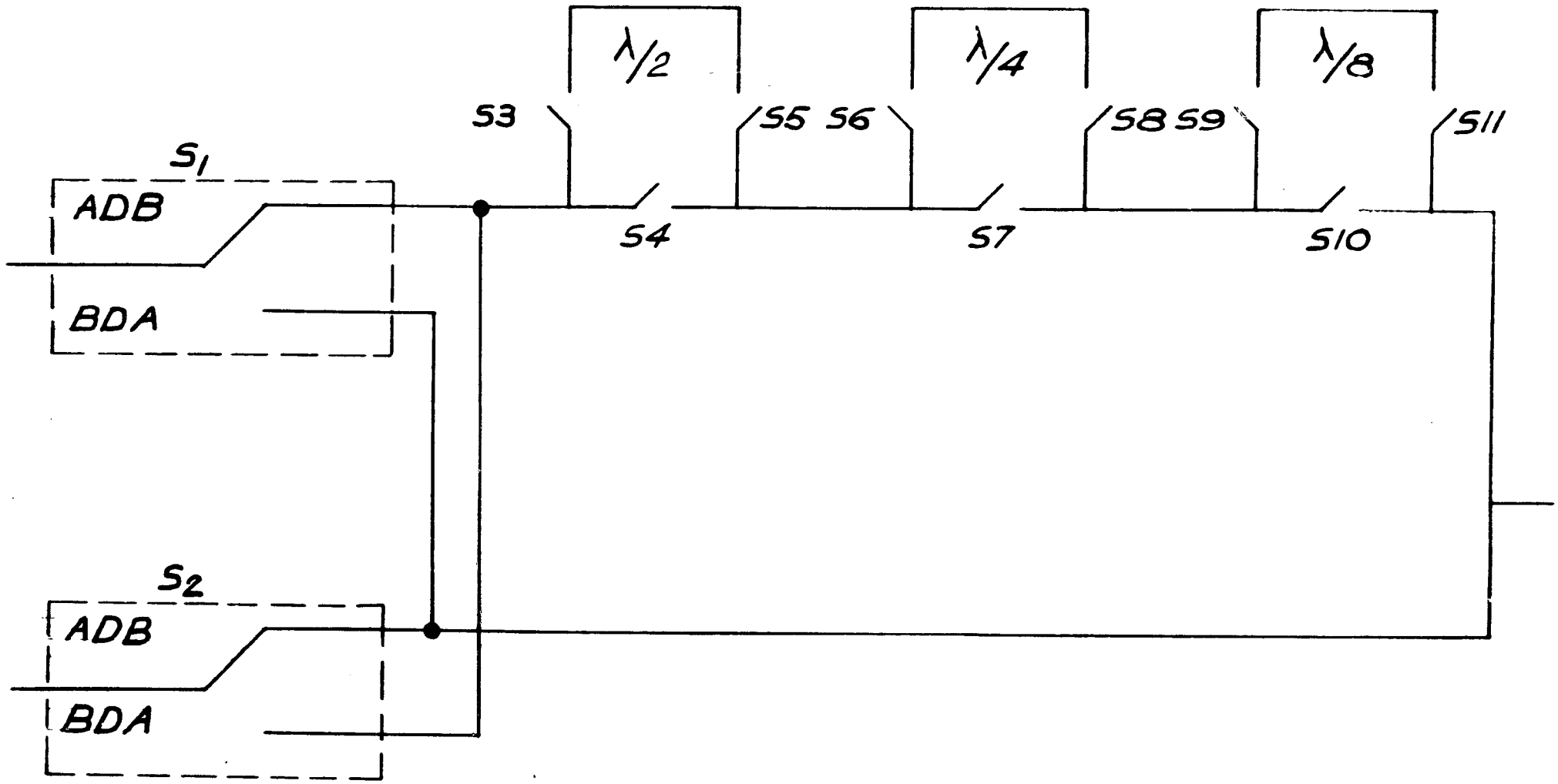

MERCURY SWITCHING NETWORK
FIG. 5.1.1-1

large array, the switching function may be automated by the use of mercury relays.

5.1.2 Performance Characteristics

The measured variations in VSWR with delay time for the phasing circuit is shown in Table 5.1.2-1.

TABLE 5.1.2-1

Time Delay	VSWR
λ/8	1.25
λ/4	1.22
3 λ/8	1.19
λ/2	1.25
5 λ/8	1.30
3 λ/4	1.19
7 λ/8	1.19

Phasing accuracies better than 5° are readily obtained. The small excess phase due to the mercury switch is compensated for by the foreshortening of the length of the delay cables. The switch shunt capacity is about .6 pf which corresponds to an isolation of 37 db. The actual measured isolation for a typical single pole switch is 34 db.

Insertion loss was measured at high (40 watts) and low (microwatt) power levels and in both cases the measured insertion loss per switch was much less than .1 db (it is very difficult to accurately measure very low losses). The switch performance at high power levels is important because the addition of the transmitting function to the array will require high power switching at the dipole level and the mercury switch appears to be a good choice to perform this function.

5.2 R.F. Amplifier Design

5.2.1 Design Approach

For a dual polarization 50 db antenna system, approximately ten thousand R.F. amplifiers are required. In production quantities, amplifier cost is a prime consideration. Also amplifier performance such as gain and phase stability, noise figure, packaging and reliability impose requirements which increase cost. The following sections describe an amplifier developed by the Center for Space Research specifically for use in this array because an acceptable low cost amplifier is not available as an "off-the-shelf" item.

The R.F. amplifier provides (1) signal gain at each element to maintain antenna noise figure below 5 db and

(2) band limiting over the 70 MHz to 80 Mhz frequency range. Cable losses between the antenna element and amplifier degrade the system noise performance. In order to minimize these losses the amplifier should be located as close to the element as possible. Additional system noise considerations are presented in Section 2.8.

The amplifier is located close to the antenna element, accordingly packaging and power distribution is a problem. For example, if the amplifier is located above the ground, it will be subjected to wider temperature variations, than if it is buried. However, a buried amplifier is subject to water immersion which complicates the amplifier packaging. As a practical matter, the advantage of moderate temperature variations has been judged to be worth the added packaging complexity.

The amplifier requires a regulated 15 volt D.C. source, which is supplied to the field amplifiers via the center conductor of the amplifier R.F. output cable. A filter network at the amplifier output separates the R.F. and D.C. voltages. The power fuse is located in the central electronics enclosure so it is easy to replace. This power distribution system aids in installation and trouble shooting since every amplifier in each pilot array may be tested from a central point.

A block diagram of the amplifier showing the input matching network, transistor, wideband output transformer,

biasing networks and three section Butterworth bandpass filter buffered by a T pad is given in Figure 5.2.1-1. In this circuit, a Germanium transistor is used in the common emitter configuration. This Motorola type MM5000 device was selected because of its desirable characteristics namely, low noise, high gain and low cost. The maximum allowable operating temperature (100°C) is well above the estimated maximum operating temperature (40°C) for the amplifier environment.

Another scheme that was evaluated utilized a Butterworth filter at the amplifier input. Input filtering is desirable because the high level, out of band, signals are attenuated before they mix in the transistor base emitter junction and because of this attenuation, the level of the spurious in-band signals is reduced. However, the filter insertion loss will increase system noise figure by about 1 db. This approach has been discarded in favor of the one shown in Figure 5.2.1-1 where the filter is in the amplifier output circuit. This approach is satisfactory because the expected site RFI environment is low (see Section 2.8.3).

5.2.2 Amplifier Performance

A variety of measurements have been made with the circuit of Figure 5.2.2-1, the results of which are

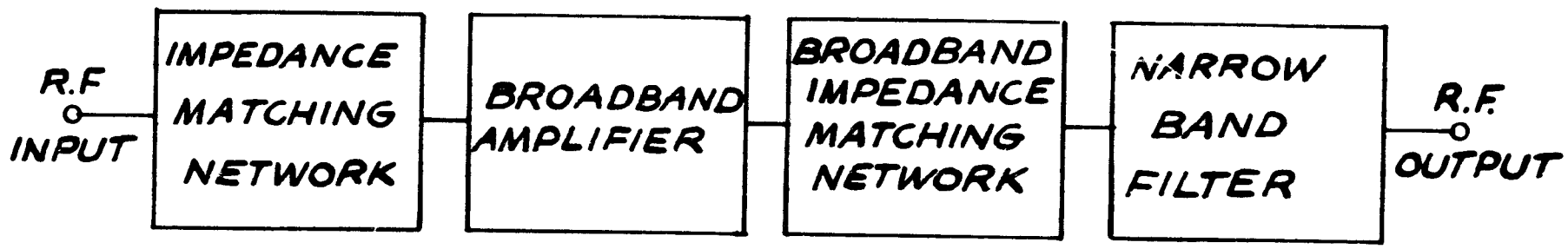

AMPLIFIER'S FUNCTIONAL BLOCK DIAGRAM
FIG. 5.2.1.-1

summarized in Table 5.2.2-1. In general, noise figure and gain have not been a problem. Typical measurements show that a noise figure of less than 3 db is easily obtained. The inherent gain of the transistor is 23 db while net circuit gain is approximately 17 db. Figure 5.2.2-2 shows the normalized gain versus frequency function of several representative amplifiers. The shape of this curve (band limiting) is primarily determined by the Butterworth filter. The measured gain is flat to within $\pm 1/2$ db over the 70 to 80 MHz frequency band.

Differences in gain, phase, and time delay between amplifiers will degrade array performance. To minimize these differences, gain and phase trimming adjustments are provided (Figure 5.2.2-1). Capacitor C_5 controls the amplifier gain over a 4 db range, and capacitor C_7 provides for a phase adjustment up to 20° in the amplifier. Figure 5.2.2-3 shows the phase-frequency characteristic of an amplifier for several settings of the phase adjustment. Note that the slope of all three curves is approximately the same which is an important consideration in the measurement characterization of circuit time delay.

In order that a network reproduce nonsinusoidal signals without distortion all the signal frequency components must be equally delayed. Since time delay of a network is the derivative (with respect to frequency) of the phase-frequency function, a linear phase-frequency curve is required for

Gain: @ 75 MHz 1[illegible] db min

Noise Figure: 2.7 db max 2.5 db typical

VSWR:

Frequency	Input VSWR
70 MHz	1.7 max
75 MHz	1.3 max
80 MHz	1.5 max

Gain Compression: -20 db[illegible] for 1 db gain compression and Δ13° phase shift

Power Supply: +15 v @ 4 ma

Phase Shift Spread Between Amplifiers:

Frequency	ΔϕShift
70 MHz	7°
75 MHz	0°
80 MHz	10°

Time Delay: 38 NS $\pm$ 5 NS

TABLE 5.2.2-1 Measured Amplifier Characteristics

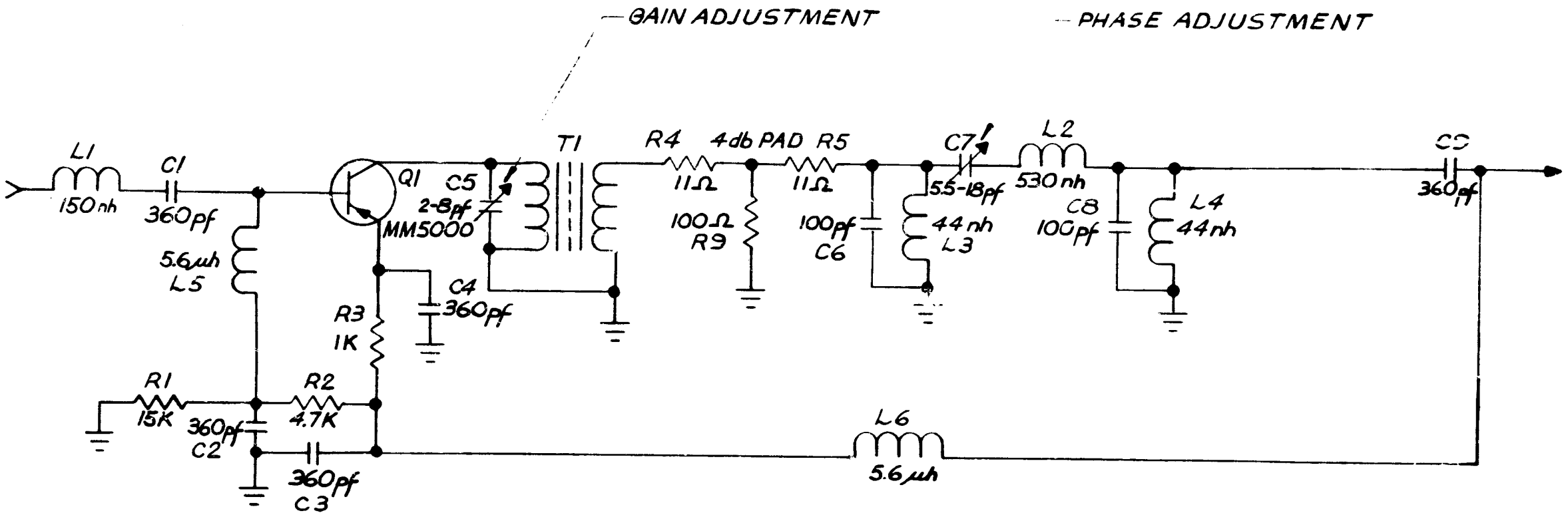

75MHZ R.F AMPLIFIER

FIG. 5.2.2-1

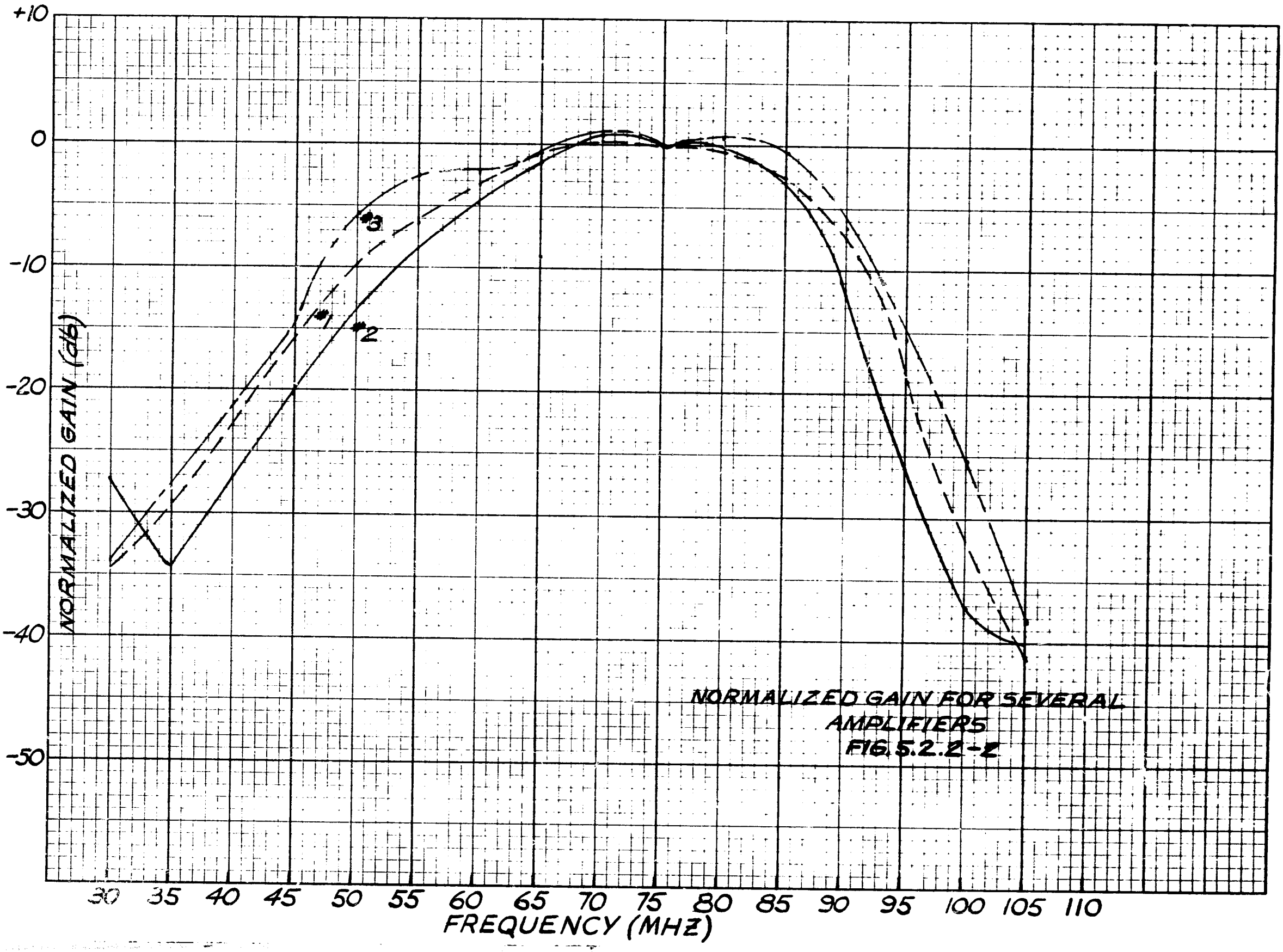

NORMALIZED GAIN FOR SEVERAL AMPLIFIERS
FIG. 5.2.2-E

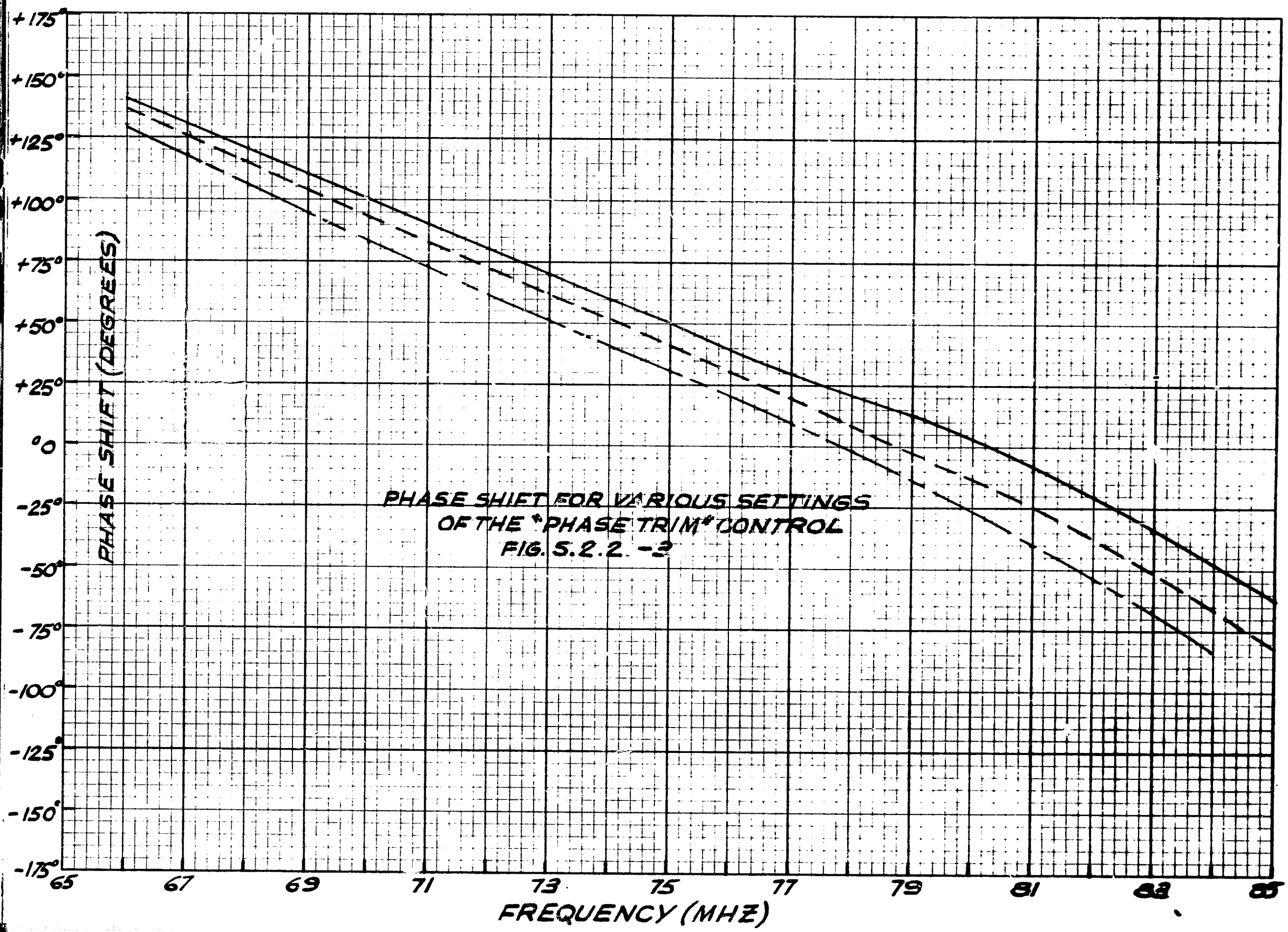

PHASE SHIFT FOR VARIOUS SETTINGS
OF THE "PHASE TRIM" CONTROL
FIG. 5.2.2 -2

distortionless transmission. The amplifier circuit given in Figure 5.2.2-1 has a linear phase function over the frequency bands of interest. Time delay measurements were made by graphically differentiating the curves given in 5.2.2.3. These results are summarized in Table 5.2.2-2. As shown, the maximum observed time delay variation is 9 nanoseconds which is small compared to the allowed limits of 200 nanoseconds set for the system. This limit is chosen to be small compared to the bit length of transmitted pulse.[1] Nominal time delay is 38 nanoseconds. Approximately 22 nanoseconds of this is due to the Butterworth filter, while the remainder is due to device and other component delays.

5.2.3 M.I.T. Phased Array Amplifier Specifications

Signal Frequencies: 69.7200 MHz ± 500 KHz
74.7000 MHz ± 500 KHz
79.6800 MHz ± 500 KHz

Gain: 18 db ± 1/2 db @ 74.7000 MHz with no operator adjustment required.

Band Pass: The gain between 69.2200 MHz and 80.1800 MHz shall be within ± 1/2 db of the gain at 74.7000 MHz. The gain at 60.08 MHz and 89.72 MHz shall be at least -3 db with respect to the gain at 74.7000 MHz. For frequencies less than 60.08 MHz and greater than 89.72 MHz the gain shall monotonically decrease and the ratio between the 60 db bandwidth and the 3 db bandwidth shall be not greater than 6:1.

Noise Figure: ≤ 3 db

Gain Compression: The minimum input signal level for 1 db gain compression shall be -16 dbM.

TABLE 5.2.2-2

TIME DELAY SPREADS MEASURED BETWEEN AMPLIFIERS

Frequency	TIME DELAY (nanosecs)			
	Amplifier #1	Amplifier #2	Amplifier #3	Spread Between Amplifiers
70 MHz	30 NS	39 NS	35 NS	9 NS
75 MHZ	26 NS	32 NS	32 NS	6 NS
80 MHz	30 NS	35 NS	36 NS	6 NS

Input Impedance: Nominal 50Ω VSWR ≤ 1.3:1

Output Impedance: Nominal 50Ω VSWR ≤ 1.3:1

Phase Shift Spread: The phase spread between amplifiers shall not exceed 22° when measured at any input signal frequency (listed above). This specification is illustrated in Figure 5.2.3-1(A) for further clarity. The measurement setup is shown in Figure 5.2.3-1(B).

Time Delay Spread: The time delay spread between amplifiers should satisfy the requirements outlined in the following table. These specs are illustrated in Figure 5.2.3-2 for further clarification. The measurement setup is shown in Figure 5.2.3-1(B).

Frequency (MHz)	Time Delay (nanoseconds)
69.7200±500 KHz	t_{d1} ± 100 nanosec
74.7000±500 KHz	t_{d2} ± 100 nanosec
79.6800±500 KHz	t_{d3} ± 100 nanosec

Cross Modulation: Cross modulation shall be measured using the techniques described in References 1 and 2. The desired signal is 75 MHz at a level of -40 dbM (2.2 mv). The spurious signal is 70 MHz and is 30% amplitude modulated with 400 cps. The spurious signal level for 1% cross modulation shall be greater than -30 dBM (7 mv).

Long Term Effects: All specifications listed above must be maintained for at least two years without adjustment under field conditions.

Packaging: Approximate physical dimensions 2" x 3" x 5". Enclosure suitable for direct earth burial with a temperature range extending from 0°F to 140°F and maximum humidity of 100%. The input signal connector must be compatible with RG8A/U coaxial cable and the output connector must be compatible with Phelps Dodge semi-rigid coaxial cable type FXA-38-50H. The required +15 V shall be supplied through the center conductor of this semi-rigid coaxial cable.

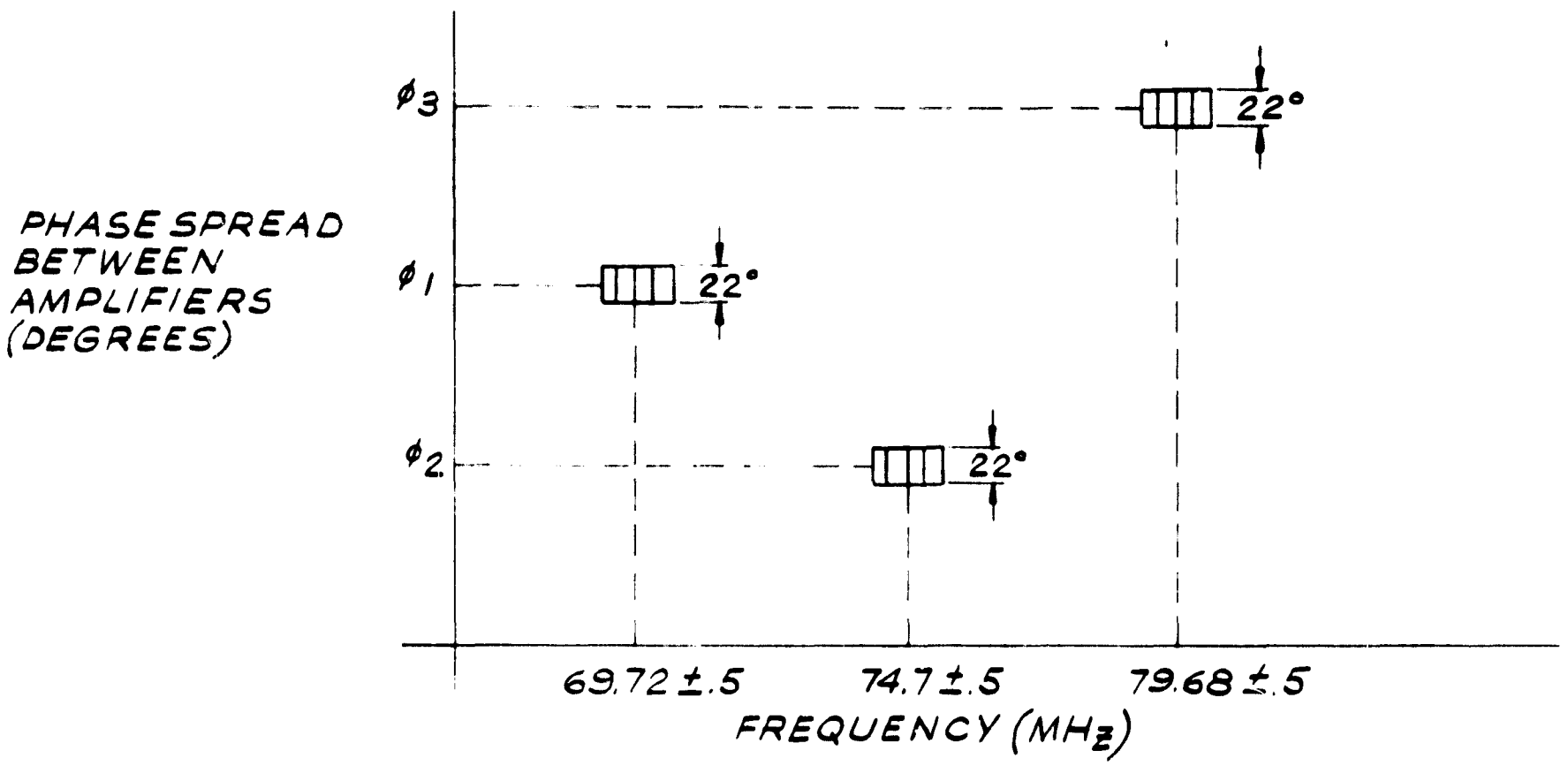

PHASE SPREAD BETWEEN AMPLIFIERS
(a)

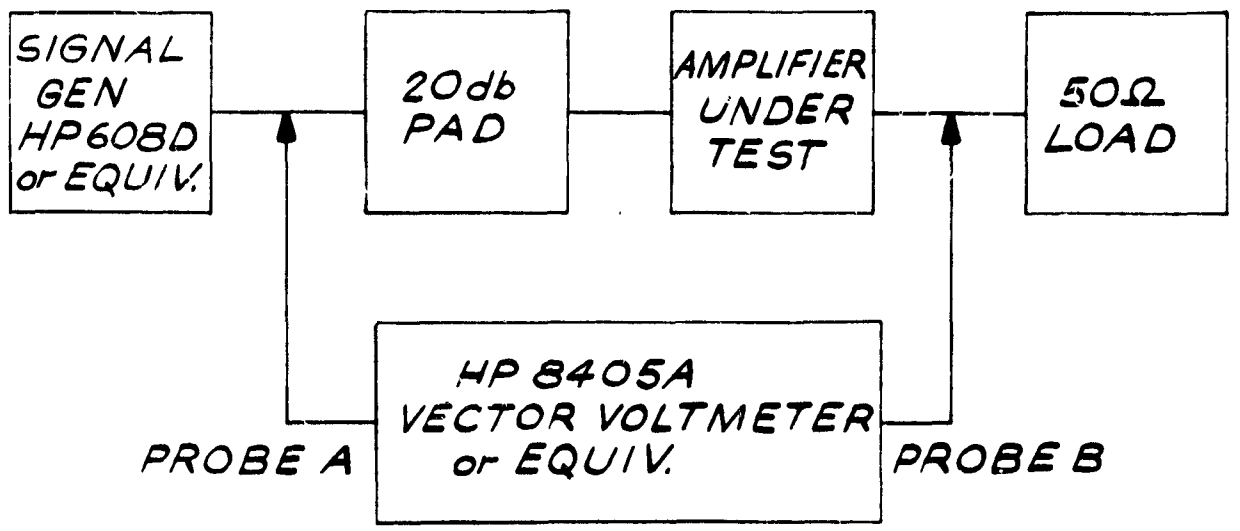

TEST SETUP FOR MEASUREMENT OF AMPLIFIER PHASE SHIFT AND AMPLIFIER TIME DELAY
(b)

PHASE SPREAD BETWEEN AMPLIFIERS

FIG. 5.2.3 – 1

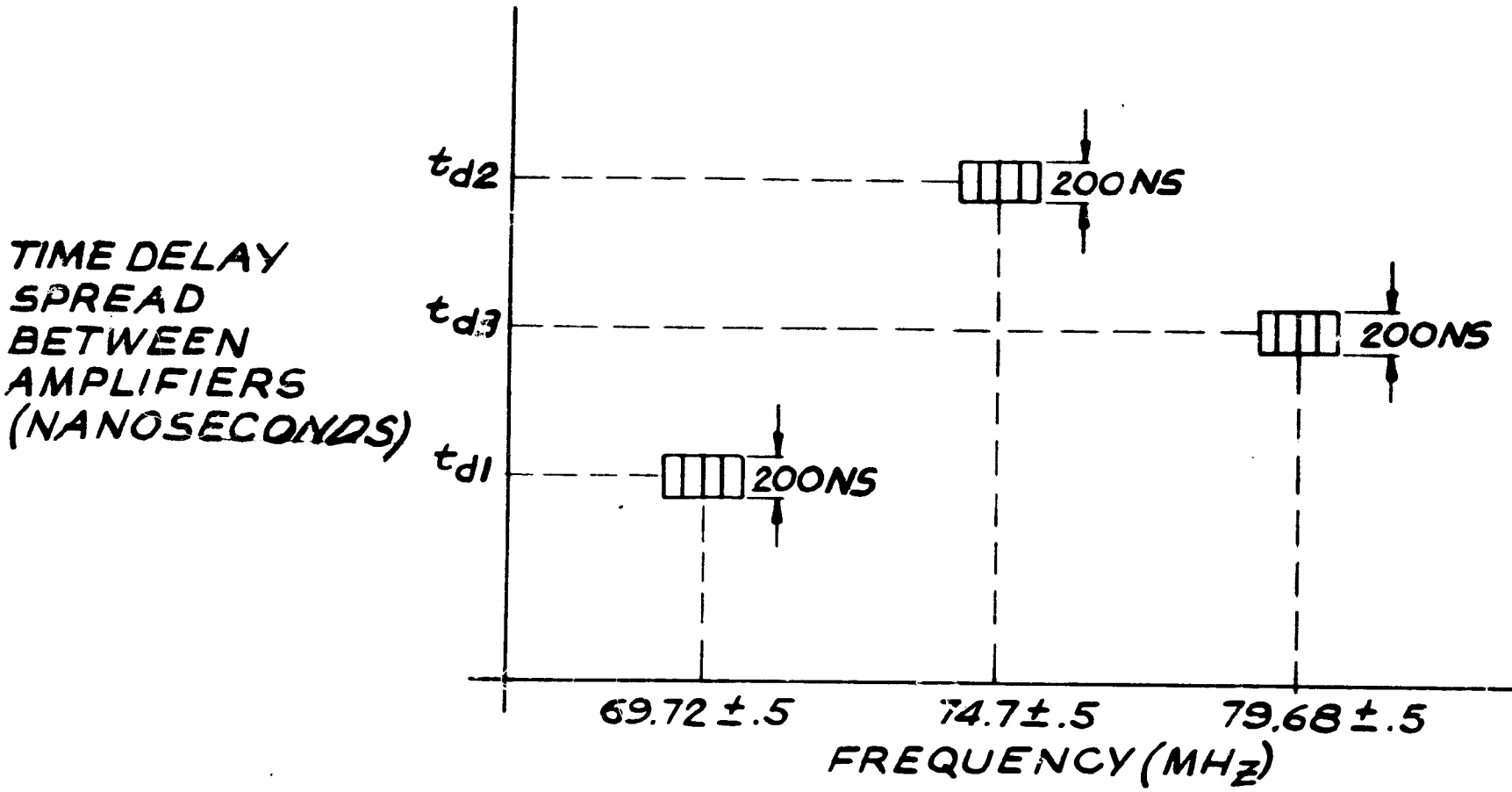

TIME DELAY SPREAD BETWEEN AMPLIFIERS
FIG. 5.2.3.-2

Temperature Range: 0°F to 140°F

Supply Voltage: +15 V

Cross Modulation References:

1) E.F. McKeon; "Cross Modulation Effects in Single-Gate and Dual-Gate Mos Field-Effect Transistors", RCA Application Note AN-3435

2) M. Akgun; "Cross Modulation and Non Linear Distortion in RF Transistor Amplifiers", IRE Transactions on Electron Devices (October, 1959) pp 457-467

5.2.4 Packaging

The basic packaging objective is to provide the amplifier with a waterproof environment. In addition the packaging design must be relatively inexpensive and easily implemented on a production basis. The system outlined below satisfies all these requirements.

In the design shown in Figure 5.2.4-1, the amplifier printed circuit board is constructed with all components on one side and the opposite side of the printed circuit board is a ground plane. After the components have been assembled onto the board, a plastic cover approximately 2 x 3 x 1/2 inches is cemented to the board to enclose all of the components except a short section of printed circuit line and several lugs which are provided for input and output cable interconnection. The printed circuit board and cover assembly is then inserted into an aluminum electrical outlet box, as shown in Figure 5.2.4-1. This non-corrosive enclosure is inexpensive,

Figure 5.2.4-1 - Completed Package Showing Component Layout and Cable Interconnections

and provides good R.F. shielding and mechanical support for the input and output cables.

After the printed circuit board and cover are inserted into the box, the input and output cables are hard soldered to the printed circuit board lugs. Mechanical support for the cables is maintained by a cable clamp and rubber grommet assembly. Next STYCAST V-B encapsulant (manufactured by Emerson Cummings) is poured into the box in order to water-proof the entire assembly. The rubber grommets are used with the cable clamps to prevent the encapsulant from leaking before it cures. The completed unit is shown in Figure 5.2.4-2 along with the cable clamps. Note that the clamp used has a split ring which is compressed around the aluminum jacketed cable by means of set screws which insures good electrical contact between the cable and the enclosure. This technique is used because soldering or welding aluminum is not practical. Finally inside the box a ground strap connects the amplifier ground to the enclosure.

Since the electronic components are inside the plastic case, the effect of the encapsulating material on the amplifier performance is minimum. The heat generated during the curing process has caused some deformation of the plastic cover, however, a plastic exhibiting a higher melting temperature should alleviate this condition. We are continuing to investigate encapsulants having the properties of low exotherm and rapid curing time. Material curing properties are especially important

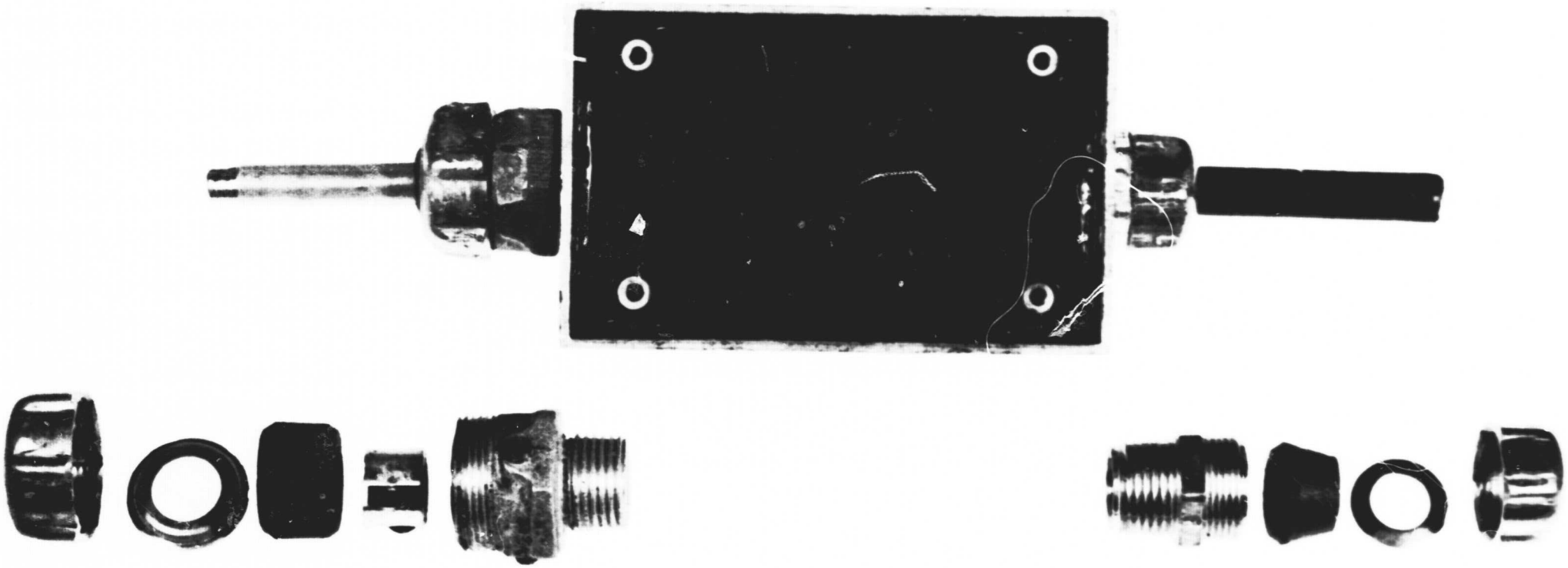

Figure 5.2.4-2 - Completed Package with Exploded View of Connectors

since the final assembly (i.e. the packaging operations) must be accomplished at the site in a production type of operation. At the present writing the STYCAST V-B is the most promising material.

5.3 Time Delay Circuits

5.3.1 Design Approach

As indicated in Figure 2.3.4-1, there are five types of time delay circuits which are used to coherently combine the signals from the Double-Tee elements within a pilot array. For purposes of analyzing time delay requirements, the aperture may be considered an array of point sources and the element type need not be specified. The spacing of the point sources and the desired scan angle from the zenith determine the length of the various delay lines. For reduction of undesirable grating lobes the array elements have been spaced such that the physical area occupied by each dipole is approximately equal to the dipole electrical area.

In the system outlined in Section 2.3.4, the spacing between the phase centers of the Double Tee elements is 1.780λ. For a scan angle of 52° from the zenith, the maximum time delay between these phase centers would be $(1.780\lambda \sin 52°)$ or 1.40λ. If the time delay increments are adjustable in $\lambda/8$ steps, then a four-bit network of the IW type, having a maximum delay of $1\ 7/8\lambda$ is used which

permits scanning almost to the horizon.

The inherent periodicity of the array geometry not only simplifies the control of time delay circuits because all of the W networks require the same time delay setting as a function of beam scanning angle, but also simplifies the design of the time delay network. All of the time delay and summation networks are basically the same. The only differences being between the range of the time delay. For example, networks W and Y have 1 7/8λ maximum delay, while networks X and Z have 3 7/8λ maximum delay. Network T has a 7 7/8λ maximum available delay.

5.3.2 Performance Details

The design of the W circuit shown in Figure 5.3.2-1 is typical of all the time delay circuits. Basically, it consists of a double-pole, double-throw R.F. switch, a switched delay line and a summation network. The function of the double-pole, double-throw switch is to permit eitner of the inputs to be delayed with respect to the other input. This is a necessary function because if the array is pointed in a southerly direction then input B must be delayed with respect to input A and for a northerly direction then input A must be delayed with respect to input B.

The time delay is obtained in the switched delay line sections. Circuit type W consists of four cables with electrical lengths λ, λ/2, λ/4 and λ/8. These cables are

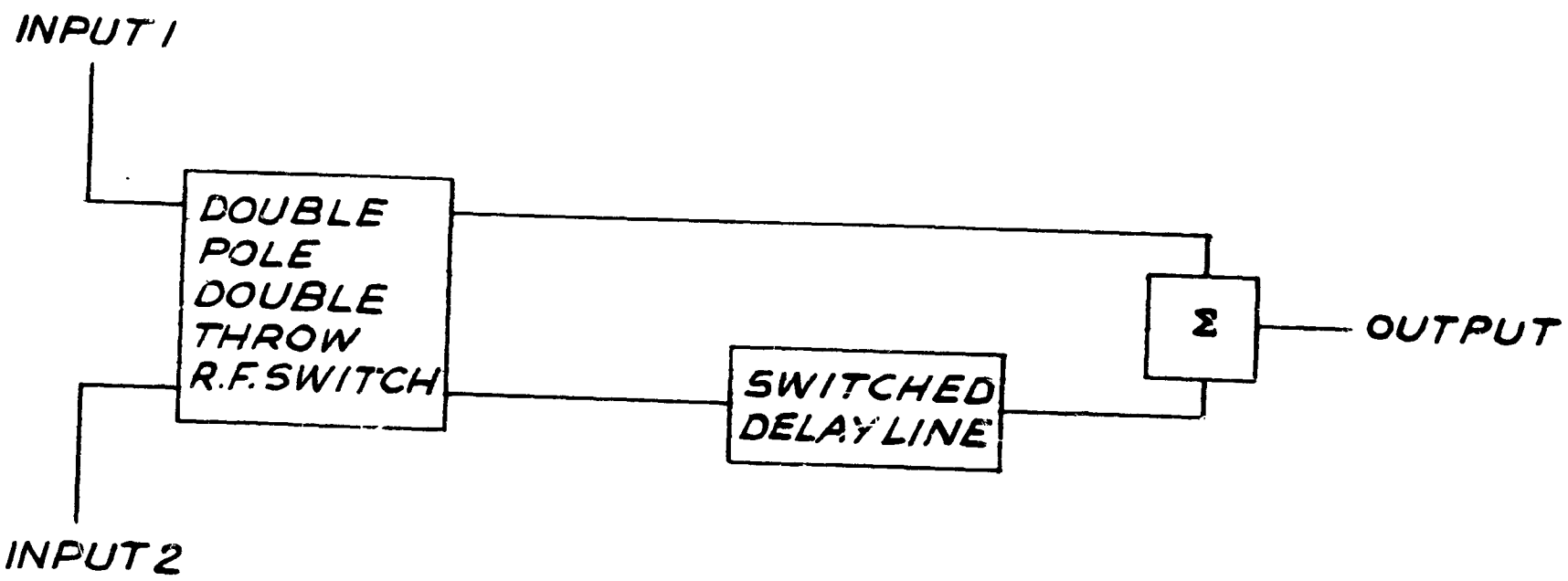

TIME DELAY NETWORK w AND y

FIG. 5.3.2 -1

switched in and out of the signal path as a function of the desired array look angle. Schematic diagram 104-400023 shows two complete time delay and summation networks. Refering to this diagram, if it is desired to have input A delayed with respect to B (southern pointing array) and a signal delay of $\lambda/2$, the dc inputs BDA, L_5 out, L_4 in, L_3 out, and L_2 out are made positive 6V with respect to ground. All other control inputs are held at ground potential. The R.F. signal from input A, is switched directly into a fixed delay line and goes to the coherent power combiner TOHJ-302H. The R.F. signal from input B, is connected to the delay line section where diodes D_4, D_6, D_8, D_{10}, and D_{13} have been made to conduct by the above selection of dc input voltages. When D_6 and D_8 are conducting, a delay of $\lambda/2$ is given to the signal arriving from input B. This signal is coherently combined in the power combiner with the signal from input A. The signals from inputs A_2 and B_2 are summed in the same manner.

Typical performance curves for type "W" networks are shown in Figures 5.3.2-2, 5.3.2-3 and 5.3.2-4. There are four delay line sections in circuit 1W, and therefore, the delay from 0 to 1.75λ occurs in 16 increments. The delay in degrees as a function of the step number has been plotted in Figure 5.3.2-2 closely approximate a straight line. The phase error as a function of step number is plotted in 5.3.2-3 for both halves of the network. Note that the maximum error is about 7°. Finally Figure 5.3.2-4 shows the variation of signal

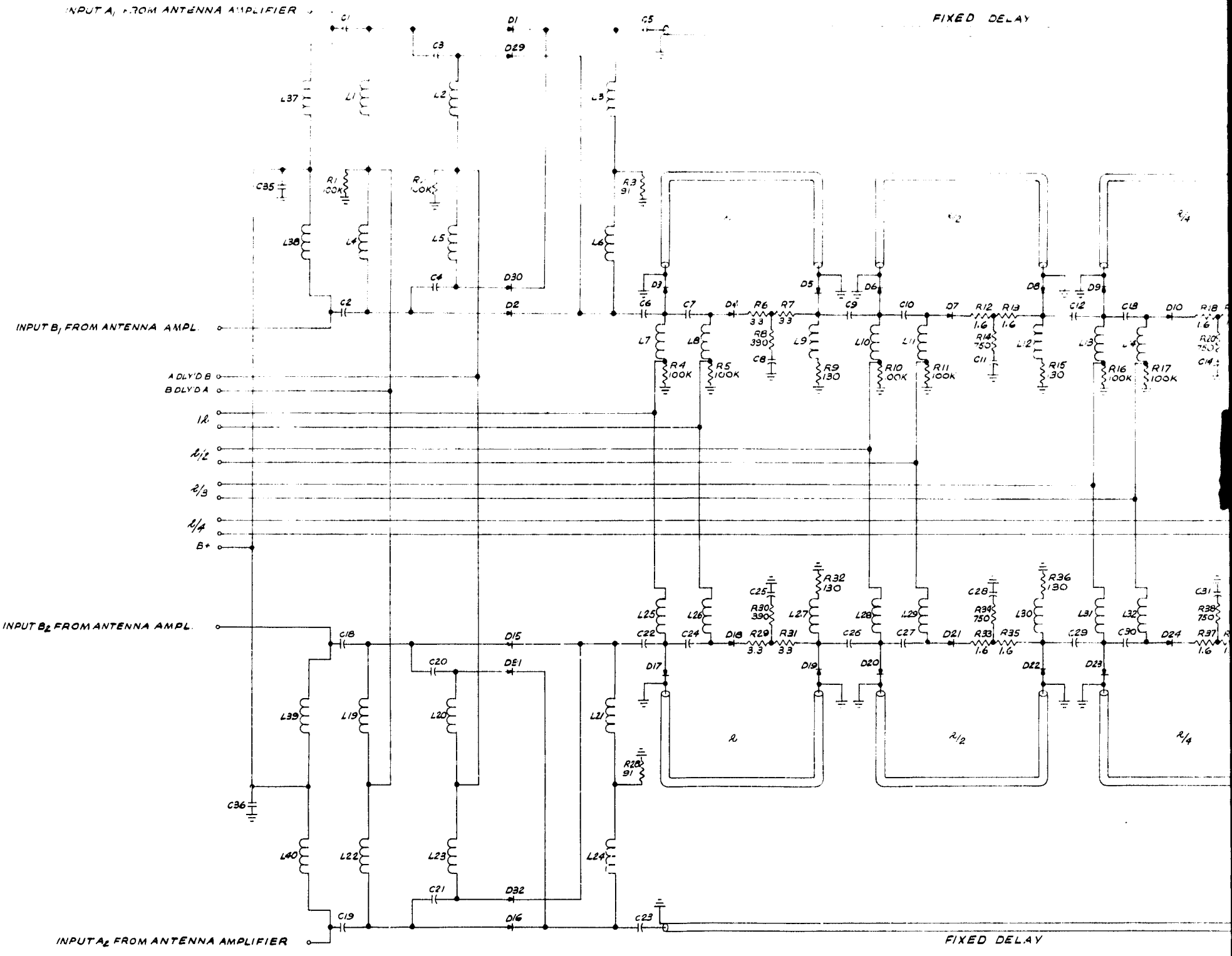

INPUTS

- A_1
- A_2
- B_1
- B_2

OUTPUTS

- A_1
- B_1

BOARD TERMINAL IDENTIFICATION

GND
A DLY'D B
B DLY'D A
λ: T_{IN} L_6 T_{OUT}
λ/2: T_{IN} L_4 T_{OUT}
λ/4: T_{IN} L_3 T_{OUT}
λ/8: T_{IN} L_2 T_{OUT}
B+

CABLE LENGTH, RG58/U CABLE
λ = 254.5 cm
λ/2 = 127.5 cm
λ/4 = 49.8 cm
λ/8 = 28.5 cm
FIXED DELAY = 185 cm

UNLESS OTHERWISE SPECIFIED
ALL CAPACITORS ARE 360 pf
ALL CHOKES ARE 5.6 μh
ALL DIODES ARE IN 903

Fold Out
a

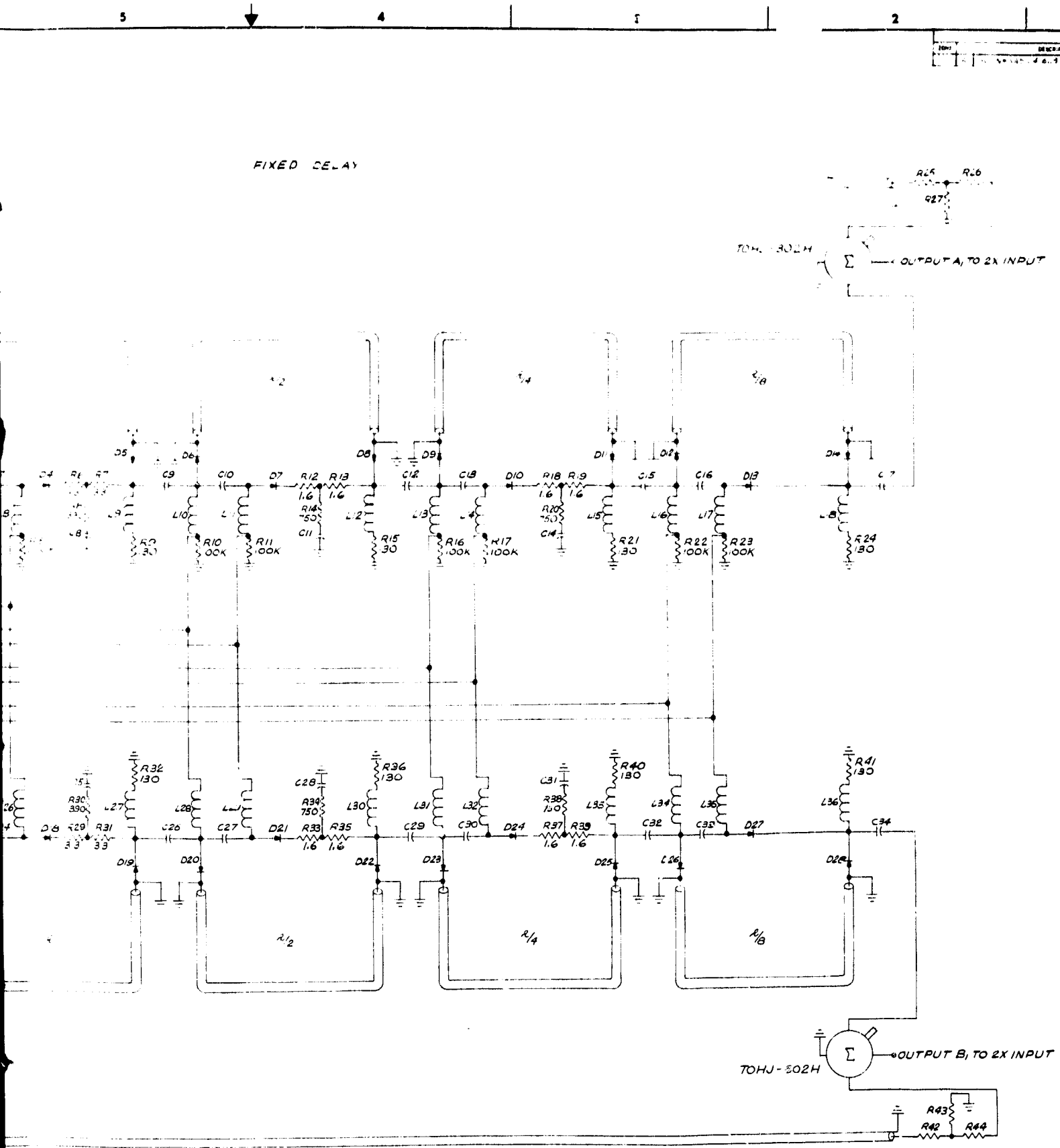

UNLESS OTHERWISE SPECIFIED
ALL CAPACITORS ARE 360pf
ALL CHOKES ARE 56 μh
ALL DIODES ARE IN 903

B

FIND NO.	QTY REQD	PART OR IDENT. NO.	NOMENCLATURE OR DESCRIPTION	MATERIAL & SPECIFICATION

LIST OF MATERIALS

UNLESS OTHERWISE SPECIFIED CAPACITOR VALUES ARE IN μf
RESISTOR VALUES ARE IN OHMS
ELECTRICAL TOLERANCES = ±5%

DIMENSIONS ARE IN INCHES
TOLERANCES ON FRACTIONS DECIMALS ANGLES
± ± ±
DO NOT SCALE THIS DRAWING

MATERIAL

DRAWN Mark Bauknight 10CT'68
CHECKED
APPROVED
APPROVED
1ST APPROVED DATE

CENTER FOR SPACE RESEARCH
MASSACHUSETTS INSTITUTE OF TECHNOLOGY
CAMBRIDGE, MASS.

TYPE IW TIME DELAY

SIZE E | CODE IDENT NO. | DRAWING NO. 104-400023 (A)
SCALE | SHEET 1 OF 1

DEGREES PHASE SHIFT vs TIME DELAY
IW PHASE SHIFTER #3
FIG. 5.3.2-2

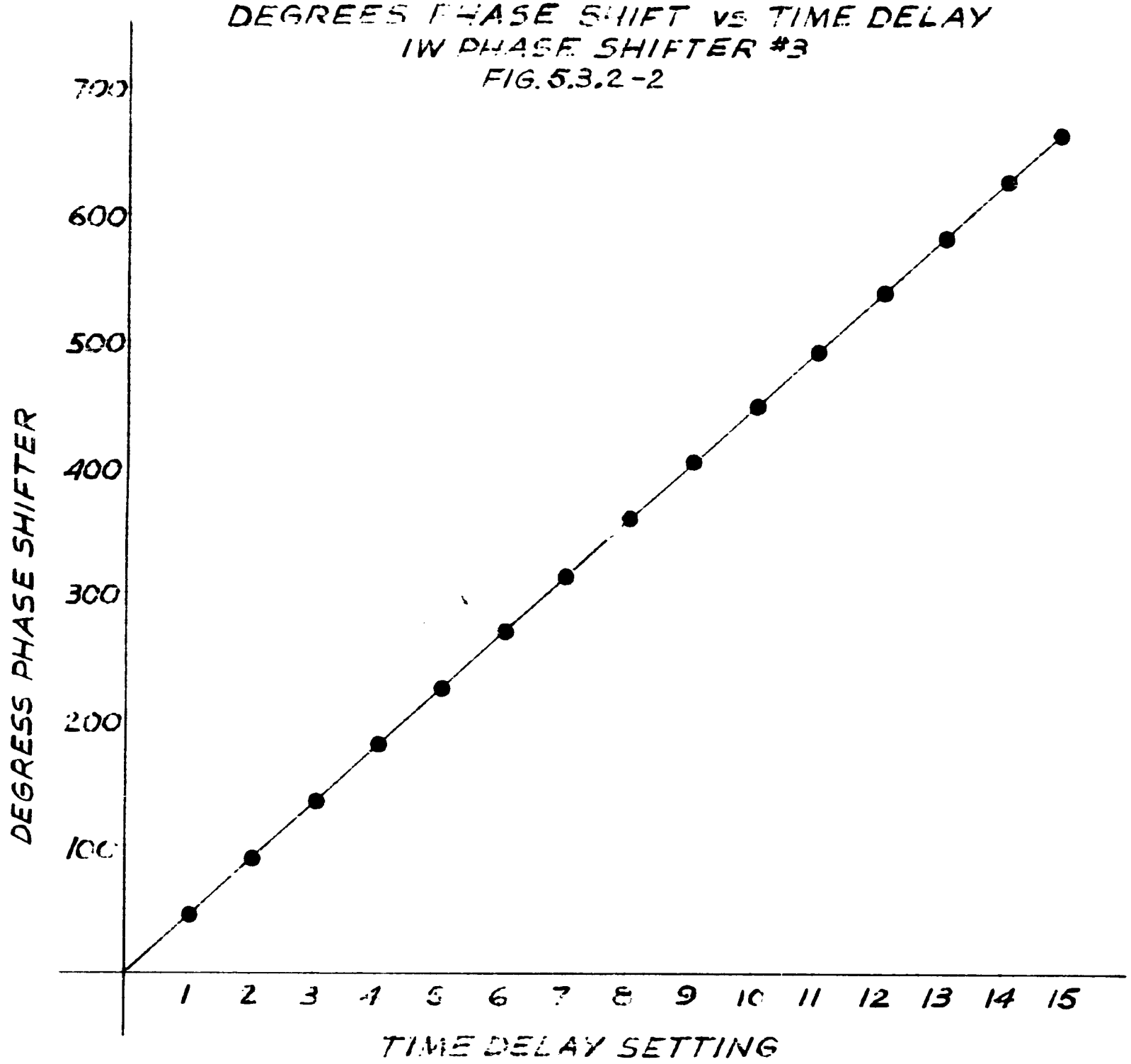

ERROR DEGREES IN PHASE SHIFTER #3

FIG 5.3.2-3

CHANNEL 1- ——
CHANNEL 2- ——

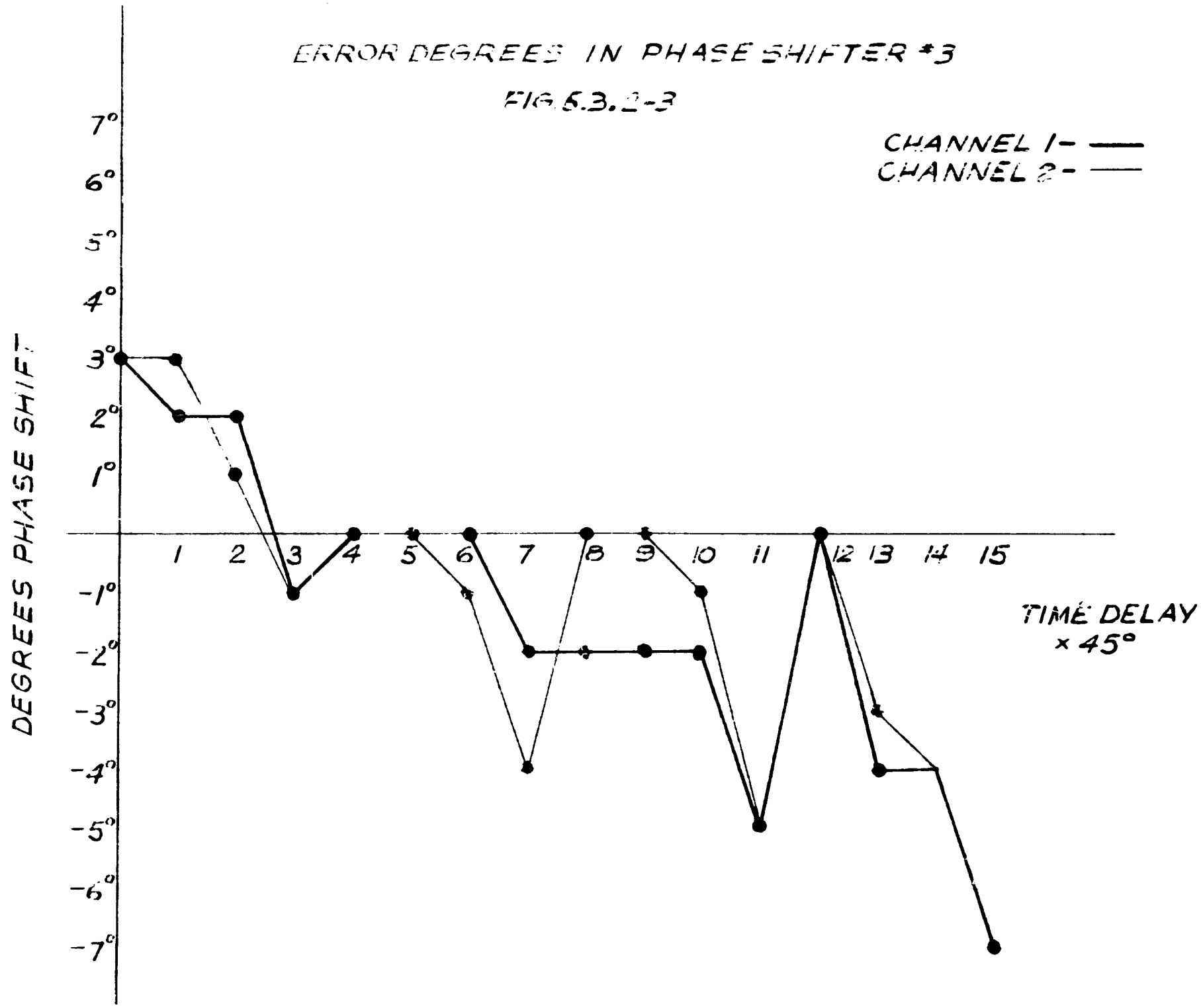

COMPARISON SIGNAL A/SIGNAL B db
IN PHASE SHIFTER #3

FIG. 5.3.2-4

CHANNEL 1 - - - - - -
CHANNEL 2 ———

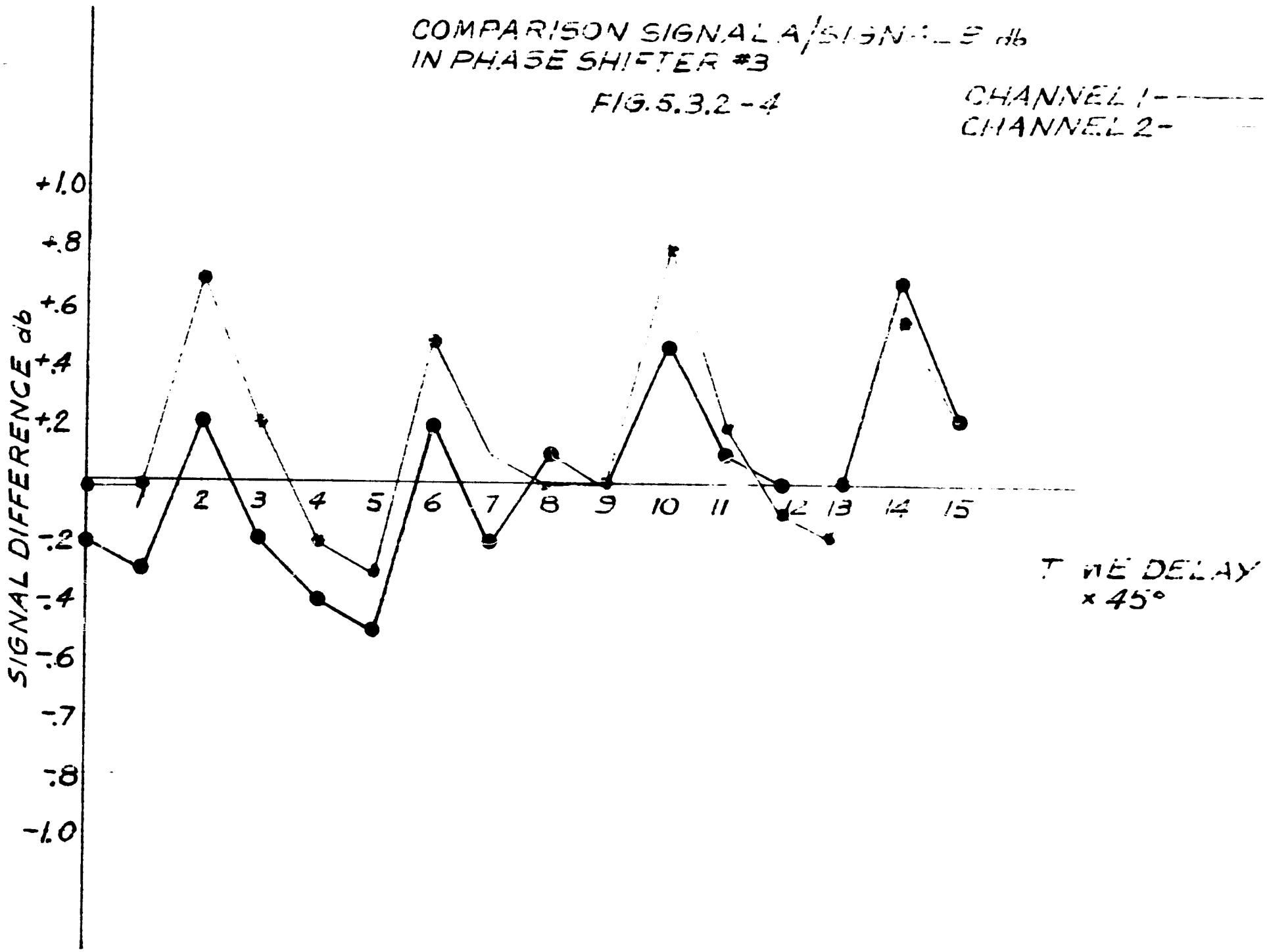

amplitude for each half of the circuit as a function of step number. Here the nominal insertion loss is 5 db and each section has been compensated with a resistive pad to equalize the amplitude response. Typical total variation in amplitude is less than 1 db.

5.3.3 Packaging

The central electronics enclosure for a pilot array, contains five time delay circuit board types: 1W; 2X; 3Y; 4Z and 5T. There are a total of 17 time delay circuits for each polarization which are distributed according to the following table:

Circuit Board Type	Number
1W	8
2X	4
3Y	2
4Z	2
5T	1

The 1W, 2X and 3Y boards have two complete sets of time delay circuits while the 4Z and 5T each have one set. The 3Y board includes a stage of R.F. amplification to make up for the insertion loss of time delay circuits 1W and 2X. The 4Z and 5T boards have only one time delay network due to the increased volume required by the relatively long lengths of cable attached to these boards.

All of the time delay networks are packaged in the same way. Single sided circuitry is used throughout. All components, except the long delay and interconnecting cables are mounted on one side of the board. The entire reverse side of the board is utilized as a ground plane except for small regions opposite to the component land areas. The boards are rectangular (9 inches x 10 inches) with a small (5 1/2 inches x 3 inches) cut out centered along the top edge. Turret terminals are located near this cutout, which provides a channel for the D.C. and control wires. The R.F. cabling and interconnection is accomplished by hard soldering the center conductor of the coaxial cable to a land area and soldering the outer braid to two turret terminals. No connectors are used in the R.F. cabling system. The R.F. cables which are coiled and tied on the ground plane side of the board are held in place by an aluminum back plate which is located about one inch from the ground plane. The back plate is held in position by four stand offs. A photograph showing this packaging arrangement is given in Figure 5.3.3-1.

Electrically the layout is simple. All resistance, inductance and capacitance values are standard preferred values the only exception being the coherent power combiner which is manufactured by Olektron Corporation of Dudley, Massachusetts. The land areas to which component solder connections are made have been located on a rectangular grid

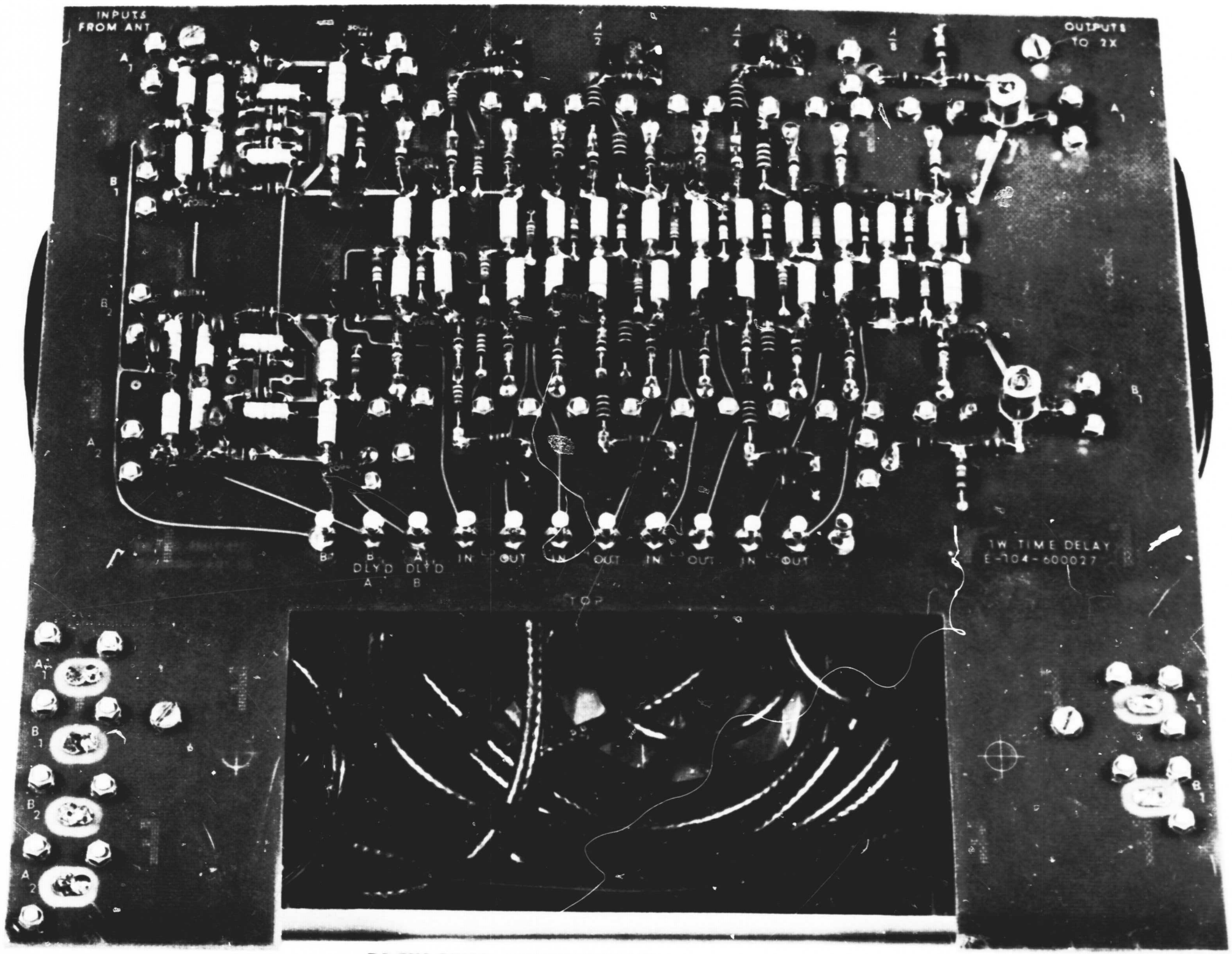

PACKAGING ARRANGEMENT
OF R.F. CABLES
Figure 5.3.3.-1

1/4 inch x 1/2 inch. This type of layout has been designed to aid in circuit assembly. The circuits will function properly when assembled to a high quality "commercial practice" specification. There are no special or critical areas where higher grade assembly practice is required. After the components and cables have been mounted, but before the aluminum back plate is added, the entire circuit is dipped in a radio frequency lacquer (Qmax A-27) manufactured by the Q-max Corporation of Marlboro, New Jersey. This substance protects against oxidation and corrosion and has excellent R.F. properties. More details of the physical properties of Qmax are given in Section 6.

5.3.4 Diode Switched Time Delay Circuit Specifications

	Network Type		
	1W and 3Y	2X and 4Z	5T
Maximum Relative Delay	1 7/8 λ	3 7/8 λ	7 7/8 λ
Number of Delay Increments	16	32	64
Insertion Loss	4 db ± 1/2 db	5 db ± 1/2 db	8 db ± 1/2 db

For all circuit types:

Operating Frequency: 69.72 MHz ± 500 KHz
74.70 MHz ± 500 KHz
79.68 MHz ± 500 KHz

Time Delay Increments: 1.67 nsec ± .42 nsec

Input Output Impedances: 50 ohms nominal V.S.W.R. = 1.3:1

Electrical Configuration: Two equal amplitude signals, delayed up to the maximum relative delay specified above, coherently combined into one output. A double-pole, double-throw switch (diode) must be included at the input circuit as shown in Figure 5.3.2-1.

Control Voltages: 6V @ 30 ma per delay line section plus 6V @ 50 ma for each double throw switch. Broad type 1W to be designed to permit 15 V @ 8 ma to be supplied to the field amplifiers.

5.4 Logic System Circuits

5.4.1 General Comments

In Section 4, it was shown how three digital numbers, properly truncated, control each array polarization. In this phased array design, the control numbers will be transmitted from a central control building to the field electronics via multi-conductor telephone cable as was done for the presently existing narrow band 128 dipole pilot system. Laboratory experiments using the 400 foot telephone cable (Phelps Dodge catalogue no. EB025) have been used to simulate the phase control link. The 50 db array would have 140 such

control links which sends the command signals to the central electronic enclosure where they are translated into time delays for the various R.F. signals. The source of these commands is not critical. They may originate from a small on-site computer, like the PDP-8, or a special purpose control system. In either case, the processing circuits at the pilot array level will remain the same.

In the following two sections short descriptions are given of (1) a manually operated array control system which has proved to be useful in the test and debugging of the various logic circuits and (2) the logic circuits which are used at the pilot array level to control the field time delay circuits.

5.4.2 Manual Receiver Control

At the pilot array level, the three numbers required to control the array are pulse sequences of variable length. The manual control which generates the pulse sequences is documented by drawings 104-800015, 104-400038, and 104-400037. The overall systems block diagram shown in Figure 104-800015 indicates the various circuit functions that must be performed in the control building, i.e. B+ control, repetition rate control, beam directions, number selection, etc. The control function essentially consists of generating 3 pulse sequences, the first of which may be 0 to 15 pulses long, the second 0 to 31 pulses

8 7 6 5

D C B A

STEP PULSE GENERATOR
DRIVER
TEST POINT
SET PULSE SHAPING
SET CONTROL SWITCH
INTER-COLUMN TIME DELAY SELECT 0-15 PULSES (N_2)
CONVERTER
DRIVER
TEST POINT
PULSE SHAPING
4 BIT COUNTER AND GATES
DRIVE
INTRA-COLUMN TIME DELAY SELECT 0-31 PULSES (N_3)
CONVERTER
DRIVER
TEST POINT
PULSE SHAPING
5 BIT COUNTER AND GATES
DRIVE
INTER-COLUMN TIME DELAY SELECT 0-63 PULSES (N_1)
CONVERTER
DRIVER
TEST POINT
PULSE SHAPING
6 BIT COUNTER AND GATES
DRIVE
REP RATE CONTROL SWITCH
ONE SHOT
DRIVER
TEST POINT
CLEAR PULSE SHAPING
BEAM DIRECTION SWITCH NS
PULSE GENERATOR
DRIVER
TEST POINT
PULSE SHAPING
TEST POINT
TO 24 PLACES; N
BEAM DIRECTION SWITCH EW
PULSE GENERATOR
DRIVER
TEST POINT
PULSE SHAPING
TEST POINT
TO 7 PLACES; NET
POWER CONTROL SWITCH - PANEL
FIELD POWER SWITCH
TO POWER SUPPLY IN FIELD
FIELD PULSE SWITCHES (6)
1

Fold Out

8 7 6 5

REVISIONS						
ZONE	LTR	DESCRIPTION	DR	CHK	DATE	APPROVED

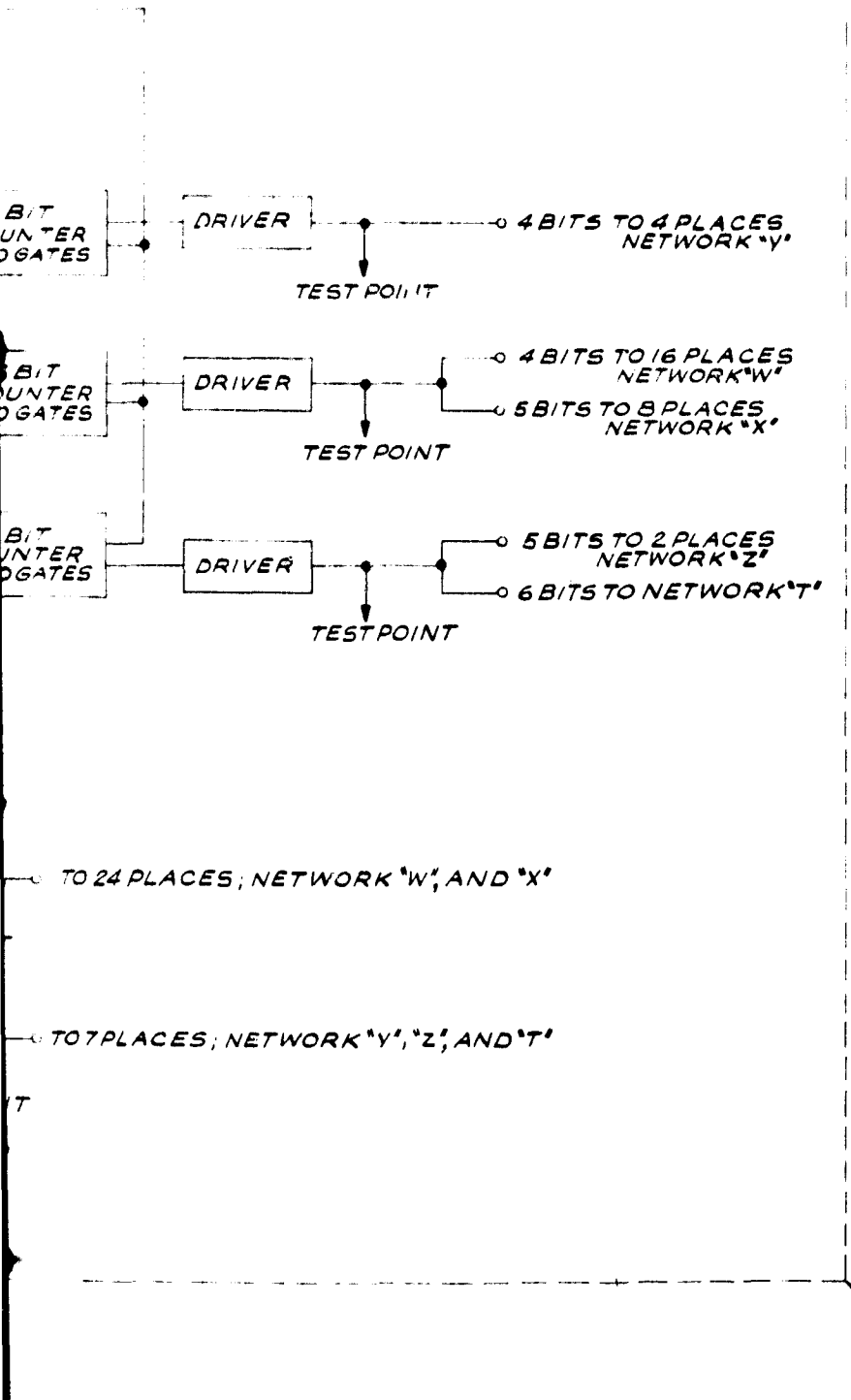

FIND NO.	QTY REQD	PART OR IDENT. NO.	NOMENCLATURE OR DESCRIPTION	MATERIAL OR SPECIFICATION
2	1	T-104-900036	DIGITAL CONTROL CIRCUIT	
1	1	T-104-900037	MANUAL RECEIVER CONTROL	

LIST OF MATERIALS

NEXT ASSY	USED ON
APPLICATION	

UNLESS OTHERWISE SPECIFIED
CAPACITOR VALUES ARE IN μf
RESISTOR VALUES ARE IN OHMS
ELECTRICAL TOLERANCES = ±5%

DIMENSIONS ARE IN INCHES
TOLERANCES ON
FRACTIONS DECIMALS ANGLES
± ~ ± ~ ± ~
DO NOT SCALE THIS DRAWING

MATERIAL

DRAWN Mark Jazukiewicz March 69
CHECKED
APPROVED
APPROVED
MIT APPROVED DATE

CENTER FOR SPACE RESEARCH
MASSACHUSETTS INSTITUTE OF TECHNOLOGY
CAMBRIDGE, MASS.

LOGIC SYSTEM BLOCK DIAGRAM PER POLARIZATION

SIZE	CODE IDENT NO.	DRAWING NO.
D		104-800015

SCALE ~ SHEET 1 OF 1

104-800015

B

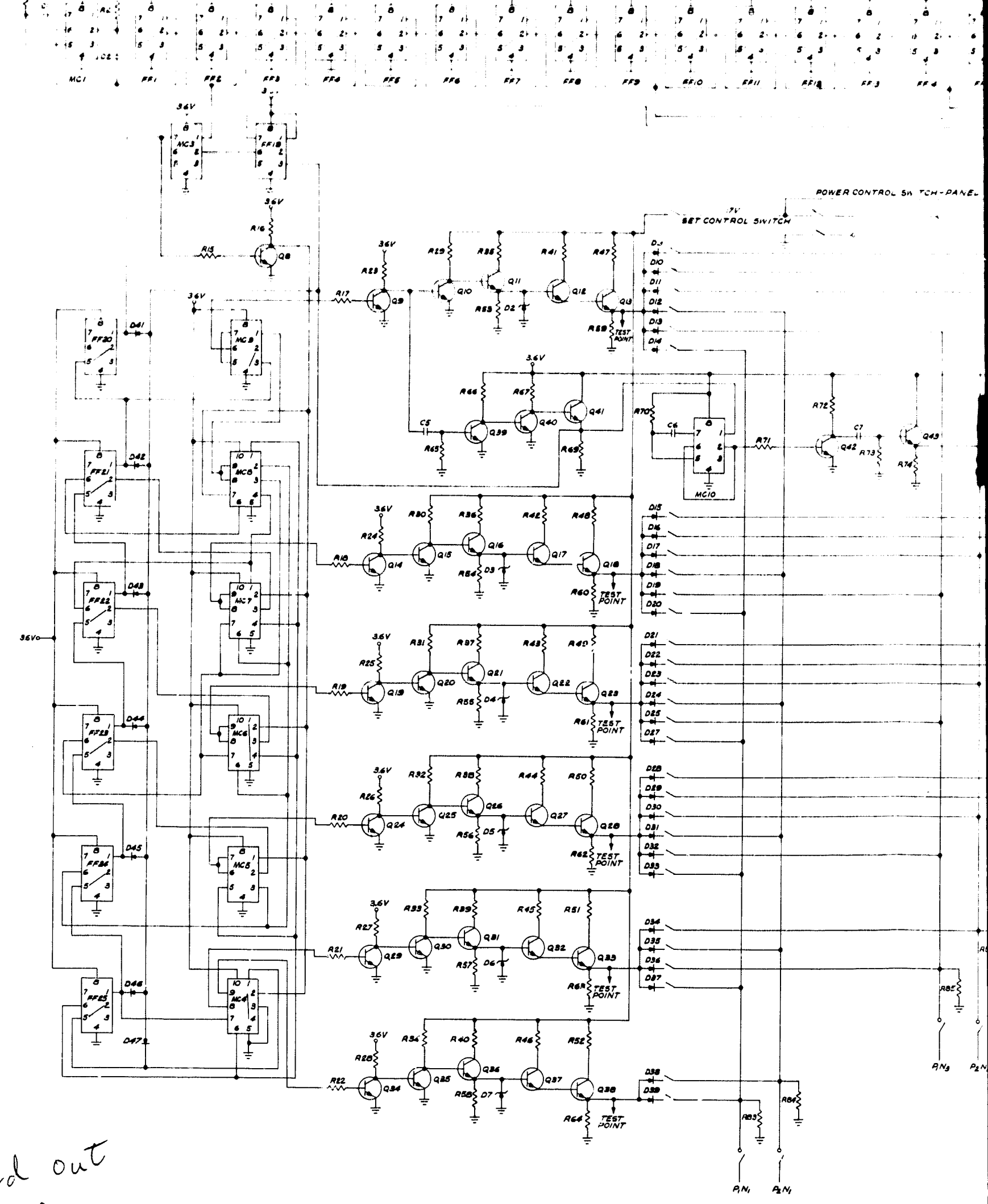
3.6V
MC1
FF1
FF2
FF3
FF4
FF5
FF6
FF7
FF8
FF9
FF10
FF11
FF12
FF13
FF14
MC3
FF15
R16
R15
Q8
R17
Q9
R23
R29
R35
R41
R47
Q10
Q11
Q12
Q13
R53
D2
R59
TEST POINT
POWER CONTROL SWITCH-PANEL
SET CONTROL SWITCH
D9
D10
D11
D12
D13
D14
MC9
FF20
D41
MC8
FF21
D42
MC7
FF22
D43
MC6
FF23
D44
MC5
FF24
D45
MC4
FF25
D46
D47
3.6Vo
R65
C5
R66
R67
Q39
Q40
Q41
R69
R70
C6
MC10
R71
R72
C7
Q42
R73
Q43
R74
R24
R30
R36
R42
R48
Q14
Q15
Q16
Q17
Q18
R54
D3
R60
TEST POINT
D15
D16
D17
D18
D19
D20
R19
R25
R31
R37
R43
R49
Q19
Q20
Q21
Q22
Q23
R55
D4
R61
TEST POINT
D21
D22
D23
D24
D25
D27
R20
R26
R32
R38
R44
R50
Q24
Q25
Q26
Q27
Q28
R56
D5
R62
TEST POINT
D28
D29
D30
D31
D32
D33
R21
R27
R33
R39
R45
R51
Q29
Q30
Q31
Q32
Q33
R57
D6
R63
TEST POINT
D34
D35
D36
D37
R85
P1N3
P2N3
R22
R28
R34
R40
R46
R52
Q34
Q35
Q36
Q37
Q38
R58
D7
R64
TEST POINT
D38
D39
R84
R83
P1N1
P2N1

Fold out
a

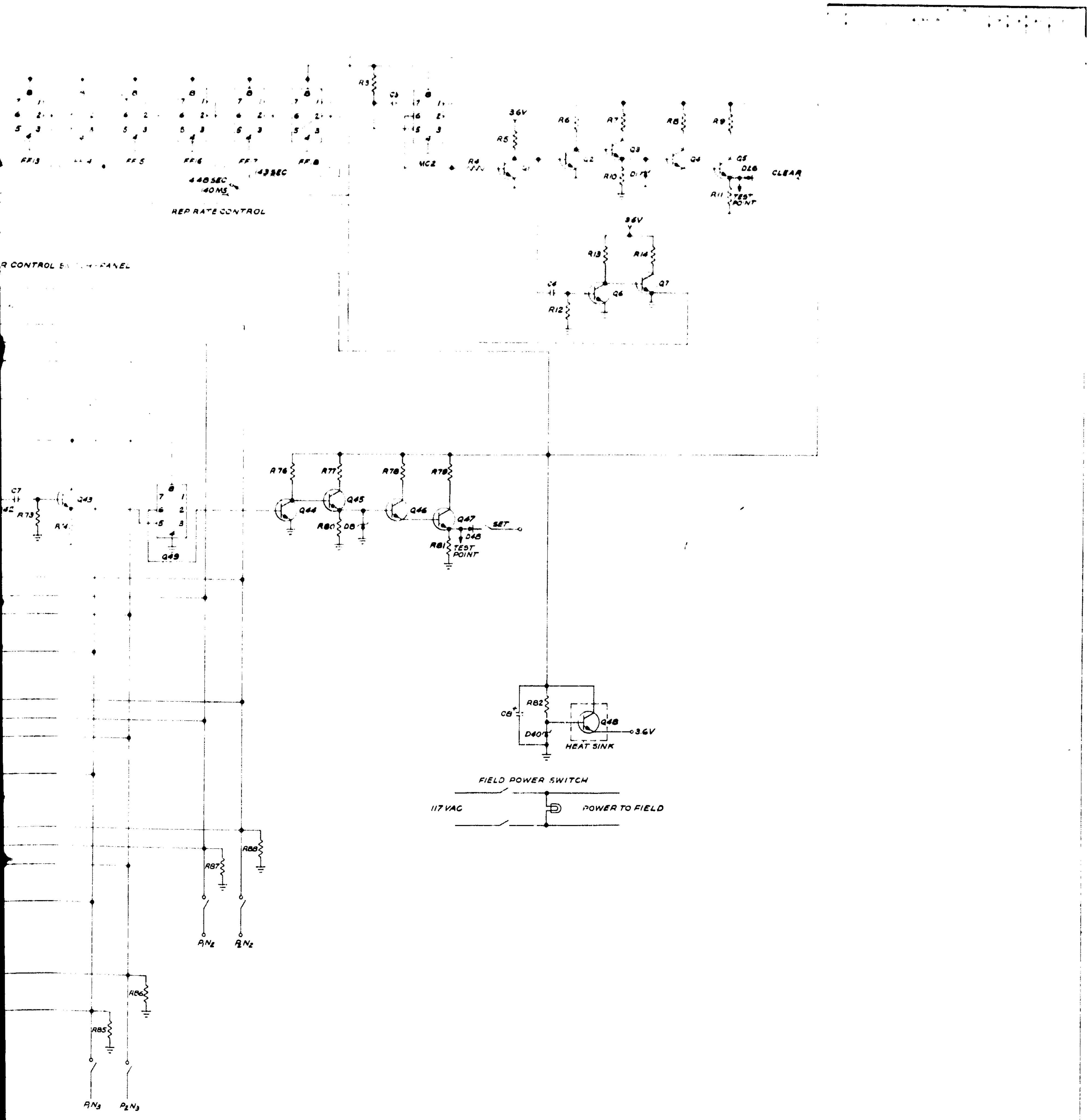

B

UNLESS OTHERWISE SPECIFIED CAPACITOR VALUES ARE IN μF RESISTOR VALUES ARE IN OHMS ELECTRICAL TOLERANCES ±5%

DIMENSIONS ARE IN INCHES TOLERANCES ON FRACTIONS DECIMALS ANGLES

DO NOT SCALE THIS DRAWING

MATERIAL

NEXT ASSY | USED ON

APPLICATION

LIST OF MATERIALS

CENTER FOR SPACE RESEARCH
MASSACHUSETTS INSTITUTE OF TECHNOLOGY
CAMBRIDGE, MASS

DRAWN H. Jasukiewicz

CHECKED

APPROVED

APPROVED

MANUAL RECEIVER CONTROL

SIZE J | CODE IDENT NO | DRAWING NO 104-400037

SCALE ~ | SHEET 1 OF 1

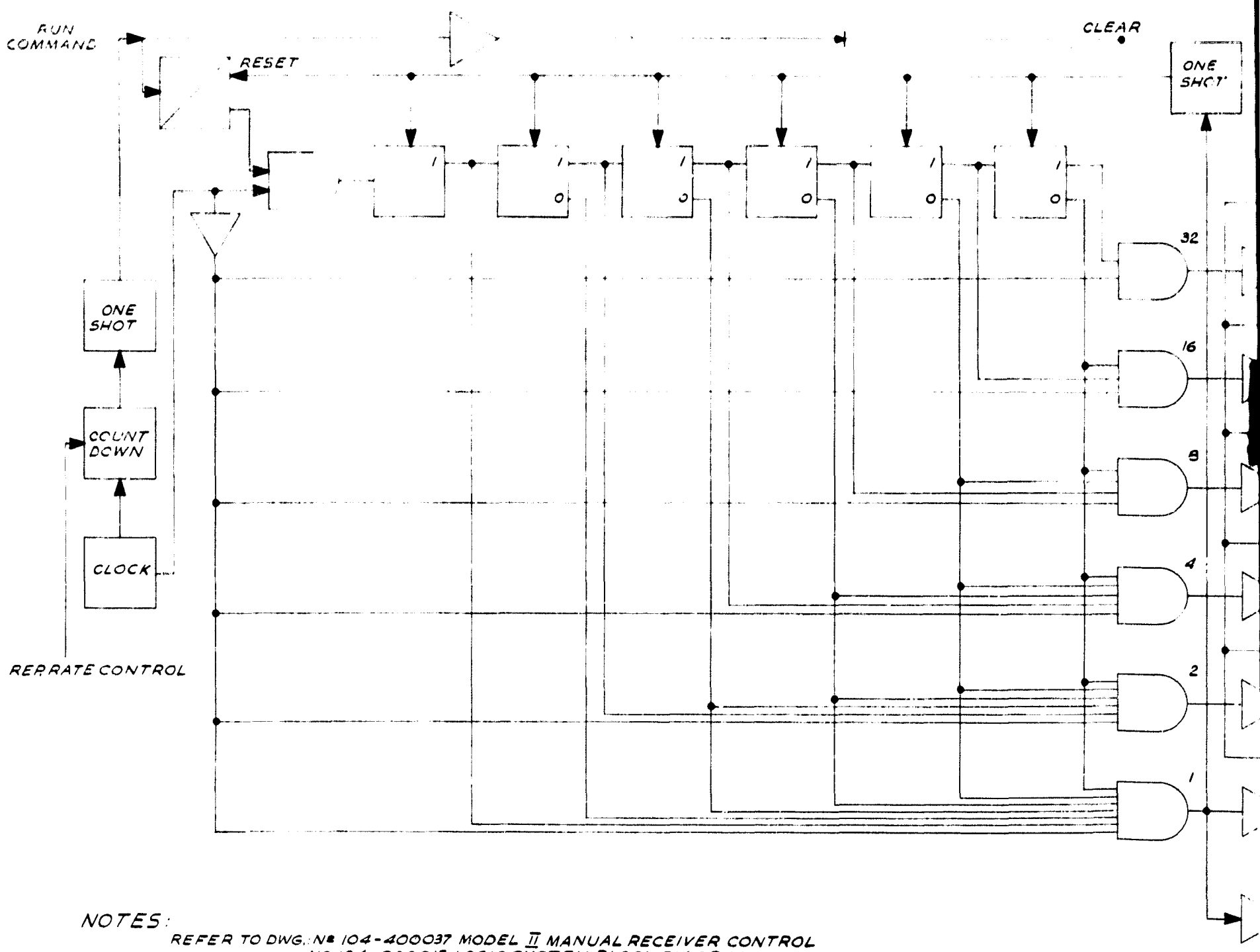

NOTES:

REFER TO DWG. Nº 104-400037 MODEL II MANUAL RECEIVER CONTROL
Nº 104-800015 LOGIC SYSTEM BLOCK DIAGRAM
BEAM DIRECTION SWITCHES, PANEL B+ SWITCH,
AND FIELD POWER SWITCHES NOT SHOWN.

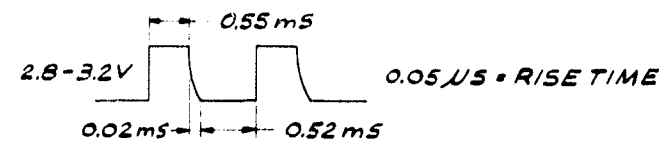

SWITCHES AT OUTPUT OF N_1, N_2, N_3, SET, AND
CLEAR ARE FIELD PULSE SWITCHES.
ALL OUTPUTS: 1 PER POLARIZATION

Fold out
a

ZONE	REVISIONS	DESCRIPTION	BY	CHK	DATE	APPROVED

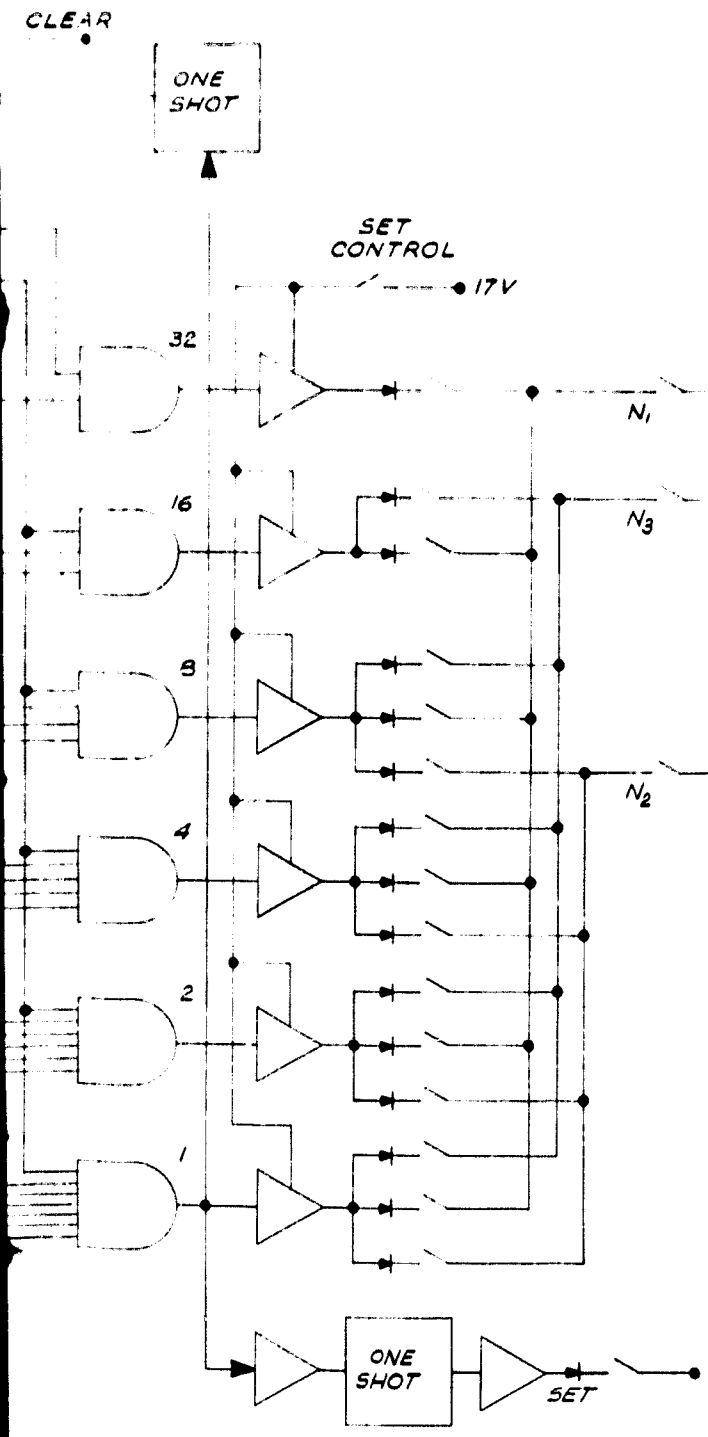

FIND NO.	QTY REQD	PART OR IDENT. NO.	NOMENCLATURE OR DESCRIPTION	MATERIAL OR SPECIFICATION

LIST OF MATERIALS

NEXT ASSY	USED ON
APPLICATION	

UNLESS OTHERWISE SPECIFIED
CAPACITOR VALUES ARE IN μf
RESISTOR VALUES ARE IN OHMS
ELECTRICAL TOLERANCES ±5%

DIMENSIONS ARE IN INCHES
TOLERANCES ON
FRACTIONS DECIMALS ANGLES
± ~ ± ~ ± ~
DO NOT SCALE THIS DRAWING

MATERIAL

DRAWN	Mark Jazukiewicz	FEB 69
CHECKED		
APPROVED		
APPROVED		
MIT APPROVED		DATE

CENTER FOR SPACE RESEARCH
MASSACHUSETTS INSTITUTE OF TECHNOLOGY
CAMBRIDGE, MASS.

MANUAL RECEIVER CONTROL LOGIC DIAGRAM

SIZE	CODE IDENT NO.	DRAWING NO.
D		104-400038

SCALE ~ SHEET 1 OF 1

B

1 March 69

long and the third 0 to 63 pulses. These sequences are sent to the central electronic enclosure where they control the various time delay circuits.

The logic diagram for the generation of these sequences is shown in Figure 104-400038. It consists of a clock, count-down chain, six stage counter, along with six gates and six line driver circuits. The count-down chain provides the basic repetition rate control. The circuit is designed to permit selection of three different rates at which the central pulses are generated. The clock pulses also drive the six stage counter and the gates. The outputs from the counter and clock are logically combined in the gate circuits to yield six output signals. These signals are the pulse sequences 2^n where n = 0,1,2,3,4,5. The manual receiver control output numbers are obtained by combining the desired number of output pulses from these six lines by means of switches.

This basic control system, only slightly modified, has been used to control both the electronic time delay circuits described in Section 5.3 and the phase shift circuits used in the 128 element narrow band dipole array (Section 7.2). In both cases the necessary circuits were constructed from commercially available integrated circuits.

5.4.3 Digital Control Circuits

The pulses generated by the central control system are transmitted over a buried telephone cable to the central electronics enclosure. Here they are processed and used to drive the R.F. time delay circuits. A block diagram of this control circuit is shown in Figure 5.4.3-1. It consists of a differentiator, power amplifiers, (drivers) counters, driver gates, SCR drivers and an SCR power control circuit. Three signals are required to convert the pulse sequence into a unique time delay. The format of these signals is shown in Figure 5.4.3-1. The control cycle begins when a clear pulse arrives which activates the SCR power control. The function of this pulse is to momentarily remove the B+ voltage supply from the SCR and thereby render all SCR's non-conducting. Following the clear pulse the control numbers (a sequence of n pulses defining a unique time delay) are supplied to the differentiator. After amplification the resultant series of pulses is supplied serially to the counter. In this circuit, 4,5 and 6 bit counters (corresponding to the length of pulse sequence) are used. Each counter has a unique state for each pulse sequence, which is transferred to the SCR drivers and hence the time delay circuits remain in a given state until the next clear pulse arrives and starts the cycle over again. The rate at which the array is controlled is determined by the length of time interval

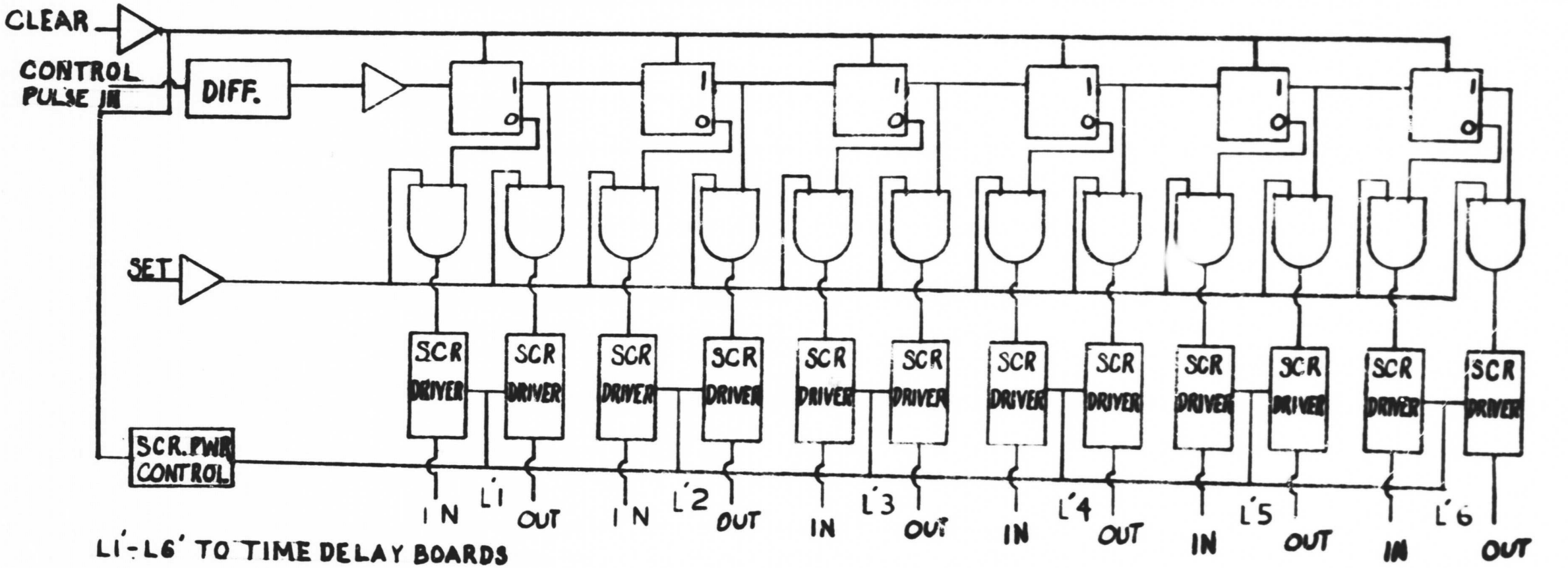

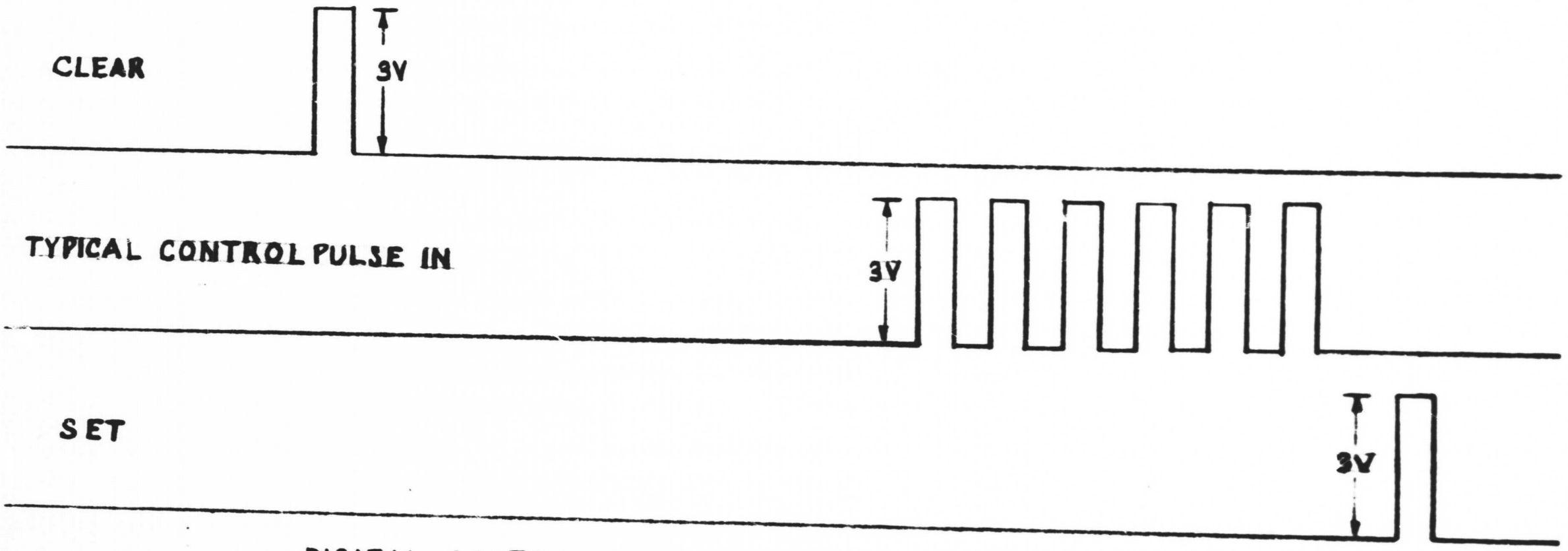

DIGITAL CONTROL UNIT LOGIC BLOCK DIAGRAM FIG. 5.4.3-1

between clear pulses which may be varied by a control clock at the central building.

The gates, register element and amplifiers are all designed with standard commercial quality integrated circuits. There are no special requirements with regard to speed or power considerations imposed on these devices. However, because of the large number of time delay circuits in parallel, the SCR drivers must handle currents of the order of an ampere. An SCR was selected precisely because of its ability to switch high currents at relatively low device cost. The complete circuit diagram of the digital control circuit is given in 104-400036.

5.5 Power Supply

Power supply requirements are, of course, dependent upon the size of the installation under consideration. In Table 5.5-1 the power requirements are listed for a dual polarization pilot array (32 Double-Tee elements per polarization). After consideration of the power levels involved and the reliability that is required, we concluded that the power supply could be a purchased unit.

Discussions with potential suppliers permitted us to draw definite conclusions regarding size, cost and design features available as options. Figure 5.5-1 shows the installation scheme for the power supply. The main power switch is located in the operators building. This switch

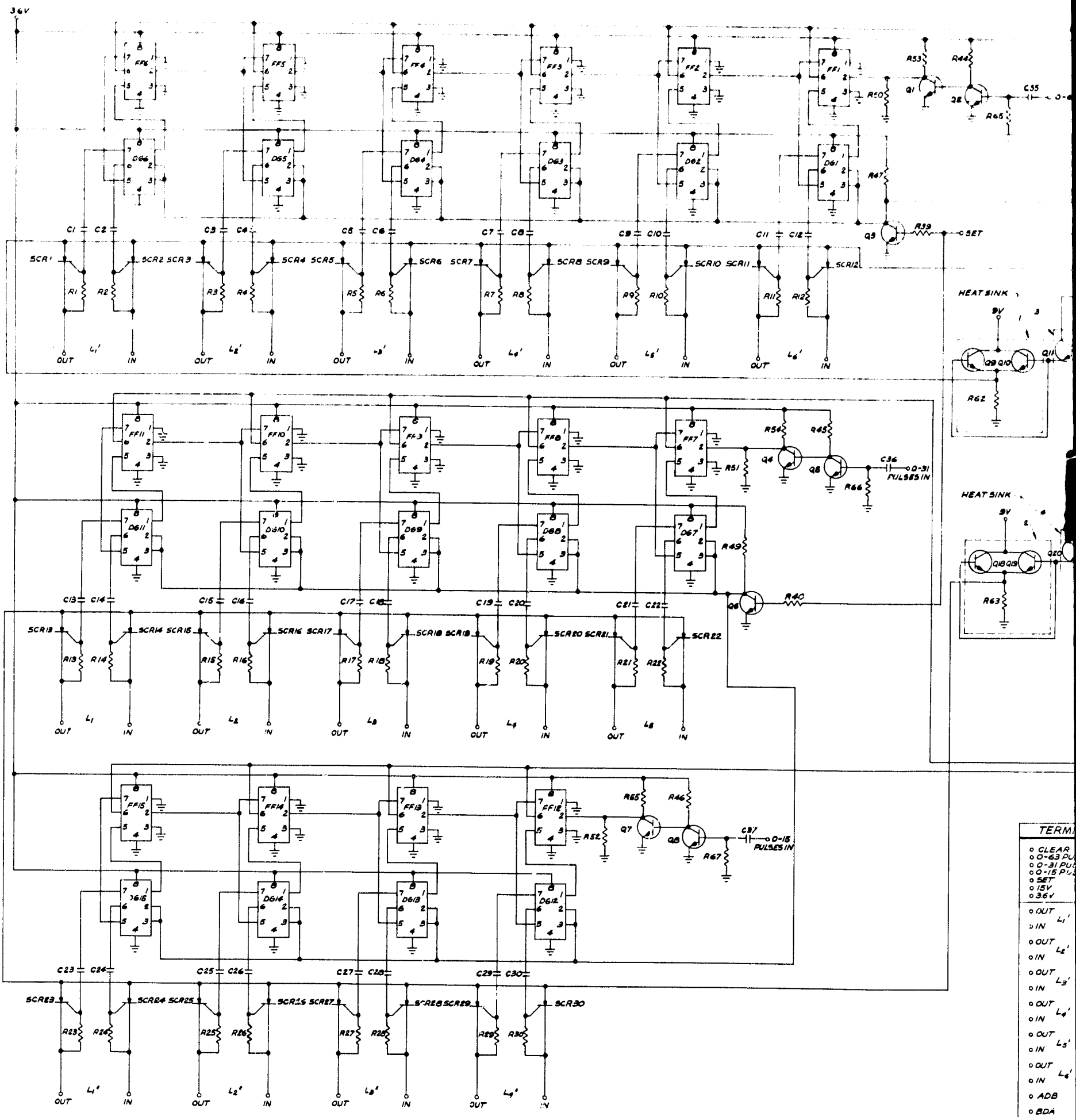
36V
FF6
FF5
FF4
FF3
FF2
FF1
DG6
DG5
DG4
DG3
DG2
DG1
C1 C2
C3 C4
C5 C6
C7 C8
C9 C10
C11 C12
SCR1
SCR2 SCR3
SCR4 SCR5
SCR6 SCR7
SCR8 SCR9
SCR10 SCR11
SCR12
R1
R2
R3
R4
R5
R6
R7
R8
R9
R10
R11
R12
OUT
IN
L1'
L2'
L3'
L4'
L5'
L6'
R53
R44
Q1
2E
C55
O-
R65
R50
R47
Q9
R39
SET
HEAT SINK
9V
Q9 Q10
Q11
R62
FF11
FF10
FF9
FF8
FF7
DG11
DG10
DG9
DG8
DG7
C13 C14
C15 C16
C17 C18
C19 C20
C21 C22
SCR13
SCR14 SCR15
SCR16 SCR17
SCR18 SCR19
SCR20 SCR21
SCR22
R13
R14
R15
R16
R17
R18
R19
R20
R21
R22
L1
L2
L3
L4
L5
R54
R45
Q4
Q8
C36
O-31
PULSES IN
R66
R51
R49
R40
Q6
HEAT SINK
9V
Q18 Q19
Q20
R63
FF15
FF14
FF13
FF12
DG15
DG14
DG13
DG12
C23 C24
C25 C26
C27 C28
C29 C30
SCR23
SCR24 SCR25
SCR26 SCR27
SCR28 SCR29
SCR30
R23
R24
R25
R26
R27
R28
R29
R30
L1'
L2'
L3'
L4'
R65
R46
Q7
Q5
C37
O-15
PULSES IN
R67
R52
TERM
CLEAR
0-63 PU
0-31 PU
0-15 PU
SET
15V
36V
OUT L1'
IN
OUT L2'
IN
OUT L3'
IN
OUT L4'
IN
OUT L5'
IN
OUT L6'
IN
ADB
BDA
(ADB)'
(BDA)'
(ADB)''
(BDA)''

Fold out

a

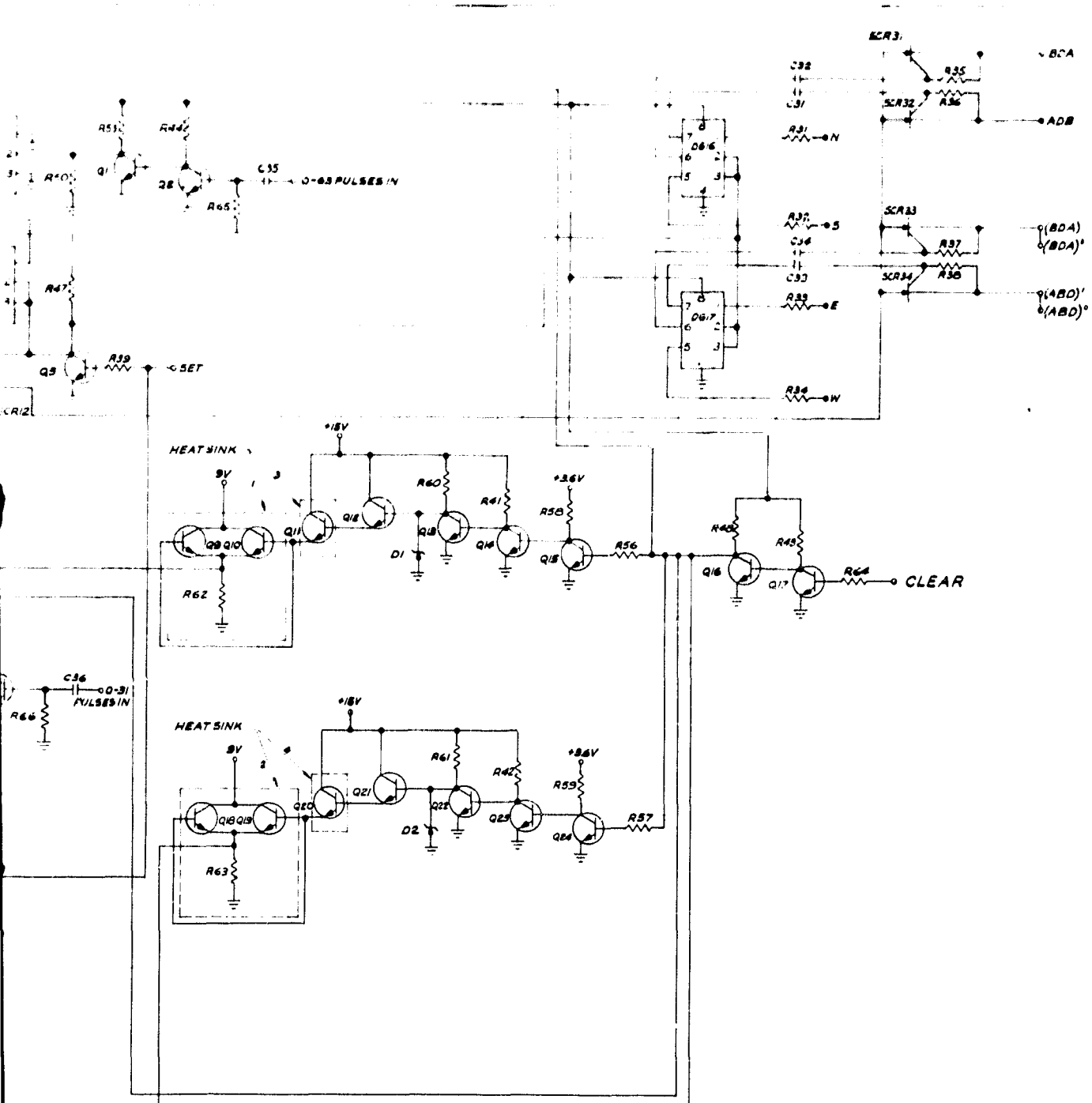

TERMINAL BOARD IDENTIFICATION

o CLEAR o 0-63 PULSES IN o 0-31 PULSES IN o 0-15 PULSES IN o SET o 15V o 3.6V	o 5 o N o W o E o = o 9V	
o OUT L_1' o IN L_1'	o OUT L_1 o IN L_1	o OUT $L_1°$ o IN $L_1°$
o OUT L_2' o IN L_2'	o OUT L_2 o IN L_2	o OUT $L_2°$ o IN $L_2°$
o OUT L_3' o IN L_3'	o OUT L_3 o IN L_3	o OUT $L_3°$ o IN $L_3°$
o OUT L_4' o IN L_4'	o OUT L_4 o IN L_4	o OUT $L_4°$ o IN $L_4°$
o OUT L_5' o IN L_5'	o OUT L_5 o IN L_5	
o OUT L_6' o IN L_6'		
o ADB		
o BDA		
o(ADB)'		
o(BDA)'		
o(ADB)°		
o(BDA)°		

B

FIND NO	QTY	PART OR IDENT NO	NOMENCLATURE OR DESCRIPTION	MATERIAL OR SPECIFICATION

LIST OF MATERIALS

UNLESS OTHERWISE SPECIFIED CAPACITOR VALUES ARE IN μf RESISTOR VALUES ARE IN OHMS ELECTRICAL TOLERANCES ± 5%

DIMENSIONS ARE IN INCHES TOLERANCES ON FRACTIONS DECIMALS ANGLES ± — = — ± —

DO NOT SCALE THIS DRAWING

MATERIAL

NEXT ASS'Y | USED ON

APPLICATION

DRAWN Mark Horowitz 11/28/67

CHECKED

APPROVED

APPROVED

MIT APPROVED DATE

CENTER FOR SPACE RESEARCH
MASSACHUSETTS INSTITUTE OF TECHNOLOGY
CAMBRIDGE, MASS.

DIGITAL CONTROL CIRCUIT

SIZE J | CODE IDENT NO | DRAWING NO 104-400036

SCALE — | SHEET 1 OF 1

TABLE 5.5-1

Power Supply Requirements for a Dual Polarization Pilot Array Installation (32 Antenna T Elements per Polarization)

Power Requirements	Application
+15V @ 2 1/2 Amps	RF amplifiers and SCR clear pulse amplifiers
+9V @ 15 Amps	SCR clear pulse amplifiers
+3.6V @ 1 Amp	Integrated circuit logic modules

THREE POWER SUPPLIES MOUNTED EXTERNALLY
TO FIELD ELECTRONIC ENCLOSURE

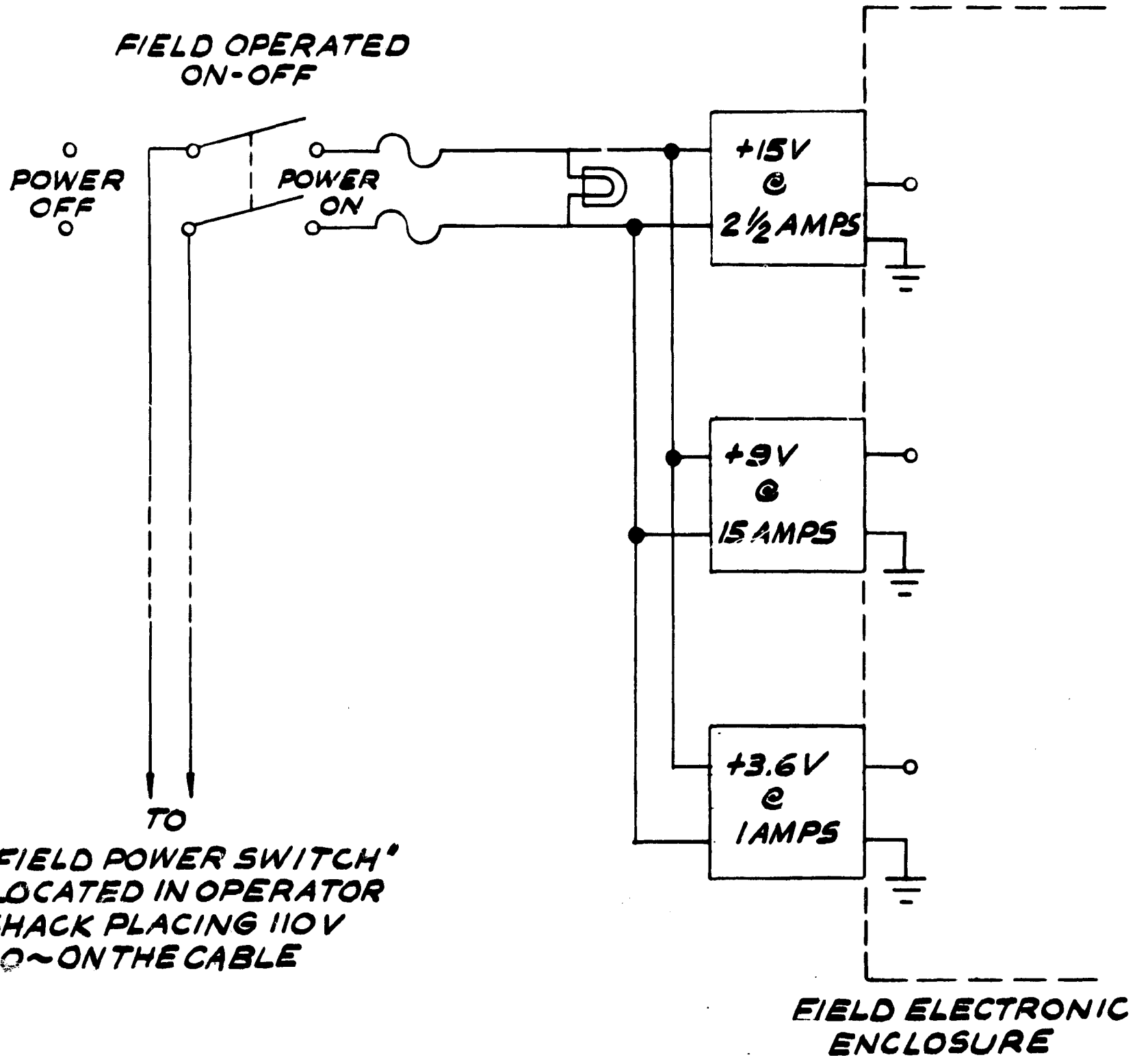

POWER SUPPLY LAYOUT

FIG. 5.5-1

places A.C. excitation across the three power supplies. They are externally mounted onto the field electronic enclosure. This eliminates any thermal problems that might arise from having the units enclosed with the phase shifters, etc. It also alleviates a severe space restriction that is caused by locating the power supplies within the central enclosure. The containers must be designed to withstand outside weather conditions. Investigation has shown that the size to be expected for suitable "off-the-shelf" power units will be about 10" x 5" x 5" each. Commercial units having suitable voltage and current capabilities and voltage tolerances less than $\pm$1% with respect to line and load variations are readily available. Other features such as automatic current limiting and transient suppression networks are also available and a suitable combination of options will be purchased to specification. This is very important since all of the digital logic modules for example could be destroyed quickly under certain power supply transient conditions. For each pilot array there are 64 R.F. amplifiers each of which are buried in the ground and requires +15 V. To insure that a possible short circuit in one amplifier will not short the entire +15 V supply, thereby shutting down the system. each line that feeds individual amplifiers is separately fused. Thus, if one amplifier fails the rest of the system will continue to function.

5.6 References

1 Baker, R.H. et al. "Conceptual Design of a Small Solar Probe," M.I.T. CSR TR-69-1, (January, 1969).

CHAPTER 6

6.0 MECHANICAL AND ENVIRONMENTAL CONSIDERATIONS

6.1 System Packaging

The primary objective in packaging is to protect the system from the environment at a reasonable cost. The design concepts presented in this section are the results of a lengthy study of all the various aspects of the array from performance through reliability. Additionally, the concepts are based on the eight years of field experience with the existing El Campo facilities.

6.1.1 Protecting Material

Printed circuit boards must be protected from moisture and corrosion, without interfering with the electrical properties of the components on the board. A low loss factor and high dielectric strength are important characteristics of the material used.

The boards within the central enclosure are unencapsulated but are coated with Q-Max A27 Radio Frequency Lacquer. This material possesses good dielectric strength (1965 volts per mil average) and repels moisture. Also tests of prolonged

exposure to humidity show that the long term stability is good. In an ambient of 99°F and 98% relative humidity, the surface resistance is greater than 1.73×10^{14} ohms. The volume resistivity is high 7.12×10^{14} ohms. The loss factor at 30 mhz and higher is .003. And the Q-dax lacquer is fungi-resisting.

The dipole amplifiers, which are buried; and therefore must be waterproof must also be protected in a material that will not alter their electrical performance.

The encapsulant used for the amplifiers (STYCAST V-B, Emerson and Cuming, Inc.) is a modified epoxide casting resin which has been specifically formulated for encapsulated electrical circuitry. It exhibits good flow properties and rapid cure at room temperature, low shrinkage, and is convenient to work with. Additional properties are:

STYCAST Type V-3

Hardness, shore D	70
Volume Resistivity ohm-cm	10^{13}
Dielectric Strength volts/mil	800
Dielectric Constant, 60 cycles	6.8
Dissipation Factor, 60 cycles	0.016
Surface resistivity, ohms	10^{13}
Flammability	Self-extinguishing

6.1.2 Central Electronics Enclosure

The central electronics enclosure must be waterproof, dustproof, yet accessible. In order to avoid excessive temperatures, the enclosure must be shaded and raised above the ground by at least six inches. A single roof attached to four posts accomplishes this and allows air convection. The electronic boards are assembled into the enclosure from the top into guides mounted on a rack. The cables enter at the side of the enclosure through rubber grommets and are soldered directly to the circuit boards. (Figures 6.1.2-1 and 6.1.2-2).

6.1.3 Mechanical Specifications

The purpose of an enclosure is to protect the enclosed elements from the environment; particularly weather, dust, animals, and insects. Direct burial amplifier enclosure that appears to be satisfactory is constructed from 12 gauge steel which is either painted with a hard enamel or hot-dipped galvanized.

6.2 Dipole and Double-Tee Element Assembly Design and Test

The basic element that has been proposed for the array is a group of six dipoles in a "Twin-Tee" arrangement which is shown in Figure 2.2-1. Phasing within the Twin-Tee is done manually by inserting or removing cable lengths at appropriate

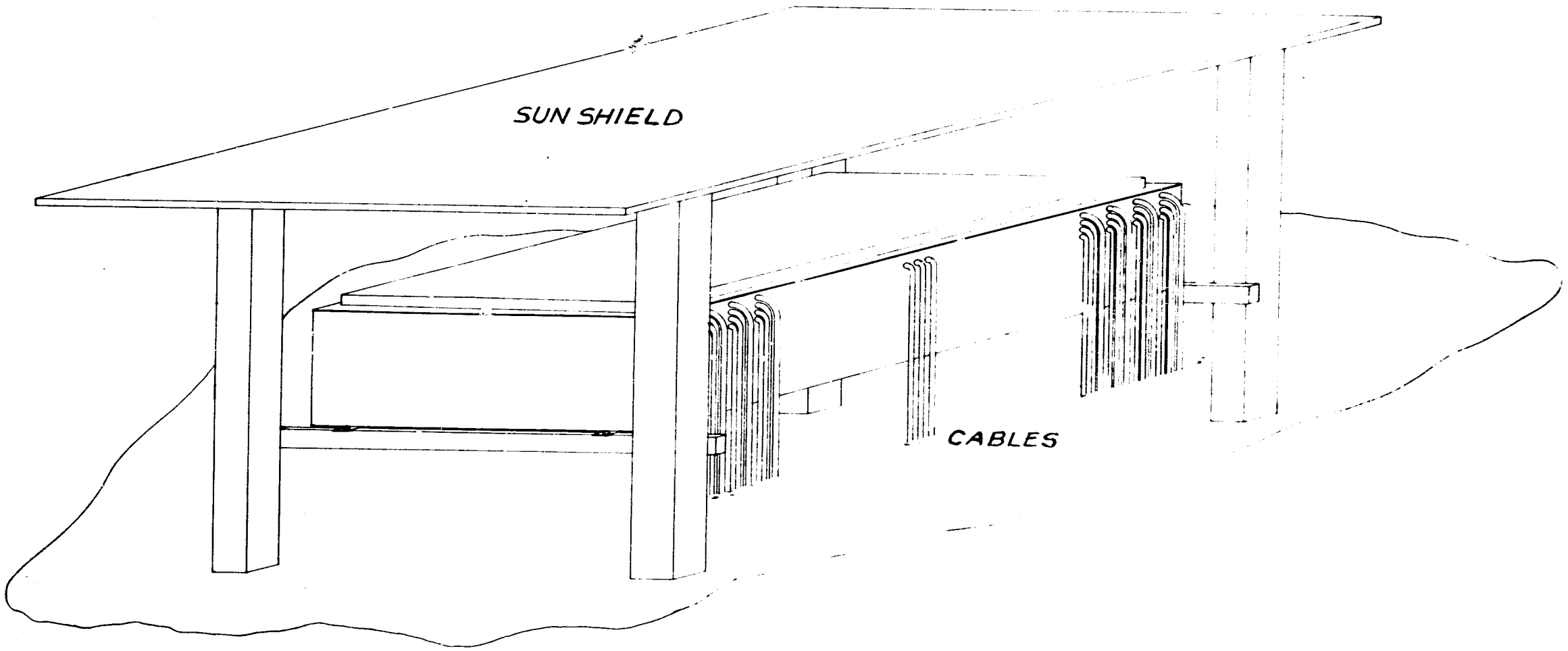

FIG. 6.1.2-1
ENCLOSURE

PACKAGING OF CENTRAL
ELECTRONIC ENCLOSURE

FIG. 5.1.2-2

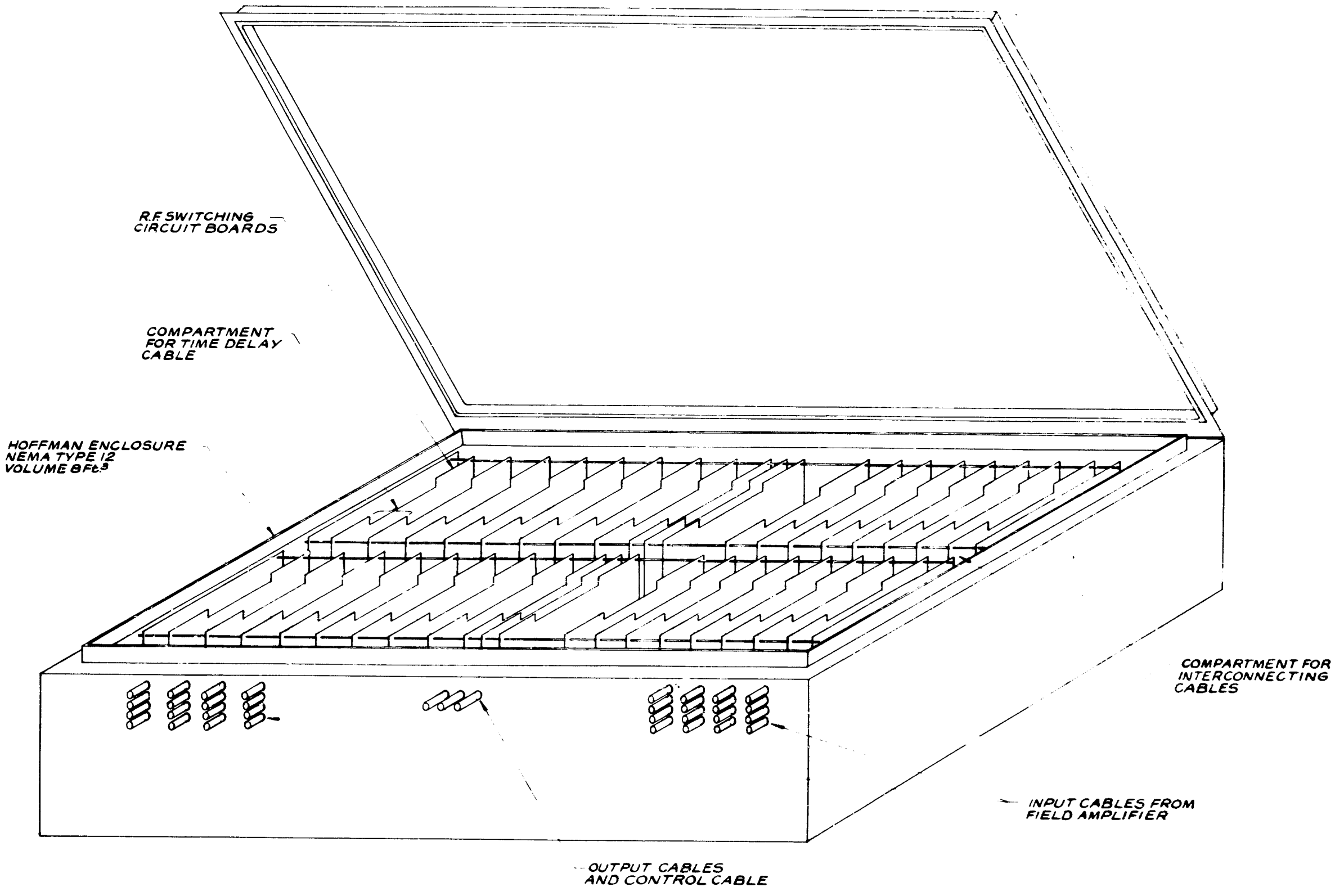

points.

The beamwidth of the Twin-Tee will limit the viewing time for a given source to about two hours each day, and will require manual phasing about six times per year as the sun changes in declination.

The Twin-Tee element is a compromise in the interest of economy. The antenna performance would be improved if a separate amplifier and automatic phase shifter were used with each dipole.

6.2.1 Dipole Materials

A 1 1/2" diameter × 0.050 wall aluminum tube was selected for the dipoles on the basis of past experience with both 1" and 1 1/2" thin-walled tubing. This tubing is light in weight which reduces the cost and alleviates the mounting problem. Experience with the 1" tubing in a narrow-band 75 MHz pilot array has shown that occasionally a dipole is broken by a worker in the field. 1 1/2° tubing is much stronger.

The tubing is tightly fitted to a pine dowel impregnated with paraffin. This wooden mount is cheap, easy to mount, and has high electrical resistance. Such wooden mounts that have been in service for over two years show no signs of deterioration.

The posts are 4" × 4" Penta treated pine. They are inserted into a 3 foot hole in the ground and backfilled with sand.

6.2.2 Single Dipole Dimensions and Characteristics

A nominal dipole height above ground of 1/4 wavelength was chosen to provide broad angular coverage, high gain, and resistive admittance. The actual height above the physical surface with no ground screen is not critical, and this should decrease the requirement of ground flatness for the final array. The optimum height is slightly above the 74.7 Mhz, 1/4λ level. Some of these experimental results are tabulated in Table 6.2.2-1.

A dipole length of 63" tip-to-tip was chosen as the best compromise for length on the basis of admittance. This length consists of two 32" aluminum tubes plus the 4" wooden spacer. Some of the measured admittances as a function of length are shown in Table 6.2.2-2.

The dipole admittances with and without a balun were measured for a large number of feed cable lengths. The Smith-chart plot of these results shows that a balun is not needed. The pattern of points for the dipole without the balun is actually closer to the chart center. The reason for this is the unavoidable inductance introduced by the balun connecting leads.

The best feed geometry was determined experimentally to be that which minimizes the inductance of the feed wires. This implies short, thick leads. A satisfactory arrangement using only a braid and center conductor of the RG-11 A/U cable

TABLE 6.2.2-1

Measured admittances of a single 1 1/2" × 64" tip-to-tip dipole above El Campo soil in October, 1968, fed with RG-11 cable having no balun and short conductors at the feed point. The nominal frequencies of 70, 75, and 80 refer to actual frequencies of 69.72 Mhz, 74.7 Mhz, and 79.68 Mhz, respectively. The height L is the 1/4λ point and is 3' × 5/16"

Height Above Ground	Frequency	Admittance (mhos)
L + 12"	70	16 + j7
	75	17 + j2
	80	12 - j3
L + 6"	70	17 + j6
	75	16 + j1
	80	11 - j3
L	70	18 + j6
	75	16 - j0
	80	10 - j4
L - 6"	70	19 + j6
	75	17 - j2
	80	10 - j5
L - 12"	70	22 + j3
	75	20 - j4
	80	10 - j7

TABLE 6.2.2-2

Dipole admittance as a function of tip-to-tip length for a 1 1/2" dipole with a 4" wooden mount, no balun, and short RG-11 feed conductors. The dipole height was 1/4λ at 75 MHz.

Length	Frequency	Admittance (mmhos)
69"	70	18 + j5
	75	14 - j2
	80	9 - j3
68"	70	18 + j7
	75	15 - j0
	80	10 - j3
67"	70	16 + j8
	75	16 + j1
	80	11 - j3

was worked out. A sketch of the feed is shown in Figure 6.2.2-1. Figure 6.2.2-2 shows cable mounting details.

6.2.3 Cable Harness

A diagram of the Twin-Tee layout with the harness details is shown in Figure 2.2-1. The total effective mismatch and attenuation loss of this harness is 0.6 db. This was determined experimentally by connecting two harnesses together back-to-back and measuring the loss through both.

Cable interconnections were made as shown in Figure 6.2.3-1 and then potted in epoxy. This potted connection was tested under water and may be directly buried under the ground. It was used in all Twin-Tee tests reported here.

6.2.4 Twin-Tee Test Range

A transmitting dipole was attached to the top of our 250 foot tower, and it was excited by a signal generator in the site building. The 6-element Twin-Tee array was installed south of the tower at a distance to require a Twin-Tee phasing of 28° north to see the tower top. The tower top is in the far field of the Twin-Tee.

A reference dipole to monitor the field strength from the tower dipole was installed about two wavelengths away from the near point of the Twin-Tee.

DIPOLE CABLE ATTACHMENT DETAILS

FIG. 6.2.2-1

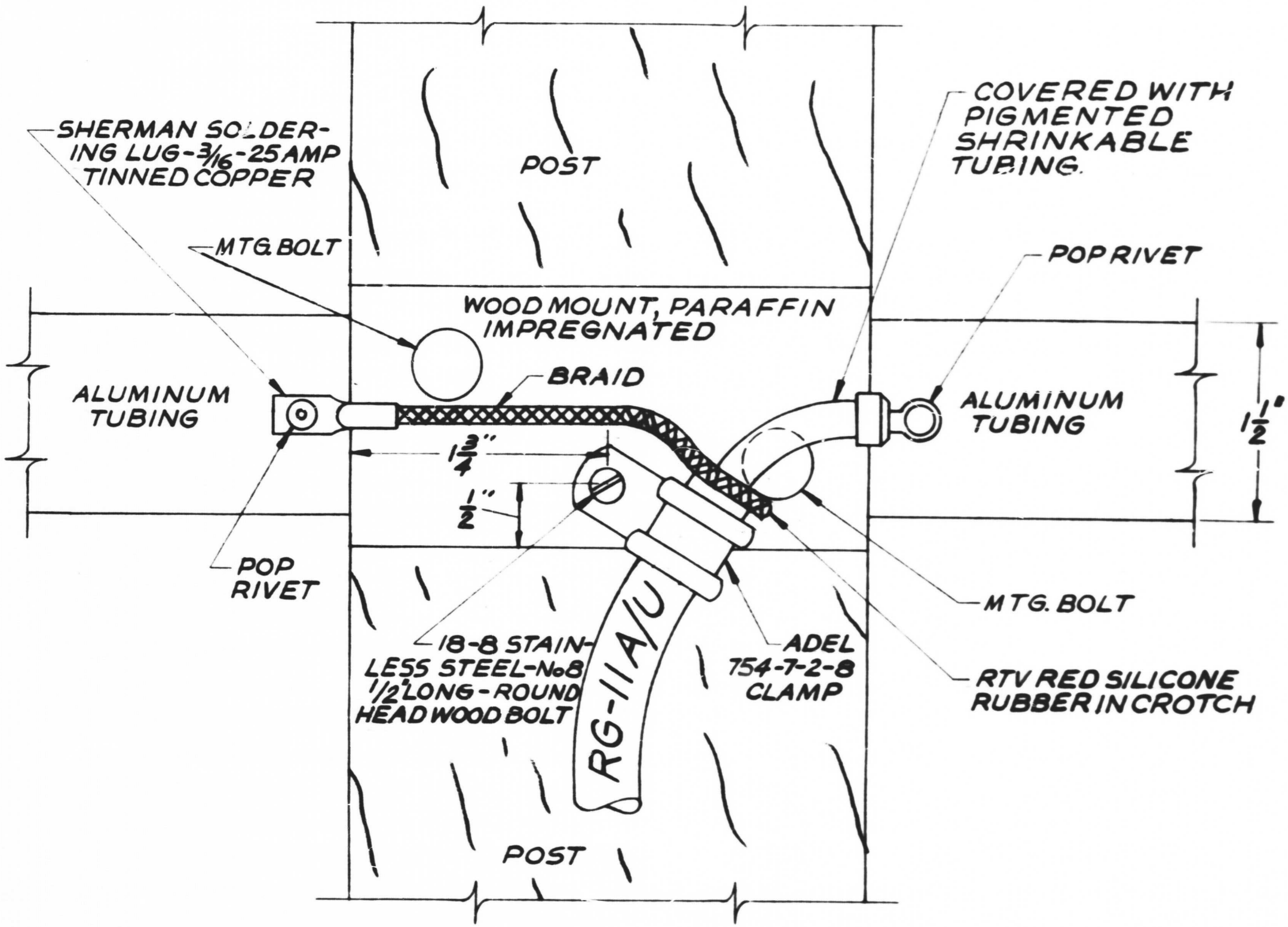

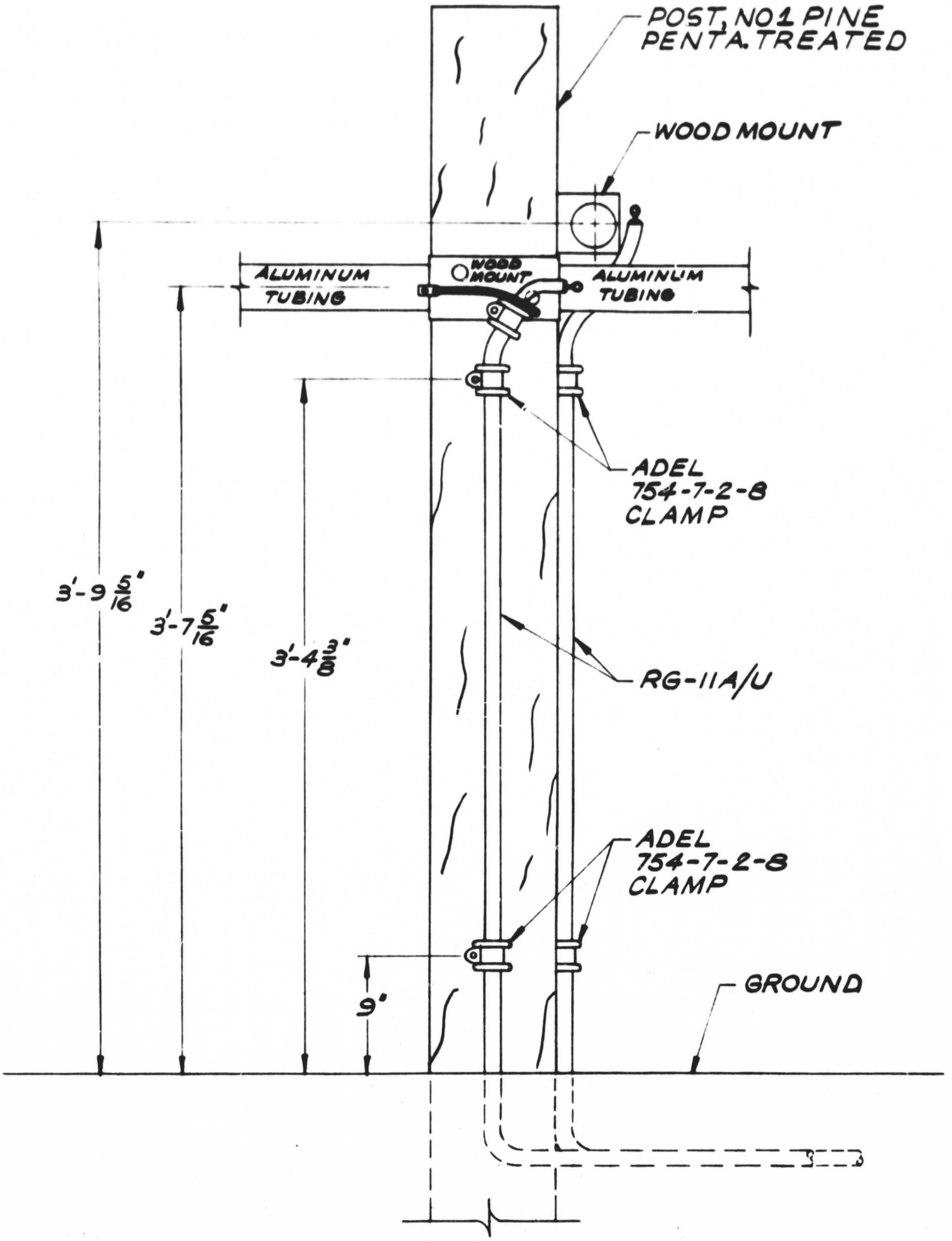

DIPOLE MOUNTING DETAILS
FIG. 6.2.2-2

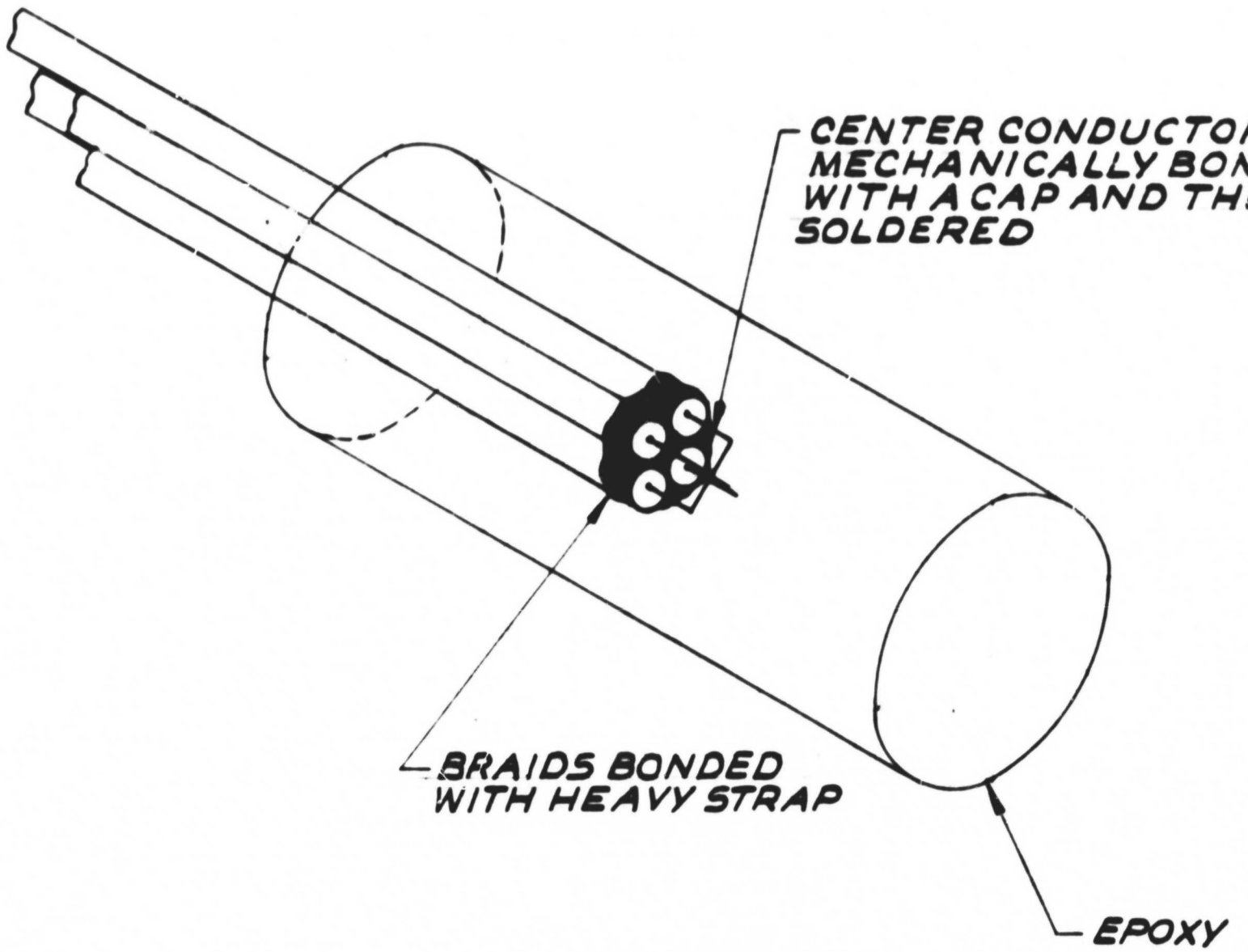

CABLE INTERCONNECTORS
FIG.6.2.3-1

6.2.5 Twin-Tee Admittances

The measured admittances of the 6-element Twin-Tee antenna under various phasing conditions are listed in Table 6.2.5-1. The ideal admittance here should be 20 millimhos.

These admittances are quite acceptable, and much better than expected.

6.2.6 Pattern From Tower Dipole

The tower dipole produces a complex gain and phase pattern in the vicinity of the Twin-Tee. The rms variation in power level among the six dipoles was 25% or 1 db, and the rms phase variation among the six dipoles was 79°. This is attributed to tower reflections, and not to mutual impedances of the dipoles, because each dipole except the one under test was disconnected.

6.2.7 Twin-Tee Antenna Gain

In spite of the non-ideal tower pattern the Twin-Tee gain measurements look very good. The ideal gain at 30° N is 7.5 db relative to a single dipole, and this is about what was measured. The gain measurements are given in Table 6.2.7-1. These measurements are for a single Twin-Tee.

The gains listed in Table 6.2.7-1 are actually larger than expected especially since the harness loss is 0.6 db. This means that the largest gain that should be expected would

TABLE 3.2.5-1

Admittance of the Twin-Tee Antenna

Phase Angle	Frequency	Admittance (mmhos)
30°N	70	23 + j2
	75	23 + j0
	80	24 + j3
60°N	70	23 + j4
	75	20 - j5
	80	24 + j1
30°E	70	24 - j2
	75	20 - j3
	80	21 + j5
60°E	70	20 - j9
	75	19 + j4
	80	17 - j1
30° SW	70	28 + j0
	75	20 - j0

be 7.5 db at 28° h. The only explanation is experimental error.

Greater north-south sky coverage can be had from the north-south dipoles by bending them as shown in Figure 6.2.7-1. This improved horizon gain is had at the cost of less gain near the zenith direction. If the array is installed near the equator, the bent dipole of Figure 6.2.7-1 will not be necessary. That a bent dipole is desirable for northern latitudes can be understood by considering the following equation for the power gain pattern of a single dipole one quarter wavelength above a perfect ground reflector.

$$P = \frac{\cos^2 [\pi/2 \cos A \sin Z]}{1 - \cos^2 A \sin^2 Z} \sin(h_r \cos Z) \qquad (6.2.7\text{-}1)$$

(See "Antennas" by Kraus, p. 303)

where P = relative power gain,

A = azimuth angle measured from axis of dipole

Z = zenith angle.

h_r = height of dipole above ground = $\frac{2\pi h}{\lambda}$ in radians.

As an example, note that the gain loss is about 2 db for a zenith angle of 30° and azimuth of 0°. At a zenith angle of 50° the gain loss can be as much as 5 db from that at the zenith. Figure 6.2.7-1 shows the pattern, in two planes, of a half wave dipole one quarter wavelength above a good ground screen.

TABLE 6.2.7-1

Gain measurements of the Twin-Tee antenna on November 7, 1968. Location of transmitting dipole is fixed at 28°N.

Phase Angle of Twin-Tee	Frequency	Gain Relative to Single Dipole 1/4λ Above Ground (db)
28°N	70	7.3
	75	7.3
	80	7.6
30°E	70	-4.3
	75	-13.6
	80	-10.7
60°E	70	-14.1
	75	-5.5
	80	-17.3
30°SW	70	-3.8
	75	-9.1
	80	-18.1
60°SW (grating lobe condition)	70	1.0
	75	0.3
	80	1.9
60°N	70	-2.6
	75	-4.4
	80	-1.2

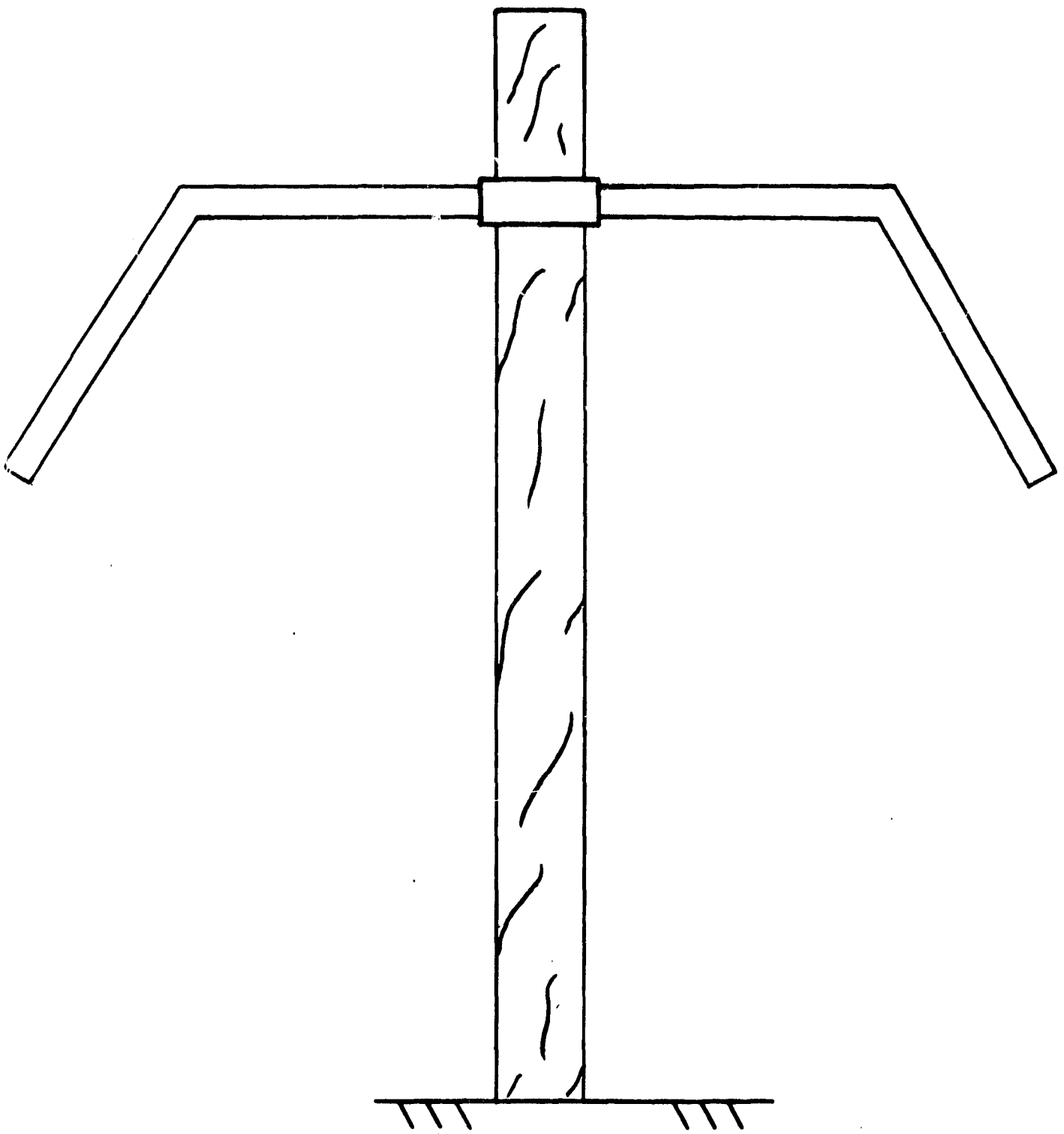

A BENT DIPOLE THAT HAS A 2 DB FLATTER SKY PATTERN THAN A SIMPLE DIPOLE

FIG. 2.7-1

PATTERN OF A HALF WAVE DIPOLE ONE QUARTER WAVELENGTH ABOVE A GOOD GROUND SCREEN.

FIG. 6.2.7-2

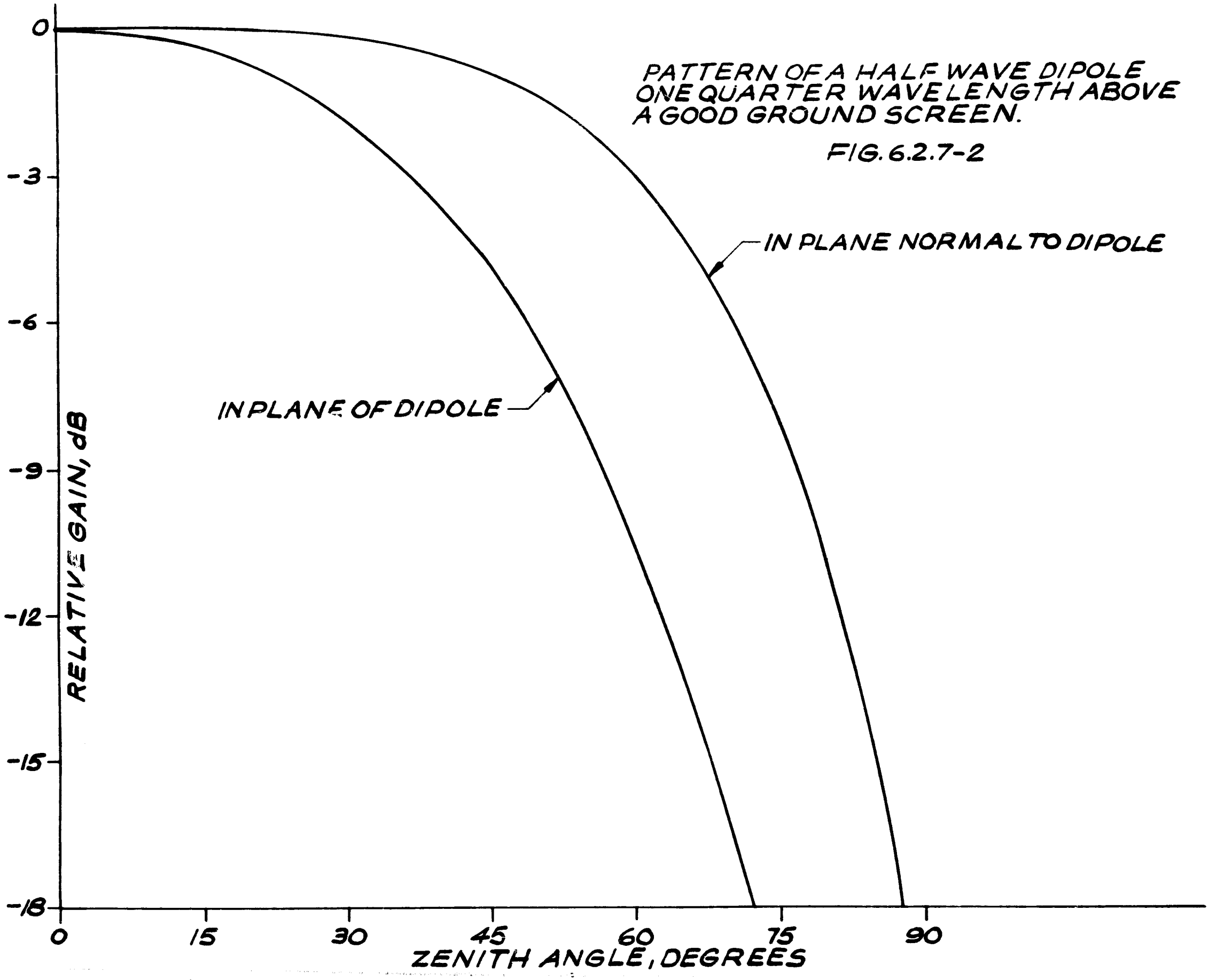

6.2.8 Twin-Tee Pattern Tests with Helicopter

Several pattern and gain measurements of a Twin-Tee array were made at El Campo on February 13, 1969, using a helicopter to fly the radiating sources. The measured patterns when the array was phased to the zenith angle of zero degrees are shown in Figures 6.2.8-1 and 6.2.8-2. A single dipole one-quarter wavelength above ground was used as the calibrating element. The absolute gain of the Twin-Tee above that of the single dipole was about 6.5 db at all three frequencies compared to a theoretical value of 7.78 db for a zenith-looking array.

6.3 Environmental Conditions

The city of El Campo is located in the south-central Texas Coastal Plain about 80 miles south-west of Houston. The climate, although classified as humid subtropical, is pleasant because of the prevailing sea breeze (about 10 mph) from the nearby Gulf of Mexico. Weather Bureau records show there are about 120 days per year that the maximum temperature exceeds 90°. The average maximum temperature in July is 83°. There are on the average only 11 days per year when the temperature drops below 32° and it is very rare that below freezing temperatures extend into the afternoon. The annual rainfall averages 40 inches and because the ground is extremely flat, occasionally temporary flooding of one to

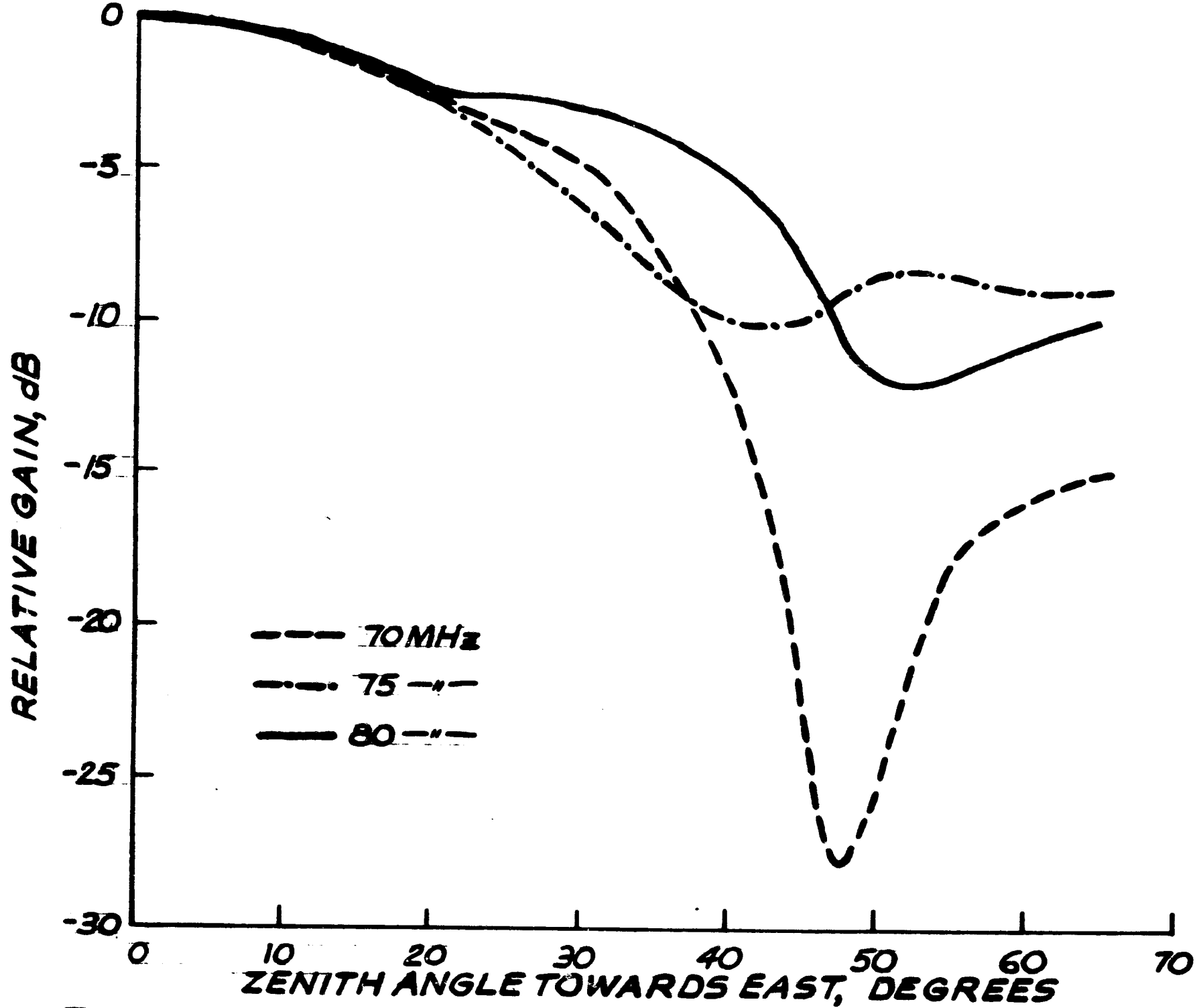

TWIN-T PATTERN AS MEASURED WITH HELICOPTER. THE LONGER AXIS OF THE TWIN-T WAS NORTH-SOUTH, AND IT WAS PHASED TO LOOK AT THE ZENITH.

FIG. 6.2.8-1

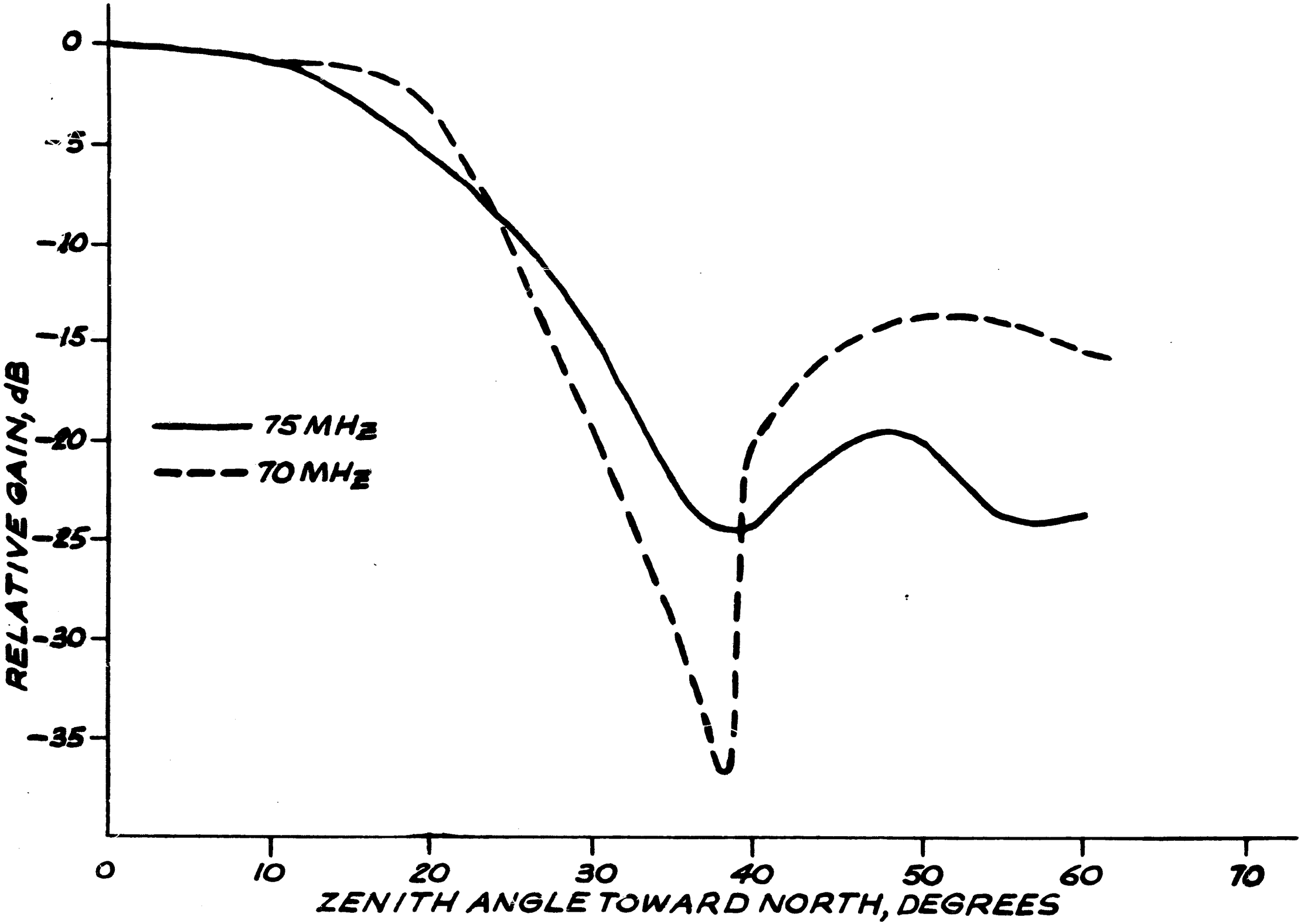

TWIN-T PATTERN AS MEASURED WITH HELICOPTER. THE LONGER AXIS OF THE TWIN-T WAS NORTH-SOUTH, AND IT WAS PHASED TO LOOK AT THE ZENITH.

FIG. 6.2.8-2

two inches in depth (once or twice per year) does occur in the low lying areas after heavy thunder storms. Hurricanes and tornadoes are rare in this area. The last hurricane was in 1961 when the eye of Hurricane Carla passed within 30 miles of the station; however, it did no damage to the 1000 dipole-38 MHz array.

Operational experience of the past several years at El Campo with the large 38 MHz arrays shows that cables and electronics should be buried in the ground to provide a stable temperature environment. The soil at El Campo is a homogeneous mixture of loam, clay, and sand and there are no rocks. Consequently, trench digging is inexpensive. The soil temperature and fluctuation level is dependent upon soil depth and ground surface conditions; the greatest fluctuations occurring with bare uncultivated soil and the least with grass covered soil. Based upon soil temperature data of Figure 6.3-1 and Tables 6.3-1 and 6.3-2, we recommend that cables and preamps be buried at a depth of two feet.

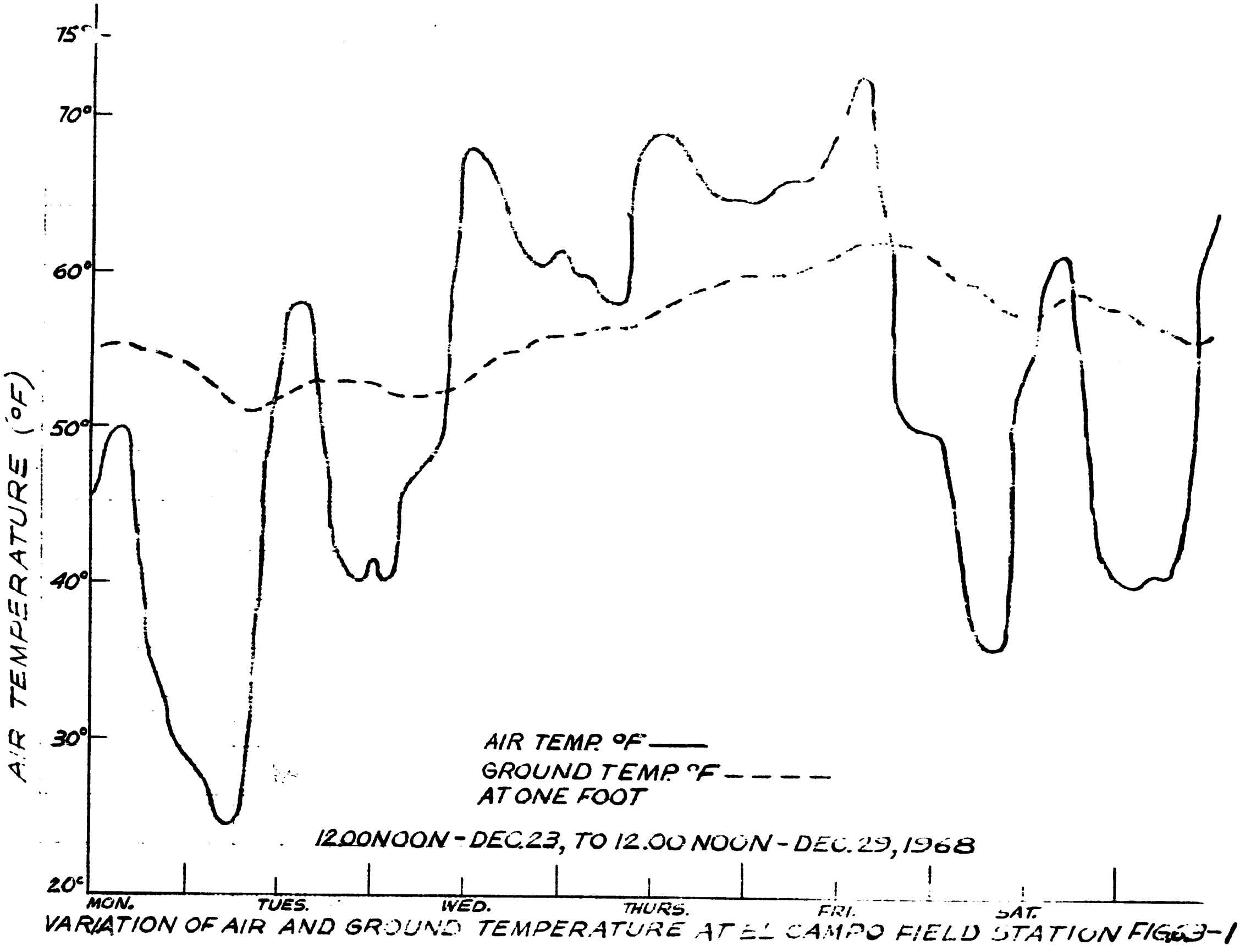

VARIATION OF AIR AND GROUND TEMPERATURE AT EL CAMPO FIELD STATION FIG 3-1

TABLE 3.3-1

Mean soil temperature by months for 1954-1956
Depth 6", Temple, Texas, Texas A&I University

Month	Maximum			Minimum			Average		
	1954	1955	1956	1954	1955	1956	1954	1955	1956
January		51.8	49.1		47.8	44.3		49.6	46.3
February		52.8	53.3		48.5	48.2		50.5	50.3
March	53.6	62.8	66.6	49.0	56.6	53.6	51.3	59.6	60.1
April	65.4	70.7	75.7	60.4	65.9	62.0	62.8	66.8	68.9
May	70.3	79.9	81.3	62.8	71.3	71.5	66.3	75.6	77.7
June	81.7	82.6	91.2	73.3	73.9	75.0	77.3	78.2	84.6
July	91.4	88.0	101.7	80.0	79.5	84.3	85.1	83.4	93.0
August	86.0	83.1	100.3	76.7	77.9	83.1	81.0	80.4	82.5
September	79.2	80.3	81.4	71.0	75.5	80.3	74.9	78.1	82.5
October	68.5	71.5	76.3	61.3	63.7	68.5	64.7	67.3	72.5
November	53.0	61.6	58.7	47.7	51.7	52.2	40.2	56.6	55.4
December	49.1	52.2	53.9	44.5	46.7	47.4	46.6	49.0	51.1
Yearly average	69.8	69.7	75.0	62.7	63.8	64.6	65.0	66.2	69.6

TABLE 6.3-2

Soil Thermograph Data for 1956

Depth 6 , Temple, Texas, Texas A&M University

Day of Month	December			August		
	Maximum	Minimum	Average	Maximum	Minimum	Average
1	56.0	46.5	51.2	105.0	86.0	95.5
2	56.0	47.0	51.5	102.0	86.0	93.5
3	58.0	50.0	54.0	104.5	83.0	93.5
4	60.0	56.0	58.0	107.0	85.0	96.0
5	62.5	58.5	60.5	106.0	86.0	96.0
6	64.0	61.0	62.5	104.0	88.0	96.0
7	65.0	60.5	62.7	108.0	87.0	97.5
8	61.5	54.0	57.2	108.0	87.0	97.5
9	54.0	49.5	51.7	109.0	87.0	98.0
10	53.5	46.0	49.7	109.0	88.0	98.5
11	57.0	50.0	53.5	108.5	87.0	97.5
12	58.0	51.0	54.5	108.0	87.0	97.5
13	56.0	50.0	53.0	109.5	89.0	99.0
14	54.0	48.0	51.0	112.5	89.5	100.5
15	53.5	48.0	50.7	112.0	90.0	101.5
16	54.0	46.0	50.0	110.0	90.0	100.0
17	60.0	53.0	56.5	100.0	87.0	93.5
18	56.0	44.0	50.0	100.0	91.0	95.5
19	46.5	44.0	45.2	101.0	90.0	95.5
20	50.5	45.0	47.7	90.0	85.0	87.5
21	52.0	46.0	49.0	88.0	78.0	83.0
22	57.0	50.0	53.5	91.0	76.0	83.5
23	53.0	46.0	49.5	93.0	77.0	85.0
24	48.0	42.0	45.0	94.0	79.0	86.5
25	47.0	40.0	43.5	91.0	79.0	85.0
26	48.0	40.0	44.0	88.0	82.0	85.0
27	48.5	41.0	44.7	90.5	81.0	85.5
28	48.0	41.0	44.5	93.0	83.0	88.0
29	50.0	42.0	46.0	94.0	85.0	89.5
30	52.0	43.0	47.5	95.0	86.0	90.5
31	53.0	44.0	48.5	95.0	86.0	90.5
Average	53.9	47.8	51.1	100.8	85.1	92.9

CHAPTER 7

7.0 APPENDICES

7.1 Site Survey Report

7.1.1 A Discussion of Desirable Site Characteristics

On June 9, 1965, a meeting of radio and radar astronomers from all over the country was held at the University of Maryland to discuss problems associated with the selection of sites for large astronomical arrays. The 20 participants were asked to vote on the relative importance of nine site characteristics. The results of this poll placed the nine characteristics in the following order:

Topology (flatness)

Interference

Latitude

Climate

Local Accommodations

Access

Longitude

Geology

Owners

The twenty participants consisted largely of technical people who would be responsible in some way for the performance

of the antenna. Had all the participants been people who were intending to live at the site, "local accommodations", including schools, would undoubtedly have been placed high. Had the participants had in mind a dipole array, "latitude" would probably have been placed second, because low latitude is more desirable for a dipole array than for other types of arrays. Furthermore, radio interference is not as serious for the dipole array because of its low silhouette to the ground. Had the participants been people who were to be responsible for the procurement of the land, "owners" would undoubtedly have been placed higher in the list. Had the participants been people who were interested in the array, but not directly responsible for the technical performance of the antenna, "climate", "local accommodations", and "access" would probably have been placed higher in the list. "Longitude" indicates proximity to the home office and is relatively unimportant. "Owners" refers to the cost and availability of the land. "Geology" determines the ease of post-hole digging and trench digging, and the dielectric constant of the ground reflector, and affects flooding possibilities. "Topology" is important because of the expense of excavating land.

"Radio interference" is important when low signal strengths are to be received, and is not likely to be as important at 75 MHz as it would be at lower frequencies. When mountains surround the site at an elevation of 5° or more, radio

interference is not a serious problem. The site should not be near a large city because of industrial and amateur radio interference. To avoid ignition noise, the site should be at least one or two miles from a busy highway.

"Latitude" is important for several reasons, especially for a dipole array. The sun and planets are all near the ecliptic, and this means that arrays nearer the equator scan to smaller zenith angles. An array that is required to scan to a smaller zenith angle has the following advantages: (1) The antenna characteristics are more uniform over the entire scanning region. (2) Frequency sensitivity is not as great a problem. (3) Mutual coupling among dipole elements is not as serious. (4) The projected aperture is larger for a given amount of real estate. (5) The single dipole pattern is more uniform over the scanning region. (6) The array gain is greater when the zenith angle is small. (7) For a given dipole spacing, grating lobes are much less likely to exist. (8) Radio interference is less likely to be a problem.

"Climate" is important for several reasons. (1) In a good climate more outside work can be done per year. (2) Snow and ice are not problems for southern latitudes. (3) Corrosion of metal and leakage across insulators is not a problem for dry climates. (4) Changes in ground conductivity is not a problem for dry climates. (5) In a tropical climate or in a very dry climate the fire hazard is not a problem.

"Local accommodations" are important for the people who must work at the site and especially for those who must live at the site and send their children to school. There should be facilities in the area for housing occasional visitors, but if necessary these can be constructed on the site. Of more importance are local services and supply sources such as electricians, plumbers, air conditioning technicians, mechanics, and railroad and truck lines.

7.1.2 Site Surveys

In February 1966, several possible sites for the Sunblazer array in West Texas, New Mexico and Arizona were visited. The report of this field trip is given in Section 7.1.3. None of these sites were at a lower latitude than El Campo, but they were in a much drier climate. The sites of this group that appear better are Sierra Madera, Nine Point Mesa, Santiago Peak, Alkali Flats, Bone Spring, Road Forks, and possibly Kitt Peak although the Kitt Peak site is likely not flat enough.

In August 1967, about 30 sites were visited in Puerto Rico. The report is the field trip is given in Section 7.1.4. The principal advantage of these sites is the low latitude, and for this reason they should be considered. Several sites are sufficiently flat but little is known at present about ground reflectivity, radio interference, and land availability

and cost. Known disadvantages of Puerto Rico are quality of labor, cost and availability of supplies, and schools. Access and climate would not be problems.

Other possible sites that have been visited are Goldstone, South Texas, and St. Croix in the Virgin Islands. NASA's Goldstone site ranks very high as far as "owners" and "climate" are concerned, but low for "latitude" and "topology". The 35° latitude should eliminate it from consideration.

Several sufficiently flat sites west and south of Corpus Christi, Texas, were visited. Compared to the El Campo site these have advantages of somewhat drier climate and a two-to-three degree less latitude. Otherwise they are very similar to El Campo. Whether or not a two degree gain in latitude is worth the unknowns of a new site and a moving operation is questionable.

A possible site on St. Croix was visited. This site is very attractive as far as latitude is concerned, and would be better than Puerto Rico as far as schools and the language barrier are concerned, but flatness and availability require more investigation.

Other possible sites that have not been visited are the Florida Everglades and one of the Hawaiian Islands. These have latitudes of 25° and 20° respectively.

One problem that may be encountered in a remote site is the availability of sufficient power for the transmitter. A peak power of 2 MW should be available.

7.1.3 Report of Field Trip to Locate Possible Sites for Future VHF Phased Arrays (C.F. Kaye, J.C. James, February 1-4, 1966)

The main criteria used to determine suitable sites were:

1) Flatness of ground over an area of at least one mile in diameter.
2) Absence of large rocks so that post holes could be easily dug.
3) Low average humidity.
4) Low latitude but within boundaries of the United States.
5) Presence of surrounding mountains that would serve to shield unwanted radio interference and to shield our site from known radio astronomy stations; and to a lesser extent.
6) Accessibility.
7) Cost of land.

A total of twelve sites were at least partially investigated. Of these twelve there are five that appear to be more desirable. These five, (discussed in the order they were visited) along with a general description and other notes are as follows:

1) Sierra Madera, Texas. This site is located in the north-central part of Sierra Madera topograhic map about 15 - 20 miles south of Fort Stockton, Texas, in a valley just east of Madera Mountain. There are several possible sites in the general area.

The land is used for cattle grazing except for one cultivated plot where gravity-flow irrigation was used. The ground condition was generally good but some areas may be rocky.

2) Nine-point Mesa, Texas. This site is on the north-central or north-east part of the Nine-point Mesa topographic map about 50 miles south of Marathon, Texas. This site is almost completely surrounded by mountains which rise to three or four degrees above the horizon. The land is owned by Mr. John M. Moss, Box 515, Marathon, and can probably be purchased for $20 per acre. The flat area may be less than one mile in diameter. There are a few small rocks near the surface.

3) Santiago Peak, Texas. This site is on the central and east-central part of the Santiago Peak topographic map and is located about 27 miles south of Marathon. Seems to be very flat and large in extent. Mountains rise about three degrees on the west, about two degrees toward the south and east and about one degree to the north. The land consists of compacted abode mud and is not rocky. This land is owned by Mr. Pope and can probably be purchased for $20 an acre.

4) Alkali Flats, New Mexico. This site is about 10 miles east of Tucson. Water covered some of the

area due to recent rains. An area could probably be found near the mountains so that a very effective screen would be provided on the west. The mountains on the east rise about one or two degrees. The site is located four miles north-east of Road Forks, New Mexico, and most is government land.

5) Kitt Peak, Arizona. This site is in the northern part of the Alambre Valley just east of the Kitt Peak Observatory, and was not thoroughly investigated. It appears to be flat when viewed from the mountain and it may be rocky. The shielding by mountains is very good on all sides. There could be power line interference from Kitt Peak. The site is on the Papago Indian reservation about 50 miles south east of Tucson. The Kitt Peak observatory probably has a lease in perpetuity from the Papago's that includes this site.

Three of the sites were judged to be a little less desirable than the five listed previously. They are, (in the order they were visited) as follows:

6) Bone Spring, Texas. This site is located at the left center of the Bone Spring topographic map and is about 40 miles south of Marathon, Texas. It is at least one-half mile by one-half

mile in extent and is not rocky. The mountains rise to the south about five degrees and to the north about two degrees. The land can probably be purchased for $20 per acre and is owned by Mr. Houston Hart, Matrax Land Company, Box 2171, San Antonio, Texas.

7) Cochise Playa, Arizona. This site is very flat over an area about ten miles in diameter. Water covered the site to perhaps a depth of one or two feet due to recent rains which began in November 1965. Water had covered the site for two months but this is unusual. Normally there may be some water during July or August for a few days. The site is 80 miles east of Tucson and five miles from Wilcox. The mountain ranges are about two degrees toward the east and west.

8) Road Forks, New Mexico. This site is south and east of Road Forks which is 140 miles east of Tucson. The land appears to be very flat and not rocky. The mountains to the east and west are perhaps two degrees in elevation. The northern part of this area is part of the alkali flats but the southern part is farm land which was reported to cost between $50 and $800 per acre, however, some of the land is government owned.

The following four sites were judged to be less desirable than the previous eight sites.

9) China Lake, N.E. Texas. On the north-east corner of the China Lake map. The land was rough and rocky with no mountain protection.

10) Playas Valley, New Mexico. Located 11 miles east of Aminas on Route 9. Water was in the playa which was about one mile wide and 14 miles long. Mountain coverage was about two degrees to east and west. This site is very remote.

11) Ryan airport area about 15 miles west of Tucson. The land appears to be generally level but probably quite valuable. The land is not rocky and the mountain elevations to the east and west are between one and two degrees.

12) Pitoikam site on the Papago Indian Reservation. This site is 71 miles west of Tucson and is very rocky. The mountain protection was only good toward the east.

The cost of the land for the Texas sites is probably about $20 per acre, and probably more for those in Arizona and New Mexico unless they are government lands. The latitudes of the Texas sites vary between 29° and 31°, and the latitudes of the Arizona and New Mexico sites are near 32°. The average humidity of all sites investigated was sufficiently low.

There are other sites that should be investigated. Some of these are: (1) Dry Salt Lake about 75 miles east of El Paso, (2) Yuma desert area in southwest Arizona, and (3) the White Sands area.

7.1.4 Report of Preliminary Investigation for Possible Antenna Site Locations on the Island of Puerto Rico, (August 1967)

There are several possible sites in Puerto Rico that are sufficiently flat. Radio interference could be serious and a radio interference monitor at the possible sites in Puerto Rico has not yet been made. The probability of interference is made smaller because of the separation of Puerto Rico from the U.S. mainland, but is made larger because of proximity to areas over which our government has less control. Any site within 10 miles of a large city such as San Juan may be bothered with industrial radio noise. The presence of mountains near a site should decrease the probability of interference as long as a relay station is not on top of it. To be of much benefit the mountains should be higher than four or five degrees when viewed from the site. At some of the Puerto Rico sites, mountains will be an advantage but some ignition noise should be expected at all sites investigated. Low latitude is an advantage because this decreases the range of zenith angles over which the array must be phased. This in turn leads to more uniform antenna characteristics over the scanning range. The Puerto Rico sites are very good in this respect because the

entire island is between 18° and 18 1/2° north latitude. The living accommodations, schools, quality of local labor, and shipping time from supply sources are not as good as in the United States. The climate and access of most of the Puerto Rico sites are very good. The humidity is satisfactory for the coaxial-line construction that we are proposing. Electric power will likely not be a major problem at any of the proposed sites. The ground consistency seems to be good for digging post holes and burying cables at all sites investigated; however, weeds and grass will likely be a problem. Some of the sites may be swampy at times, and the cost of the land has not been investigated. Most of the possible sites were covered with sugar cane.

The site search was started by screening all the 7 1/2 minute series topographic maps of Puerto Rico and the Virgin Islands. All flat areas of 1/2 mile or larger in diameter were marked as possibilities. There were more than 30 such possibilities in Puerto Rico.

On August 28, 29, and 30, 1967, twenty possible sites were visited by C.F. Kaye and J.C. James. Comments on each site are listed as follows along with the name of the quadrangle on which the site is located. The sites are listed in the order in which they were visited.

1) Carolina. Has power line nearby. Partly in sugar cane and partly cow pasture. Ground not rocky nor marshy. North of the hamlet of Hoyo Mulas. Several likely plots. Flat. About 5 miles

east of San Juan city limits.

2) Rio Grande. Several small plots near Highway 187. About 10 miles from city limits of San Juan. Largest possible plot is about 1/2 mile in diameter.

3) Punta Puerca. On Roosevelt Roads Naval Reservation. Too hilly, rocky, and bushy. The site of interest as selected from the map is now the Naval Base garbage dump.

4) Naguabo. East of intersection of Highways 3 and 31. Small. Elevation changes about four feet in 1/2 mile. Southern part of this plot is more flat and more swampy. Near town of Daguao.

5) Naguabo. North of Punta Santiago. Just inland from a coconut grove. Route 3 is between a nice beach and the coconut grove. Flat, sandy soil covered with sugar cane. According to map the Blanco River may limit the plot size to about 3/4 mile in diameter. There are mountains to the west and north in the direction of San Juan.

6) Aumacao. West and north of Punta Santiago. Similar to site 5. We only viewed the site from Route 925 (a back road). According to the map it is at least one mile in diameter and very flat. Covered with sugar cane. One or two degree mountains in direction of San Juan should provide

some shielding. This site is about 25 air-line miles from San Juan.

7) Humacao. A reasonably flat site southeast of town of Rio Abajo. Covered with sugar cane. Near site No. 6. Mountains to west and north.

8) Santa Isabel. On south side of island where there is less rainfall. Two and one-half hours from down town San Juan by Route 1. Several fairly-flat areas all around town of Santa Isabel. These sites are not as flat as others. All possible sites covered with sugar cane.

9) Sabana Grande. Large, very flat area in Lajas Valley. Covered with sugar cane. Soil okay. There may also be other less flat sites in Valle do Lajas on quadrangles San German and Guanica. Mountains on all sides except west. Looks good.

10) San German. Fairly flat sites west northwest of town along Route 2. Covered with sugar cane.

11) Aguadilla. Flat, sandy area on coast about two miles southwest of Aguadilla. On U.S. Naval Reservation. A tall tower is being constructed for Naval communications. May be marshy at times.

12) Aguadilla. On Ramsey Air Force Base. We did not go on base but guard said that the entire area that we were interested in is now covered with buildings.

13) Bayande. Ten miles west of San Juan along coast. Large, flat areas some of which are swampy. U.S. Navy has antennas in one area. Best plot may be about one mile directly west of Naval installation. Dorado Hilton Hotel is nearby.

14) Vega Alta. Northeast of Dorado. Has power line through center of small plot and has many fences. Not much sugar cane. Some pasture. Does not look very good.

15) Vega Alta. Large, level plot northwest of town of Ceiba. Soil okay. Sugar cane. Along Rio Cibuco.

16) Barceloneta. South and Southwest of town of Manita. Flat and covered with sugar cane. Too near Route 2. The Manita River bisects site. Soil okay.

17) Barceloneta. Northwest of town of Manita. Route 2 is too close.

18) Barceloneta. Just east of Manita River near town of Barceloneta. Not flat enough, too near Route 2, and a new proposed highway will bisect it.

19) Barceloneta and Arecibo. Large, flat area seven miles long and one and one-half miles wide between highways 681 and 682. Covered with sugar cane. Soil okay.

20) Arecibo. One or two possible sites along Arecibo River. Covered with sugar cane. The largest site is three miles south of town of Arecibo, which is too near town. Another site is two miles farther up the river is only 1/2 mile wide but is protected by mountains. Automobile ignition from Route 10 may be a problem. This site is only about four or five airline miles from the Arecibo dish.

Conclusion: The best site is probably 6, 9, or 13 and possibly 15, 19 or 20. The next step is to decide whether or not any Puerto Rico site is desirable from the point of view of living accommodations, labor supply, and equipment supply time, and if so, investigate the availability, and cost of several likely plots. Then, a more careful investigation of size, flatness, radio frequency interference, ignition noise, and seasonal flooding should be made.

7.2 128 Dipole Narrow Band Pilot Array (75 MHz) Experience Summary

The narrow-band 75 MHz pilot array antenna consists of 128 dipoles which is just sufficient to see the strong sources of Cygnus and Cassiopeia. The sun also is strong enough to be used but it often is variable and so is not reliable as a test source.

In this pilot antenna, the large line problem was solved by placing amplifiers in the field close to the dipole elements. The phasing problem was solved by providing an automatic phase-shift network at each dipole in the field. The outputs of all amplifier and phase shift circuits then were combined properly and brought back to the main receiving building. Schematically, the circuit arrangement was in the following order: antenna element, amplifier, phase shifter, and power combiner as shown in Figure 7.2-1.

The pilot antenna was first completely installed last February and March (1968). The dipoles had been installed during the previous summer. The ground had been prepared and surveying done prior to that. Just after the installation last March, the recording system was worked out so that signals could be recorded on a calibrated chart. One problem that was immediately apparent was that the amplifiers in the field had too much gain. This produced a high level output and required a special system for calibrating the receiving building. The calibrating system included a PRD noise generator followed by a power amplifier of known noise figure and gain. After the recording system was installed and the calibration system worked out, the source Cygnus was immediately seen. This source appeared at the proper time and with the approximate correct amplitude. The problem of determining the correct amplitude required a knowledge of the line losses, the average gain of the receivers in the field, and the allotted gain of the antenna

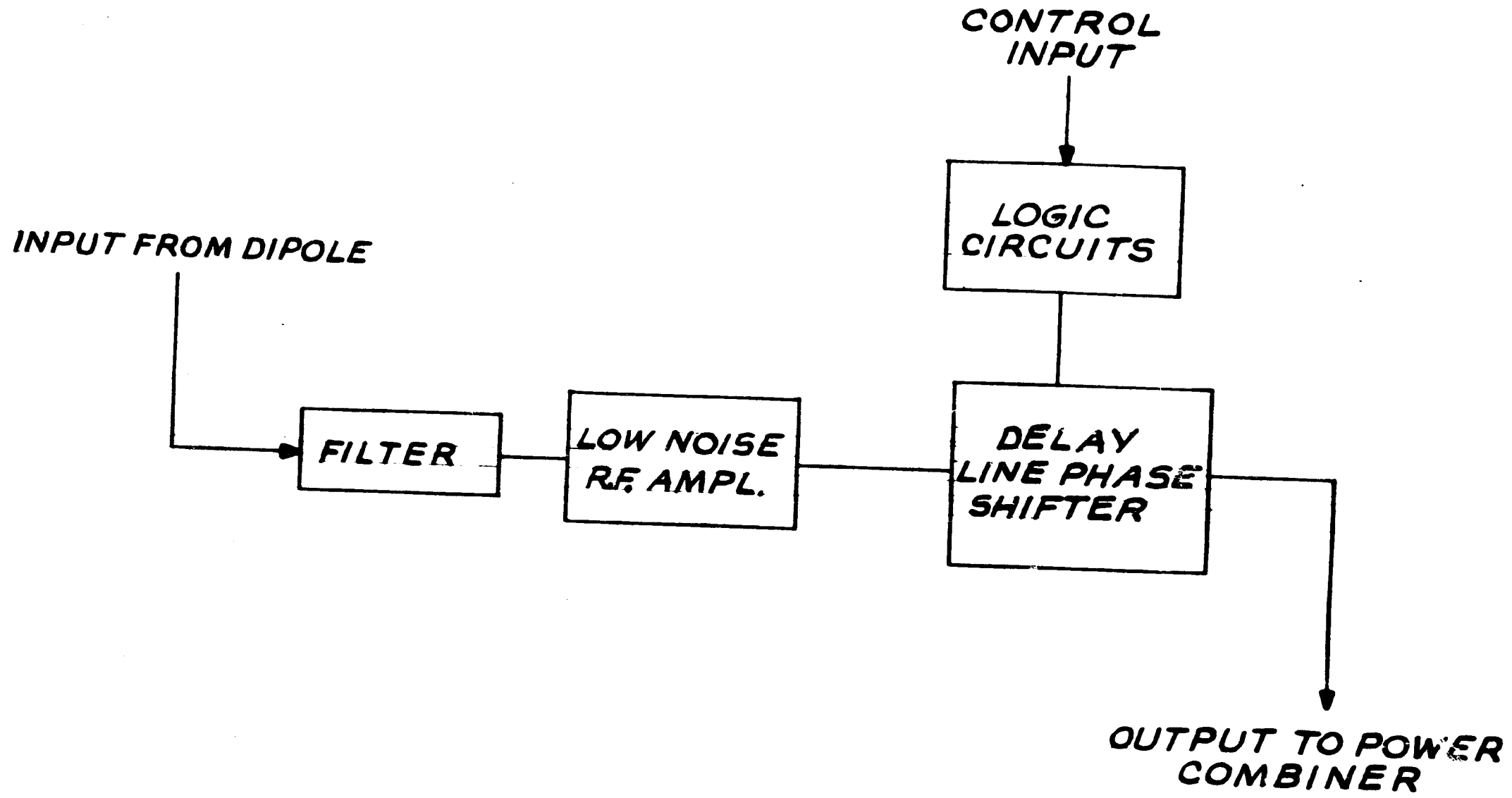

DIPOLE RECEIVER DIAGRAM
FIG. 7.2-1

array itself. A system was worked out whereby the line losses could be accurately measured. This system used a cable of the 1/2 inch Foamflex type which appeared to have stable gain and phase characteristics so that a signal could be transmitted from the receiving shack along this cable to a particular point in the field. After the line losses were measured and properly accounted for, and the gain of the amplifiers was taken into account, the entire array had the expected gain. The first step in verifying this result was to measure the gain and phase of all amplifiers in the field. This job was completed on May 3, 1968. After measuring the gains and phase shifts they were then adjusted to be a constant value within limits.

Subsequent tests showed that the gain of the array was still approximately as expected, and perhaps 1/2 db higher when looking near the zenith. However, on some occasions when looking at the zenith angle of 25 degrees or more, the gain dropped more than should have been expected.

In midsummer 1968 another problem became apparent. This was the corroding of the circuit boards in the field due to condensation during the nighttime, and to leakage of rain through the plastic covers which by this time were becoming somewhat frayed. Plastic waste cans were installed in place of the plastic covers to stop the leakage and condensation. However, the gain and phase shifts of all the circuits had to

be adjusted again. This job was completed in the fall of 1968. Also during this time, the phase length of all the buried cables were again checked and found to be approximately the same lengths as when they were installed. Small adjustments however, were made in the line lengths so that for long runs the phase length tolerance was within $\pm 5°$.

The degradation of gain with large zenith angle was not solved until December 1968. Apparently the problem was due to different output impedances of the combiner board amplifiers. This resulted in different outputs from the various bays of the antenna when the power supply voltage was removed from all bays except one. The output of a particular bay would depend upon which bay was being looked at. For example, the output of bay No. 1 might be considerably higher than bay No. 2 when the antenna was phased to look at the zenith. In December, the combiner networks, which sum the outputs of four receiving boxes, were changed to resistive combining networks. These resistive combiner circuits had losses, and served to equalize the impedances of all bay outputs. After this modification was introduced and sources Cygnus and Cassiopeia were again looked at, the problem of degradation of gain with zenith angle was not apparent. For some as yet unexplained reason these reactive combining networks apparently cause a loss of gain when the antenna was phased to a large zenith angle.

When proper account is now taken of the gains of the field units and the line losses, the gain of the antenna array is

slightly higher than expected. It is difficult to believe that the efficiency of the antenna is 100 percent which is what the results show. However, all the measurements have been checked carefully and it is not believed that this final result is in error by more than one db. Figures 7.2-2, 7.2-3, 7.2-6, and 7.2-7 give typical performance data of pilot array and Tables 7.2-1 and 7.2-2 give typical system calculations.

During the winter and early spring of 1967, a 16 acre square area was chosen for a final 75 MHz array. The pilot array was to be a partially filled strip through the center of the final array. The area was chosen well away from the public road in order to avoid ignition noise. The entire 16 acre plot was leveled at a cost just under $2,000. This leveling consisted of removing about 6" of dirt along a high ridge through the center of the plot and depositing the removed dirt along each side of the plot. A dirt road and one wooden bridge was constructed to the site area. Power lines at 440 V, 60 cps, were buried in a trench from the main site building to the 16 acre plot, and this power line had outlets distributed over the region of the pilot array. A sheep-proof fence was constructed around the plot, a well was dug, and Bermuda grass was planted to prevent mud.

An 8' by 8' receiving and control shack was constructed at the center of the pilot array. The shack had heating and air conditioning and was well insulated. The floor was 1 1/2 feet

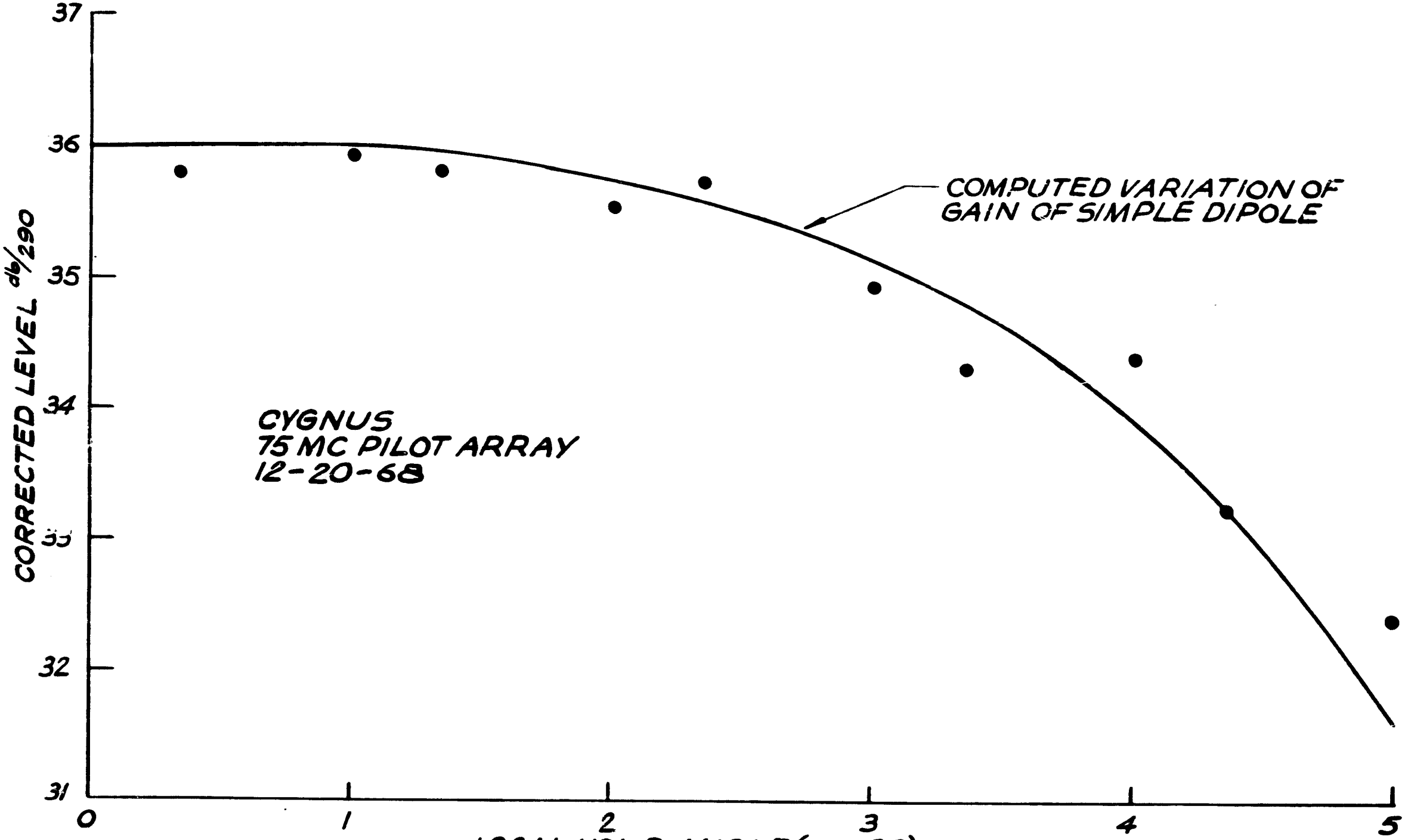

ANTENNA OUTPUT LEVELS - CYGNUS

FIG. 7.2-2

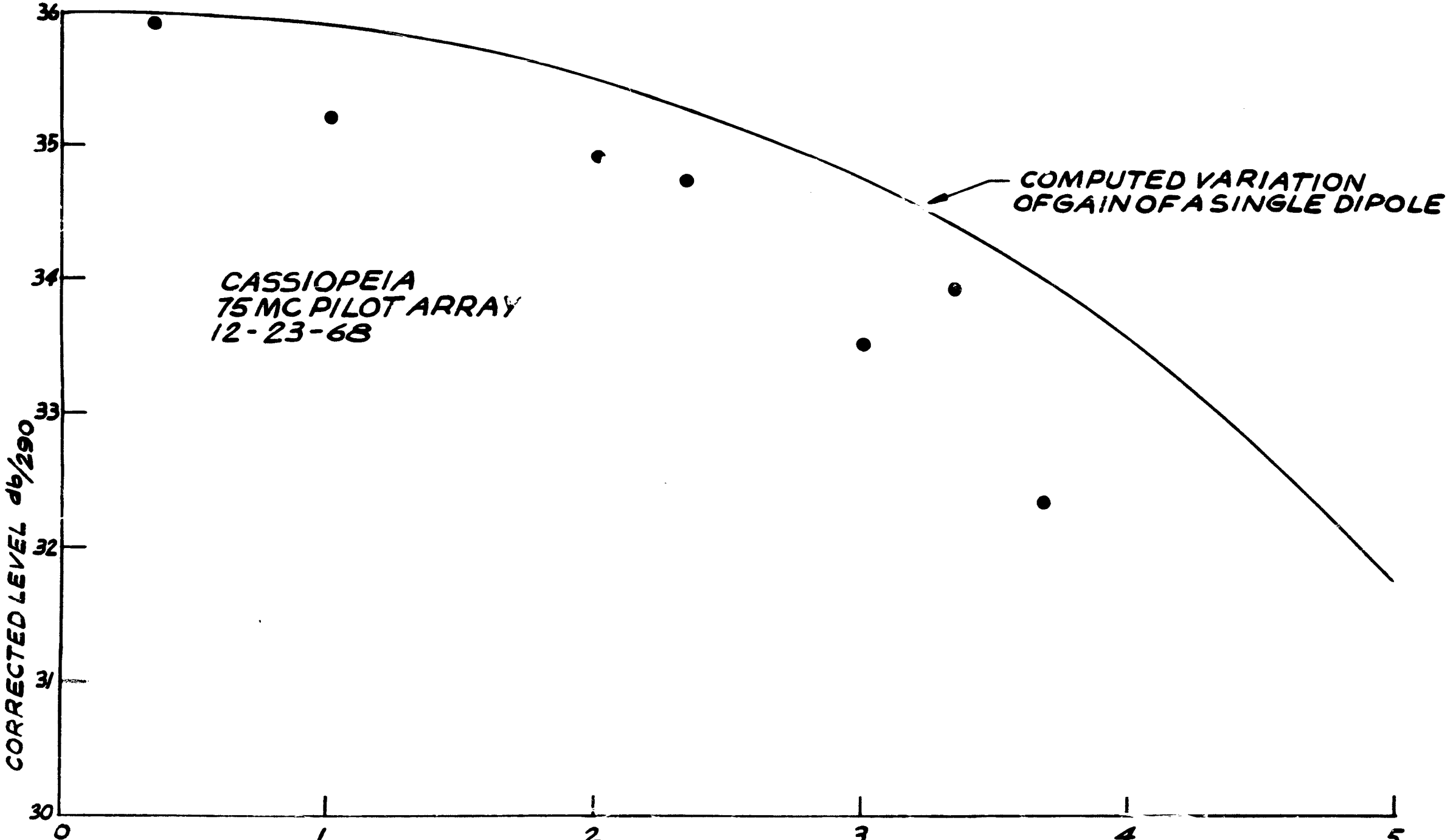

ANTENNA OUTPUT LEVELS - CASSIOPEIA

FIG. 7.2-3

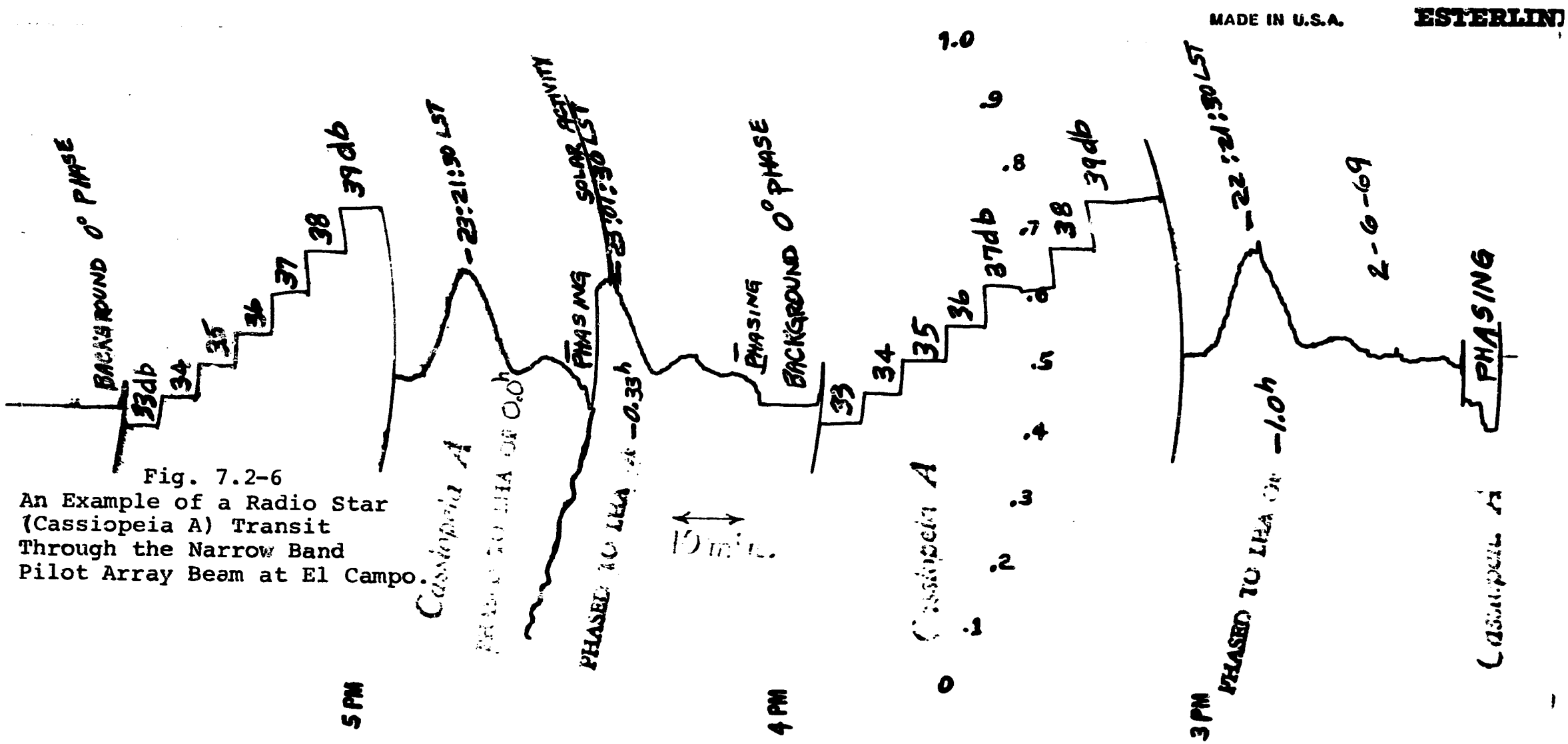

Fig. 7.2-6
An Example of a Radio Star (Cassiopeia A) Transit Through the Narrow Band Pilot Array Beam at El Campo.

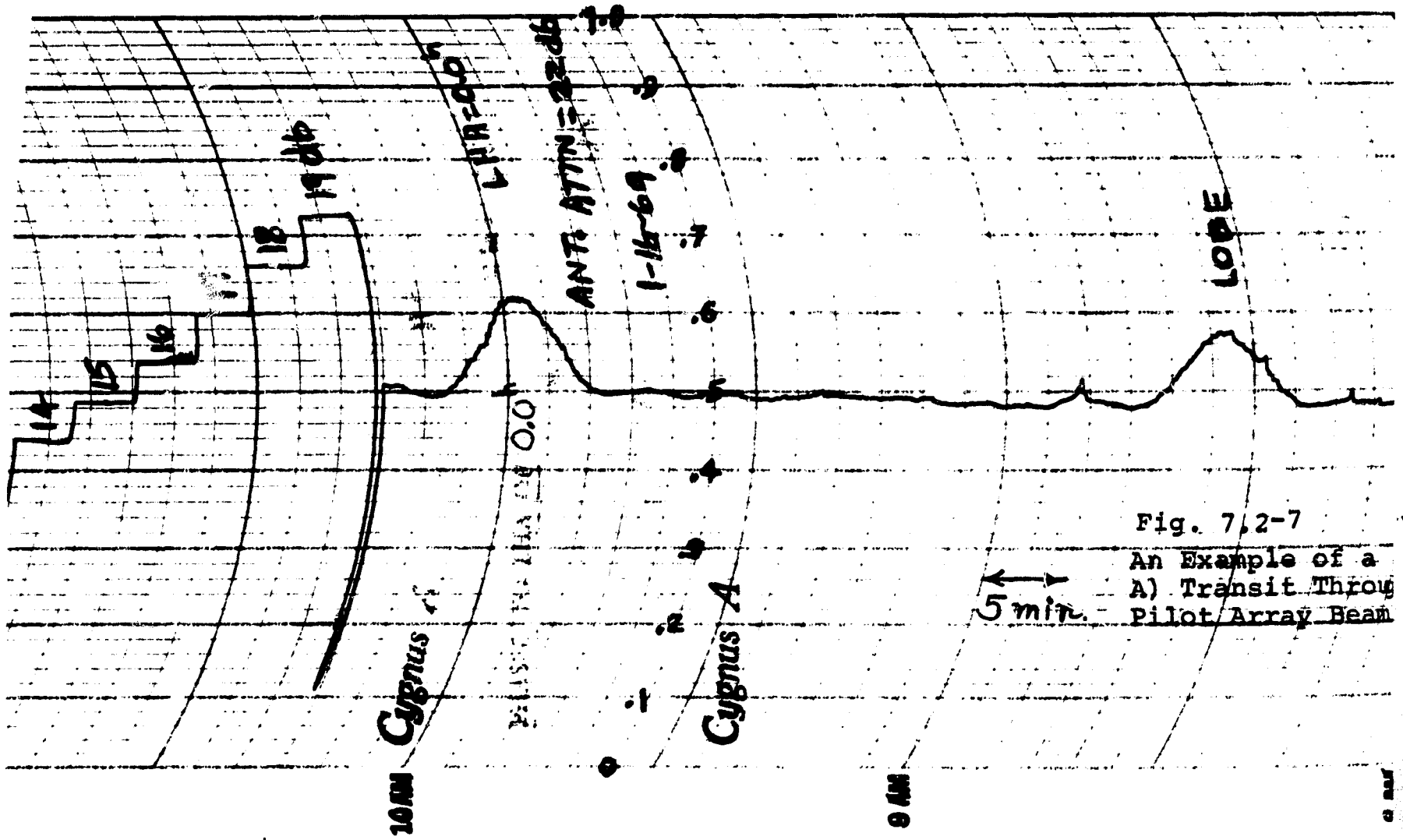

Fig. 7.2-7
An Example of a
A) Transit Throug
Pilot Array Beam

Fold Out
a

APOLIS, IND., U.S.A. **CHART NO.** 4305-C

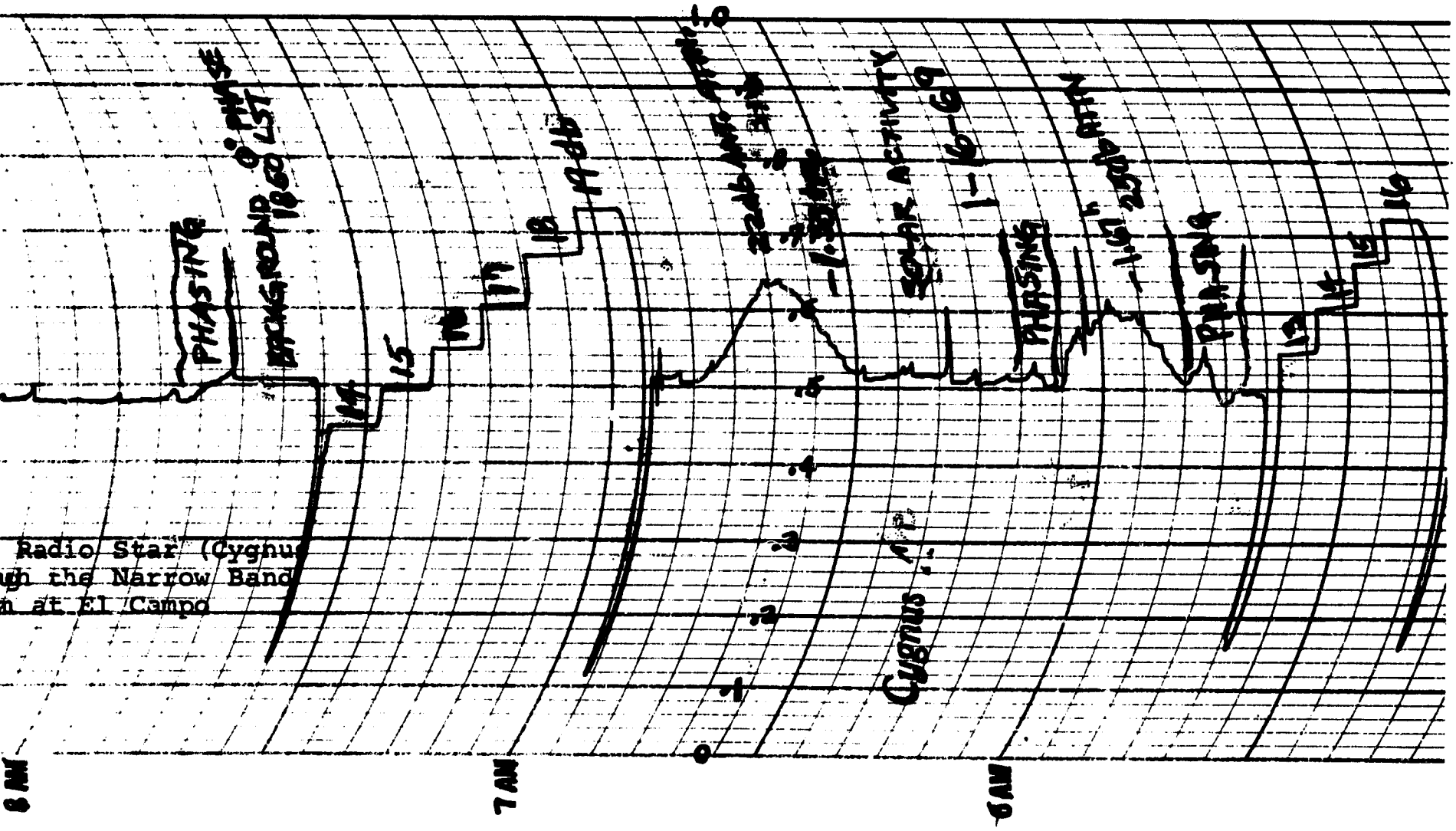

Radio Star (Cygnu
gh the Narrow Band
n at El Campo

B

above the ground level so that cables could be fed through the floor. The four corners of the shack were anchored in concrete in case of a hurricane. The location of the shack with respect to the 8 bays of the pilot array is shown in Figure 7.2-4.

The east-west alignment of the array was determined by Polaris sightings. The locations of the bays and dipoles were accurately surveyed on the basis of a dipole spacing of 0.6300 wavelengths at 75.000 MHz. Trenches for cables were also accurately placed. The physical layout of a typical bay is given in Figure 7.2-5.

Power lines were first installed and next the 4" x 4" wooden posts. The posts were placed about 3 feet in the earth and backfilled with sand. Control and R.F. cables were then placed in 2 foot trenches. Afterwards, dipoles were installed, and finally the receiver and phase shifters.

The control cables were 25 pair and 6 pair, 22 AWG copper conductors with 5 mil shields. This cable has a pulse rise time degradation of 0.1 microsecond for the first 900 feet, and has a characteristic impedance of 120 ohms. The R.F. cables were RG-8 A/U, RG-11 A/U and 1/2" Foamflex.

There were 128 crossed dipoles and 32 receiving boxes. Each box contained 4 receivers, 4 phase shifters, and one combiner board with amplifiers.

Junction boxes for the control cables were outdoor, telephone type enclosures. They were quite satisfactory. Junction covers for the Foamflex cables were heavily galvanized.

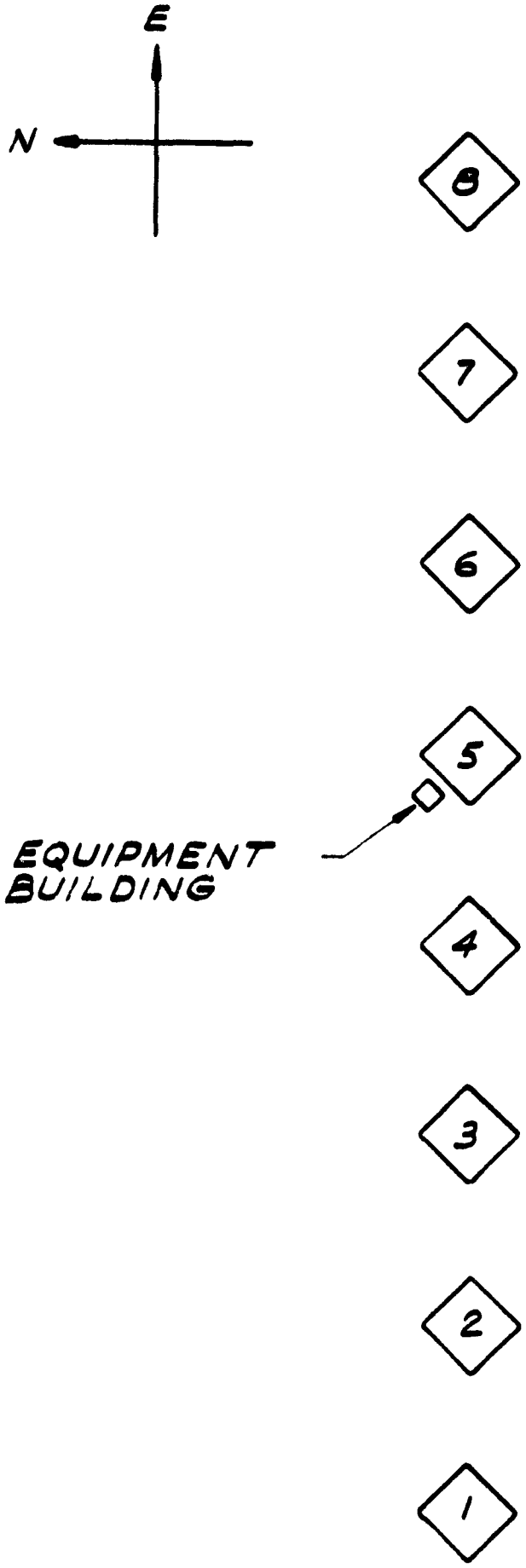

75 MC ARRAY BAY IDENTIFICATION
FIG. 7.2-4

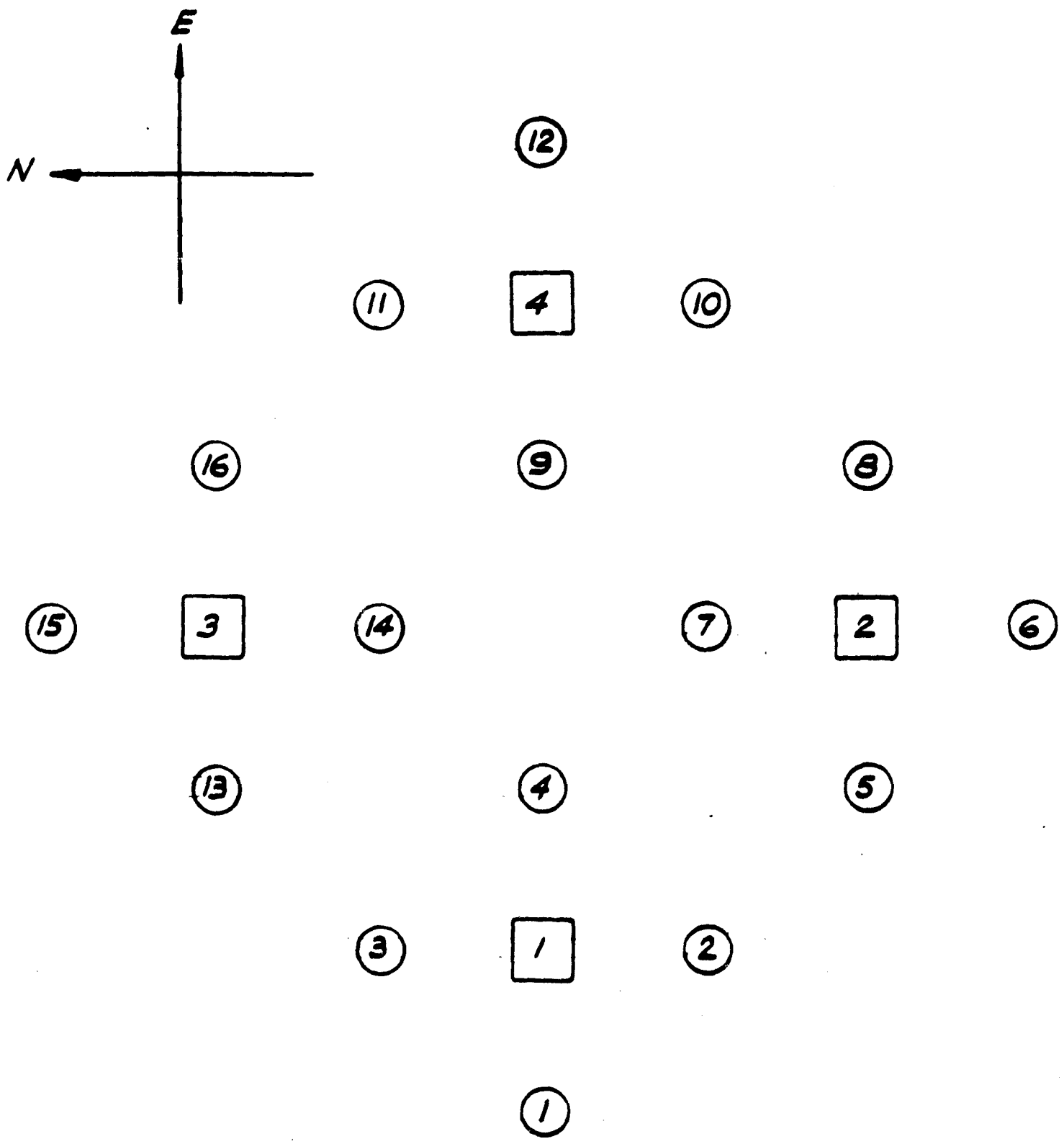

NOTES

(1) DIPOLE IDENTIFICATION

[1] RECEIVER BOX IDENTIFICATION

75Mc ARRAY - DIPOLE IDENTIFICATION AND RECEIVER BOX IDENTIFICATION

FIG. 7.2-5

steel buckets mounted on steel rods driven in the ground.

Phasing of the array consisted of setting four toggle switches for each of the 128 elements. Computer computations for this phasing were made at Wharton Junior College and M.I.T.

The main pilot array beam was 1° x 20°. Separated east and west of this main beam were two side lobes of half intensity. The long axis of the beams were north-south.

The antenna gain amounts to about 6 to 7 db per dipole for near zenith sources, but less for off-zenith sources. This is near the maximum possible gain and amounts to approximately 90 percent efficiency. The pointing accuracy was good. Some improvement in design, packaging, and placement of the field electronics packages is required.

This pilot array has demonstrated that the basic idea is sound. The gain and pointing accuracy exceeded the expectations.

The separation of the dipoles appears to be near optimum and the details of dipole construction and mounting are good. This has been demonstrated by the antenna performance and the lack of mechanical problems during the past 1 1/2 years. The wooden, pentachlorophenol treated, posts and the wax impregnated wooden mounts show no signs of deterioration. The coaxial cables with foam dielectric are inexpensive, have low loss, have good phasing stability, and are free from mechanical damage and the deterioration caused by weather when buried under ground.

Experience with the operation of the array has shown that what might be called a simple modification to one unit turns out to be a job of major proportions for 128 units. It is especially important to completely work out all the desired details of the electronics for the large array in the pilot array stage.

The enclosure or "box" for the field electronics has not been completely satisfactory. It was physically too large, it leaked water during rain, it corroded, and it had no ventilation. Snails, opossums, dirt dobbers and other insects and animals shorted the connector terminals on top of the box. The plastic and fabric bags that covered the box initially had a lifetime of about six months. In fact, it is likely that our greatest problem with the electronics began when these bags began leaking. The solid plastic trash cans that now cover the boxes perform much better. For the next phase of testing, the circuit boards will be covered directly with moisture-proof paint.

The combination of wind, rain, sunshine, heat and mechanical motion is a much stronger weathering agent than is water alone. Consequently, it is normally better to have the electronics, cables, etc. under the ground. On one occasion the gain of the pilot array dropped several decibels within a few minutes time when a cold norther blew in. Most of this drop was due to a loose connection in one of the boxes. The wind aggravated the connection but the combiner board is also temperature sensitive. Normally, however, weather conditions do not

strongly affect the gain; that is, rainfall does not short out the dipoles, nor does it cause any effect on the gain of the amplifiers except through box leakage.

The field electronics require some modification for a large array. The front-end R.F. amplifier on each circuit board caused no particular problems, but it had more gain than was necessary. The phase shifting network and the combiner amplifier did require maintenance. On three occasions during the first year all the electronic boxes were brought to the work bench, checked, repaired and adjusted. Part of the problem was corrosion of the circuit boards and other components. The field electronics were not packaged for ease of servicing.

Future field electronics should be rugged, reliable, and stable with changes in temperature, supply voltage and time. They should be completely water proof. The noise figures should be less than three db and the output impedances should be constant and stable. They must have a very low failure rate. The amplifier and phase shifter should not be a sophisticated laboratory device. During design much attention should be paid to practical problems that may arise in the field. This can be done by maintaining very close contact with experienced field personnel or by having the design work done at the field station.

The phasing board and circuits in the control shack were quite satisfactory. The noise figure of the Nems-Clarke

Receiver would have been too high had the field receiver gains not been excessive. The 1/16 wavelength phasing increment is not necessary. It would have been somewhat more convenient to have had a selected number of pre-wired boards for phasing to certain angles, and for future arrays, of course, the phasing must be automatic.

The control of the B+ voltage of each bay from the control shack was a definite advantage in trouble shooting.

It was found through experimentation that each dipole and its amplifier could be quickly checked for failure by radiating an R.F. signal near each dipole. The problem of keeping check on field units in the large array is not believed to be as great a problem as some would expect.

All designs should proceed with a proper consideration of the entire system and not just the particular part being designed. For example, a better impedance match might be had between the dipole and input amplifier, if the dipole were not one-quarter wavelength above ground. If the dipole were lower to the ground there would also be better sky coverage. Other possibilities are that feed cables could become part of the matching network, or the amplifier may match directly to the parallel combination of several dipoles. This principle of paying attention to the performance of the final overall system as each part is designed will be especially important if a transmitting feature is to be added later.

Perhaps an inverted V-shaped dipole should also be tested in search of an antenna element with greater sky coverage. Such a dipole having each arm bent downward 30° should provide a 2 db improvement in the flatness of coverage.

TABLE 7.2-1

COMPUTATIONS OF ANTENNA GAIN USING THE CYGNUS SOURCE

From "List of Constants" the Cygnus level at a zenith angle of zero should be	11.8 db
Correction for dipole pattern	- .3
Average field receiver box gain	39.8
Line and transforming section losses	- 4.1
Resistive combiner loss	-11.5
Expected level	35.7 db
Actual recorded level corrected for background noise level (12/20/68)	36.0 db

COMPUTATIONS OF ANTENNA GAIN USING THE CASSIOPEIA A SOURCE

From the "List of Constants" the Cassiopeia level at a zenith angle of zero should be	13.5 db
Correction for dipole pattern	- 1.8
Average field receiver box gain	39.8
Line and transforming section losses	- 4.1
Resistive combiner loss	-11.5
Expected level	35.9 db
Actual recorded level corrected for background noise level (12/23/68)	36.0 db

TABLE 7.2-2

LIST OF CONSTANTS FOR 75 MHz PILOT ARRAY

Simple half-wave dipole one-quarter wavelength above perfect ground.

Gain 7.2 db (at zenith)

Effective area $0.42\lambda^2$

Actual area allotted each dipole spaced on a 0.63λ x 0.63λ grid.

Actual area $0.40\lambda^2$

0.63λ at 75 MHz = 8.2619 feet

λ at 75 MHz = 13.1142 ft. = 3.99721 meters

Actual area of 128 element pilot array is $128 \times (0.63 \times 3.99721)^2 =$ $811.72\ m^2$

One U.S. yard = 3600/3937 Meters (by act of Congress)

k = Boltzman's constant = 1.38024×10^{-23} watt sec/deg.

Loss in 1/2 inch Foamflex, 0.7 db/100'

Loss in RG 8A and RG 11A, 1.7 db/100'

Temperature phase change of RG 8A, -200 ppm/oC

Temperature phase change of Foamflex, 25 ppm/oC

FLUX DENSITIES AT 75 MHz

Cassiopeia A	$2.2 \times 10^{-22} w/m^2/cps$
Cygnus A	$1.5 \times 10^{-22} w/m^2/cps$
Taurus A	$1.9 \times 10^{-22} w/m^2/cps$
Virgo A	$2.4 \times 10^{-22} w/m^2/cps$

TOTAL POWER INCIDENT ON AN 812 SQ. METER APERTURE AT NORMAL INCIDENCE FROM FOLLOWING SOURCES. T IS THE EFFECTIVE TEMPERATURE OF 1/2 THIS POWER EXPRESSED IN db ABOVE 290°

Source	Power (10^{-20}w)	T(db/290°)
Cassiopeia A	18	13.5
Cygnus A	12	11.8
Taurus A	1.5	2.7
Virgo A	2.0	4.0

POWER GAIN OF A HORIZONTAL HALF-WAVE DIPOLE IN FREE SPACE RELATIVE TO ITS MAXIMUM GAIN (which is 2.15 db over isotropic) IS GIVEN BY

$$P_{fs} = \frac{\cos^2 [\pi/2 \cos A \sin Z]}{1 - \cos^2 A \sin^2 Z}$$ (Kraus, Antennas, p. 308)

where

A = azimuth angle measured from axis of dipole, and

Z = zenith angle

POWER GAIN OF A HORIZONTAL HALF-WAVE DIPOLE SPACED A HEIGHT h RADIANS ABOVE A PERFECTLY REFLECTING GROUND IS

$$P = P_{fs} \sin^2 (h \cos Z)$$

This gain P is relative to the maximum gain of 7.2 db over isotropic

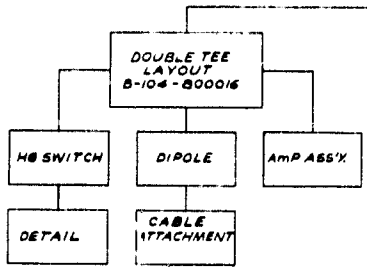
DOUBLE TEE LAYOUT B-104-800016
HB SWITCH
DIPOLE
AmP ASS'Y.
DETAIL
CABLE ATTACHMENT

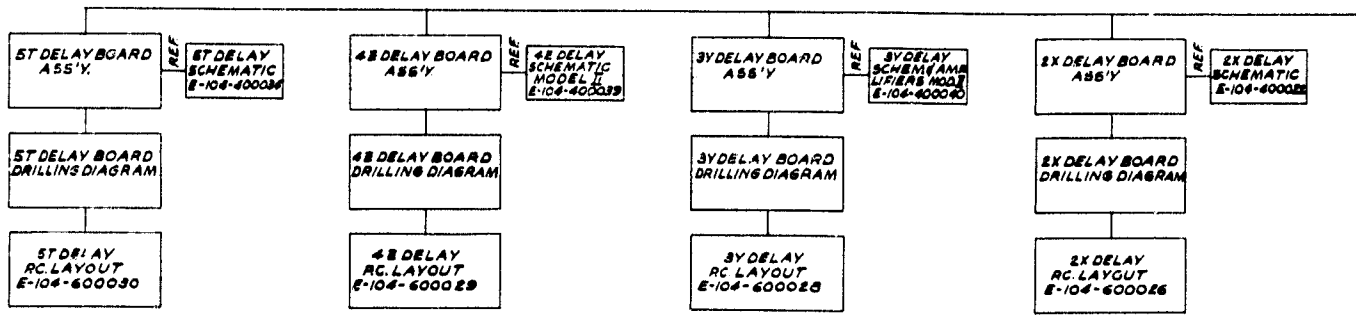
5T DELAY BOARD ASS'Y.
REF
5T DELAY SCHEMATIC E-104-600034
5T DELAY BOARD DRILLING DIAGRAM
5T DELAY RC. LAYOUT E-104-600030
4E DELAY BOARD ASS'Y.
REF
4E DELAY SCHEMATIC MODEL II E-104-600039
4E DELAY BOARD DRILLING DIAGRAM
4E DELAY RC. LAYOUT E-104-600029
3Y DELAY BOARD ASS'Y
REF
3Y DELAY SCHEMATIC AMP LIFIERS MODEL E-104-600040
3Y DELAY BOARD DRILLING DIAGRAM
3Y DELAY RC LAYOUT E-104-600028
2X DELAY BOARD ASS'Y
REF
2X DELAY SCHEMATIC E-104-600026
2X DELAY BOARD DRILLING DIAGRAM
2X DELAY RC. LAYOUT E-104-600026

Fold Out
a

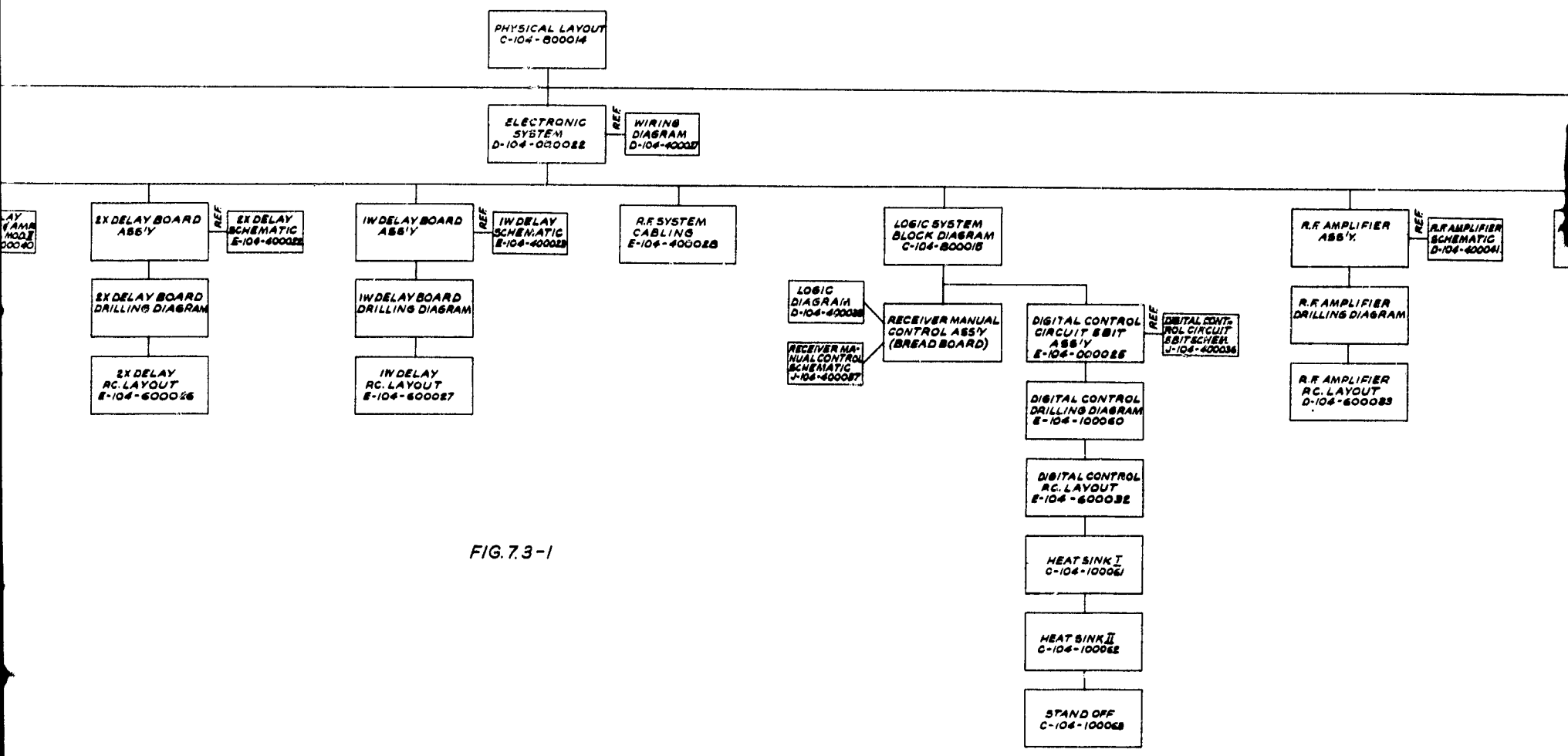
PHYSICAL LAYOUT C-104-800014
ELECTRONIC SYSTEM D-104-000022
REF
WIRING DIAGRAM D-104-400037
2X DELAY BOARD ASS'Y
REF
2X DELAY SCHEMATIC E-104-400022
2X DELAY BOARD DRILLING DIAGRAM
2X DELAY RC. LAYOUT E-104-600026
1W DELAY BOARD ASS'Y
REF
1W DELAY SCHEMATIC E-104-400023
1W DELAY BOARD DRILLING DIAGRAM
1W DELAY RC. LAYOUT E-104-600027
R.F SYSTEM CABLING E-104-400028
LOGIC SYSTEM BLOCK DIAGRAM C-104-800018
LOGIC DIAGRAM D-104-400038
RECEIVER MANUAL CONTROL ASS'Y (BREAD BOARD)
RECEIVER MANUAL CONTROL SCHEMATIC J-104-400087
DIGITAL CONTROL CIRCUIT 8 BIT ASS'Y E-104-000025
REF
DIGITAL CONTROL CIRCUIT 8 BIT SCHEM. J-104-400036
DIGITAL CONTROL DRILLING DIAGRAM E-104-100060
DIGITAL CONTROL RC. LAYOUT E-104-600032
HEAT SINK I C-104-100061
HEAT SINK II C-104-100062
STAND OFF C-104-100063
R.F AMPLIFIER ASS'Y.
REF
R.F AMPLIFIER SCHEMATIC D-104-400041
R.F AMPLIFIER DRILLING DIAGRAM
R.F AMPLIFIER RC. LAYOUT D-104-600033

FIG. 7.3-1

B

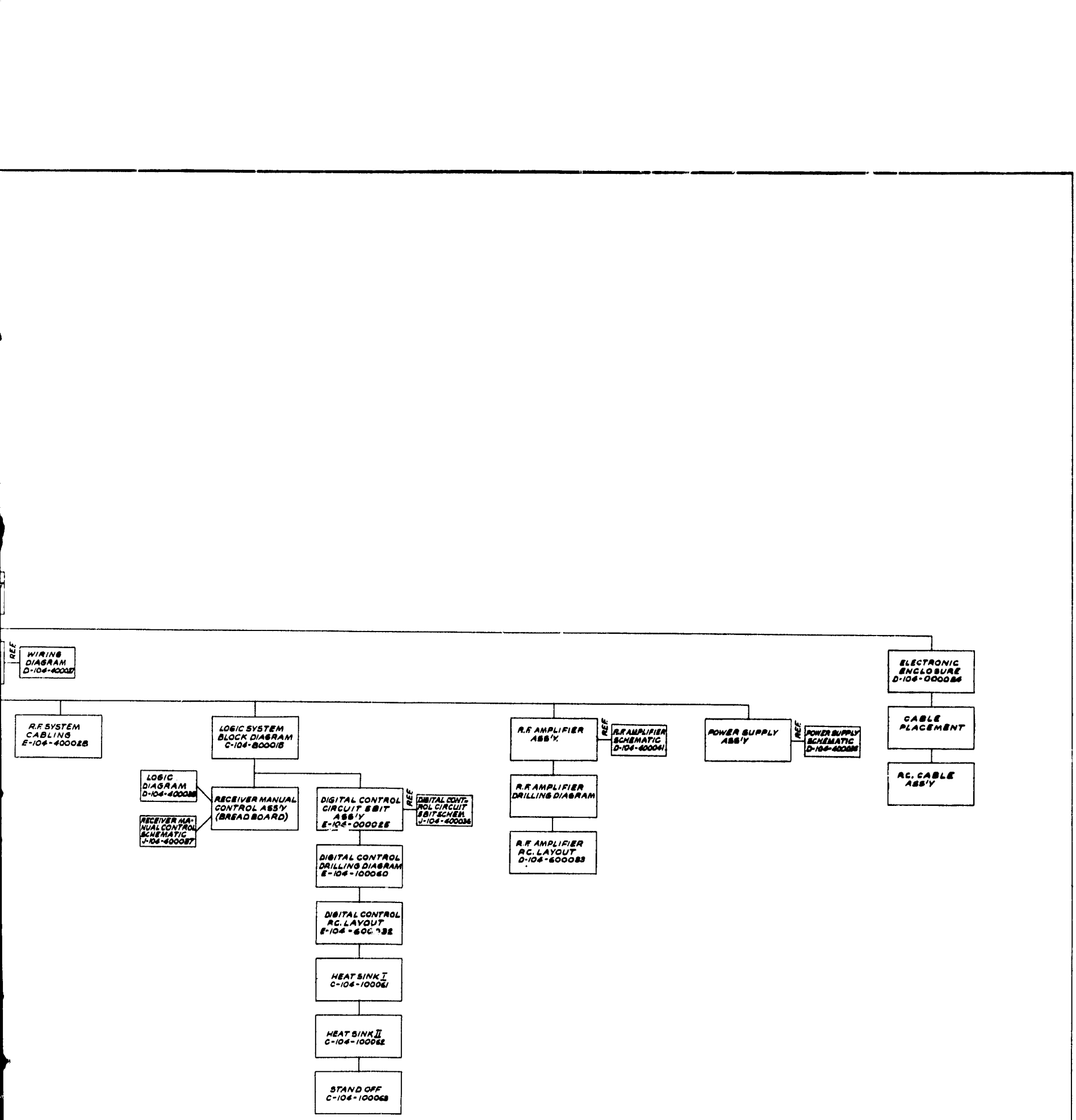
WIRING DIAGRAM D-104-400037
REF
R.F SYSTEM CABLING E-104-400028
LOGIC SYSTEM BLOCK DIAGRAM C-104-800018
LOGIC DIAGRAM D-104-400035
RECEIVER MANUAL CONTROL ASS'Y (BREAD BOARD)
RECEIVER MANUAL CONTROL SCHEMATIC J-104-400037
DIGITAL CONTROL CIRCUIT 8 BIT ASS'Y E-104-000055
REF
DIGITAL CONTROL CIRCUIT 8 BIT SCHEM. J-104-400036
DIGITAL CONTROL DRILLING DIAGRAM E-104-100060
DIGITAL CONTROL P.C. LAYOUT E-104-600032
HEAT SINK I C-104-100061
HEAT SINK II C-104-100062
STAND OFF C-104-100063
R.F AMPLIFIER ASS'Y.
REF
R.F AMPLIFIER SCHEMATIC D-104-400041
R.F AMPLIFIER DRILLING DIAGRAM
R.F AMPLIFIER P.C. LAYOUT D-104-600083
POWER SUPPLY ASS'Y
REF
POWER SUPPLY SCHEMATIC D-104-400038
ELECTRONIC ENCLOSURE D-104-000084
CABLE PLACEMENT
A.C. CABLE ASS'Y

B

C

7.4 Financial Analysis

The following cost estimates were proposed by the Center for Space Research, Laboratory for Space Experiments. They have been carefully analyzed in the light of our collective experience with the phased array over the past three years.

The figures represented in our estimates were predicted on actual cost data wherever practicable and we have every reason to believe they depict the entire cost picture. But they are still estimates, and as such, are subject to revision as future costs become actual. Notwithstanding this, we submit the following statements for your consideration and evaluation.

	El Campo maintanence 10/1/68 - 3/31/70	Pilot Array 10/1/68 - 6/30/69	Expanded 40db Array 5/1/69 - 4/30/70	50db Array 6/1/70 - 12/31/71	Transm.
alaries & ages	42,220	163,594	310,748	462,788	
aterials & ervices	122,400	83,914	387,800	1,938,032	
ravel	9,000	10,000	10,000	12,000	
ther					
a)		3,000 (Maintain 128 dipole narrowband array)			
b)		28,000 (Documentation)			
c)		104,000 (Support not funded)			
otal	173,620*	392,508	708,548	2,412,820	1,309,000

* Cost is estimated at 246K if support for array not forthcoming.

SUMMARY ARRAY COSTS

EL CAMPO SITE OPERATION

(10/1/68 - 3/31/70)

I.	Salaries & Wages			
	A. 1 Proj. Engineer (25%)			
	B. 1 Proj. Technician			
	C. 1/2 Secretary			
	D. Mgt. & Support			
	E. Overhead (25%)			
	F. Benefits			
	TOTAL Salaries, Wages, Expenses, etc.			$ 42,220*
II.	Materials & Services			
	A. Maintan. of Facility	@	5,300	95,400
	B. Outside, Misc. Purch.	@	1,500	27,000
	TOTAL Materials & Services			122,400
III.	Travel	@	500	9,000
	TOTAL SITE OPERATION			$ 173,620

* Total salaries, wages, including overhead and benefits, will increase by 73K; total will then be 246.6K if array does not support some of site personnel.

DETAILED SUMMARY

PILOT ARRAY

(10/1/68 - 6/30/69)

I. Salaries, Wages & Management

A. Salaries

1. 1 Proj. Eng.
2. 1 Site Eng. (75%)
3. 1 E. Eng.
4. 1 E. Eng.
5. 1 Mech. Eng. (50%)
6. 1 Programmer (50%)

B. Wages

1. 1-1/2 Proj. Tech.
2. 1 A Tech
3. 1 B Tech
4. 1 C Tech
5. 1 Machinist (50%)
6. 1 Draftsman

TOTAL Salaries & Wages	Site	$ 24,614	
	MIT	65,025	
C. Management			
1. Tech. & Admin. Mgt.			
2. Gen. & Admin. Support			
TOTAL Salaries - Indirect		13,500	
D. Overhead @ 50.5% (MIT)		39,655	
25% (Site)		6,154	
E. Benefits @ 14.2%		14,646	
TOTAL Labor & Overhead			$ 163,594.00

PILOT ARRAY

II. Materials & Services

A. Hardware & Digging for 14db element

1.	Post hardware & hole digging (6 posts & associated hardware @ $12/dipole)	$72/14db element	
2.	Mercury switches #14 @ 3.50	49/14db element	
3.	Cable 16λ @ 3.85/λ	61.60/14db element	
4.	Trenches 5.25λ @ 3.30/λ	17.33/14db element	
	Sub-Total	$199.93/14db element	
5.	Installation Labor	28/14db element	
6.	2 Amplifiers @ 38.47	76.94/14db element	
	Sub-Total Hardware & Labor 14db Element	304.87	

TOTAL Hardware & Digging Cost for Elements: [318.30/14db Element x 32 elements] $ 9,775.84

B. Cost from 14db Element to Pilot Center

1.	Cable 740λ @ 3.85/λ	2,849.00	
2.	Trenches 88λ @ 3.30/λ	290.40	
	Sub-Total	3,139.40	
3.	Central Electronics Box	4,599.00	
	Sub-Total Element to Pilot Center		7,738.40

TOTAL Material Cost - Elements $17,514.24

C. Site Preparation

1.	Power	18,500
2.	Gravel Road	3,000
3.	Surveying	500
4.	Construction of suitable facility (complete with water, air conditioning)	10,000
TOTAL Site Preparation		32,000

III. Capital Equipment

A. MIT/LSE

Power Amplifier Receiver	$1,400	
RF voltmeter	700	
Vector Impedance Meter	2,700	
IF Strip	1,000	
Time Domain Reflectometer	1,500	
Standing Wave Indicator	1,300	
Probes	800	
TOTAL MIT/LSE Capital Equip.	9,400	

B. Site Capital Equipment (Included part of C/E required in 40db Array) 25,000

TOTAL Capital Equipment $34,400

IV. Travel

20 man trips (MIT) to site @500/trip 10,000

TOTAL Travel 10,000

V. Maintain & Continue Operation of 128/dipole Narrowband Array 3,000

VI. Documentation (including final report) 28,000

VII. Previous Support, not funded (as of 9/30/68) 104,000

TOTAL Materials & Services 288,914.24

TOTAL PILOT ARRAY (Labor, Materials & Travel) $392,508.24

EXPANDED 40db ARRAY

(5/1/69 - 4/30/70)

I. Salaries, Wages & Management

A. Salaries & Wages

1. 1 Proj. Eng. (MIT)
2. 1 Proj. Eng. (Site, 75%)
3. 1 E. Eng. (MIT)
4. 1 E. Eng. (Site)
5. 1 E/M Eng. (Site)
6. 1 Mech. Eng. (50%)
7. 1 E.A. (Site)
8. 1 Programmer (50%)
9. 2 Proj. Tech. (Site)
10. 1 C Tech
11. 1 A Tech
12. 2 B Tech (Site)
13. 1 A Tech
14. 1 B Tech
15. 1 Draftsman
16. 1 Machinist (50%)

TOTAL Wages	Site	$ 104,328	
	MIT	74,100	
B. Management			
1. Lab Tech & Admin. Mgt.			
2. Gen. & Admin. Support			
TOTAL Management Salaries		26,400	
TOTAL Salaries & Wages			$ 204,828.00
C. Overhead (50.5%)	MIT		50,752.00
	Site		26,082.00
D. Benefits (14.2%)			29,086.00
TOTAL Expenses & Salaries, etc.			$ 310,748.00

40ch. EXPANDED-ARRAY-

II. Materials & Services

A. Hardware & Digging for 14db Element

1.	Post hardware & hole digging (6 posts & associated hardware)	$108/14db element
2.	Mercury switches #14 @ $2	28/14db element
3.	Cable 16λ @ 3.27/λ	52.32/14db element
4.	Trenches 5.25λ @ 3.30/λ	17.33/14db element
	Sub-total	$205.65/14db element
5.	2 Amplifiers @ 27.37	54.74/14db element
6.	Installation Labor	24/14db element
	Sub-total Hardware & Labor	284.39/14db element

TOTAL Hardware & Digging Expense
[$284.39/14db element x 32 (9,100.48/pilot unit) x 15] $136,507.20

B. Cost from 14db Element to Pilot Center

1.	Cable $2349 x 15 - less 15% discount (2421.65 x 15)	36,324.75
2.	Trenches $290 x 15 plus additional trenching 56λ @ 3.30/λ	4,350 184
	Sub-total Trenches	4,534.00

3. Central Electronic Box @ 3343.32 x 15	50,149.80	
Sub-total to Element Central Electronics		91,008.55
TOTAL Hardware & Digging Cost Expanded Array		$227,515.75*

III. Site Preparation

Grading & surveying of expanded array area $3,000

IV. Capital Equipment

A. MIT/LSE

HP 608 Signal Generator 2 @ $1450	$2,900	
Tektronix Sampling Scope		
661 Main Frame 2 @ 1200	2,400	
5T3 Timing Unit 2 @ 850	1,700	
451 Sampling Unit 2 @ 1475	2,950	
Automatic Network Test Equipment		
Wiltron 310B Indicator	3,485	
Wiltron 311 V20 Resolver	2,950	
Wiltron Sweep Generator		
610B Frame	1,450	
6105 Plug in	1,950	
Sub-total MIT/LSE Capital Equip.		19,785

B. Site

Computer	30,000	
Tape Recorders	35,000	
Time 7 Frequency Stand.	7,500	
Gen. Test Equipment	15,000	
Facilities Improvemt.	15,000	
Sub-total Site Capital Equip.		102,500

---

* This cost is exclusive of control cable cost at the expanded array level estimated at $3,300.

C. TOTAL Capital Equipment		122,200.00
V. DC Power Distribution for RF Transmitter		20,000.00
VI. Extra Maintanence		15,000.00
TOTAL MATERIALS & SERVICES		387,800.75
VII. Travel		
40 man trip vendor @ 150	6,000	
8 man trip MIT to site @ 500/trip	4,000	
TOTAL Travel		10,000.00
TOTAL EXPANDED ARRAY COST		$ 700,548.75

50db ARRAY

(6/1/70 - 12/31/71)

I. Salaries, Wages & Management

A. Salaries & Wages

1. 1 Proj. Eng. (MIT)
2. 1 Proj. Eng. (Site, 75%)
3. 1 E. Eng. (MIT)
4. 1 E. Eng. (Site)
5. 1 E/I Eng. (Site)
6. 1 Mech. Eng. (50%)
7. 1 E.A. (Site)
8. 2 Proj. Tech. (Site)
9. 1 Programmer (50%)
10. 1 C Tech
11. 1 A Tech
12. 1 B Tech (Site)
13. 1 A Tech (Site)
14. 1 B Tech (Site)
15. 1 B Tech
16. 1 Draftsman
17. 1 Machinist (50%)

TOTAL Wages	Site	$174,876	
	MIT	115,723	
B. Management			
1. Lab Tech. & Admin. Mgt.			
2. Gen. & Admin. Support			
TOTAL Management Salaries		44,490	
C. Overhead (50.5%)	MIT	80,892	
	Site	43,710	
D. Benefits (14.2%)		47,578	
TOTAL Expenses & Salaries, etc.			$ 462,788

50Ω ARRAY

II. Materials & Services

A. Hardware & Digging Costs

1.	Post hardware & digging (6 posts & associated hardware, installed)	$100/14db element
2.	Mercury switches #14 @ 1.50	21/14db element
3.	Cable 10λ @ 3.05/λ	48.20/14db element
4.	Trenches 5.25λ @ 2.97/λ	15.59/14db element
	Sub-total	185.39/14db element
5.	Amplifiers @ 17.75	35.50/14db element
6.	Labor of wiring	20/14db element
	Sub-total Hardware & Labor	240.89/14db element

TOTAL Hardware & Digging Expense [240.89/14db element x 32 (7,708.48 pilot unit) x 124] $955,851.52

B. From Element to Central Electronics

1.	Cable ($2849 less 308)		
	1994.30 x 124	247,293.20	
	Additional cable	62,000.00	
			309,293.20
2.	Trenches $261 x 124	32,364.00	
	*Additional trenches	3,000.00	
			35,364.00
3.	Central Electronics @ $2601 x 124		322,524.00

TOTAL MATERIAL COSTS-Elements $1,623,032.72

* Trenches to Pilot shack.

III.	Power Distribution for Transmitter	180,000.00
IV.	Road (completely encircling array)	35,000.00
V.	Capital Equipment	100,000.00
	TOTAL MATERIALS & SERVICES	1,938,032.72
VI.	Travel	12,000.00
	TOTAL 50db ARRAY	$2,412,820.72
VII.	Automatic Mercury Switching at Element Level	400,000.00
VIII.	Transmitter 500KW	1,300,000.00
		$4,112,320.72

SUMMARY

Methods of Construction - Cost Comparison

I. Building Array by Steps

A. Total Cost Pilot Array	$ 392,508.24	
B. Total Cost 40db Expanded Array	708,548.75	
C. Total Cost 50db Array	2,410,820.72	
GRAND TOTAL to Build Array by Steps		$ 3,511,877.71

II. Building 50db Array W/O Intermediate Steps

A. Labor	136,830.00	
B. I & S	1,700,360.00	
C. Extra Cable	62,000.00	
D. Capital Equip.	200,000.00	
E. Power Busses	200,000.00	
F. Travel	30,000.00	
TOTAL		3,189,100.00

N.B. Therefore, difference between building Array by M.I.T. by eight intermediate steps or in one effort is approximately $323,000.

Step Method		No/Steps
Adding Transmitter:		
$3,511,877.71	(Transmitter	$3,190,000.00
1,300,000.00	in 1972)	1,300,000.00
$4,811,877.71		4,490,000.00
	Transmitter 1970	3,190,000.00
		1,500,000.00
		4,690,000.00

7.5 Description of the Sunblazer Program

7.5.1 Mission Considerations

7.5.1.1 Scientific Mission Objectives

The primary objective of the Sunblazer program is to measure the electron density profile with good accuracy over the 5 to 100 solar radii distance from the sun where it has only been inferred with considerable ambiguity from radio star occultation measurements. A secondary objective is to measure unambiguously the scale of turbulence in the inner corona and the outward moving velocity of the inhomogeneities in the inner corona. Additional objectives include observations of Faraday rotation or pulse splitting to infer some qualitative information about the existence of a general solar magnetic field, and to carry a variety of particles and fields experiments to the .52 A.U. region of interplanetary space.

In addition to experiments involving the spacecraft, quite significant radio and radar astronomy experiments may be performed with the antenna alone. Some of these possibilities are discussed in Section 1.4.

7.5.1.2 Other On-Board Experiments

The present spacecraft weight is approximately 28 pounds exclusive of any on-board experiments. The 5-stage Scout is

capable of placing a payload of 55 pounds into a .65 A.U. orbit. The word "payload" in this case applies to all weight appended to the fifth-stage rocket casing. There are at least 10 to 15 pounds of engineering telemetry which has been put aboard the 5-stage Scout vehicle for performance-testing which presumably could be removed on later launches. We would expect that this additional weight could be used for additional science on Sunblazer. A large number of suggestions for quite meritorious experiments have been proposed, relating mostly to particles and fields experiments in the .52 and .65 A.U. region that Sunblazer will traverse.

All of the proposed experiments are typically those that count events over say a one-day period and require the contents of a counter to be transmitted back once a day or so for the experiment to be accomplished; these are quite suitable for the low data rate transmission system that Sunblazer will have.

7.5.2. Description of the Sunblazer Spacecraft

7.5.2.1 The Launch Vehicle and Spacecraft Orbit

In the interests of economy for this series the standard four-stage Scout launch vehicle modified by an additional "velocity package" fifth-stage will be utilized to provide the solar orbital injection velocity for the Sunblazer spacecraft. The five-staged Scout performance is given in Figure 7.5.2.1-

SOLAR PROBE MISSIONS

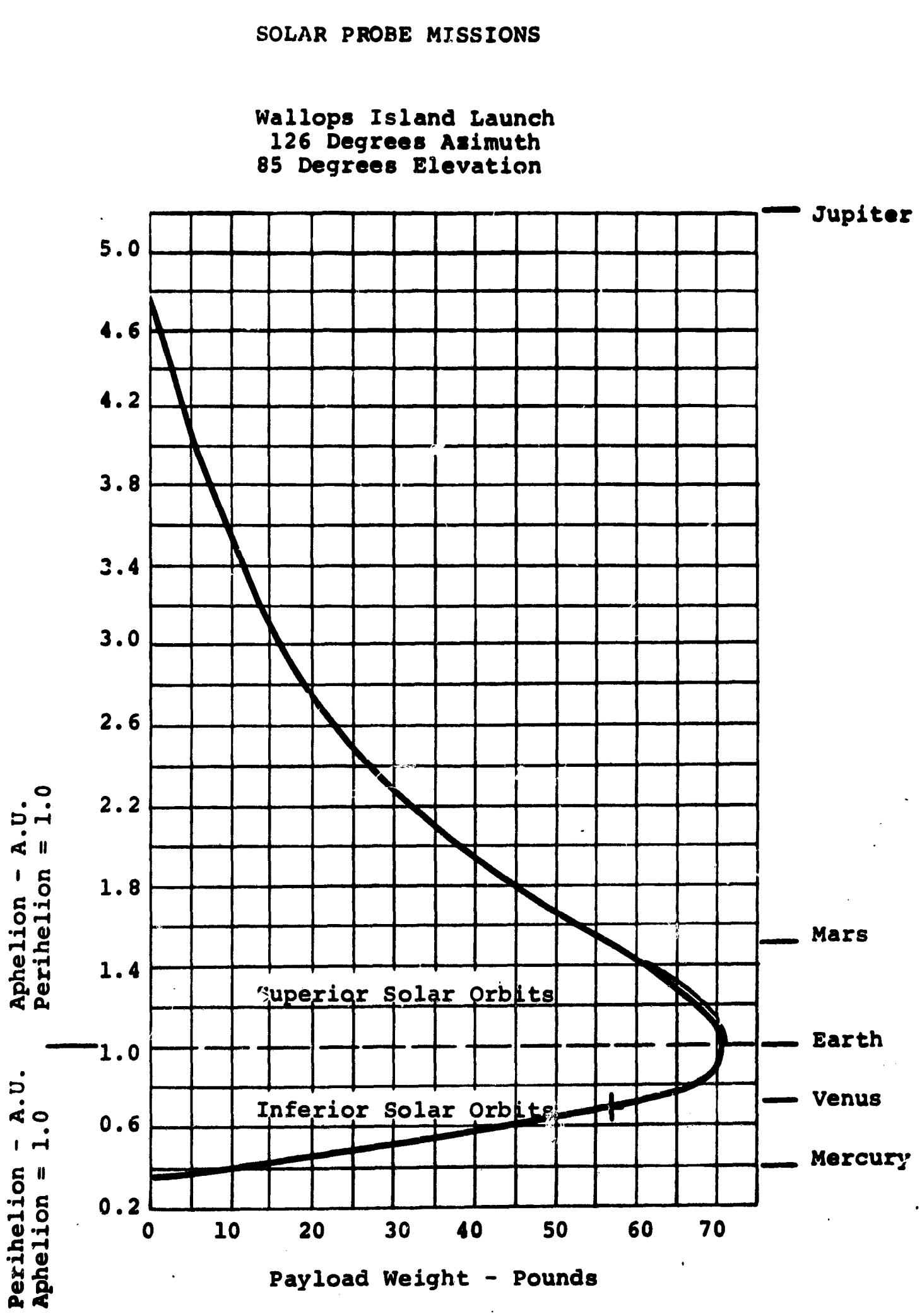

Figure 7.5.2.1-1 Solar Probe Performance Using Scout Fifth Stage-Wallops Station

and indicates that approximately a 57 pound payload may be put into a 0.65 A.U. perihelion solar orbit. This orbit was selected because it included three superior conjunctions which are generated by the relative motions of the spacecraft and the earth as shown in Figure 7.5.2.1-2. The selected orbit permits the spacecraft to apparently remain within a subtended angle of 3 degrees from the sun for a period greater than 6 months.

7.5.2.2 Some Basic Spacecraft Design Requirements

Within the size and weight limitations of the spacecraft the following requirements were imposed:

1) Thermal survival of the apparatus at 1.0 A.U. and 0.65 A.U.
2) The generation of 2 kilowatts of transmitted R.F. power.
3) An earth pointing antenna beam pattern for the delay experiment at superior conjunction.

These three basic requirements are satisfied by designing a spacecraft which is aligned with a projected solar radius throughout the entire orbit.

Thermally, one side of the spacecraft always faces the sun and is cooled by the opposite side which acts as a heat sink and radiator to cold space.

With solar cells spaced on the sun facing side of the spacecraft, the available power to solar cell weight ratio is optimized since all cells are constantly illuminated.

Figure 7.5.2.1-2

MOTION OF SUNBLAZER RELATIVE TO THE EARTH

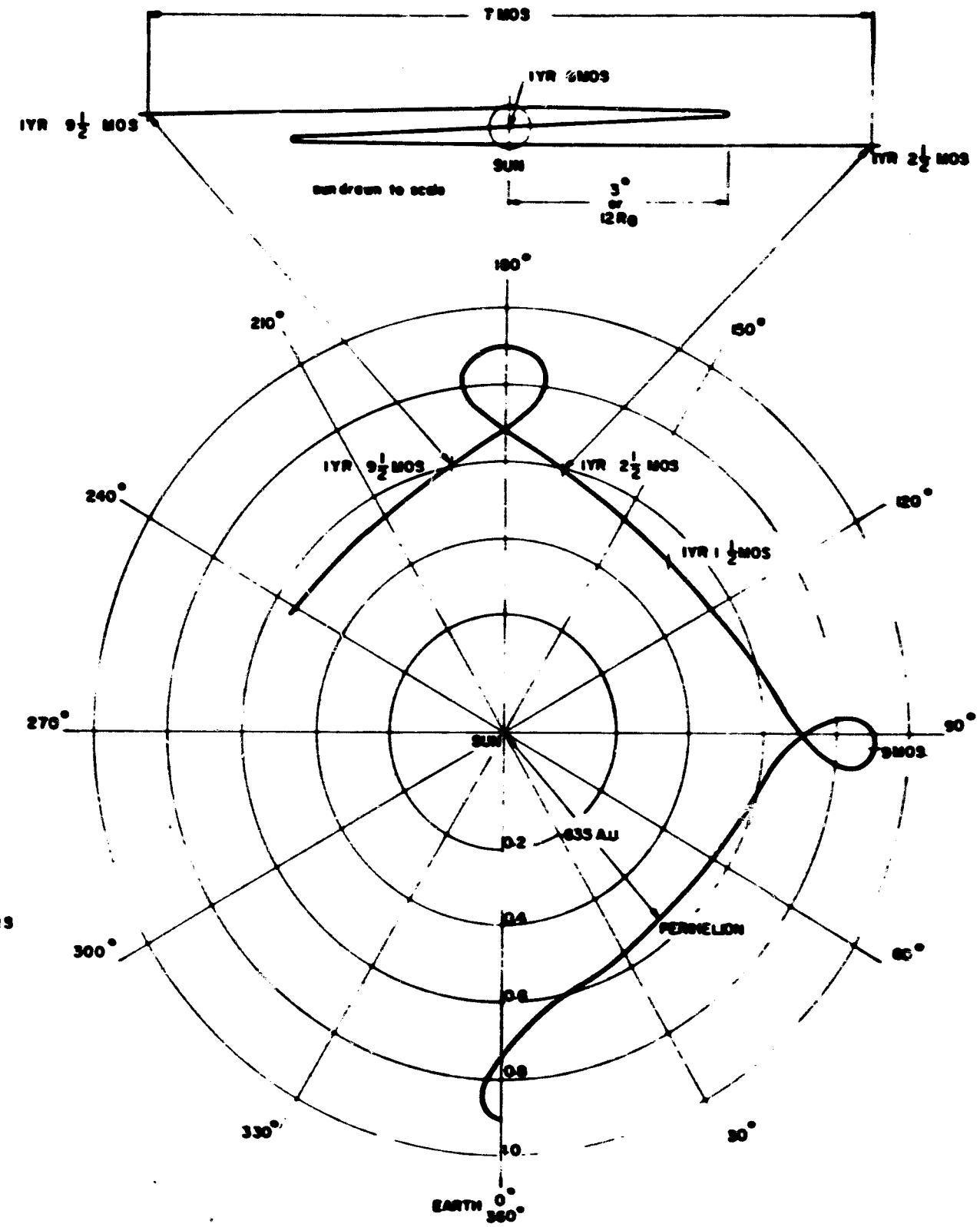

LAUNCH - JULY 4
ORBITAL PERIOD - $\frac{3}{4}$ YR
SEMI-MAJOR AXIS - .82548 A.U.
INCLINATION: 3 degrees
ORBITAL ECCENTRICITY - .234673
TIME TO SUPERIOR CONJUNCTION - $1\frac{1}{2}$ YEARS
PERIHELION DISTANCE - .635 A.U.

During superior conjunction which is the primary region of scientific interest, the spacecraft antenna beam pattern is automatically aligned with the earth.

7.5.2.3 The Spacecraft Configuration

Shown in Figure 7.5.2.3-1 is the main body of the Sunblazer spacecraft, it consists of a solar cell mounting platform and, attached to its rear portion, a cylindrical radiator which also houses the cruciform structured electronics subassembly.

Orientation of the platform-radiator assembly to the sun is maintained by the use of four triangular shaped, rear canted solar sails which have an adjustable pitch angle in their longitudinal axis. Control of the sail pitch angle is maintained by a solar aspect and spin rate detector mounted in the spacecraft's spin axis on the solar cell platform. Logic and amplifier circuits associated with the aspect sensor provide the control signals to pitch the sails.

Solar pressure on the sails which are behind the center of mass, generates the required torques to erect the spacecraft's spin axis into alignment with the sun.

The spacecraft's main radiating antenna is a quarter wave dipole configuration mounted at the rear edge of the platform. Due to the volume constraints and the forces involved during spin up and despin, both the sails and antenna are designed as deployable members which are activated after injection when the spacecraft has been despun to a slower rate.

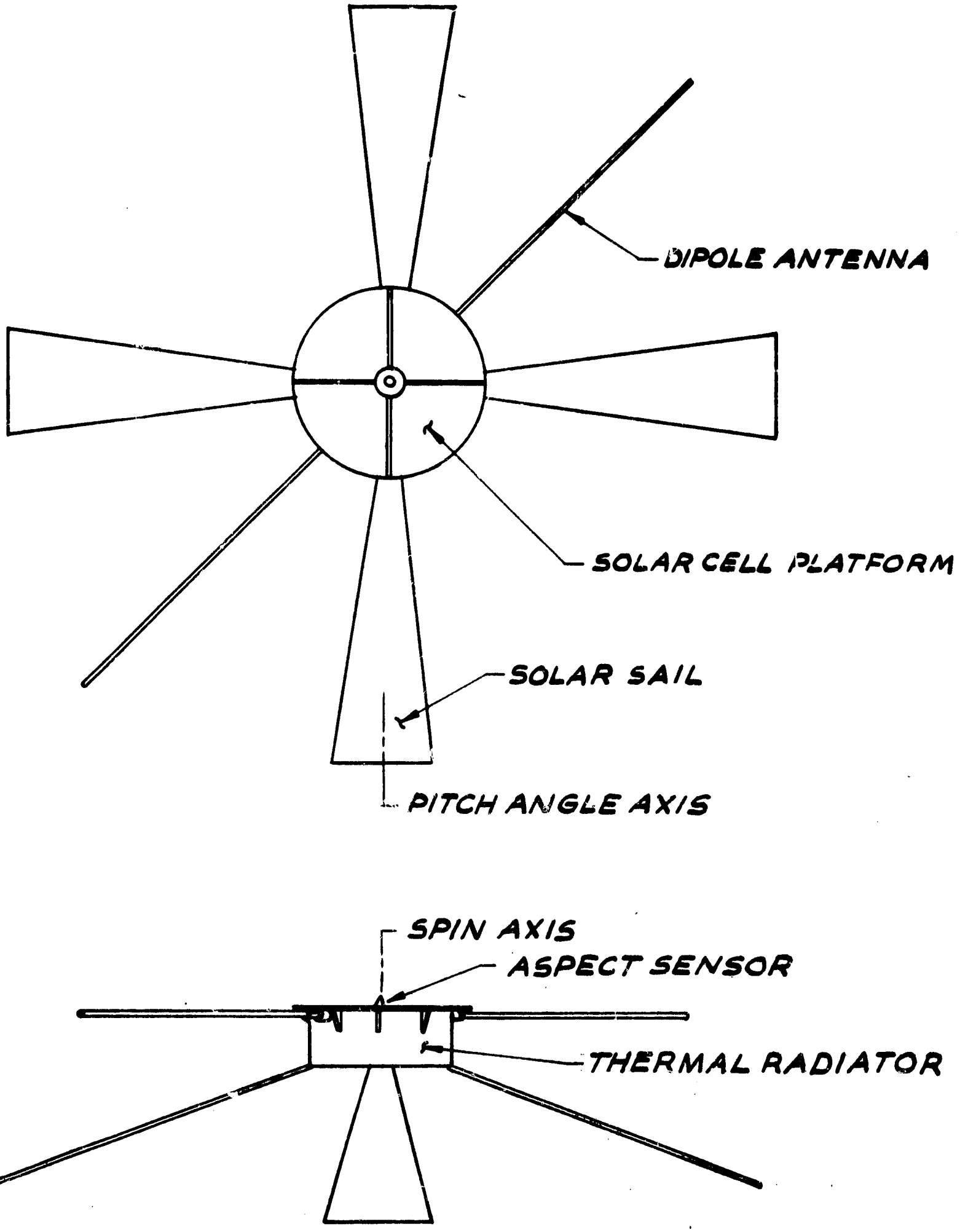

SUNBLAZER SPACECRAFT CONFIGURATION

FIG. 7.5.2.3-1

7.5.2.4 Spacecraft Power

The solar cell array is made up of sixteen paralleled series strings of forty 1 x 2 centimeter cells, which will supply about 18 watts of power at 1.0 A.U. and about 30 watts at 0.65 A.U. This changing power profile is tracked by a special D.C. to D.C. converter to provide near maximum continuous power to a capacitive energy storage system. Present capacitor technology provides about 30 Joules of energy storage per pound. Approximately 15 percent of the Sunblazer's weight has been allocated to the main transmitter's energy storage system which has been designed to provide subsystem redundancy.

A battery operated, 50 watt beacon transmitter is also included on board the spacecraft to provide initial tracking and telemetry data. The signals from the beacon transmitter are radiated from the solar sails.

7.5.3 Propagation and Communication Considerations

7.5.3.1 The Propagation Experiment

Many studies have been made of the extent to which the turbulent coronal plasma should be expected to distort a pulse. This occurs by means of frequency broadening which would arise from the motion of the turbulent refractive inhomogeneities or, correspondingly, from the delay distortion which would occur in the time domain through the dispersive

nature of the medium or through multipath. We have concluded, on the basis of both theoretical studies and the examination of the data provided by radio star occultation and by the Mariner 4 frequency broadening measurements that a 3 millisecond pulse at 75 MHz has an excellent probability of being detected in as close as 5 solar radii, and further that this pulse can be composed of 25 microsecond elementary pulses distinguished by phase reversal modulation. In effect, then, we would have 25 microsecond resolution and should be able to identify any multipath contributions as well as to identify contributions arriving on different magnetoionic propagation modes. The large advantage that this pulsed group-delay method has over the kind of sinusoidal modulation employed in the Pioneer propagation experiment is that the periodicity of the modulation precludes the possibility of identifying multipath and other perhaps unanticipated propagation modes, and makes difficult if not risky the interpretation of the delay data.

The other, in our view, great deficiency of the Pioneer experiment is that the delay measurements are made on the uplink for matters of engineering convenience, but the interpretation must be then done by a relatively inept machine and not by the scientific observer who is available if downlink transmissions can be made adequate, as we believe they are in Sunblazer. In Pioneer, for example, all possibility of scintillation measurements, frequency broadening measurements,

Faraday rotation measurements are excluded unless an extremely complicated receiver on the spacecraft is postulated. We are convinced from an engineering viewpoint that the I.I.T. propagation measurement has been proved feasible.

7.5.3.2 Communication System

This section of the report is concerned primarily with the communication system constraints and performance requirements that are germane to the design specification of the receiver complex and phased array antenna. To provide perspective for this discussion we start by reviewing briefly the major system constraints that are discussed in detail in other sections of this report and in the companion reporting specific to the Sunblazer spacecraft. Like most system designs, the final configuration is reached by a series of compromises between these various constraints and is aimed toward the achievement of an optimal balance between maximum performance and minimum total system cost.

A fundamental criteria is that the Sunblazer experiment must be conducted economically both to minimize the cost/effectiveness ratio for the immediate propagation experiment and to facilitate a continuing program of deep space exploration experiments at the university level. This requirement leads immediately to the choice of a relatively low cost launch vehicle and the acceptance of a consequent modest lifting

capability. The resultant restriction of spacecraft size and weight is manifested principally by restrictions on the spacecraft complexity and the available spacecraft power. These limitations, in turn, restrict the choice of communication strategy.

Other important constraints are dictated by the nature of the transmission medium that is to be investigated and the scientific data sought in the propagation experiment. A regime of maximum interest will occur when the spacecraft approaches superior conjunction. At this time the medium will introduce appreciable distortions and perturbations in the communication path that will affect the received signal adversely. Indeed, the signal design is chosen deliberately to accentuate the effect of the medium so that the magnitude of the perturbations can be measured with tolerable accuracy.

These various constraints combine to require the transmission from the spacecraft of relatively short pulses with high, but restricted, peak power and the accurate measurement of the time of receipt of these pulses in the face of perturbations induced by the medium and a very long communication range. In turn, these factors combine to dictate a minimum required system signal-to-noise ratio and hence to establish the required gain of the phased array antenna.

7.5.3.2.1 Spacecraft Constraints

The average power available in the spacecraft is limited by the size of the solar cell array that can be carried. As

shown in the companion report concerned with the Sunblazer spacecraft, the available power in the region of superior conjunction will be about 15 watts. Some part of this is lost by inefficiencies in the power conversion processes, and in the fixed power drains imposed by the spacecraft timing and control circuits. Consequently, the average power available at each of the two carrier frequencies used in the prime propagation experiment is limited to about 6 watts. This, of course, is a significant constraint on the communication system strategy and performance.

The peak power of each transmitted pulse is limited both by the average power constraint and by the availability of suitable lightweight, reliable, spaceworthy transmitter components. Available transistors permit a single output stage to generate about 70 watts of R.F. power. A larger total peak power is secured by combining the outputs of many such stages in parallel. In principle, any desired number of stages could be used to achieve any arbitrary peak power level. Practically, however, difficulties in properly phasing the individual outputs over the required frequency band restrict the total number of paralleled stages to about 30 to 40 with a consequent total peak power output of the order of 2 or 3 kilowatts. This restricted peak power combined with the long transmission range as the spacecraft approaches superior conjunction precludes the use of incoherent envelope detection and

makes necessary the use of a coherent detection technique. With this technique the proper criteria for system capability is not the average power or peak power but is the energy contained in each received pulse.

The transmitted pulse energy is constrained by two important considerations: the pulse repetition rate required by the propagation experiment, and the nature of the energy storage device in the spacecraft power conversion sub-system. To obtain a data sample rate adequate for the experiment it is necessary to use a pulse repetition rate of the order of one pulse per second. Since the available average power, per carrier, is 6 watts, this implies a maximum transmitted pulse energy of the order of 6 Joules. This is within the range of capability of a capacitor energy storage sub-system, a desirable qualification since it avoids the use of an active temperature control mechanism that would be required if chemical batteries were used as the main energy reservoir. Both considerations, therefore, point to the same optimal transmitted pulse energy of 6 Joules.

Unfortunately, this energy has to be radiated in a nearly omni-directional pattern. A truly high gain spacecraft antenna is precluded because it is not feasible to carry star sighting and pointing mechanisms in a small inexpensive spacecraft. A small improvement is achieved by emphasizing the radiation pattern toward the front of the spacecraft which is normally pointed toward the sun. This causes a reduction in received

signal energy when the spacecraft is near the earth and viewed from the rear; however, in this time region the range is relatively short so this reduction is an acceptable price to pay for the improvement obtained when the spacecraft is near superior conjunction and pointing simultaneously toward the sun and toward earth. To avoid unacceptable penalties in critical portions of the spacecraft orbit, however, the directional gain has to be limited to about 3 db.

7.5.3.2.2 Communication Constraints Imposed by the Medium

A parameter of immediate significance here is the communication channel coherence time. This describes the maximum time duration for which the channel may be expected to maintain phase stability. That is, it defines the maximum pulse duration that may be used if the receiver is to take full advantage of the detection improvement possible with coherent integration of the total received signal energy.

The companion Sunblazer spacecraft report characterizes the expected parameters of the communication channel in terms of the probable behavior of the transmission medium. It is shown that the channel coherence time may be as little as 3 milliseconds when the spacecraft approaches superior conjunction. Combining this time with the allotted 7 Joules per pulse, we see that the required transmitted pulse peak power is 2 kilowatts. This is within the range of capability of the transmitter and is, therefore, an acceptable requirement.

7.5.3.2.3 Receiver Constraints

In order to extract the signal from the noise background it is necessary to use a correlation technique in which the received signal is compared with a multiplicity of locally generated postulated signals to determine the presence and time of arrival of the received pulse. The efficacy of this procedure is related in a non-linear manner to the signal-to-noise energy ratio. Several system performance parameters degrade rather rapidly when this ratio becomes less than about 6 db. This, therefore, represents a minimum threshold energy ratio that must be achieved to ensure acceptable detection accuracy.

The design value of the signal-to-noise energy ratio must be greater than the threshold value by an amount sufficient to offset a variety of probable detection inefficiencies. These include possible degradation in the spacecraft transmitter, reduction in the receiving antenna gain caused by beam distortion when the antenna is pointed away from the zenith, slight losses caused by less than perfect pointing of the receiving antenna at the very distant spacecraft, a less than perfect knowledge of the instantaneous received frequency, fading and multipath interference induced by the medium, and localized increases in the galactic background noise. Proper allowance for these disturbing factors requires the system to be designed to yield a nominal signal-to-noise energy ratio of the order of 16 db.

7.5.3.2.4 Signal-to-Noise Ratio

For the type of communication system involved here the parameter of prime interest in determining system performance is the signal-to-noise energy ratio; that is, the ratio of the energy in each received pulse to the background noise spectral density, or noise power per unit bandwidth. This ratio may be shown as:

$$\left(\frac{S}{N}\right)_{energy} = \frac{E_t G_t A_e}{4\pi R^2 kT}$$

or, substituting:

$$A_e = \frac{\lambda^2 G_r}{4\pi}$$

$$\frac{S}{N} = \frac{E_t G_t \lambda^2 G_r}{(4\pi R)^2 kT}$$

where E_t is the energy of the transmitted pulse, in Joules

G_t is the directional gain of the transmitting antenna

A_e is the effective area of the receiving antenna, in meters^2

R is the communication range, in meters

k is Boltzmann's constant, in Joules per degree Kelvin

T is the total equivalent noise temperature of the observed background and the receiver front end, in degrees Kelvin

λ is the wavelength of the R.F. carrier, in meters

G_r is the directional gain of the receiving antenna

Rearranging this, we can stipulate a required design value for the ground antenna gain is:

$$G_r \geq \frac{\left(\frac{S}{N}\right)(4\pi R)^2 kT}{L_t G_t \lambda^2}$$

Now, it has been shown that the energy of the transmitted pulse is 6 Joules, that the directional gain of the transmitting antenna is limited to 3 db, and that the received signal-to-noise energy ratio is required to be 16 db. It is shown elsewhere that the maximum range is 2 A.U., or 3×10^{11} meters, and that the chosen frequency is 75 megahertz with a consequent wavelength of 4 meters. The average galactic background noise temperature at 75 megahertz is 1850 degrees Kelvin and the equivalent noise temperature of the receiver front end is 665 degrees Kelvin.

Substituting these values:

$$G_r \geq \frac{40(4\pi \times 3 \times 10^{11})^2 (1.38 \times 10^{-23})(2.52 \times 10^3)}{(6)(2)(4^2)}$$

$$\simeq 1.035 \times 10^5 \simeq 50 \text{ db}$$

As we have seen in other sections of this report, performance of this order can be achieved at reasonable cost. It has also been shown that the resultant antenna facility offers numerous fringe benefits in the form of additional unique scientific

observations that can be made, thus, in effect, prorating this cost among several investigative programs. We therefore close the system design loop justifying the original choice of a modest cost launch vehicle, with the consequent restriction of spacecraft complexity, in a total system configuration that is practical to implement and that is near optimal on both an economic and scientific basis.

7.5.4 Tracking Requirements

Tracking and communications are not problems even if the normal NASA tracking nets are not used. The angle and Doppler information we get on Sunblazer from the phased array will be sufficiently accurate to establish the orbit with enough precision for the propagation experiment. For the propagation experiment, the only important parameter is the displacement of the ray path from the solar center and the actual locations of the terminals, assuming that both are well outside of the region of greatest electron density, are unimportant. Even so, from the angle and Doppler measurements we expect to be able to locate the spacecraft within 10,000 km^3 with high reliability.

There is no up-link contemplated in the Sunblazer mission, and the modest amount of telemetry indicated will be multiplexed on the same 75 MHz carrier emanating from the spacecraft.

7.6 Transmitter Considerations

7.6.1 General System Constraints

An antenna is required to receive signals transmitted from the Sunblazer satellite. An antenna array that is operable over the range 70 to 80 MHz has been proposed for this purpose. It will consist of 27,000 crossed dipole elements, will be electronically steerable, and will have a total gain of 50 db over isotropic. As previously proposed, the Sunblazer antenna will only be able to receive. A proposal has been made for a transmitting function to be incorporated as the antenna is first constructed. The simultaneous construction of the basic receiving array and the transmitting feature will save much time and expense in the long run.

The Sunblazer program is designed to learn more of the physics of the solar corona and interplanetary space by transmitting a series of controlled radio signals through the corona and space. The transmitters will be on the Sunblazer satellite, whose orbit will place it in position behind the sun. With the proposed transmitting function the Sunblazer antenna can also be used to study the backscattering properties of the solar corona and of all planets within the orbit of Saturn.

In the receiving configuration the received signal from each group of six dipoles is amplified, fed through an electronic phase shifter, and then added to similar phase-shifted outputs

of other elements and fed to the main receiver. In the transmitting configuration a signal of proper frequency and modulation is fed to the vicinity of each six-dipole element through the same lines and phase shifters, and then before being fed to the radiating elements is amplified by a solid-state power amplifier. This design requires 4,480 power amplifiers, switches to remove or insert the proper amplifier, a wire line from the control room to control the switching functions, and a primary-power distribution system. As a basis for analysis a system that will radiate one million RF watts is assumed. This requires a 250-watt amplifier at each of the 4,480 six-dipole elements.

7.6.2 Solar Radar Studies

7.6.2.1 Need for New Solar Radar Investigations

The sun is fairly well understood as far as atomic and ionic processes are concerned, but many macroscopic phenomena are not understood at all. The present theories of ionized plasma have been unable to explain the solar corona. The behavior of a hot ionized plasma in the presence of a magnetic field is very complicated. The phenomena of the appearance and development of sunspots, plage regions, flares, prominences and surges have been well observed and documented optically, but have not been explained. Prior to the El Campo solar radar studies there were many theories as to why the coronal

temperature was two million degrees, even though the photospheric temperature was only six thousand degrees and the energy came from nuclear processes at the center of the sun. Radar studies have shown that wave motions that could heat the corona are always present in the corona out to about 1.6 solar radii, where Brandt (1967) has shown that the deposition of energy must cease.

To help untangle the complicated problem of plasma behavior in the sun, more radar observations are needed. Plasma motions can be observed by radar much better than they can by optical or radio emission. Radar, undoubtedly, has a future in explaining the solar corona, but only preliminary radar studies have yet been made. The only significant scientific studies that have been made were those at 38 MHz by MIT at El Campo, Texas. In 1959, a group at Stanford University demonstrated on three occasions that solar echoes could be received at 26 MHz, but have not been able to do so since, in spite of numerous attempts and an enlarged antenna. No other successful experiments have been reported, although it is known from private sources that attempts were made at 49 MHz in Peru and at 40 MHz in Puerto Rico.

Solar radar experiments are badly needed over the frequency range from 20 MHz to 200 MHz. More system sensitivity and more angular resolution, than the present El Campo system has, would help considerably in the interpretation of the data. Experiments at 75 MHz would permit coronal levels as near the

sun's center as 1.15 solar radii to be studied. The deepest penetration of the 38 MHz signal is about 1.35 solar radii, which is 2.3 times as far from the photosphere as the 1.15 level.

Radar studies at 75 MHz could lead to a determination of the coronal absorption and mean temperature to the 1.15 solar radii level. Of more importance would be the variation in temperature and energy deposition as a function of events in the chromosphere. The velocities of plasma waves at the 1.15 level should help considerably in deciding what type of waves heat the corona. In general such experiments should teach us more about both the sun and plasma physics.

7.6.2.2 Solar Radar Results to Date

Solar radar experiments have been performed at 38 MHz near El Campo, Texas, since 1961. During this time much has been learned about how to use radar to explore the sun in addition to learning new facts of solar physics. For example, it has been found that the frequency sensitivity of the antenna causes a decrease in the quality of the integration process, especially when certain types of solar noise bursts are present.

The echo intensity, or radar cross section, is variable on both a long time basis of several years and a short time basis of several days. The echo signal is fairly constant over a 16-minute interval except for a very small amount of

fading at times with a period of five to ten minutes. The cross section is usually appreciably stronger when active regions are on the disk. A large amount of Doppler spreading is always present whether the sun is active or not. The Doppler bandwidth between the half power points is 30 to 40 KHz, and this is much larger than the 1 KHz that might be explained by the rotation rate of the sun. More energy is received at positive Doppler shifts than at negative shifts. Some echo components have only small amounts of Doppler shift and spreading. The echo appears to have equal energies in both linear and circular polarizations.

The main part of the echo is reflected from some sort of wave motion in the corona. These wave motions could be, and very likely are, the mechanism by which the corona is heated. The waves are moving in a predominately radial direction with velocities between 100 and 200 Km/s. Because of multiple reflections, and possibly some wave motions in the direction of the photosphere, there are negative Doppler components in the larger-delayed part of the main echo. The intensity of the main echo changes because of changes in the coronal temperature, changes in the intensity and number of shock waves, changes in the size and shape of the corona, and changes in interplanetary plasma that focuses the radar energy.

The solar radar cross section tends to be considerably larger during the decreasing portion of the sun-spot cycle for some unexplained reasons.

Some echo components arise from irregularities in the high corona out to three or more solar radii from the sun's center. These irregularities are moving radially outward at 10 to 20 KM/s. Their densities change much more slowly with distance from the sun than does the mean density of the corona. Echoes from these show up in the early range intervals and also in the late range intervals. The late echoes are due to signals that are first reflected from the shock waves in the corona, then from a backside of the high corona irregularities, and then again from the shock waves. The late echoes have a large amount of Doppler spreading whereas, the early echoes have a very small amount of Doppler spreading. This should be expected because the shock waves impart a large Doppler spreading to the signal. These high-corona echoes may be moving along with the solar wind, and if so, radar provides a measure of the solar wind velocity in the high corona. However, Dessler (1967) has shown on theoretical grounds that the solar wind velocity in the high corona should be supersonic, and if so, the high corona echoes are reflected from coronal irregularities that are not participating in the solar wind.

7.6.2.3 Solar Echo Studies at 75 MHz

Several factors enter into the computation of the expected signal-to-noise ratio for a solar radar experiment at 75 MHz; namely, average transmitted power, antenna gain, antenna beamwidth,

Doppler spreading of the echo, background noise level, coronal absorption, and radar cross section. It is convenient, and perhaps more significant, to predict the relative performance of the proposed 75 MHz system and the known 38 MHz system rather than compute the received energy of the 75 MHz system only. At 38 MHz the cross section has varied from about $0.2\pi R_\theta^2$ to $20\pi R_\theta^2$ with 500 KW of transmitted power and a 35 db gain antenna (R_θ is the radius of the photosphere). The cross section was typically between 0.5 and $1\pi R_\theta^2$. The signal-to-noise ratio should be no less than it was for the 38 MHz system in order for a significant experiment to be performed.

From the radar equation, the relative sensitivity, S, of the proposed 75 MHz system and the present 38 MHz system is given by:

$$S = \left(\frac{\text{signal}}{\text{noise}}\right)' / \left(\frac{\text{signal}}{\text{noise}}\right) = \frac{P_T'}{P_T}\left(\frac{G'}{G}\right)^2 \frac{A_o'}{A_o}\left(\frac{\lambda'}{\lambda}\right)^{5/2} \frac{N}{N'} \qquad (7.6.2.3\text{-}6)$$

where P_T, G, A_o, λ, and N are respectively; transmitted power, antenna gain, solar radar cross section, wavelength, and background noise temperature at 38 MHz; and where the primes refer to similar parameters at 75 MHz. The 5/2 power for the wavelength ratio arises because the effective area of the receiving antenna varies as $G\lambda^2$, and because the Doppler bandwidth is assumed to vary inversely as the wavelength. For a detection procedure employing signal integration, the signal-to-noise ratio varies inversely as the square root of the

bandwidth. For the 38 MHz system N is about equally divided between galactic and solar noise, and a typical antenna temperature is 20,000 degrees. At 75 MHz the photosphere should be approximately resolved, and so in the absence of grating lobes the antenna temperature would be about 100,000 degrees. The cross section at 75 MHz is an unknown quantity, and is dependent among other things on coronal absorption. For a one-million-degree corona the two-way absorption for the central ray is computed to be 7 db at 38 MHz and 14 db at 75 MHz (James, 1968). For rays at the limbs the attenuation is 1 and 2 db, respectively. The temperature in the vicinity of the reflection strongly affects the attenuation. For example, for the central ray at 75 MHz the computed attenuation is 3 db at 3 million degrees and 36 db at 1/2 million degrees. The solar temperature is likely about one million degrees at the 75 MHz reflecting level. The type of reflecting irregularity (shock wave, Alfren wave, plasma density irregularity, etc.) will, of course, also affect the cross section.

On the basis that both N'/N and A_o/A_o' are 7 db, the value of relative sensitivity is computed to be

$$S = 12 \text{ db} \qquad (7.6.2.3\text{-}2)$$

for $P_T' = 1000$ KW and $G' = 50$ db. This value of S allows a margin for error in the prediction of A_o'.

7.6.3 Planetary Experiments

7.6.3.1 General Discussion of Reasons for Doing

A radar study of planets is another very important reason for including a transmitting facility in the antenna design. Planetary studies yield information on orbits, surface features, rotation rates, ionospheres, magnetic fields, and interplanetary plasma. When the reflection is from the surface rather than the ionosphere, such as is the case for the dark side of Venus and for Mars, something can be learned about surface roughness and composition. Reflections from ionospheres could lead to much information of scientific value such as atmospheric composition and density.

Radar echoes from planets would be modified by the interplanetary medium thus providing a means of studying interplanetary plasma from an earth-based laboratory. Results of such studies would have application to solar physics and space communications. The interplanetary effect on the echo should vary inversely as the square of the frequency and so 75 MHz should be more sensitive than higher frequencies to the plasma effect. The integrated electron density between earth and the planet can be measured directly when the system sensitivity is high enough to permit short pulse measurements. For Venus, at inferior conjunction, a pulse width of about 20 microseconds and a receiver bandpass of about 300 KHz would be required to detect an average electron density of 10/cc.

For a signal-integration detection system the sensitivity varies inversely as the square root of the receiver bandpass and so, as the bandwidth was increased from 1 Hz to 0.3 MHz to accommodate the narrow pulse, the sensitivity would decrease 27 db. This means that a sensitive system would be required to measure weak interplanetary electron densities, but a 50 db gain, 1 MW-transmitted-power system would be sufficient to make such measurements using the planet Venus and, perhaps, Mars.

The transmission properties of the solar corona could be studied by an earth bound radar system when planets were used as reflectors. This principle has been used previously, for example, to study transmission properties of aurora by using the moon as a reflector. (See James, et al, 1960.) The planet Mercury would be quite useful for this purpose because it is in position behind the corona a good percentage of the time. This technique, because of the two-way passage through the corona, would not result in data as easily interpreted as that from the Sunblazer satellite, but it would have advantages of repeatability and flexibility. The backscattered power from Mercury when behind the corona would only be about 0.2 watt for the 1 MW, 50 db radar transmitter, but this is both the average and peak power and so could easily be received in a relatively narrow pass band.

7.6.3.2 Computations of Echo Power

The proposed 70 - 80 MHz antenna will have a gain of 50 db over an isotropic radiator. In the computations to follow it will be assumed that the total radiated power is 1 MW, which is only 10 watts per dipole and a power that can be reasonably obtained. The present El Campo array transmits a total power of 500 KW, which is about 500 watts per dipole.

The radar system sensitivity for a given planetary target is determined by the ratio of the received echo power to the background noise fluctuations. This ratio should be at least 5 dB in order to identify the echo in the presence of noise.

The background noise is conveniently expressed in terms of noise temperature, T, or in terms of db with respect of the standard room temperature of 290°. The relation between available noise power in watts, P, and noise temperature is:

$$P = kTB \qquad (7.6.3.2\text{-}1)$$

where k is Boltzman's constant (1.38×10^{-23} w/m^2/cps) and B is effective bandpass in cps. At 75 MHz the background noise for planetary experiments will consist of receiver front-end noise plus cosmic noise. For the proposed antenna the front-end noise will be the average noise figure of the receivers in the field, and so the front-end noise temperature will be about 3 db/290°. When the sun or a strong radio star is not

in the beam, the cosmic noise temperature will vary from about 2 db to 12 db with the higher values falling along a narrow region near the galactic equator (Milky Way). The antenna assumes the mean sky temperature of the region falling within the beam, regardless of beam size. In the computations to follow, the sky temperature was taken to be 3 db/290°, which leads to a total background temperature of 6 db/290° when the receiver noise is included.

The received echo power is computed by the radar equation,

$$P_R = P_T \frac{G_T}{4\pi R^2} A_O \frac{A_R}{4\pi R^2} \rho \qquad (7.6.3.2\text{-}2)$$

where P_R is received echo power in watts,

P_T is transmitted power in watts,

G_T is transmitting antenna gain over an isotropic radiator,

R is the target range in meters,

A_O is the target cross section in square meters,

A_R is the effective aperture of the receiving antenna in square meters, and

ρ is the polarization misalignment factor. For a linearly-polarized antenna ρ will have an average value of 1/2 for random polarization angles.

The following substitutions will be made in order to simplify the radar equation:

$P_T = 10^6$ watts

$G_T = G_R = 50$ db or 10^5

$R = 1.496\ V \times 10^{11}$ meters, where V is range in astronomical units.

$$A_R = G_R \frac{\lambda^2}{4\pi}$$

$\lambda^2 = 15.98\ m^2$ at 75 mHz

$\rho = 1/2$

With these substitutions the radar equation becomes

$$P_R = \frac{A_o}{V^4} \times 8.04 \times 10^{-32} \text{ watts.} \qquad (7.6.3.2\text{-}3)$$

The cross section, A_o, is the projected area of the planet (πr^2) times the backscattering reflectivity. The reflectivity is a parameter to be measured and is not accurately known except in the case of Venus and even here it fluctuates greatly with time from near zero to 200%. (See James, Ingalls, and Rainville, 1967.) The reflectivities of the planets are discussed by Pettengill (1968), and are largely the bases for the reflectivity assumptions listed in Table (7.6.3.2-1). The listed value for Saturn and Ganymede (one of Jupiter's moons) is no more than a typical value for planets that have been observed. The reflectivity for Jupiter is probably larger

TABLE 7.6.3.2-1

Predicted values of signal-to-noise ratio for radar studies at 75 MHz with a 50 db antenna and 1 MW transmitted power. Values of estimated reflectivity and Doppler bandwidth, and round-trip times are also listed. Max and min refer to the largest and smallest distances of the body from the earth within the next ten years. A_o is radar cross section, and P_R is received echo power. Background noise temperature is assumed to be 6 db/290°.

		MERCURY	VENUS	MARS	JUPITER	GANYMEDE	SATURN
Round-Trip Time (Mins)	MIN.	10.0	4.8	6.1	69.9	69.9	142.1
	MAX.	23.3	26.3	43.2	108.1	108.1	175.4
Reflectivity (%)		6	15	7	8	10	10
A_o ($10^{12} m^2$)		1.10	18.1	2.54	1290.	1.92	1146.
P_R (10^{-20} watts)	MIN.	68	20600	1090	33.	.05	1.7
	MAX.	2.3	17.4	0.45	5.7	.009	0.7
Bandwidth (cps)		2	2	100	100	2	100
$\frac{S}{N}$ (db) No Signal Integration	MIN.	13	38	8	-7	-18	-20
	MAX.	-1.5	7	-25	-14	-26	-23
$\frac{S}{N}$ (db) With 5 Mins. Integration Time	MIN.	27	52	31	15	-4	4
	MAX.	12	21	-3	8	-12	-1
$\frac{S}{N}$ (db) Signal Integration For Round-Trip Time	MIN.	29	52	31	21	2	10
	MAX.	15	43	2	15	-5	7

than 8% at 75 MHz.

For the above radar system the signal-to-noise ratios for several possible planetary targets were computed using Equations (7.6.3.2-1) and (7.6.3.2-3), and are presented in Table 7.6.3.2-1. The MAX and MIN values refer to the known maximum and minimum distances of the bodies from the earth. The listed values for receiver bandwidth are based on known values of Doppler spreading except for the cases of Jupiter, Ganymede, and Saturn. For these bodies the Doppler spreading was estimated on the basis of their size, spin rate, and expected roughness.

The results of these computations are that the proposed radar system should be capable of studying Mercury, Venus, Jupiter, Saturn and the interplanetary space between these bodies and earth, at all points of their orbits. It would indeed be a significant experiment to study these planets at both superior and inferior conjunction. The radar system would also be capable of studying Mars each day except for a period of 8 months out of each 25.6 months; i.e., Mars could be seen on 70% of the days. Ganymede could not be studied unless its reflectivity were greater than 20%. The detectability of Saturn would be doubtful, if its reflectivity were less than 10%.

7.6.4 Primary Power System

7.6.4.1 System Design

The design here is based on 5000 or more power amplifiers spaced uniformly over the array and supplying a total R.F. power of one megawatt to the antenna elements. The primary power for these amplifiers is at 25 or more volts DC. The 25 volt distribution will be from a number of rectifier stations spaced uniformly over the array. Each rectifier station will be fed by a 3 phase, 60 Hz power at 4160/2400 volts, and will in turn supply 25-volt circuits with 100 to 200 amperes each. Each rectifier station will be housed in an all weather cubicle and will contain a 3 phase, 100 KVA transformer, a bank of solid state rectifiers, 200 ampere DC circuit breakers, meters, and current transformers.

The 4160 volt power will be supplied through four air circuit breakers, and may be tripped by overload currents in any of the substations. Transmitted power will be monitored by measuring power at the 4160 volt level and computed from the known efficiency of the transmitting units. This efficiency can be checked periodically by actually measuring the power output of sample units. At this power-density level an operator can work in the field with the R.F. power on. More than the required amount of primary power is at present available from the power company at the El Campo substation.

In the cost analysis that follows, the efficiency of the power amplifiers has been assumed to be 63%, and that of

the rectifying and secondary power distribution system 87%. The efficiency of the primary power system should be more than 95% so that the overall efficiency should be 50% or more. These are conservative estimates. The nominal 25 volt secondary voltage output at each rectifying station will actually be about 29 volts under full load. The total power output of the transmitting system can be varied by adjusting the level of the 75 MHz exciter signal fed from the control room to the power amplifiers in the field.

There are several factors to consider when deciding the design efficiency of the 25 VDC conductors. The initial cost of these conductors will be considerable, but this cost is less when the efficiency is low. This cost will be cut about 40% for example when the efficiency is dropped from 90% to 80%. A lower efficiency means less reserve in case the R.F. power should be increased in the future. The lower limit of efficiency will be set by the current-carrying capacity of the conductors. Poor efficiency means poor voltage regulation at the power amplifiers, but this need not be high. A low efficiency means a larger power bill for a given R.F. power output. Each additional KW of maximum power demand will cost about $1.25/month. Each additional KWh will cost about one cent. For a transmitter "on" time of 2 hours per day, the additional power cost due to a lowered efficiency would be about $2/month/KW, or about $480/KW for 20 years.

The optimum efficiency can be estimated by taking a specific example. Suppose one aluminum, direct burial, conductor is to supply amplifiers for 50 dipoles with 118 amperes at 25 volts, and that these amplifiers are 391 feet from the rectifying station. (This would be a realistic example if there were 60 rectifying stations.) Suppose the conductor consists of n strands of AWG 1 cable which costs $140/1000 feet. Allow $20/KW for additional transformer and rectifier capacity. Then the total cost for cable, additional rectifiers and additional power for 20 years is

$$T = 110n + 0.5(\pi 8^2 \cdot \frac{15}{n}) \qquad (7.6.4.1\text{-}1)$$

The resistance of 782 feet of AWG 1 cable is 0.15 ohms. From the equation above, the minimum value for T occurs for n = 3.2, for which the cable cost is $363 and the cable power loss is $312 for 20 years. The voltage drop in the conductors would be 5.5 volts, and the efficiency of the distribution system would be 82%. The design efficiency used in the cost analysis that follows is 87%.

7.6.4.2 Conductors for D.C. Power

To determine the cost of cable for one station we shall proceed with the calculation on the basis of 60 stations, and then scale the result after the optimum number of stations is determined.

Let the area fed by each station be divided into nine equal squares with a rectifying station at the center as shown in Figure 7.6.4.2-1. The heavy solid lines represent large aluminum feeder buses each carrying 118 amps to 50 dipoles. The dotted lines represent copper lines branching from each aluminum line. There are 3 two-wire dotted lines for each of the eight groups and eight smaller two-wire copper lines for the central group. For purposes of cost estimation we will assume that the following cables are needed:

1) 8 Al wires 270' long each carrying 118 amps
2) 8 Al wires 135' long each carrying 118 amps
3) 144 Cu wires 100' long each carrying 15 amps

An overall line efficiency of 87% is assumed. The 87% efficiency determines the IR drop in the feeder lines as follows

$$0.87 = \frac{IV}{IV + I^2R} = \frac{V}{V + IR} = \frac{R_L}{R_L + R} \qquad (7.6.4.2\text{-}1)$$

$$IR = V\frac{1 - 0.87}{0.87} = 0.149V \qquad (7.6.4.2\text{-}2)$$

For V = 25 volts, IR = 3.7 volts.

The best division of resistance between the aluminum and copper lines shown in Figure 7.6.4.2-2 must be determined. For both these conductors, the cost per unit length varies approximately as the resistance per 1000 feet, ρ, raised to

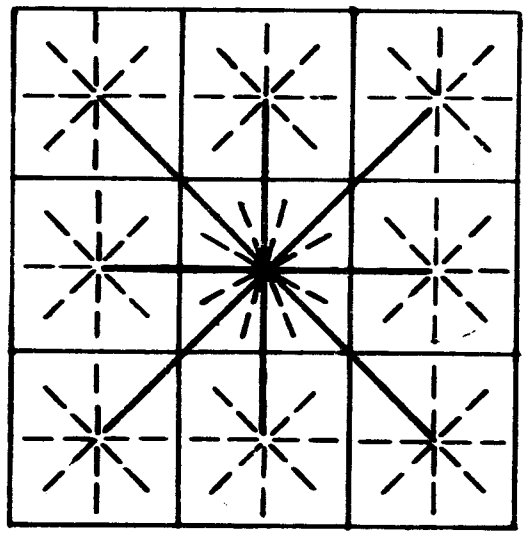

FIG. 7.6.4. 2-1
D.C. POWER BUSES AND
RECTIFYING STATIONS

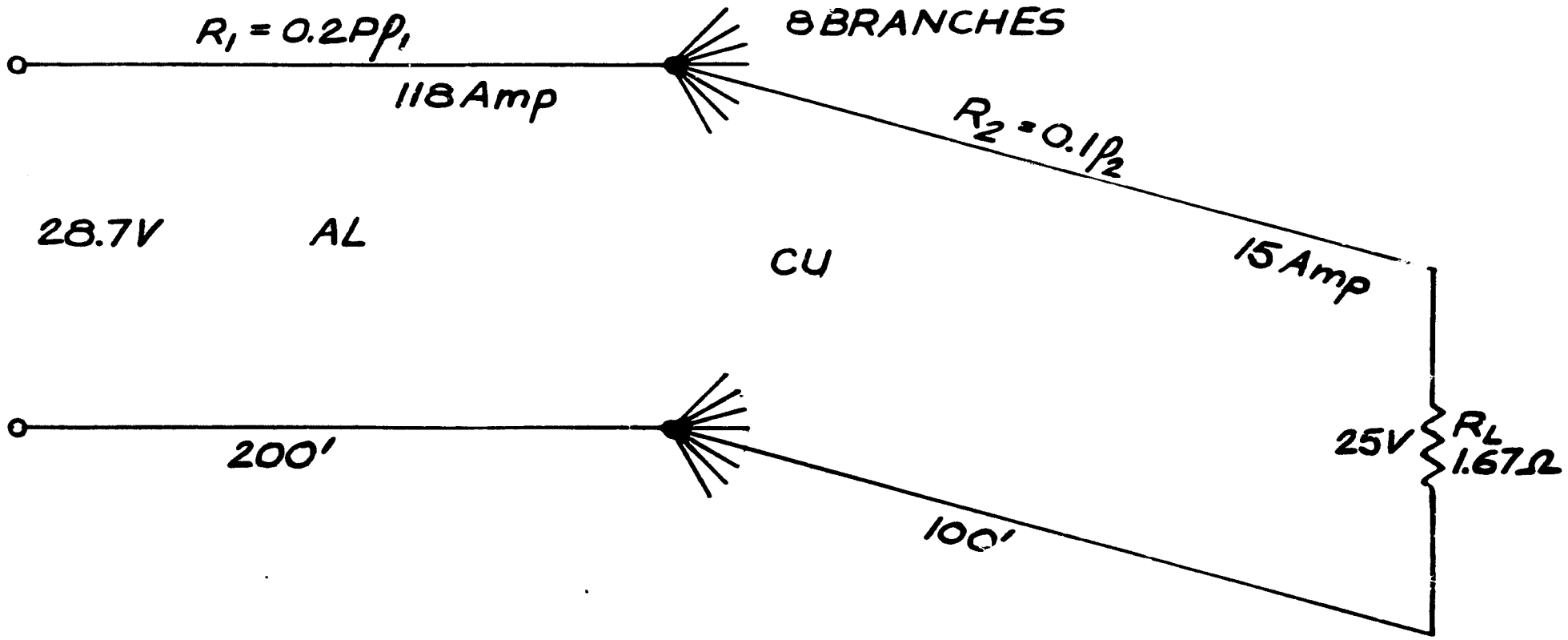

FIG. 7.6.4. 2-2
ALUMINUM AND COPPER BRANCH LINES

the -0.7 power.

Let P_1 and P_2 be respective prices* per foot of the aluminum and copper lines. Then from known prices of #8 Cu cable and 250 MCM Al cable,

$$P_1 = \frac{0.0495}{\rho_1^{0.7}} \qquad (7.6.4.2\text{-}3)$$

$$P_2 = \frac{0.0795}{\rho_2^{0.7}} \qquad (7.6.4.2\text{-}4)$$

The total cost of cable to feed the 8 outside groups then is approximately

$$T = 3200\ P_1 + 12800\ P_2 \text{ dollars} \qquad (7.6.4.2\text{-}5)$$

The relation between ρ_1 and ρ_2 can be determined from the 87% efficiency.

$$0.87 = \frac{8R_L(\frac{118}{8})^2}{8R_L(\frac{118}{8})^2 + 2(118)^2R_1 + 16(\frac{118}{8})^2R_2} \qquad (7.6.4.2.6)$$

$$0.87 = \frac{R_L}{R_L + 2R_L + 16R_1} \qquad (7.6.4.2\text{-}7)$$

---

*$110/1000' for direct burial #8 Cu
$313/1000' for direct burial 250 MCM Al.

Substitute

$$R_L = 167\Omega$$

$$R_1 = 0.2\rho_1$$

$$R_2 = 0.1\rho_2$$

to get

$$\rho_2 = 1.25 - 16\rho_1 \qquad (7.6.4.2\text{-}8)$$

Then

$$T = \frac{158}{\rho_1^{0.7}} + \frac{1017}{\rho_2^{0.7}} = \frac{158}{\rho_1^{0.7}} + \frac{1017}{(1.25 - 16\rho_1)^{0.7}} \qquad (7.6.4.2\text{-}9)$$

From $\frac{dT}{d\rho_1} = 0$, the optimum ρ_1 is 0.04 ohms/1000'. An aluminum conductor of 450 MCM has $\rho_1 = .0393$, so let this be the No 1 cable. Then

$$\rho_2 = 1.25 - 16\rho_1 = 0.62$$

An AWG 3 copper conductor has $\rho_2 = 0.628$, so let this be the No. 2 cable. From these resistivities then we have the following:

$$P_1 = 0.48 , \qquad (7.6.4.2\text{-}10)$$

$$P_2 = 0.11 , \qquad (7.6.4.2\text{-}11)$$

$$T = \$1540 + \$1410 = \$2950 . \qquad (7.6.4.2\text{-}12)$$

For the central section near the rectifiers we require eight feeder lines each delivering 15 amperes to a 1.67 ohm load. For a 3.7 volt drop in a 200 foot line, a cable having a resistivity of 1.23 ohms/1000' is required. This is approximately an AWG 11 copper line which costs about $60/1000' or about $96 per day. This when added to T yields the cost for all secondary conductors fed by each station, and is $3046.

7.6.4.3 Transformers

At each rectifying station a three-phase power transformer to convert the 4160V to the required secondary voltage will be required. The cost of such transformers varies approximately as the 0.65 power of their capacity. For 60 rectifying stations a 20 KVA unit will be required, and its cost will be about $350.00.

7.6.4.4 Rectifiers and Secondary Breakers

A bank of solid state rectifiers supplying 20 KVA at each of 60 stations will cost about $400. Each such bank will supply nine 118 ampere field circuits through nine fused switches. This set of switches with fuses should cost about $400. The cost of the rectifiers and switches for each station should vary approximately inversely as the number of stations so that the total cost of these items for the entire array is constant.

7.6.4.5 Items with Fixed Cost per Station

Some items will contribute to a fixed cost per rectifying station regardless of the number of stations. Such items are the concrete mounting pad, the weatherproof enclosure, current transformers, meters and protective devices. The cost of these items is estimated to be about $1500, including installation.

7.6.4.6 Total Cost and Optimum Number of Stations

When N is the number of rectifying stations, the total cost of supplying sufficient power at 25 VDC to each power amplifier is the sum of the following four terms.

1) $1500 N. These are fixed costs per station

2) $95,000. These are fixed costs and include rectifiers, DC switches, four 4160V air circuit breakers at $5,000 each, 4160V direct burial conductors, and installation costs.

3) $1470 $N^{0.65}$. Cost of power transformers

4) $5,870,000 $N^{-0.85}$. Cost of DC power distribution system.

The value of N optimum is obtained by equating the sum of the derivative of these four terms to zero as follows:

$$1500 + 956\ N_{opt}^{-.35} - 4.99 \times 10^{6} N_{opt}^{-1.85} = 0 \qquad (7.6.4.6\text{-}1)$$

From this equation N_{opt} is solved graphically to be

$$N_{opt} = 75 \qquad (7.6.4.6\text{-}2)$$

The above four cost items then become respectively:

1)	$112,500
2)	95,000
3)	24,300
4)	150,000

for a total of $381,800 to supply 1.59 megawatts of DC power to the power amplifiers.

7.6.5 Cost of R.F. Power Amplifiers for 50 db Array

The present cost of high power, conventional tube-type transmitters in the UHF range is a little less than two dollars per R.F. watt. It appears that the present cost using transistorized units is about the same, but the exact cost will depend

upon the particular, high power, UHF transistor used and upon the date when the transistors are purchased. At present the cost of highly selected units for spacecraft applications is two dollars per R.F. watt for the transistor alone. Less expensive units could be used for the 1 MW transmitter, but the best compromise between initial cost and field reliability can only be determined after more development and experimentation. The proposed 29 db, 192 dipole pilot array should provide a good opportunity for deciding the point of this compromise. The temperature of the power unit is a factor in determining the maximum power that it can supply, and this is another reason for proposing field tests before the final selection is made.

7.6.6 Cost of R.F. Power Amplifiers for Pilot Array

It is proposed that the transmitting feature be added to the 192 dipole array. This would require 32 or more power amplifiers which would produce a total power of 8 KW. This 29 db, 8 KW system could easily detect the moon by radar, and would provide not only a test plot for the transmitting feature but would assist materially in the evaluation of the receiving antenna.

For the pilot array the proposed power amplifiers would be located schematically as shown in the Figure 7.6.6-1. During receive, the power amplifier would be completely removed from the circuit, and during transmit, the receiver amplifier would be completely removed from the circuit and its input

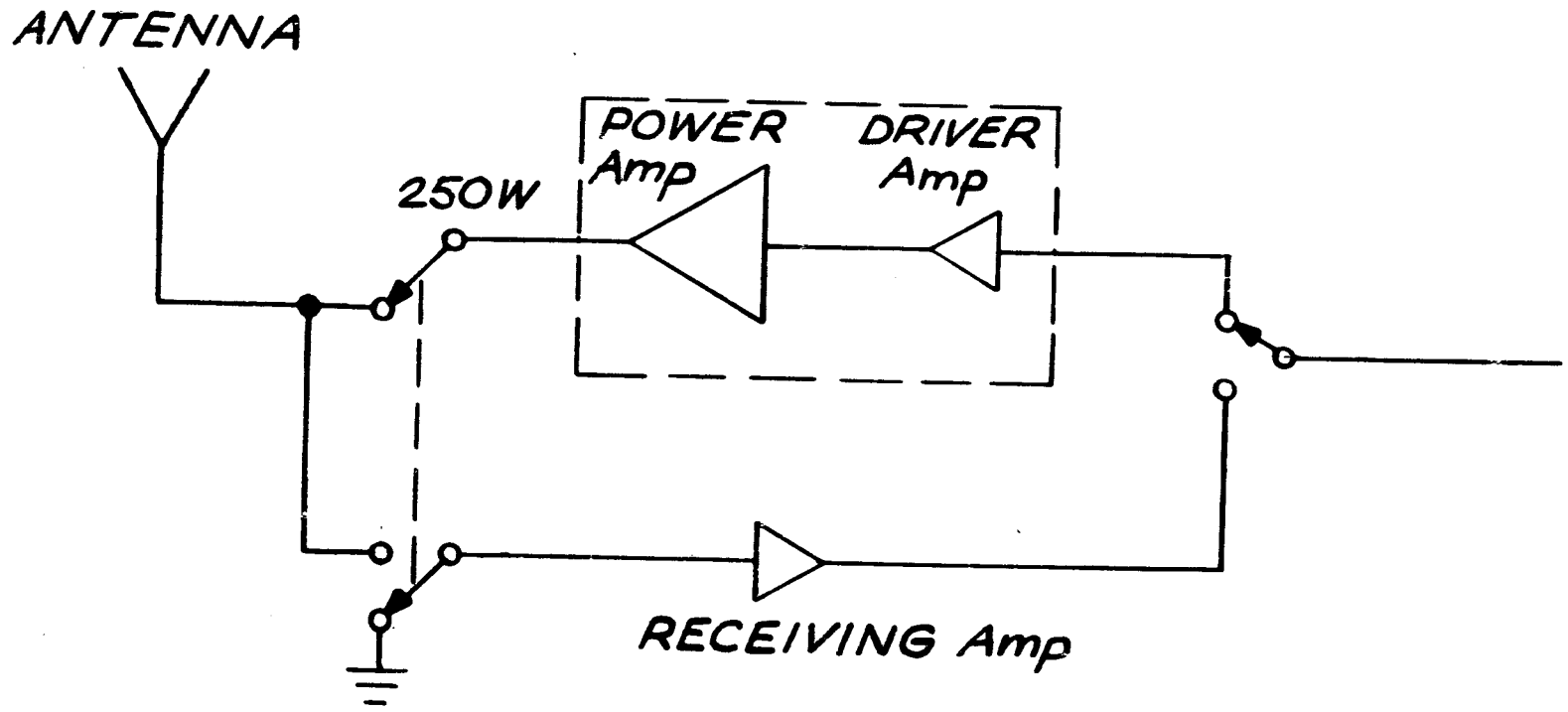

FIG. 7.6.6.-1
TRANSMITTING AND RECEIVING ELECTRONICS

terminal grounded. The power amplifier would consist of a driver amplifier followed by a power amplifier consisting of several transistors in parallel. The TR-ATR switches should consist of mechanical devices, perhaps mercury switches, on the antenna side of the amplifiers and diode switches on the other side.

The estimated cost of these 32 power amplifiers, switches and control cables is as follows:

32	250W amplifiers	$16,000
32	Mercury relays, DPDT	500
34	Diode switches, SPDT	300
	Control Wires	100
	Exciter, 5 watt	500
	Total	$17,400

7.6.7 Conclusions

Reasons are given for incorporating a transmitter feature in the Sunblazer antenna.

A cost analysis is made that shows that for an optimum primary power system of 75 rectifying stations, the power distribution cost is $380 thousand. The remaining cost is the power amplifiers themselves and this should be less than $2 million for a one megawatt radiated power system.

These cost estimates apply for the 50 db array of dipoles regardless of the number of dipoles grouped together for the

basic element.

The specific system given here is for a transmitting feature to be included in the 192-dipole pilot array. There are several benefits to be had from this pilot-array transmitter, among which is a more accurate determination of the cost of the R.F. power amplifier.

The estimated cost of the pilot array transmitter is $17,400 for the power amplifiers plus $20,000 for an initial power distribution system.

7.6.8 Bibliography

Brandt, J. C. Radar Observations and the Extent of Coronal Heating, Astrophysical Journal, 149, p 447, August (1967).

Dessler, A. J., Solar Wind and Interplanetary Magnetic Field, Reviews of Geophysics, 5, p 1-41 (1967).

James, J. C., et al, "Observed Characteristics of an UHF Signal Traversing an Auroral Disturbance", Nature, 185, p 510-512, (1960).

James, J. C., Radar Studies of the Sun, Chapter 7 of Radar Astronomy by Evans and Hagfors, McGraw Hill (1968).

James, J. C., Radar Studies of the Sun at 38 Mc/s, Astrophysical Journal, 146, p 356-366 (1966-b).

James, J. C., Ingalls, R. P., and Rainville, L. P., Radar Echoes From Venus at 38 Mc/sec, Astronomical Journal, 72, p 1047-1050, (1967).

Pettengill, G. H., Radar Studies of the Planets, Chapter 6 of Radar Astronomy by Evans and Hagfors, McGraw-Hill, (1968).

7.7 Evaluation of the Antenna Elements

7.7.1 Summary

Efforts to find a suitable element for the El Campo array have led to experimental investigations as follows:

1) The measurement of gain and radiation pattern of an array of four 1λ backfire elements. This was carried out over the frequency band 280 MHz to 320 MHz.
2) For a single 1.5λ backfire at 225 MHz, gain and impedance properties were evaluated over the equivalent frequency band.
3) The relative bandwidth of dipoles over a ground plane, as a function of dipole diameter, was investigated for single elements and a finite (1.5λ Dia.) ground plane. (Frequency 225 MHz).

7.7.2 1λ Backfire Array at 300 MHz

The 300 MHz quad of backfire elements was matched to 50Ω (within 1.1 SWR) at three different frequencies. Gain and pattern measurements were carried out at these frequencies for

1) Individual elements.
2) The combined array.
3) Cross polarization.

Terminals not used in the measurement procedure, were left open circuited.

Pattern and gain measurements were taken at 280 MHz, 300 MHz, and 320 MHz. The gain measurements are summarized as follows:

Frequency	Gain of Element (dB)	Gain of Array (db)
280	10.6	16.2
300	12.9	17.5
320	8.0	13.0

7.7.3 1.5λ Backfire Element at 225 MHz

Unless otherwise specified, the following dimensions were used for the backfire under test:

Backfire Length	1.5 λ
Director Length	0.405λ
Spacing of Directors	0.2 λ
Diameter of Directors	0.002λ
Secondary Reflector Diameter	0.475λ
Primary Reflector Diameter	1.5 λ
Support Tube Diameter	0.025λ
Dipole Diameter	0.002λ
Dipole Length	0.475λ
Dipole - Reflector Spacing	0.3 λ

7.7.3.1 Admittance Measurements

The backfire was matched at three critical frequencies only by using a double stub configuration. The mismatch is less than 1.7 SWR at all three frequencies.

Attempts to match the backfire using an unbalanced γ feed (similar to that used on the 11 element yagis) proved futile. For these tests, a 1/2" diameter rod was used as the driven element and several matching geometries tried. In general it can be said that the γ match is not suitable because the antenna impedance is too high, as there is always a step up in impedance level regardless of the geometry of the γ matching section.

7.7.3.2 Gain Measurements

Because of difficulties in obtaining an accurate reference level, the absolute gain figures (with respect to isotropic) shown below may only be accurate to within ±1 1/2 db. This estimate of accuracy is based on the variation of signal level which is measured when the reference yagi is moved to different locations.

Relative measurements as given in Table 7.7.3.2-1 may still be useful, however, e.g. variation of director length from .405λ to .421λ.

	Frequency	Mismatch Loss (db)	F.B. (db)	Yagi (db)	Abs. gain/iso. (db)
Director Length = .421λ	210	.25	-.5	-3	12
	225	.22	-3.5	-7.5	15.1
	240	.25	-12	-24.5	12.75
Director Length = .405λ	210	.5	0	-3	12.8
	225	.04	-.5	-5.5	15.9
	240	.25	-.2	-24	12.25

TABLE 7.7.3.2-1

7.7.4 Bandwidth Investigation for λ/2 Dipoles of Different Diameter (1.5λ diameter ground plane)

Originally three diameters (1/4", 1', and 2") were to be used but the results for 1/4" and 2" proved to be sufficient to illustrate the trends.

7.7.4.1 Impedance

Since the reaiation pattern and gain are slowly varying functions of dipole length, the dipoles were adjusted to give approximate resonance for <u>each</u> diameter tested as shown in Figure 7.7.4.1-1.

i.e. d = 1/4" ℓ = .475λ

d = 2" ℓ = .36λ

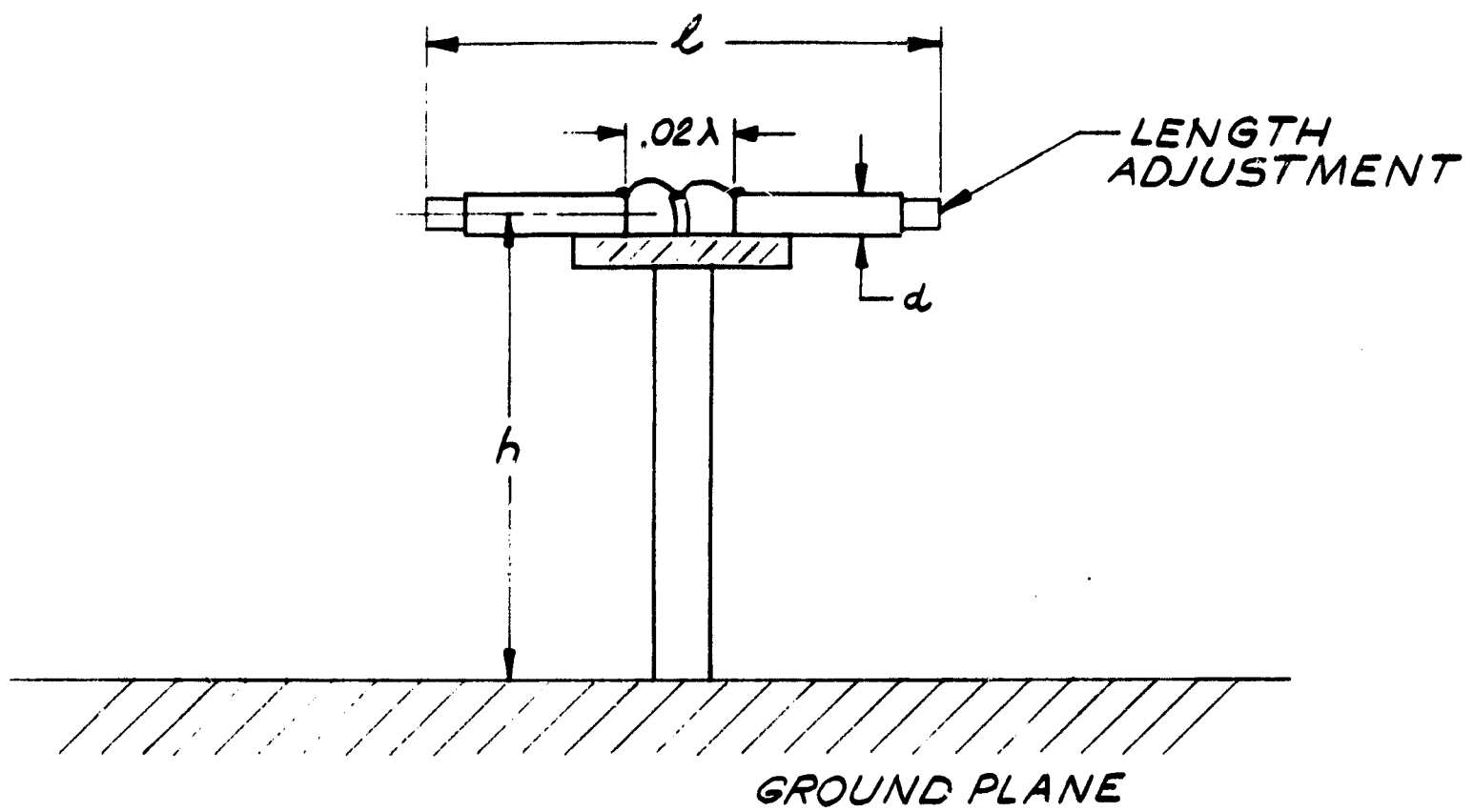

FIG. 7.7.4.1-1
DIMENSIONS OF A DIPOLE
ABOVE GROUND PLANE

Then using these values of ℓ, three different values of dipole to ground plane spacing were tried.

$h = .2\lambda, .25\lambda, .3\lambda$

Admittance plots were taken and used to find the loss due to mismatch for the gain measurement (i.e. no matching networks were used), and also to compare the B.W. of the two different dipoles. Apparently a small capacitive stub on the 1/4" dipole could give B.W. comparable to the 2" model.

7.7.4.2 Gain Measurement

Two approaches were used. One was to try to measure the absolute gain of each antenna relative to isotropic using the calibrated yagi as a reference. The other was a direct comparison between the 2" and 1/4" diameter dipoles to illustrate the degradation in B.W. of the 1/4" diameter mode <u>relative</u> to the 2" diameter version.

Results are shown in Table 7.7.4.2-1, while Table 7.7.4.2-2 represents a summary of the absolute gain measurements.

The absolute gain measurements at 240 MHz are suspect because of the fact that both the transmitting and receiving (reference) yagis have responses which are 11 db down at that frequency (relative to mid-band). Because of this, the signal strength on the reference measurement was fluctuating by ±1 db, and the actual measurement involved a change of instrument scale. It is felt that the <u>relative</u> measurements between dipoles are more reliable since there was no change of scale involved and

the signal level was steady. Furthermore, the levels measured were repeatable over periods of a day or more.

From the results of (1) and (2) there is no apparent degradation in B.W. for a single dipole above a ground plane when the diameter is reduced from 2" to 1/4".

Dipoles in an array environment require further investigation.

TABLE 7.7.4.2-1

Gain Measurement

1/4" Diameter

Freq. MHz	Dipole	Yagi	Δ	Mismatch Loss	Δ'	Net Gain isotropi (db)
1. h = .2λ						
210	-2 1/2	-3 3/4	+1 1/4	0	1 1/4	10 1/2
225	-4 3/4	-3 3/4	-1	1/2	-1/2	10 1/2
240	-21 1/4	-29 1/2	+8 1/4	1 1/4	9 1/2	9 1/2
2. h = .25λ						
210	-2 3/4	-3 1/2	+3/4	0	3/4	10
225	-5	-3 3/4	-1 1/4	1/2	-3/4	10 1/4
240	-21 1/4	-29 1/2	+8 1/4	10	9 1/4	9 1/4
3. h = .3λ						
210	-3 1/2	-3 1/2	0	1/4	1/4	9 1/2
225	-6	-4	-2	1/4	1/4	10 1/4
240	-22 1/2	-30 1/2	+8	3/4	8 3/4	8 3/4

TABLE 7.7.4.2-1 (continued)

Gain Measurement

2" Diameter

Freq. MHz	Dipole	Yagi	Δ	Mismatch Loss	Δ'	Net Gain Isotropic (db)
1. h = .2λ						
2.0	-2 1/2	-3 1/2	+1	1/4	1 1/4	10 1/2
225	-4	-3 1/2	-1/2	1/4	-1/4	10 3/4
240	-20	-31	+11	1/4	11 1/4	11 1/4
2. h = .25λ						
210	-2 1/2	-3 1/3	+1	1/4	1 1/4	10 1/2
225	-4 1/2	-3 1/2	-1	1/4	-3/4	10 1/4
240	-20	-31	+11	1/4	11 1/4	11 1/4
3. h = .3λ						
210	-3 1/4	-3 1/2	+1/4	1/4	1/2	9 3/4
225	-6	-4 1/2	+1 1/2	0	-1 1/2	10 1/2
240	-21	-31	+10	0	10	10

TABLE 7.7.4.2-2

Summary of Absolute Gain Measurements

Freq Mlz	h = .2λ		h = .25λ		h = .3λ	
	1/4	2	1/4	2	1/4	2
210	10 1/2	10 1/2	10	10 1/2	9 1/2	9 3/4
225	10 1/2	10 3/4	10 1/4	10 1/4	10 1/4	10 1/2
240	9 1/2	11 3/4	9 1/4	11 1/4	8 3/4	10

λ/2 dipole - 1.5λ diameter ground plane - gain db above isotropic